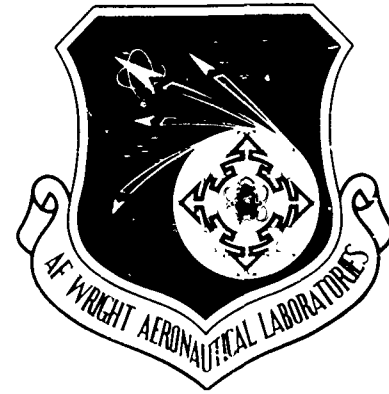


AFWAL-TR-85-2097

IMPROVEMENT OF THE CORROSION RESISTANCE OF TURBINE ENGINE BEARINGS



AD-A167 355

J. H. Mohn
H. M. Hodgens II
H. E. Munson (TRW, Bearings Division, Jamestown, New York)
W. E. Poole

Pratt & Whitney
Government Products Division
P. O. Box 2691
West Palm Beach, Florida 33402

April 1986

Final Report for Period August 1981 - August 1985

Approved for Public Release: Distribution Unlimited

Aero Propulsion Laboratory
Air Force Wright Aeronautical Laboratories
Air Force Systems Command
Wright-Patterson Air Force Base, Ohio 45433

DTIC FILE COPY

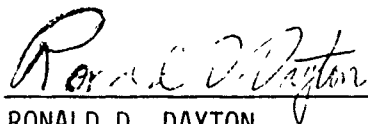
86 5 16 010

NOTICE

When Government drawings, specifications, or other data are used for any purpose other than in connection with a definitely related Government procurement operation, the United States Government thereby incurs no responsibility nor any obligation whatsoever; and the fact that the government may have formulated, furnished, or in any way supplied the said drawings, specifications, or other data, is not to be regarded by implication or otherwise as in any manner licensing the holder or any other person or corporation, or conveying any rights or permission to manufacture, use, or sell any patented invention that may in any way be related thereto.

This report has been reviewed by the Office of Public Affairs (ASD/PA) and is releasable to the National Technical Information Service (NTIS). At NTIS, it will be available to the general public, including foreign nations.

This technical report has been reviewed and is approved for publication.



RONALD D. DAYTON
Project Engineer
Lubrication Branch



HOWARD F. JONES
Chief, Lubrication Branch
Fuels and Lubrication Division

FOR THE COMMANDER:



ROBERT D. SHERRILL, Chief
Fuels and Lubrication Division
Aero Propulsion Laboratory

"If your address has changed, if you wish to be removed from our mailing list, or if the addressee is no longer employed by your organization please notify AFWAL/POSL, WPAFB, OH 45433 to help maintain a current mailing list."

Copies of this report should not be returned unless return is required by security considerations, contractual obligations, or notice on a specific document.

UNCLASSIFIED

SECURITY CLASSIFICATION OF THIS PAGE

AD-A167355

REPORT DOCUMENTATION PAGE

1a. REPORT SECURITY CLASSIFICATION UNCLASSIFIED		1b. RESTRICTIVE MARKINGS N/A	
2a. SECURITY CLASSIFICATION AUTHORITY N/A		3. DISTRIBUTION/AVAILABILITY OF REPORT Approved for Public Release; Distribution Unlimited	
2b. DECLASSIFICATION/DOWNGRADING SCHEDULE N/A			
4. PERFORMING ORGANIZATION REPORT NUMBER(S) P&W/GPD FR-18566		5. MONITORING ORGANIZATION REPORT NUMBER(S) AFWAL-TR-85-2097	
6a. NAME OF PERFORMING ORGANIZATION Pratt & Whitney Government Products Division		6b. OFFICE SYMBOL (If applicable)	
6c. ADDRESS (City, State and ZIP Code) P.O. Box 2691 West Palm Beach, Florida 33402		7a. NAME OF MONITORING ORGANIZATION Aero Propulsion Laboratory (AFWAL/POSL)	
7b. ADDRESS (City, State and ZIP Code) Air Force Wright Aeronautical Laboratories Air Force Systems Command Wright-Patterson Air Force Base, Ohio 45433			
8a. NAME OF FUNDING/SPONSORING ORGANIZATION Aero Propulsion Laboratory		8b. OFFICE SYMBOL (If applicable) AFWAL/POSL	
8c. ADDRESS (City, State and ZIP Code) Air Force Wright Aeronautical Laboratories Air Force Systems Command Wright-Patterson Air Force Base, Ohio 45433		9. PROCUREMENT INSTRUMENT IDENTIFICATION NUMBER Contract F33615-81-C-2023	
11. TITLE (Include Security Classification) Improvement of the Corrosion Resistance of Turbine Engine Bearings		10. SOURCE OF FUNDING NOS.	
		PROGRAM ELEMENT NO. 62203F	TASK NO. 06
		PROJECT NO. 3048	WORK UNIT NO. 21
12. PERSONAL AUTHOR(S) J.H. Mohn, H.M. Hodgens II, H.E. Munson (TRW Bearings Div.), W.E. Poole			
13a. TYPE OF REPORT Final		13b. TIME COVERED FROM 8-1981 TO 8-1985	
		14. DATE OF REPORT (Yr., Mo., Day) 1 April 1986	
		15. PAGE COUNT 189	
16. SUPPLEMENTARY NOTATION			
17. COSATI CODES		18. SUBJECT TERMS (Continue on reverse if necessary and identify by block number)	
FIELD	GROUP	SUB GR	
			Corrosion Resistance Test
			Wear Resistance Test
			Rolling Contact Fatigue Test
			Hot Hardness Test
			Rolling Contact Bearings
			Bearing Life Testing
			Bearing Endurance Testing
			Bearing Lubrication
			M50
			Nickel Sputter Coating
			CRB7
			Corrosion Resistant Bearings
			MRC2001
			Corrosion Resistant Alloys
			RSR565
			Corrosion Resistant Coatings
			Armoloy
			Corrosion Resistant Surface Treatments
			RSP565
			Bearing Fabrication
			Bearing Surface Finish
19. ABSTRACT (Continue on reverse if necessary and identify by block number) This final report encompasses the work accomplished by a two-phase program aimed at developing an alternate material, fabrication technique, or material treatment for turbine engine mainshaft bearings with improved corrosion resistance compared to state-of-the art VIM-VAR-M50. During Phase I, five corrosion-resistant bearing candidates (Armoloy-coated M50, nickel sputter-coated M50, wrought CRB7, RSR565, and MRC2001) were identified as the most promising. These were subjected to rolling contact fatigue, corrosion, hot hardness, and wear screening tests. The phase concluded with selection of MRC2001 as the single most promising candidate for full-scale bearing fabrication and testing. VSP (see Acc Report)			
20. DISTRIBUTION/AVAILABILITY OF ABSTRACT UNCLASSIFIED/UNLIMITED <input type="checkbox"/> SAME AS RPT <input checked="" type="checkbox"/> DTIC USERS <input type="checkbox"/>		21. ABSTRACT SECURITY CLASSIFICATION UNCLASSIFIED	
22a. NAME OF RESPONSIBLE INDIVIDUAL J.H. Mohn		22b. TELEPHONE NUMBER (Include Area Code) 305-840-5955	
		22c. OFFICE SYMBOL AFWAL/POSL	

DD FORM 1473, 83 APR

EDITION OF 1 JAN 73 IS OBSOLETE.

UNCLASSIFIED

SECURITY CLASSIFICATION OF THIS PAGE

UNCLASSIFIED

SECURITY CLASSIFICATION OF THIS PAGE

19

In Phase II, full-scale 35-mm endurance bearings were fabricated from MRC2001 and baseline VIM-VAR M50. Additionally, 110-mm performance bearings were fabricated from MRC2001. In a parallel but separately funded program full-scale 35-mm endurance bearings were also fabricated from RSP565 material and endurance tested. RSP565 is a conventional argon atomized version of the RSR565 material evaluated in Phase I. The MRC2001, RSP565 and M50 35-mm bearings were subjected to back to back endurance tests. Considering inner race failures only Weibull analysis showed no significant difference between the materials at the 95 percent confidence level.

UNCLASSIFIED

SECURITY CLASSIFICATION OF THIS PAGE

FOREWORD

This final technical report describes exploratory development work performed by the Pratt & Whitney Engineering Division under United States Air Force (USAF) Contract F33615-81-C-2023, Improvement of the Corrosion Resistance of Turbine Engine Bearings. P&W was assisted in this effort by TRW Bearings Division of TRW, Inc. The report covers the period from August 1981 to August 1985.

This program is sponsored by the Aero Propulsion Laboratory of the Air Force Wright Aeronautical Laboratories (AFWAL), Wright-Patterson Air Force Base, Ohio 45433 under project 3048, "Fuels, Lubrication and Fire Protection," Task 304806, "Aerospace Lubrication," work unit 30480621, "Improvement of the Corrosion Resistance of Turbine Engine Bearings." Mr. R. Dayton is the USAF AFWAL/POSL Project Engineer. The Pratt & Whitney Program Manager and Principal Investigator are J. H. Mohn and W. E. Poole, respectively. Test specimen preparator and material testing was conducted at TRW Bearings Division under the direction of Mr. A. T. Galbato, Manager of Research and Development.

This document is submitted in compliance with CLIN 0002 and CDRL Sequence Number 6.

Appreciation is extended to the following for their valuable assistance in this program: P. Allard (P&W), J. Artuso (AFWAL), J. W. Broch (P&W), J. N. Fleck (TRW), B. J. Killman (TRW), B. McCoy (TRW), J. R. Miner (P&W), D. Pogoshev (NAPC), and R. F. Spitzer (TRW).



Accession Per	
[Handwritten mark]	
By	
Distribution/	
Availability Codes	
Dist	Trail and/or Special
AI	

TABLE OF CONTENTS

<i>Section</i>		<i>Page</i>
I	INTRODUCTION	1
II	TECHNICAL DISCUSSION	3
	1. Background	3
	2. Corrosion Investigation	3
	3. Candidate Selection	47
	4. Phase II Bearing Fabrication and Test	116
III	CONCLUSIONS	171
	1. Summary	171
	2. Principal Results	171
	3. Conclusions	173
	4. Recommendations	173
	REFERENCES	175
	APPENDIX A — Visual Inspection Documentation of the 35-mm Endurance Ball Bearings	177
	APPENDIX B — Visual Inspection Documentation of the M50 Baseline 35-mm Endurance Ball Bearings With MRC2001 Inner Rings, M50 Balls, and Outer Rings	181
	APPENDIX C — Visual Inspection Documentation of the RSP565 35-mm Endurance Ball Bearings	185

LIST OF ILLUSTRATIONS

<i>Figure</i>		<i>Page</i>
1	Dark Staining of Silver-Plated AISI 4340 Cage at Rolling Element-Cage and Race-Cage Contact Loci (Main Shaft Bearing C, Stored in MIL-C-11796B Preservative)	5
2	Heavy, Dark Staining of Silver-Plated AISI 4340 Cage Generally Conforming to Thick-Thin Preservative Boundary Morphology (Accessory Bearing, Similar to Accessory Bearing E Stored in MIL-C-11796B Preservative)	6
3	Light Violet Staining of Silver-Plated AISI 4340 Cage at Rolling Element-Cage Contact Loci (Accessory Bearing F Stored in MIL-C-11796B Preservative)	7
4	SEM Photomicrograph and XES Spectra of Light Violet Stained Region (Area F) and Unstained Region (Area G) of Silver-Plated AISI 4340 Steel Cage Material (Accessory Bearing F)	8
5	SEM Photomicrographs and XES Spectra of Light Brown Stained and Unstained Areas of Silver Plating on AISI 4340 Cage Material (Main Shaft Bearing C)	9
6	Heavy, Dark Staining of Silver-Plated AISI 4340 Cage Analyzed Via SEM and XES in Figure 7 (Accessory Bearing E Stored in MIL-C-11796B Preservative)	10
7	SEM Photomicrograph and XES Spectra of Dark Stain on Silver-Plated AISI 4340 Cage Material (Accessory Bearing E)	11
8	AES Spectra of Stained Region of Silver-Plated AISI 4340 Steel Cage Material From Main Shaft Bearing C, Stored in MIL-C-11796B Preservative, Showing Variation of Chemical Composition With Depth	12
9	Thick-Thin Preservative Boundary Morphology as Seen Through Plastic Skin-Pack (Main Shaft Bearing N)	13
10	Dark Black Stains of M50 Steel Conforming to Rolling Element/Race Contact Morphology (Accessory Bearing F)	14
11	SEM Photomicrographs of Stained and Unstained Areas of M50 Steel Race (Main Shaft Bearing B); Indicated Areas are Examined Further in Figure 12	15
12	SEM Photomicrographs of Indicated Area in Figure 11 and Photographs of XES Spectra From Light and Dark Areas, Emphasizing Difficulty of Analyzing Lightest Stains	16
13	AES Spectra of Stained Region of M50 Steel Ball From Main Shaft Bearing C, Stored in MIL-C-11796B Preservative, Showing Variation of Chemical Composition With Depth	17

LIST OF ILLUSTRATIONS (Continued)

<i>Figure</i>		<i>Page</i>
14	SEM Photomicrographs, XES Spectra, and Chlorine X-ray Map of Adsorbed Dendrites Comprised of Sodium, Potassium, and Calcium Chloride on an M50 Steel Ball (Result of Handling Ball Without Gloves or Suitable Protective Film on Hands)	18
15	SEM Photomicrographs and XES Spectra of Lightly Stained M50 Bearing Material (Main Shaft Bearing C) Which Appears to Follow the Grain Boundary Morphology (Arrows)	19
16	SEM Photomicrographs and XES Spectra of Dark Black Stains on M50 Steel Roller Showing Apparent Enrichment of Alloying Elements (Cr, Mo, V) Relative to Iron in Location of Corrosive Attack	20
17	Typical Appearance of Service-Rejected Bearing Does Not Suggest Corrosive Attack (Mainshaft Bearing J, Service in MIL-L-7808J Oil) ..	21
18	Pitting Attack of Functional Surfaces of Service-Rejected Bearing (Main Shaft Bearing J, Service in MIL-L-7808 Oil)	22
19	Pitting Attack of Ball Previously Shown in Figure 18 (Mainshaft Bearing J, Service in MIL-L-7808J Oil)	23
20	SEM Photomicrographs and XES Spectra of Indentations (Main Shaft Bearing J)	24
21	SEM Photomicrographs and XES Spectra of Locations of Embedded Particles and Probable Autocatalytic Pitting Attack Initiated at Those Locations (Main Shaft Bearing K)	26
22	SEM Photomicrographs and XES Spectra of Area of Pitting Attack (Main Shaft Bearing K)	27
23	Section of Cage Examined Via SEM, XES, and MET Analyses for Thin Dark Stains (Accessory Bearing H)	28
24	SEM Photomicrographs and XES Spectra of Thin, Dark Stains of Silver-Plated AISI 4340 Steel Showing Mudcracked Morphology and High Sulfur Content in Locations of Corrosive Attack (Accessory Bearing H)	29
25	SEM Photomicrographs and XES Spectra of Mudcracked Morphology of Silver-Plated AISI 4340 Steel Cage and Damaged Bower 315 Steel Outer Race (Main Shaft Bearing K)	30
26	SEM Photomicrographs and XES Spectra of M50 Steel Roller Exposed to Service and Storage Environments (Accessory Bearing G)	31

LIST OF ILLUSTRATIONS (Continued)

<i>Figure</i>		<i>Page</i>
27	SEM Photomicrographs, XES Spectra, and X-ray Maps of Mudcracked Region of Figure 26 Showing Relative Enrichment of Alloying Elements Due to Leaching Away of Iron Corrosion Products	32
28	Corrosion of Main Shaft Bearing D Inadequately Preserved During Delay in Assembly	33
29	SEM Photomicrographs and XES Spectra of Mudcracking Corrosion of M50 Steel, Nonfunctional Surfaces (Main Shaft Bearing D)	34
30	SEM Photomicrographs and XES Spectra of Pitting Attack of M50 Steel Outer Race Along Phase Boundary (Main Shaft Bearing D)	35
31	Specimens (M50 Steel at Top; Silver-Plated Coupon at Bottom) Exposed to MIL-L-23699 Oil (Contaminated at Left; Control at Right) at 140°F for 24 Hours	39
32	Specimens (M50 Steel at Top; Silver-Plated Coupon at Bottom) Exposed to MIL-L-7808J Oil (Control at Left; Contaminated at Right) at 140°F for 24 Hours	40
33	Specimens (M50 Steel at Top; Silver-Plated Coupons at Bottom) Exposed to MIL-C-15074C Oil (Contaminated at Left; Control at Right) at 140°F for 24 Hours	41
34	Specimens (M50 Steel at Bottom; Silver-Plated Coupon at Top) Exposed to 0.0005 Percent Weight Sulfur (as Trityl Thiol) in Mineral Oil at 140°F for 24 Hours	42
35	Specimens (M50 Steel at Bottom; Silver-Plated Coupon at Top) Exposed to 0.0020 Percent Weight Sulfur (as Trityl Thiol) in Mineral Oil at 140°F for 24 Hours	43
36	Specimens (M50 Steel at Bottom; Silver-Plated Coupon at Top) Exposed to 0.0100 Percent Weight Sulfur (as Trityl Thiol) in Mineral Oil at 140°F for 24 Hours	44
37	Specimens (M50 Steel at Bottom; Silver-Plated Coupon at Top) Exposed to 0.0005 Percent Weight Chloride (as Trityl Chloride) in Mineral Oil at 140°F for 24 Hours	45
38	Specimens (M50 Steel at Bottom; Silver-Plated Coupon at Top) Exposed to 0.0020 Percent Weight Chloride (as Trityl Chloride) in Mineral Oil at 140°F for 24 Hours	46
39	Specimens (M50 Steel at Bottom; Silver-Plated Coupon at Top) Exposed to 0.0100 Percent Weight Chloride (as Trityl Chloride) in Mineral Oil at 140°F for 24 Hours	47

LIST OF ILLUSTRATIONS (Continued)

<i>Figure</i>		<i>Page</i>
40	Diagrammatic Representation of the Radio Frequency Diode Sputtering Chamber	51
41	SEM Photomicrograph of a Cross Sectioned "As-Received" Armoloy-Coated M50 Test Specimen	55
42	SEM Photomicrograph of the Surface of a Typical VIM-VAR M50 Baseline Test Specimen and Coating Substrate Specimen	56
43	SEM Photomicrograph of the Surface of a Typical "As-Received" Armoloy-Coated M50 Test Specimen	57
44	SEM Photomicrograph of the Surface of a Typical Polished Armoloy-Coated M50 Test Specimen	57
45	Planar Target Radio Frequency Diode Sputtering System	58
46	SEM Photomicrograph of a Cross Section of Sputtered Nickel on M50 Bearing Stock	59
47	SEM Photomicrograph of the Surface of a Typical Nickel Sputter-Coated M50 Test Specimen	60
48	Microstructure Photographs	65
49	Overall View of the Rolling Contact Fatigue Rig (Top); Closeup View of Specimen and Test Rolls (Bottom)	66
50	Weibull Plot of Baseline M50 Rolling Contact Fatigue Test Results ...	67
51	Weibull Plot of Nickel Sputter-Coated M50 Rolling Contact Fatigue Test Results	68
52	Weibull Plot of As-Received Armoloy-Coated M50 Rolling Contact Fatigue Test Results	69
53	Weibull Plot of Polished Armoloy-Coated M50 Rolling Contact Fatigue Test Results	70
54	Weibull Plot of MRC2001 Rolling Contact Fatigue Test Results	71
55	Weibull Plot of CRB7 Rolling Contact Fatigue Test Results	72
56	Weibull Plot of RSR565 Rolling Contact Fatigue Test Results	73
57	Weibull Plot of RSR113 Rolling Contact Fatigue Test Results	74
58	Composite Weibull Plot of Candidate and VIM-VAR M50 Rolling Contact Fatigue Test Results	76

LIST OF ILLUSTRATIONS (Continued)

<i>Figure</i>		<i>Page</i>
59	EDXR Analysis of Nickel Sputter-Coated Bar Outside of Roller Track (Note Nickel Lines)	77
60	EDXR Analysis of Nickel Sputter-Coated Bar Roller Track (Nickel Has Been Lost)	78
61	SEM Photomicrograph of Roller Track on Nickel Sputter-Coated Bar HN-2 (Note Flaking; Magnification: 50×)	79
62	SEM Photomicrograph of Roller Track on Nickel Sputter-Coated Bar HN-2 (Magnification: 200×)	79
63	SEM Photomicrograph of Roller Track No. 3 on Chrome-Plated Bar HA-5 (Note Pebbled Surface Outside of Roller Path; Magnification: 50×)	80
64	SEM Photomicrograph of Roller Track No. 3 on Chrome-Plated Bar HA-5 (Note Smearred Surface; Magnification: 200×)	80
65	SEM Photomicrograph of Roller Track No. 6 on Chrome-Plated, Subsequently Polished, Bar HA-3; (Magnification: 50×)	81
66	SEM Photomicrograph of Roller Track No. 6 on Chrome-Plated, Subsequently Polished, Bar HA-3 (Magnification: 200×)	81
67	EDXR Analysis of Chrome-Plated, Subsequently Polished, Bar HA-3 Outside of Track (Note Iron Lines)	82
68	EDXR Analysis of Chrome-Plated, Subsequently Polished, Bar HA-3 in Track 1 (Note That Iron is Present but Chrome is Thicker Than in Figure 67)	83
69	EDXR Analysis of Chrome-Plated Bar HA-5 Outside of Track	84
70	EDXR Analysis of Chrome-Plated Bar HA-5 in Track 3	85
71	SEM View of Typical Spall in M50 Reference Test Bar H-4 (Magnification: 110×)	86
72	SEM View of Spall in Chrome-Plated Test Bar HA-1 (Magnification: 72×)	86
73	SEM View of Spall in CRB7 Test Bar HC-2 (Magnification: 72×)	87
74	SEM View of Spall in RSR565 Test Bar HR-1 (Magnification: 72×)	87

LIST OF ILLUSTRATIONS (Continued)

<i>Figure</i>		<i>Page</i>
75	SEM View of Spall in RSR113 Test Bar HB-2 (Magnification: 72×)	88
76	SEM View of Spall in MRC2001 Test Bar HE-2 (Magnification: 72×)	88
77	Corrosion Test Fixture With Four Pairs of Specimens	89
78	Corrosion Test Setup	90
79	M50 Reference Specimens 5 and 6	91
80	Stained and Pitted End Surface M50 (Magnification: 400×)	92
81	Stained and Pitted OD Surface M50 (Magnification: 300×)	92
82	Chrome-Plated Specimens 19 and 20 After Corrosion Test (Arrows Point to Corroded Areas)	93
83	Schematic of Wear Test Apparatus	102
84	Wear Test Rig Showing Wick Lubrication	102
85	Sample Traces of Vibration Data From Wear Tests	103
86	Sample Traces of Vibration Data From Wear Tests	104
87	Bar Chart Showing Mass Change of Stationary Specimens Used in Candidate vs Candidate Wear Tests	107
88	Sections of Wear Test Bars Showing Representative Scars on M50, Armoloy-Coated M50, and RSR565 Material (Latter Two Bars Were Also Subjected to Hot Hardness Tests)	108
89	Wear Test Bars Showing Representative Scars on MRC2001, CRB7, and M50 Material (Scale Magnification Approximately 2.5×)	108
90	Rotating Wear Test Bars Showing Representative Tracks on M50 and MRC2001 Specimens (Scale Magnification Approximately 3×)	109
91	Rotating Wear Test Bars Showing Representative Tracks on MRC2001 and CRB7 Specimens (Scale Magnification Approximately 3×)	109
92	SEM Photograph of the Bottom of a Typical Wear Scar on an M50 Stationary Bar (Magnification: 100×)	110
93	SEM Photograph of the Bottom of a Typical Wear Scar on an MRC2001 Stationary Bar (Magnification: 100×)	110

LIST OF ILLUSTRATIONS (Continued)

<i>Figure</i>		<i>Page</i>
94	SEM Photograph of the Bottom of a Typical Wear Scar on a CRB7 Stationary Bar (Magnification: 100×)	111
95	Wear Scars on M50, Armoloy-Coated M50, CRB7, and RSR565 Run Against Silver-Plated Steel (RSR565 Specimen Was Discolored Subsequent to the Wear Test)	112
96	Rotating Wear Test Bars, Silver-Plated AMS 6515 Steel, Showing Representative Wear Tracks (Scale Magnification Approximately 3×) ..	112
97	Metallographic Examination of Cross Section of Wear Track on a Silver-Plated Steel Bar (Magnification: 400×)	113
98	Schematic of Hot Hardness Test Apparatus	113
99	Plot of Normalized Hardness vs Temperature for Candidates and VIM-VAR M50 Baseline Material	117
100	Typical Indentations on Hot Hardness Test Specimens	118
101	MRC207S 35-mm Endurance Test Bearing	120
102	SEM Photomicrograph of Annealed Inner Ring Segment Which Exhibited Normal Heat Treat Response	123
103	SEM Photomicrograph of Annealed Outer Ring Segment Which Exhibited Abnormal Heat Treat Response	124
104	SEM Photomicrograph of Hardened and Tempered Inner and Outer Ring Segments Presented in Figures 102 and 103 Respectively	125
105	SEM Photomicrograph of Outer Race Segment Voids/Cracks After Heat Treatment (Unetched; 100×)	126
106	Plot of Hardness Range vs Density for 110-mm Inner Ring Blanks	129
107	Part of Battery of Model A Test Machines	134
108	Schematic of TRW's Model A Test Rig	134
109	MRC2001 35-mm Endurance Bearing S/N #2 Spalled Ball	137
110	MRC2001 35-mm Endurance Bearing S/N E20 Spalled Inner Race	138
111	MRC2001 35-mm Endurance Bearing S/N E12 Outer Race Spall (20×)	139
112	M50 35-mm Endurance Bearing S/N 17 Inner Race Spall (20×)	139

LIST OF ILLUSTRATIONS (Continued)

<i>Figure</i>		<i>Page</i>
113	Composite Maximum Likelihood Weibull Distribution Plot of M50 and MRC2001 Task VII Endurance Bearing Failures	140
114	Photomicrograph of Primary Fatigue Spall of MRC2001 RCF Specimen and MRC2001 Inner Race	142
115	Thin Film Transmission Electron Micrograph of MRC2001 RCF Specimen	143
116	Thin Film Transmission Electron Micrograph of MRC2001 35-mm Endurance Bearing Ball	144
117	MRC2001 Microstructure, Grain Size, and Etch Response Comparison	147
118	MRC2001 35-mm Bearing Ring Microstructure as HIPped (1000×)	148
119	MRC2001 35-mm Bearing Ring Microstructure After HIPping, Upsetting, and Drilling (1000×)	148
120	MRC2001 35-mm Outer Ring Microstructure After HIPping, Upsetting, and Hammer Forging (1000×)	149
121	MRC2001 35-mm Outer Ring Microstructure After HIPping, Hammer Forging, and Hardening (1000×)	149
122	Tensile Residual Stress Profile of MRC2001 Inner Race S/N E22	150
123	Comparison of Typical MRC2001 and M50 Race Surface (1000×)	151
124	Residual Stress Profile of MRC2001 Test Rings	153
125	Circumferential Residual Stress vs Depth for Inner Raceways at Center Ball Track Location	159
126	Residual Stress vs Depth at Arbitrary Location on Ball	159
127	Circumferential Residual Stress vs Depth for Outer Raceways at Center Ball Track Location	160
128	Range of Inner Race Surface Finish for MRC2001, RSP565, and M50	161
129	Slinger to Prevent Adjacent Bearing Contamination	163
130	Composite Maximum Likelihood Weibull Distribution Plot of M50, MRC2001, and RSP565 Inner Race Failure Data	166
131	Typical 35-mm Bearing Component Spalls	168

LIST OF ILLUSTRATIONS (Continued)

<i>Figure</i>		<i>Page</i>
132	RSP565 35-mm Endurance Bearing S/N 4 Spalled Ball Cross Section (Endurance Time of 404 Hours)	169
133	Composite Maximum Likelihood Weibull Distribution Plot of MRC2001 and RSP565 Ball Failure Data	170

LIST OF TABLES

<i>Table</i>		<i>Page</i>
1	Storage Preservatives	36
2	History and Analysis of Used Engine Oils	37
3	Oil Analysis Results After Engine Water Washdown	38
4	List of Potential Candidates	49
5	Armoloy-Plated Bearing Applications	51
6	Preliminary Task 2 Candidate Selection	53
7	Heat Treatment of M50	61
8	Heat Treatment of MRC2001	61
9	Heat Treatment of CRB7	62
10	Heat Treatment of RSR565	62
11	Heat Treatment of RSR405	63
12	Heat Treatment of RSR113	63
13	Metallurgical Parameters of Alloy Candidates, RSR113 and VIM-VAR M50 Baseline	64
14	Rolling Contact Fatigue Test Results	75
15	VIM-VAR M50 Corrosion Test Data	93
16	Nickel Sputter-Coated M50 Corrosion Test Data	94
17	Armoloy-Coated M50 Corrosion Test Data	94
18	CRB7 Corrosion Test Data	95
19	RSR565 Corrosion Test Data	96
20	MRC2001 Corrosion Test Data	96
21	RSR113 Corrosion Test Data	97
22	Task III Ranking Summary	101
23	Wear Test Data	105
24	Wear Test Results Summary	106

LIST OF TABLES (Continued)

<i>Table</i>	<i>Page</i>
25 Hot Hardness Test Data	115
26 Summary of Hot Hardness Test Results	116
27 Task III Ranking Summary	119
28 Thermomechanical Processing of MRC2001 Race Blanks	120
29 Density Values for 110-mm Rings	121
30 Post-Heat Treat Hardness vs Density for 110-mm Outer Ring Blanks	126
31 Post-Heat Treat Hardness vs Density for 110-mm Inner Ring Blanks	127
32 Post-Heat Treat Hardness vs Density for MRC2001 35-mm Inner Race Blanks	128
33 Post-Heat Treat Hardness vs Density for MRC2001 35-mm Outer Race Blanks	129
34 Dimensional and Quality Inspection Data for MRC2001 35-mm Endurance Bearings	130
35 Dimensional and Quality Inspection Data for M50 35-mm Baseline Endurance Bearings (VIM-VAR M50 Inners, Outers, Balls)	131
36 Dimensional Inspection Data for MRC2001 110-mm Performance Bearings (Same Configuration as Forward Bearing of PWA 536343 Duplexed Pair)	133
37 Task VII 35-mm Bearing Endurance Test Log	141
38 Thermomechanical Processing of the RSP565 Race Blanks	154
39 RSP565 Heat Treat Schedule	154
40 Inspection Data for 35-mm Bearings With MRC2001 Inners, M50 Balls and Outer Races	155
41 Inspection Data for 35-mm M50 Bearings	156
42 Inspection Data for 35-mm RSP565 Bearings	157
43 Inner Race Fits and Bearing Internal Clearances	158
44 Calculated Bearing Life for the Range of Bearing Geometries and Endurance Test Conditions	164

LIST OF TABLES (Continued)

<i>Table</i>		<i>Page</i>
45	35-mm Endurance Bearing Test Results	165

SECTION I

INTRODUCTION

The objective of this "Improvement of the Corrosion Resistance of Turbine Engine Bearings Program" is to provide a bearing which is significantly more corrosion resistant than VIM-VAR (vacuum induction melt-vacuum arc remelt) M50 state-of-the-art bearings.

Improved bearing corrosion resistance can be achieved with either the use of a new corrosion resistant alloy, or by surface treating, or coating state-of-the-art M50 with a protective covering. This ~~48-month~~ two-phase program investigated all three methods: alloys, coatings, and surface treatments. In Phase I, appropriate bearing materials, surface treatments, and coatings were identified. Screening tests were performed on the most promising candidates. The single most promising candidate was selected for full-scale bearing fabrication and testing in Phase II.

The Phase I effort was broken into five tasks which will be discussed in detail in this report. Task I began with a study of the corrosion mechanism which was a continuation of an ongoing effort at P&W. In Task II, 17 candidates with potential for improving bearing corrosion resistance were identified for consideration. The 17 candidates included corrosion resistant alloys such as CRB7 (AMS5900), and BG42 (AMS5749), coatings such as the proprietary chrome plating process called Armoloy, and surface treatments such as nickel sputter-coated M50. Of these, the five most promising were selected based on available data and perceived material properties. The five highest potential candidates were Armoloy-coated M50, nickel sputter-coated M50, wrought CRB7, and powder metallurgy RSR565 and MRC2001. Task III ranked the five candidates based on rolling contact fatigue and corrosion resistance tests. From these test results, the three best candidates, Armoloy-coated M50, CRB7, and MRC2001 were selected for further evaluation. In Task IV, these three candidates were evaluated for wear resistance and hot hardness characteristics. Based on the property test results and criteria established in Task II, the most promising candidate, MRC2001, was selected in Task V for full-scale bearing development and testing. → Fu PA

The original Phase II program consisted of Tasks VI through IX. In Task VI twenty 35 mm bore size MRC207S endurance test bearings, i.e., balls, inner races, and outer races, were fabricated from the MRC2001 material and baseline VIM-VAR M50. Full engine size MRC2001 demonstration bearings were also fabricated. Bearing rolling contact fatigue (RCF) life tests were conducted in Task VII. Task VIII was to evaluate the performance characteristics of the full-scale bearing in a rig at 16,000 rpm (1.76 million DN where $D = \text{bore diameter in millimeters} \times N = \text{rpm}$) and other conditions simulating actual engine operation, and the used endurance test bearings were to be subjected to corrosion tests in Task IX.

The Task VII endurance tests were terminated when the MRC2001 bearings demonstrated unexpected low endurance life (B_{10} life for the MRC2001 bearings was 75 hours versus 977 hours for M50). An investigation determined that the grinding practice used to fabricate the MRC2001 bearings, and the test facility oil filtration system were contributing factors to the MRC2001 low endurance life.

At the conclusion of the low endurance life investigation, the then current Phase II effort was redirected. The previously defined Phase II Tasks VII through IX were terminated and Tasks 421, and 422 were constituted.

In Task 421, the surviving 35-mm MRC2001 inner races, fabricated in Task 6, were reground and fitted with new M50 balls and outer races. New M50 baseline endurance bearings were also fabricated. Endurance tests were conducted in Task 422. The purpose of the endurance

tests was to demonstrate equivalent endurance life for the MRC2001 material versus state-of-the-art M50 material.

Prior to regrinding the MRC2001 inner races a grinding study was conducted by TRW Bearings Division to optimize the MRC2001 grinding practice. Comparable surface texture, surface finish, operating internal radial clearance, and raceway fits were maintained between the two endurance test bearing lots. In addition, the endurance test rig oil filtration system was modified to include 3.3 micron lubricant filtration.

As part of a separately funded program, 20 each RSP-565 bearings were fabricated and back-to-back endurance tested with the Task 421 M50 and MRC 2001 test bearings. The grinding practice optimized for the MRC 2001 inner races was used to grind the RSP 565 races.

A total of 100,127 endurance test hours were accumulated on 55 bearings, 20 each M50, 20 each RSP565 and 15 each MRC2001. The B_{10} lives, based on inner race endurance test results, were 1253 hours, 1968 hours, and 2211 hours for MRC2001, RSP565, and M50 respectively, based on Weibull analysis. A statistical evaluation of the MRC2001 and RSP565 Weibulls determined that the rolling contact fatigue life was equivalent to VIM-VAR M50 at the 95 percent confidence level with a minimum P value of 0.3 (where $(1 - P) \times 100$ percent is the lowest level of confidence for which Weibulls would be considered the same).

SECTION II

TECHNICAL DISCUSSION

1. BACKGROUND

Current engine bearings have proven to be reliable and durable, but are often rejected for further use and discarded upon engine overhaul inspection long before their durability limits have been reached. This is due to environmental effects which degrade the bearing condition. Corrosion has been found to be the major cause of this premature bearing rejection (References 1 and 2). The expense and increased bearing usage caused by these rejections is unacceptable due to escalating labor and material costs, and the increasing manufacturing lead time required to meet the higher overall bearing demand.

Current turbine engine bearings are made from AISI M50 steel. This material, originally developed as a tool steel, was selected for turbine engine bearing use because of its good rolling contact fatigue life and high hot hardness. In its current form, VIM-VAR M50 performs well, but is sensitive to corrosion. The corrosion problem can be addressed in two ways: development of corrosion resistant bearings, or development of corrosion inhibitors for lubrication systems and storage preservatives. Two investigations have addressed corrosion inhibitors for lubrication systems (References 3 and 4). The goal of the Improvement of Corrosion Resistance of Turbine Engine Bearings Program is to provide a bearing significantly more resistant to corrosion than M50 state-of-the-art bearings.

2. CORROSION INVESTIGATION

a. Technical Approach

Corrosion is the most significant cause of gas turbine engine bearing field service rejection. Bearings rejected for corrosion have not expended their theoretical fatigue life. This effective reduction in bearing life results in higher maintenance costs associated with the inspection, repair and premature replacement of bearings.

The purpose of the corrosion mechanism investigation was to determine:

- Requisite conditions for the corrosion of stored and service bearings
- Main sources of corrosion contaminants
- Predominant corrosion mechanism.

During the corrosion investigation, representative samples from bearings rejected from both storage and service environments for corrosion were studied. The rejected bearings were analyzed for the morphology of the corrosive attack and for the chemical species present in the corrosion products. Bearing preservatives and used engine oils were also analyzed for contaminants that might cause or accelerate corrosion of the various bearing materials.

The possibility of corrosion by galvanic attack was also explored. A galvanic cell could greatly increase the rate of corrosion. It consists of two dissimilar metals immersed in a conductive solution. To address this possibility, the galvanic potential of silver M50 and silver AISI 4340 couples in an aqueous sodium chloride solution were measured and the bearing environments were analyzed for reactive chemical species which readily dissociate in water solution.

Accelerated corrosion tests of bearing materials in contaminated oils were also conducted to support hypotheses generated during the investigation.

b. Analyses of Corroded Bearings

Representative storage and service corrosion-rejected turbine engine bearings from two advanced turbofan engine types in the current USAF inventory were selected as candidates for study. A wide sampling of bearings from storage was possible due to a related P&W study which was in process at the time of this investigation. Conversations with P&W field representatives and other knowledgeable personnel led to the conclusion that the field samples received, though few in number, are typical of the majority of field rejects for corrosion.

(1) Stored Bearings

Main and accessory bearings which were rejected from storage due to corrosion were analyzed for the morphology of the corrosive attack and chemical species present in corrosion products by scanning electron microscopy (SEM), X-ray emission spectroscopy (XES), microprobe, metallography (MET), and Auger electron spectroscopy (AES) methods. Bearings examined included the following:

<u>Bearing</u>	<u>Condition</u>	<u>Preservative</u>	<u>Type</u>
A	New	MIL-C-11796B	Mainshaft
B	New	MIL-C-11796B	Mainshaft
C	New	MIL-C-11796B	Mainshaft
D	Used	NA	Mainshaft
E	New	MIL-C-11796B	Accessory
F	New	MIL-C-11796B	Accessory
G	Used	MIL-C-15074C	Accessory
H	Used	MIL-C-15074C	Accessory

All of the above bearings were of identical construction in terms of materials; balls and races being composed of M50 steel with silver-plated AISI 4340 cages. Used bearings exhibited characteristics of both storage and service environments, and provided valuable information in establishing differences and similarities of corrosion morphology and mechanisms. They are discussed further in Section II.2.b(3).

Corrosive attack of the silver-plated cages (AISI 4340 steel) during storage was manifested as stains affecting relatively large areas and ranging from very light violet to dark black in color. The morphologies of the stains generally correspond to rolling element cage contact loci and thick-thin preservative contours shown in Figures 1 and 2.

Light and dark areas (staining) associated with the thick-thin preservative contours probably only reflect the varying quantities of reactive species being made available from the corresponding volume of preservative to the silver surface. Similar logic can be applied to the rolling element cage contact loci where a thicker meniscus of preservative is often formed.



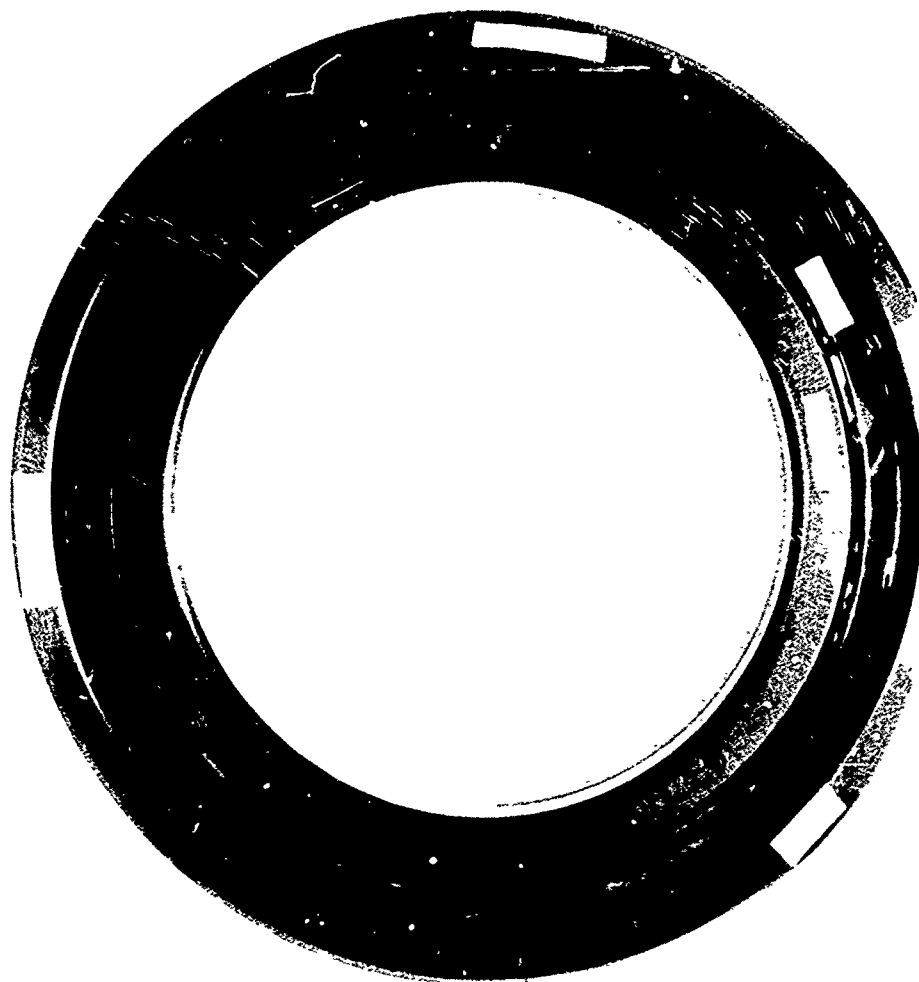
FE 352879

Figure 1 — Dark Staining of Silver-Plated AISI 4340 Cage at Rolling Element-Cage and Race-Cage Contact Loci (Main Shaft Bearing C, Stored in MIL-C-11796B Preservative)

The lightest stains observed exhibited a violet tint (Figure 3) where SEM and XES analyses (Figure 4) identified only silver and chlorine, suggesting a silver halide compound. Similar analyses of slightly darker stains, light brown in color, revealed sulfur and chlorine contamination. The light brown color is attributed to the presence of sulfur as silver sulfide shown in Figure 5. Still darker, almost black stains, sometimes with a purple tint, were characterized by much higher XES spectra for sulfur shown in Figures 6 and 7.

The AES analysis of medium to dark stains formed at ball-cage contact points (Figure 1) revealed sulfur to be the contaminant present in highest concentration, followed by chlorine, oxygen, carbon, iron, and possibly calcium. Ion sputtering of the stained surface rapidly reduced the intensities of all contaminants, restoring a bright, virtually contaminant free silver surface as shown in Figure 8. The high intensity for sulfur relative to oxygen and the rapidity with which the contaminants were removed by ion sputtering indicates the stain to be a thin film of silver sulfide, approximately 1000 to 2000 angstroms thick.

A comparison of the free energies of formation for oxides and sulfides at 25 °C reveals silver sulfide to be more stable than silver oxide (protective film on bright, unstained silver), a characteristic that becomes more pronounced at elevated temperatures. Thermodynamics, therefore, favors the substitution of sulfur for the oxygen in the protective silver oxide film if sulfur is available in a reactive state (not SO_4^{2-}). Reactive organic sulfur (as organic thiols, sulfides, disulfide, etc.) and inorganic sulfur (SO_3^{2-} , SO_2 , S^0 , H_2S , HS^- , S^{2-}), if water is present in solution with the preservative, are the primary corrodents responsible for staining and corrosion of the silver-plated components of stored bearings. Their presence in preservative media is probably due to the failure of refining techniques to remove these petroleum impurities down to the levels which would preclude visible staining of silver.



FE 352760

Figure 2. — Heavy, Dark Staining of Silver Plated AISI 4340 Cage Generally Conforming to Thick-Thin Preservative Boundary Morphology (Accessory Bearing, Similar to Accessory Bearing E Stored in MIL-C-11796B Preservative)

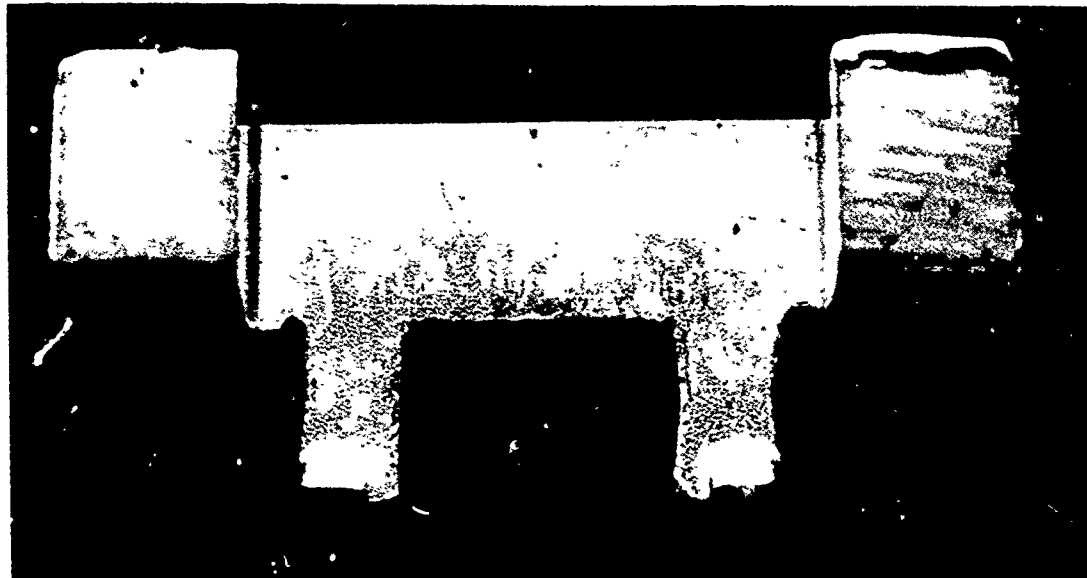
The next most important contaminant in terms of corrosive attack of stored silver-plated bearing components is chlorine, present in preservatives as chlorinated hydrocarbons, solvated chloride ions (if water is present in solution with the preservative), and chloride ions and compounds adsorbed to metal surfaces (improper handling).

Silver chloride, like silver sulfide, is more stable than the oxide at room temperature which favors the substitution of the chloride for the protective oxide and results in staining.

Sources of chloride contamination are believed to include standard petroleum contaminants (as chlorinated hydrocarbons and solvated chloride ions) and improper handling procedures such as failure to use gloves or protective film when handling bearings.

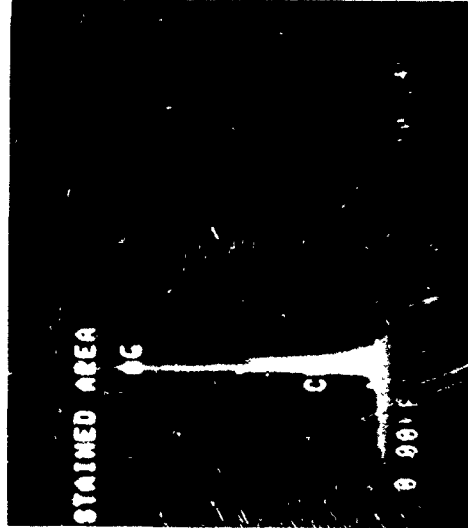
Carbon and calcium contaminants are probably due to entrapment of the saponified (agents: sodium, potassium, calcium, magnesium, lithium, and/or aluminum) hydrocarbon preservative in the corrosion product. Carbon might also have migrated the short distance from an adjacent corroding ball or roller. Similarly, the source of iron as a contaminant in the stained silver plate is probably other steel components of the bearing itself. The presence of oxygen only reflects the lack of complete conversion of the silver oxide film to sulfide and/or chloride.

Corrosive attack of stored M50 steel races and rolling elements was several orders of magnitude less severe in appearance than that of the associated silver-plated cages. However, even the lightest corrosive attack of the functional surfaces of the M50 steel components was considered much more serious than the plated cages due to the potential catastrophic failure of these parts from progressive spalling initiated at such sites. Corrosive attack of the M50 steel components varied from widespread, extremely light stains, barely discernible to the eye (and invisible to standard macrocameras, SEM, and XES), to very heavy, black or brown stains and pitting. The lightest stains generally conformed to the thick-thin preservative boundary morphology, and heavier stains to the race-rolling element contact morphology as shown in Figures 9 and 10.



FE 352814

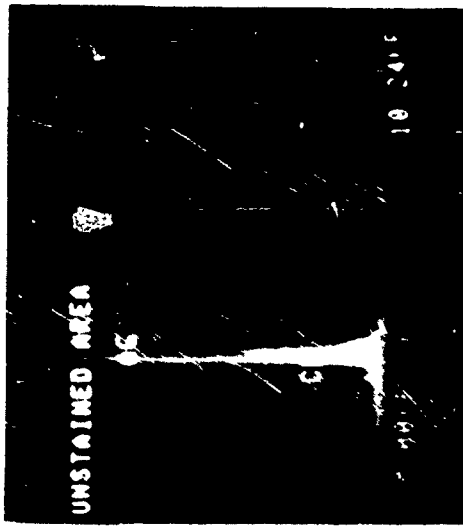
Figure 3. — Light Violet Staining of Silver-Plated AISI 4340 Cage at Rolling Element-Cage Contact Loci (Accessory Bearing F Stored in MIL-C-11796B Preservative)



XES Spectra of Stained Region F



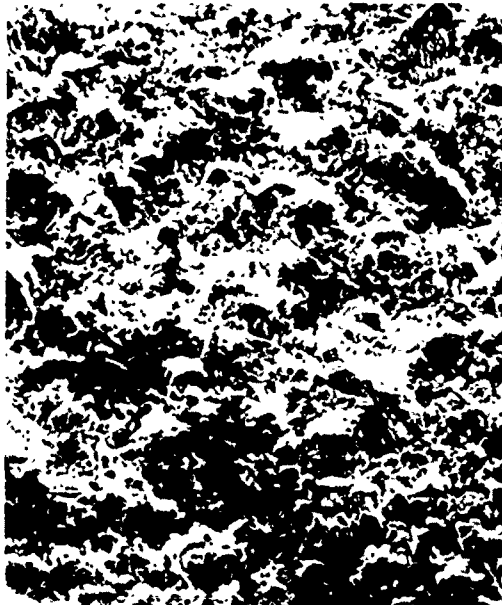
Mag 10X SEM Photomicrograph of Cage



XES Spectra of Unstained Region G

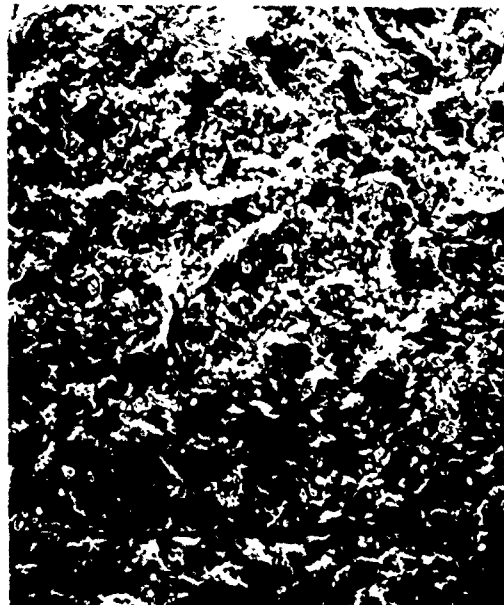
FD 230693

Figure 4. — SEM Photomicrograph and XES Spectra of Light Violet Stained Region (Area F) and Unstained Region (Area G) of Silver-Plated AISI 4340 Steel Cage Material (Accessory Bearing F)



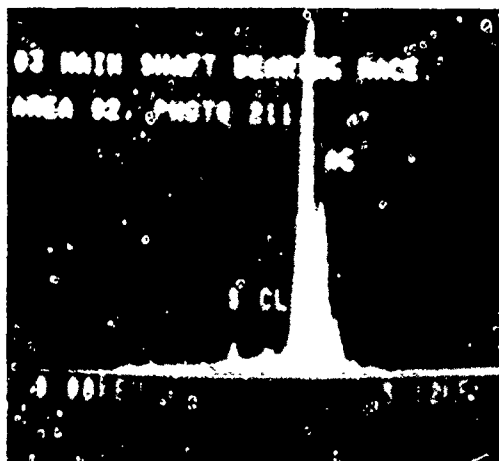
Mag 800X

Stained Silver Plate

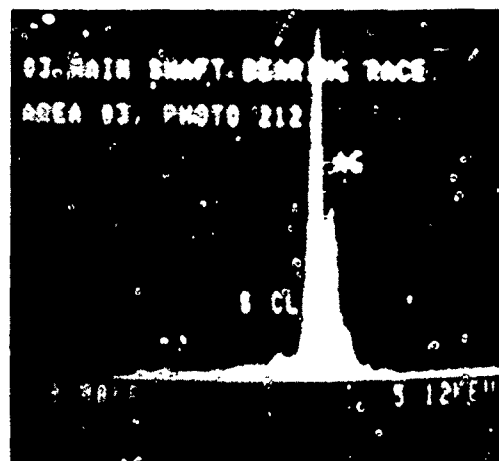


Mag 800X

Unstained Silver Plate



XES Spectra of Stained Silver Plate



XES Spectra of Unstained Silver Plate
Note Absence of S

FD 230894

Figure 5. — SEM Photomicrographs and XES Spectra of Light Brown Stained and Unstained Areas of Silver Plating on AISI 4340 Cage Material (Main Shaft Bearing C)



FE 352758

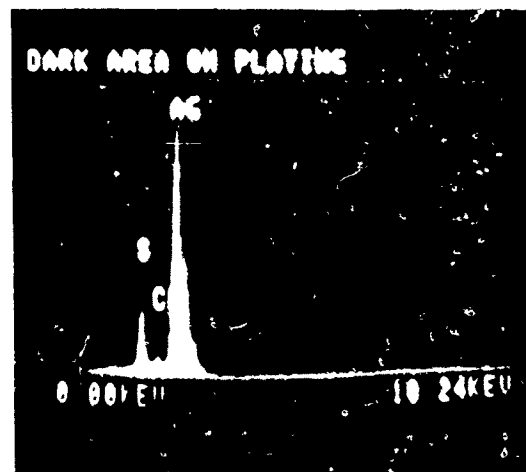
Figure 6. — Heavy, Dark Staining of Silver-Plated AISI 4340 Cage Analyzed Via SEM and XES in Figure 7 (Accessory Bearing E Stored in MIL-C-11796B Preservative)

The SEM and XES analyses of the lightest stains observed proved fruitless (Figures 11 and 12) due to the stronger background emissions of the base material through the stains (films less than 3000 angstroms composed of light elements) and noise. AES analysis of lightly stained areas of two separate mainshaft bearings (A, B) which had been protected in MIL-C-11796B, a cosmoline-type preservative revealed almost identical results. Both unstained as well as stained areas usually exhibited spectra for oxygen, carbon, calcium, sulfur, and chlorine with phosphorous, nitrogen, nickel, sodium, zinc, aluminum, and silicon observed in some locations as well. This layer of contaminants was rapidly removed by ion sputtering leaving a bright, clean base metal surface in unstained locations and a slightly thicker layer of oxygen containing material with some carbon and calcium in stained areas as shown in Figure 13. Total thickness of the layers in the stained regions was estimated to be less than 1000 angstroms.



Mag 10X

SEM Photomicrographic of Stained Cage



XES Spectra of Stained Region
Denoted at Left

FD 230895

Figure 7 — SEM Photomicrograph and XES Spectra of Dark Stain on Silver-Plated
AISI 4340 Cog Material (Accessory Bearing E)

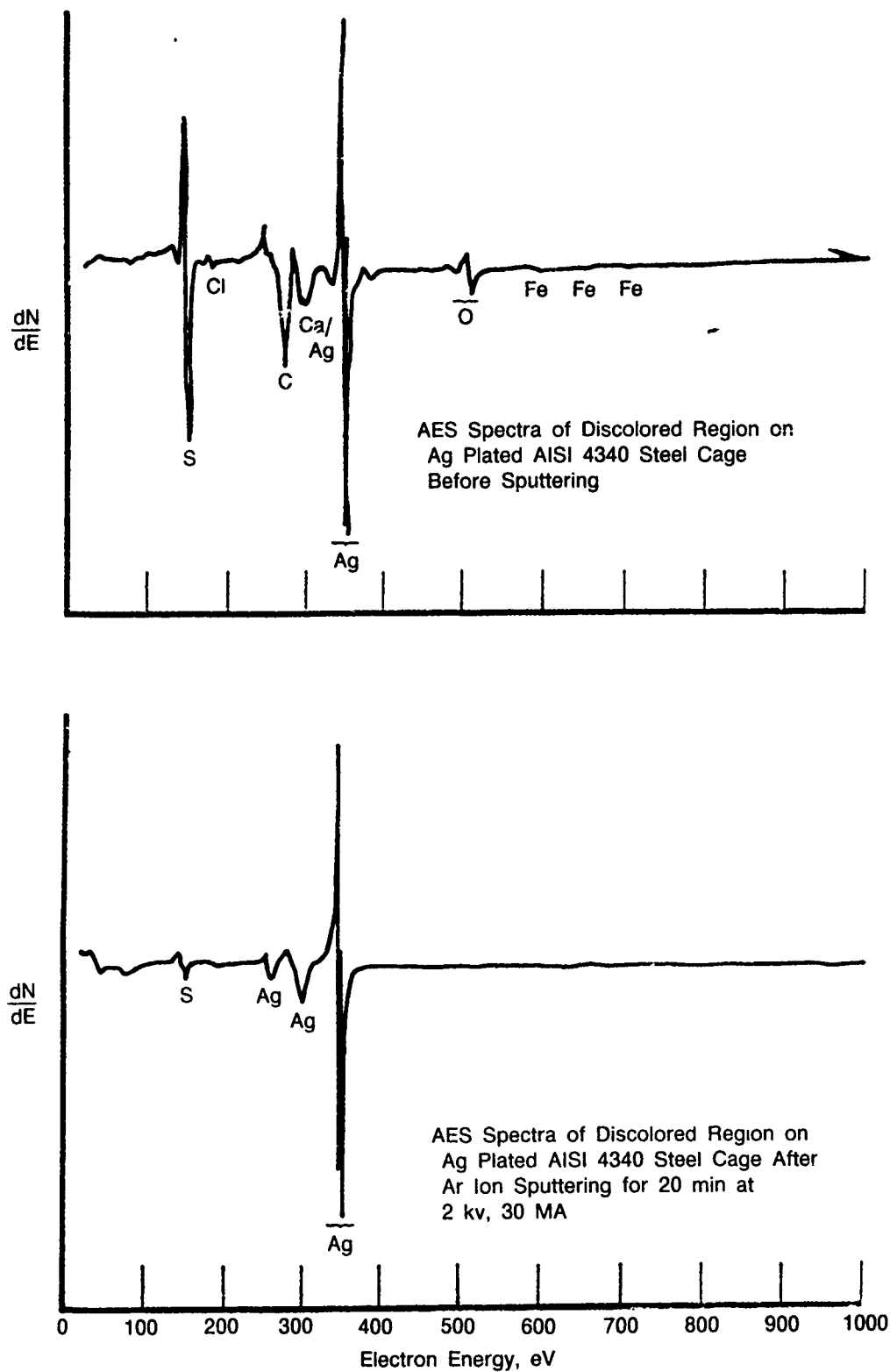
Of the contaminants encountered, chlorine, sulfur, and oxygen (present in corrosion products as chlorides, sulfides, and oxides) are considered the primary corrosidents.

Chlorides are believed to be present in the storage environment as chlorinated hydrocarbons, solvated chloride ions (if water is present in solution with preservative), and chloride ions or compounds adsorbed to metal surfaces. Sources of this contamination include standard petroleum impurities and incorrect handling techniques, shown in Figure 14.

Reactive sulfur (as organic thiols, sulfides, disulfides, etc., and if water is present, as SO_3^{-2} , SO_2 , S^0 , H_2S , HS^- , and S^{-2}) is undoubtedly a preservative contaminant, the result of residual petroleum impurities during manufacture or reduction of sulfate/sulfonate corrosion inhibiting additives.

Oxygen is available to the bearing surface via water dissolved in the preservative and by penetration of air through bearing packaging and preservatives.

Carbon may be present as a normal alloy constituent or due to entrapment of the hydrocarbon preservative in the corrosion product. Similarly, the alkali metals, lithium, sodium, and potassium plus magnesium, calcium, and possibly aluminum are frequent saponification components in greases and preservatives and may also be entrapped in the corrosion product. Corrosion inhibiting additives often contain barium, phosphorous, nitrogen, zinc, and sulfur as well. Nickel and silicon are the only two elements for which a plausible explanation cannot readily be found other than impurities in the preservative. Nickel is an alloying element of AISI 4340 steel and could find its way into the preservative if the integrity of the silver plate were breached. Silicon as a substituent of silicones may be present as a vendor proprietary ingredient or from contamination with ordinary sand (SiO_2).



FD 230887

Figure 8. — AES Spectra of Stained Region of Silver-Plated AISI 4340 Steel Cage Material From Main Shaft Bearing C, Stored in MIL-C-11796B Preservative, Showing Variation of Chemical Composition With Depth



FD 230896

Figure 9. — Thick-Thin Preservative Boundary Morphology as Seen Through Plastic Skin-Pack (Main Shaft Bearing N)

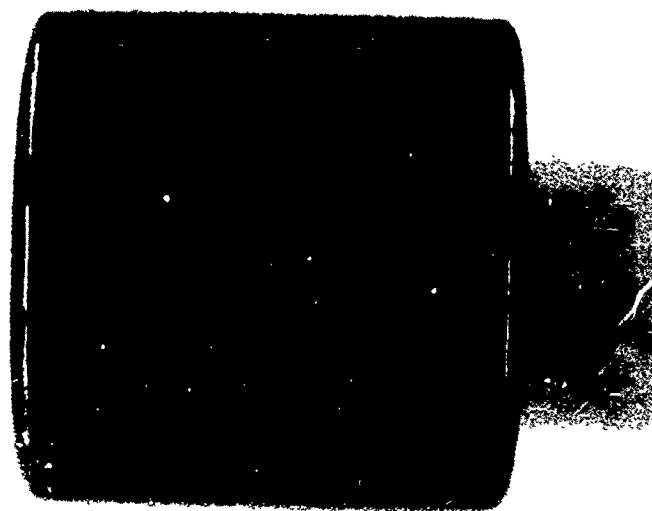
Corrosion corresponding to slightly darker stains of the M50 material (mainshaft bearing C) which was amenable to SEM and XES analyses, appeared to follow the grain boundary morphology (Figure 15). Localized stress concentration in the lattice structure along the grain boundary, i.e., grain boundary energy, rather than transgranular differences of chemistry, is believed to be a primary mechanism responsible for initiating autocatalytic pitting corrosion along grain boundaries in the storage environment.

The most severe corrosive attack of M50 components in storage was manifested by dark black stains usually conforming to rolling element-race contact morphologies (Figure 10). SEM photomicrographs of these stains revealed severe mudcracking and spalling of the mudcracked corrosion product. An XES analysis of these mudcracked regions typically revealed enrichment of the alloying elements (Cr, Mo, and V) relative to iron except in locations of spalling in which fresh unaffected surface was exposed (Figure 16). This is probably due to the leaching out of the more soluble iron corrosion products or, similarly, precipitation of less soluble alloying element corrosion products due to the decreasing concentration gradient of the attacking media from the bottom of a local pit to the surface of the alloy.

The mudcracking effect may represent the final stages of autocatalytic pitting corrosion initiated along grain boundaries (compare 200 \times photos in Figures 15 and 16) and producing a trench-shaped crevice (crack) which ultimately spalls, exposing fresh surface to further attack. This type of corrosion of functional bearing surfaces, if undetected, can result in failure.



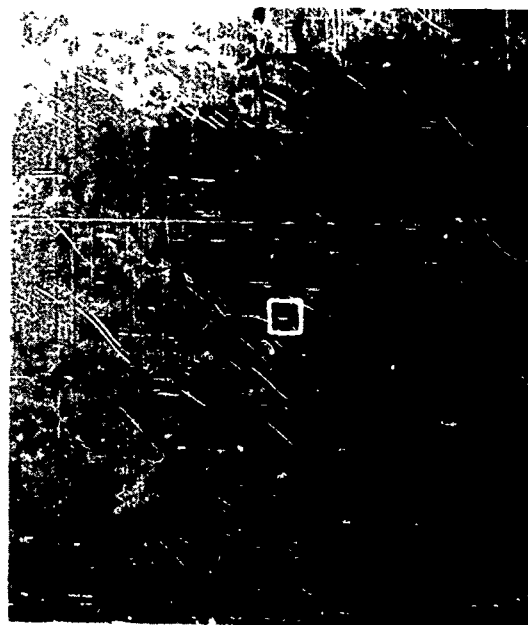
Mag 3 1/2X Corrosion of Inner Race



Mag 6X Corrosion of Roller

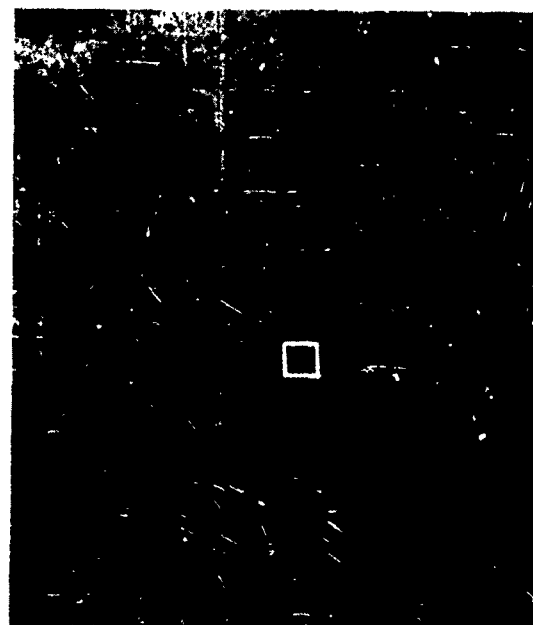
FD 230892

Figure 10 — Dark Black Stains of M50 Steel Conforming to Rolling Element/Race Contact Morphology (Accessory Bearing F)



Mag 100X

Stained Area



Mag 100X

Unstained Area

FD 230897

Figure 11 — SEM Photomicrographs of Stained and Unstained Areas of M50 Steel Race (Main Shaft Bearing B). Indicated Areas are Examined Further in Figure 12

Contaminants present in the corrosion products of the most severely attacked areas were essentially the same as those described previously, implying involvement of the same mechanism but under more severe conditions or for a longer duration.

(2) Service Bearings

Analyses of service-rejected bearings for corrosion were conducted on three main shaft bearings employing SEM, XES, microprobe, and MET techniques. Two of the bearings possessed similar material construction, i.e., M50 steel balls and races. Quantitative XES analysis of the third bearing, however, revealed the inner race base metal to have a composition similar to M50 steel, whereas the outer race and rollers exhibited spectra similar to that of BOWER 315, a high temperature carburizing grade, alloy steel. In each case, the cage material was the standard silver-plated AISI 4340 steel. The three bearings are listed below.

<u>Bearing</u>	<u>Condition</u>	<u>Oil</u>	<u>Type</u>	<u>Outer Race and Roller Material</u>
J	Used	MIL-L-7808J	Mainshaft	M50
K	Used	MIL-L-7808J	Mainshaft	Bower 315
L	Used	MIL-L-7808J	Mainshaft	M50

Other than minor physical damage, such as indenting, scratches, and wear, the silver-plated cages of the service-rejected bearings exhibited virtually no evidence of detrimental effects from the service environment, including corrosive attack of the silver plate.



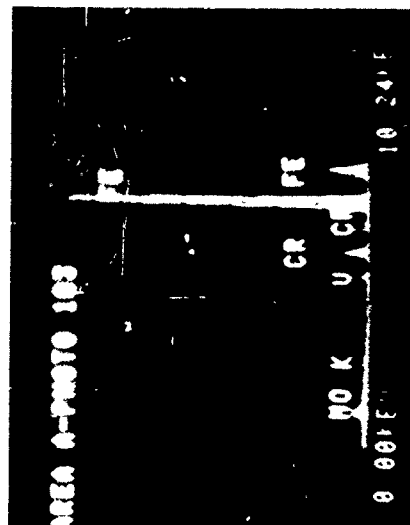
Mag 5000X

Stained Area

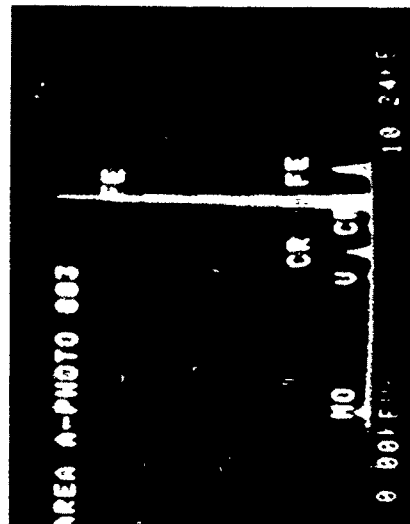


Mag 5000X

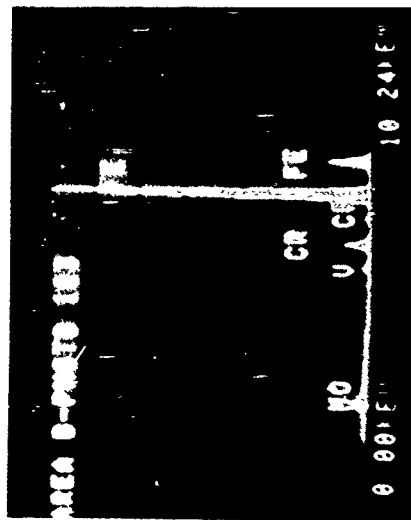
Unstained Area



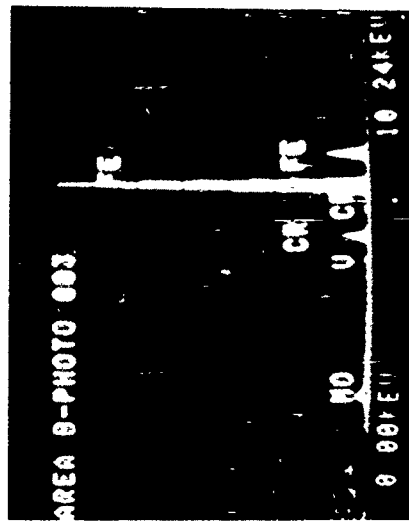
XES Spectra from Dark Region, Area A,
of Stained M-50 Steel Race



XES Spectra from Dark Region, Area A,
of Unstained M-50 Steel Race



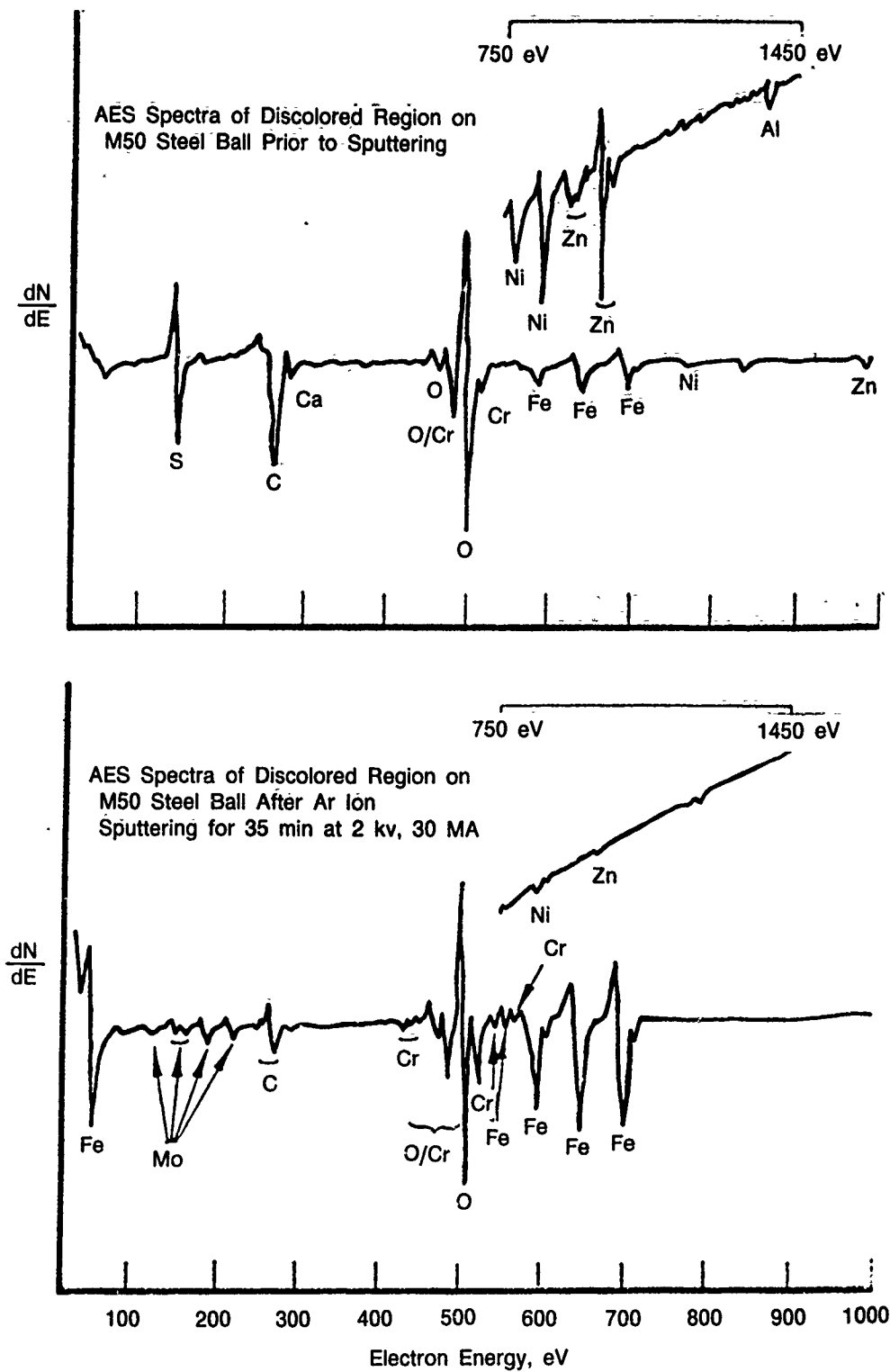
XES Spectra from Light Region, Area B,
of Stained M-50 Steel Race



XES Spectra from Light Region, Area B,
of Unstained M-50 Steel Race

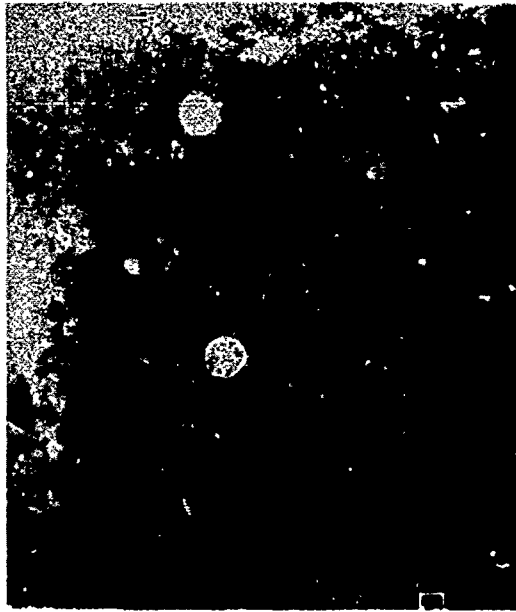
FD 230898

Figure 12. — SEM Photomicrographs of Indicated Area in Figure 11 and Photographs of XES Spectra From Light and Dark Areas, Emphasizing Difficulty of Analyzing Lightest Stains



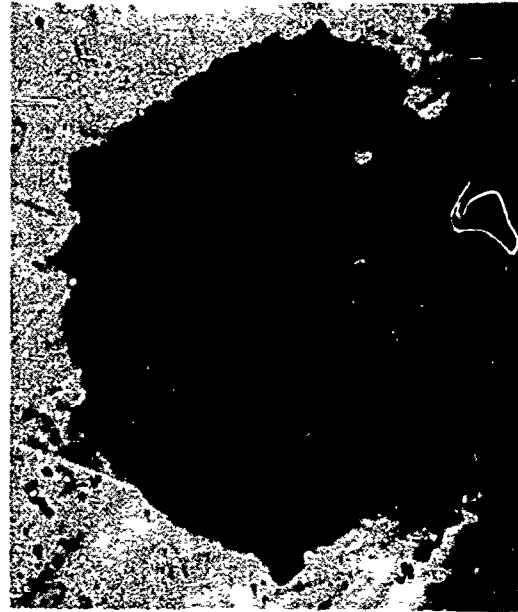
FD 230888

Figure 13. — AES Spectra of Stained Region of M50 Steel Ball From Main Shaft Bearing C, Stored in MIL-C-11796B Preservative, Showing Variation of Chemical Composition With Depth



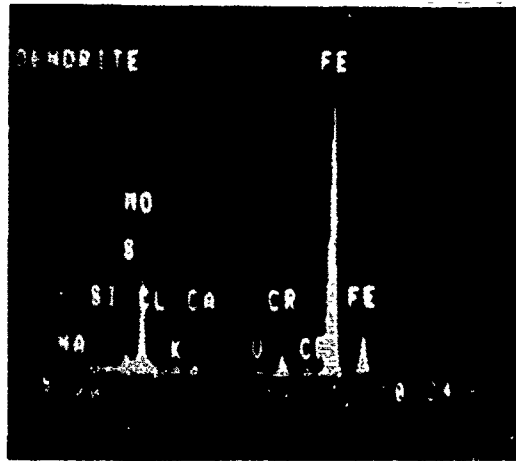
Mag 50x

Surface of Contaminated Ball
Indicated Area Enlarged at Right



Mag 2000x

Enlarged Area Showing Dendrite
Network of Chloride Crystals



XES Spectra of Dendrite



Chloride X-Ray Map of Above Area

FD 230899

Figure 14. — SEM Photomicrographs, XES Spectra, and Chlorine X-ray Map of Adsorbed Dendrites Comprised of Sodium, Potassium, and Calcium Chloride on an M50 Steel Ball (Result of Handling Ball Without Gloves or Suitable Protective Film on Hands)



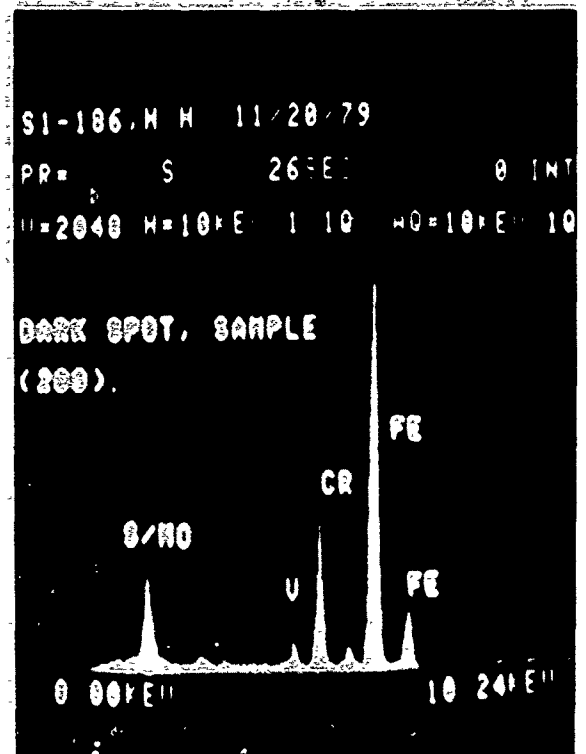
Mag 200X



Mag 500X

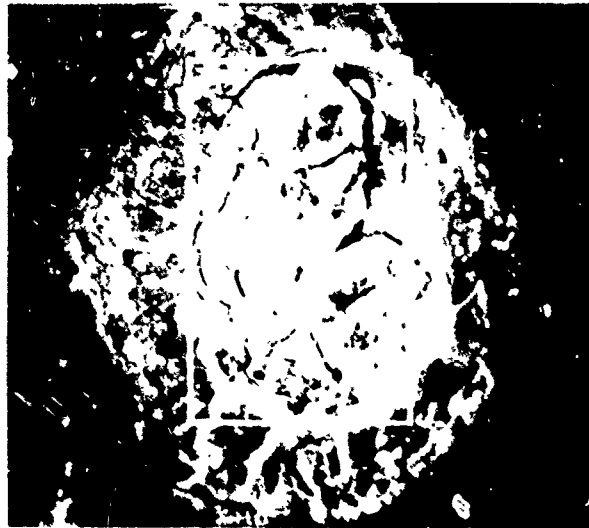


Mag 2000X

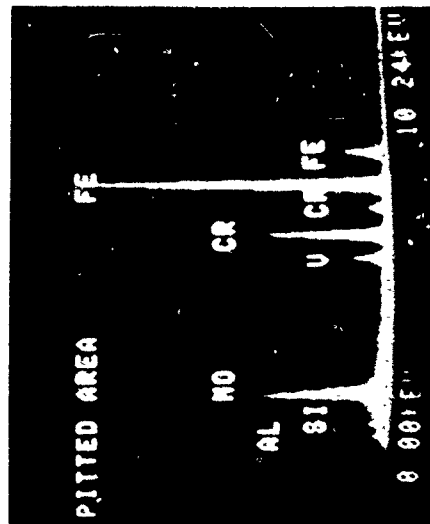


FD 230889

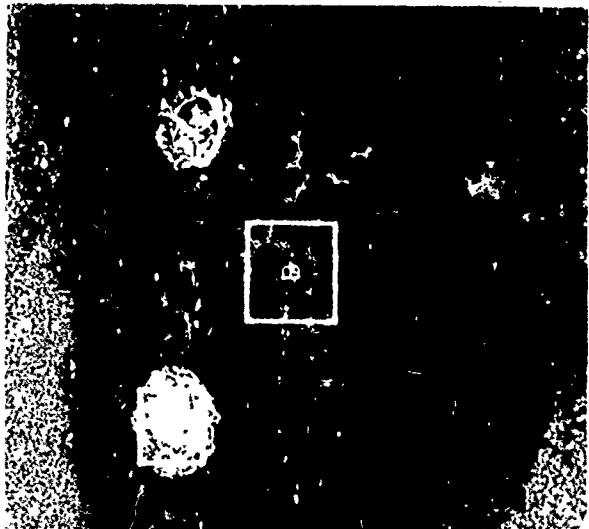
Figure 15. — SEM Photomicrographs and XES Spectra of Lightly Stained M50 Bearing Material (Main Shaft Bearing C) Which Appears to Follow the Grain Boundary Morphology (Arrows)



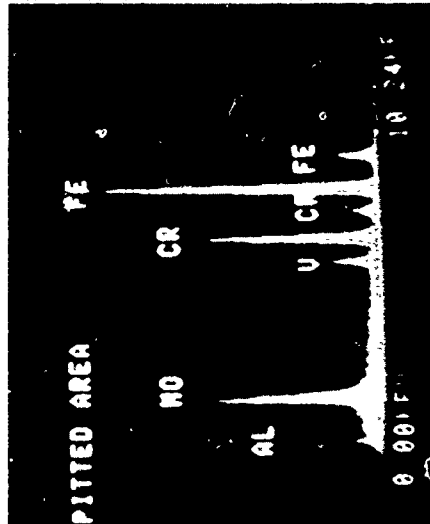
Mag 900X



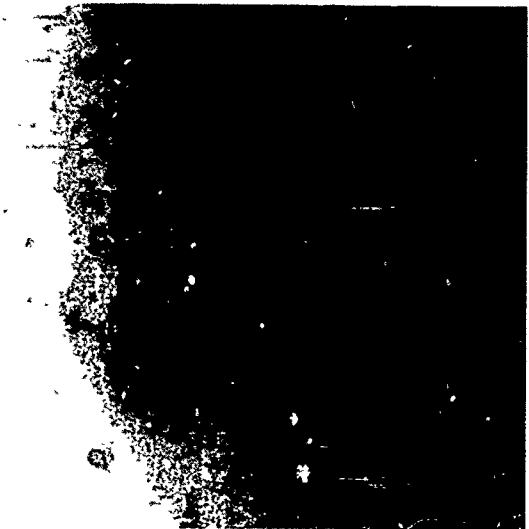
XES Spectra in Pit, Area A



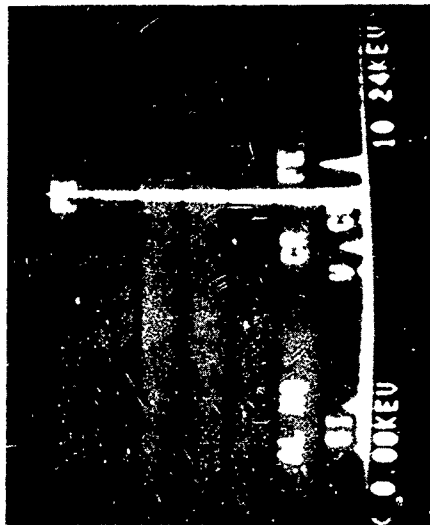
Mag 200X



XES Spectra in "Mudcracked" Region, Area B



Mag 20X

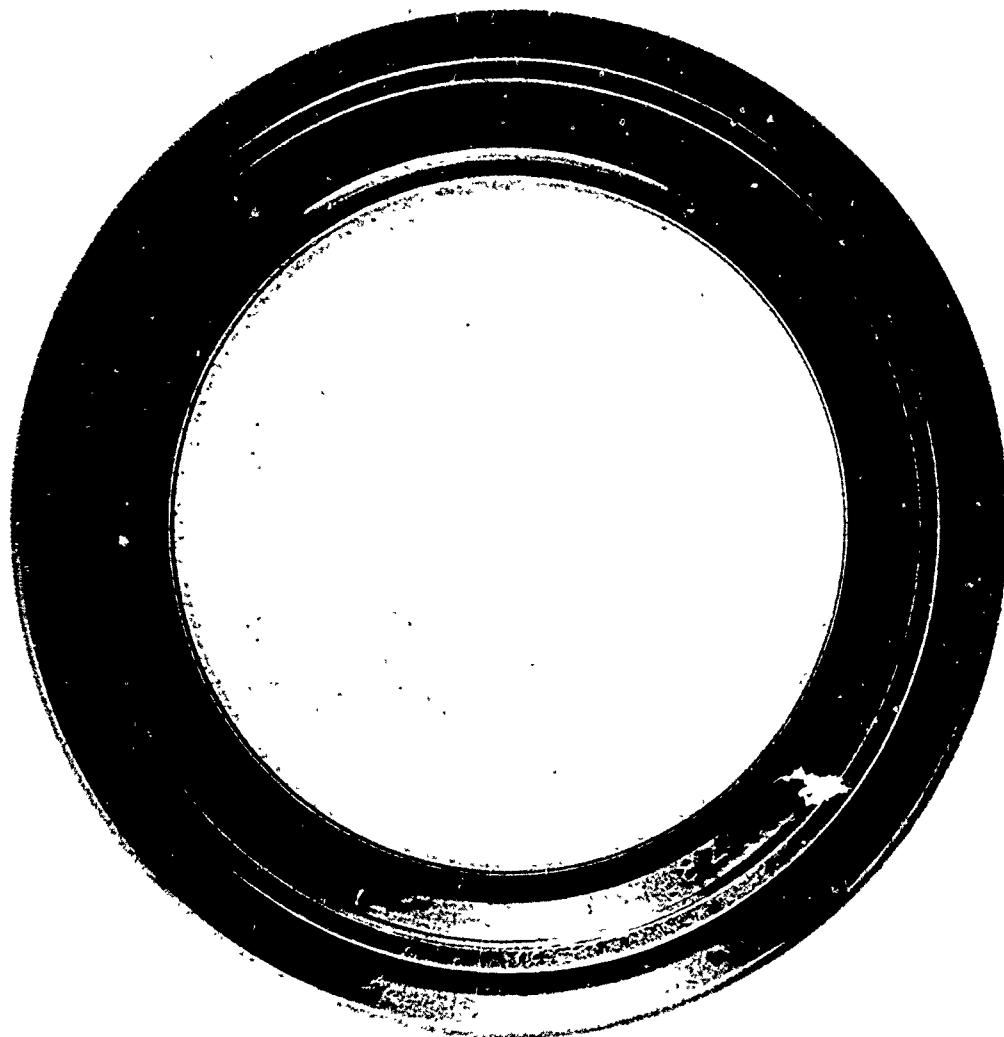


XES M-50 Base Metal Spectra

FD 230900

Figure 16. — SEM Photomicrographs and XES Spectra of Dark Black Stains on M50 Steel Roller Showing Apparent Enrichment of Alloying Elements (Cr, Mo, V) Relative to Iron in Location of Corrosive Attack

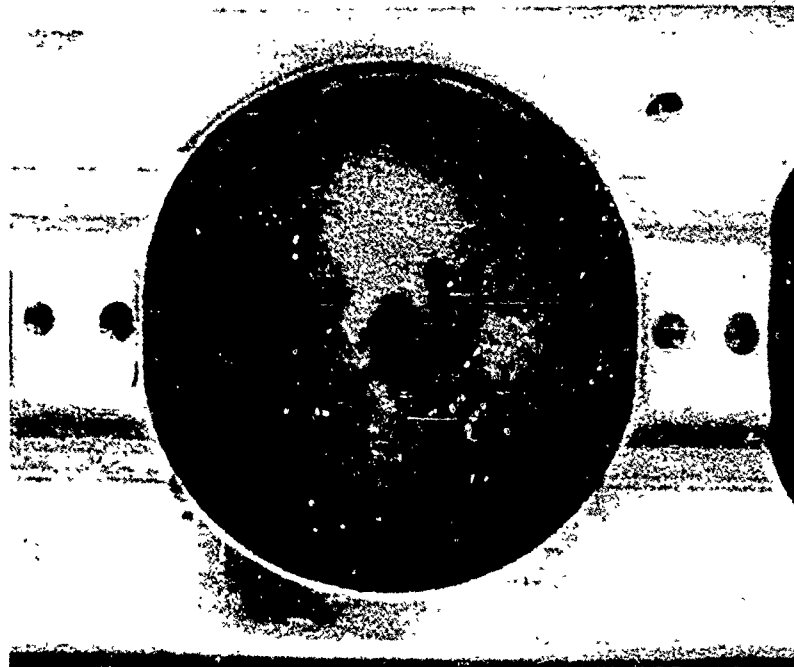
Corrosive attack of M50 and BOWER 315 steel rolling elements and races of service bearings was less evident than that of stored bearings (Figure 17). Staining of the alloy surface was not encountered. Rather, the morphology of the corrosive attack of these bearing components was confined to almost microscopic pitting which, though widespread, was difficult to see except at higher magnification (Figures 18 and 19).



FE 352762

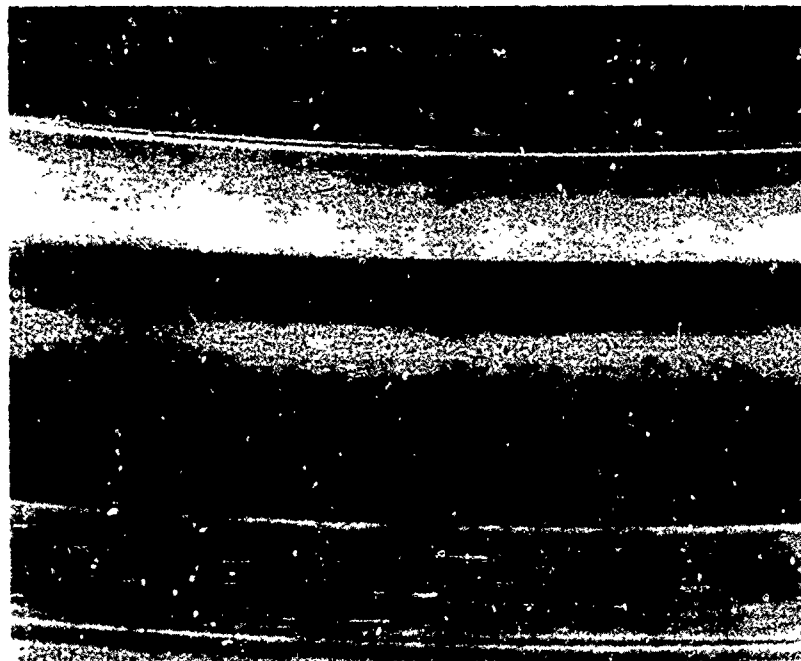
Figure 17. — Typical Appearance of Service-Rejected Bearing Does Not Suggest Corrosive Attack (Manshaft Bearing J, Service in MIL-L-7808J Oil)

On examination, the most common functional surface condition encountered with the rejected service bearings was indentation from contaminants entrained in the oil. Aluminum and silicon (probably as oxides) were the usual contaminants associated by SEM and XES analyses with indentations (Figure 20). The relatively higher proportion of aluminum encountered suggests contamination with residuals from some manufacturing process as opposed to common sand or dust contamination, since the silicon/aluminum ratio for most sands is greater than 1:1.



Mag 5X

Pitting Attack of Ball



Mag 3 3/4X

Pitting Attack of Outer Race

FD 230890

Figure 18. — Pitting Attack of Functional Surfaces of Service-Rejected Bearing (Main Shaft Bearing J, Service in MIL-L-7808 Oil)

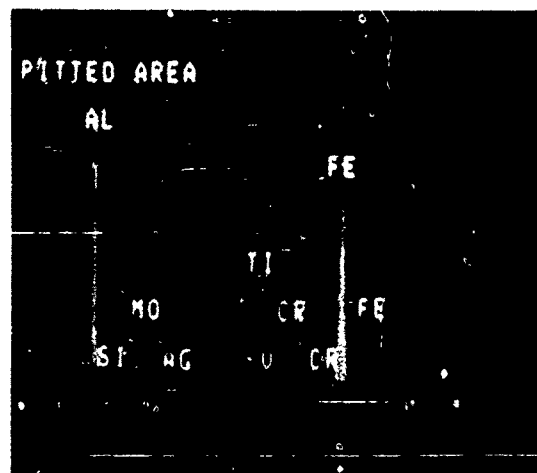


FE 352766

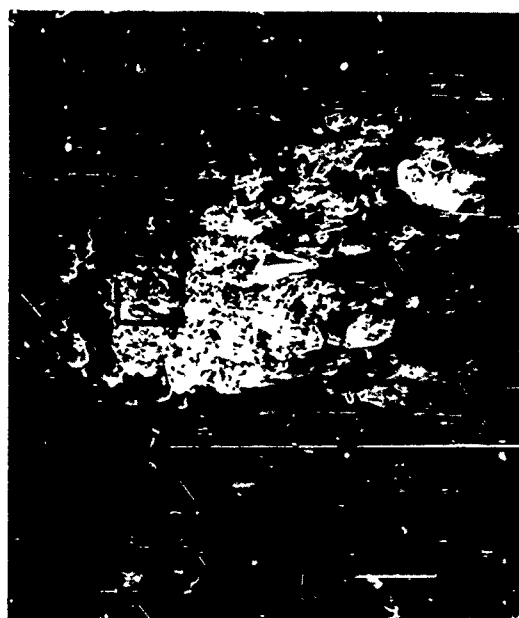
Figure 19 — Pitting Attack of Ball Previously Shown in Figure 18 (Mainshaft Bearing J, Service in MIL-L-7808J Oil)



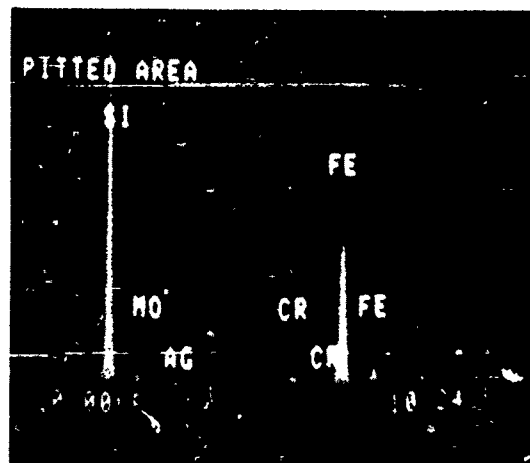
Mag 200X
Indented Region of M-50 Outer Race



XES Spectra of Dark Spot
Note High Aluminum Content



Mag 200X
Indented Region of M-50 Inner Race Showing
Corrosion - Like Pitting Morphology



XES Spectra of Indicated Area
Note High Silicon Content

FD 236801

Figure 20 -- SEM Photomicrographs and XES Spectra of Indentations (Main Shaft Bearing J)

Corrosion-like morphologies were found in the regions of some indentations (Figure 20). In the absence of static exposure to a relatively corrosive environment (storage with MIL-C-11796B), it is postulated that corrosive attack is more readily initiated at locations of physical damage rather than at grain boundaries. Small particles embedded in functional surfaces provide relatively large areas of closely conforming surfaces which are very amenable to capillary adsorption of water in the system (and attendant reactive species). Thus, an area of physical damage is easily converted to a site for autocatalytic pitting attack as seen in Figures 21 and 22.

The XES analysis revealed little evidence of contamination of the corrosion site by potentially reactive species. This is to be expected, since the corrosion damage was probably experienced during a period of extended idleness when water condensed from the air and/or oil in the bearing housing, and corrosion products (scale) along with contaminants were dislodged and entrained in the oil upon subsequent engine operation. In addition, bearings are generally inspected only after thorough cleaning. The rejected service bearings examined in this program had been packaged in MIL-L-8188 oil during shipment to prevent further corrosion, all of which served to mask the chemical species responsible for the corrosion.

The morphology of service-related corrosion sites was similar to that of the freshly exposed material of a recent spall in a region of storage-related corrosion. This suggests that after initiation, a similar mechanism of corrosion is at work in both the stored and service bearing, but the physical environment of the service bearing subsequently dislodges the corrosion product (scale).

(3) Stored, Service Bearings

Bearings which exhibited characteristics of both service and storage environments are described in this section.

Originally considered as corrosion-rejected bearings from service, examination via SEM, XES, and MET analyses revealed evidence of corrosive attack that could not be explained on the basis of previous experience with service bearings and the hypotheses generated as a result of this experience. A review of the history of these bearings showed that all had seen a *storage* environment of one sort or another.

All of the *used* bearings examined were of similar material construction, i.e., M50 steel balls and races with silver-plated AISI 4340 steel cages.

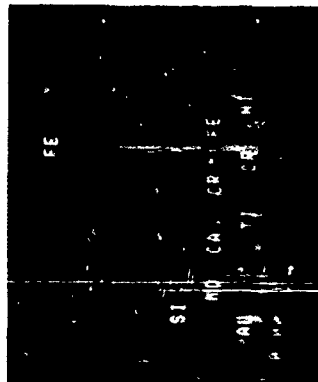
For the most part, corrosion of the silver-plated AISI 4340 steel resembled that of bearings subjected to a storage environment. The cage of one accessory bearing exhibited a feature not previously encountered with silver plating, i.e., mudcracking. Examination of thin, dark stains of the cage (Figure 23), via SEM and XES analyses, revealed heavy mudcracking and pitting (spalling) similar to that seen on M50 steel components subjected to a severe storage environment (Figure 24). Mudcracking of the silver plate is not serious in terms of precipitating a failure of the cage, but spalls can cause indenting of functional surfaces (Figure 25), and may progress to flaking of the silver plate.

Corrosive attack of the silver plate leading to the mudcracking morphology may be due to autocatalytic pitting attack involving formation of an aqueous sulfur concentration cell during storage. Incorrect handling (skin moisture) and saturation of the preservative due to condensation are the most probable sources of water contamination.

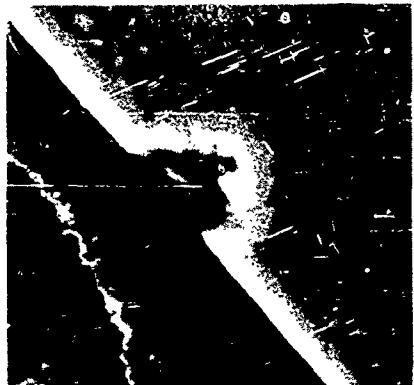


Mag 3000X

Embedded Particle in Functional Surface of Rolling Element

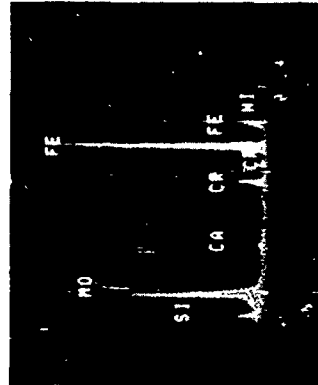


XES Spectra of Region With Embedded Particle Above



Mag 8000X

Embedded Particle in Functional Surface of Rolling Element

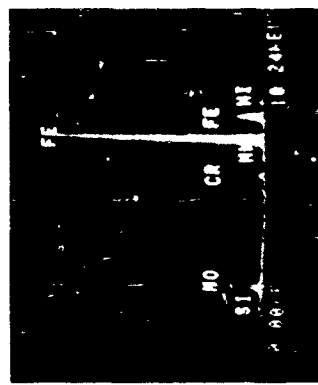


XES Spectra of Region With Embedded Particle Above Higher Concentration of Alloying Elements May be Due to Leaching Effect of Corrosive Attack



Mag 1500X

Site of Probable Autocatalytic Pitting Attack



XES Spectra of Bower 315 Base Material for Comparison

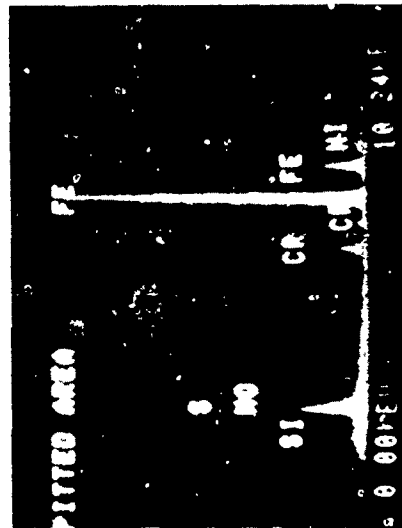
FO 234802
8956001
811 688

Figure 21 — SEM Photomicrographs and XES Spectra of Locations of Embedded Particles and Probable Autocatalytic Pitting Attack Initiated at Those Locations (Main Shaft Bearing K)

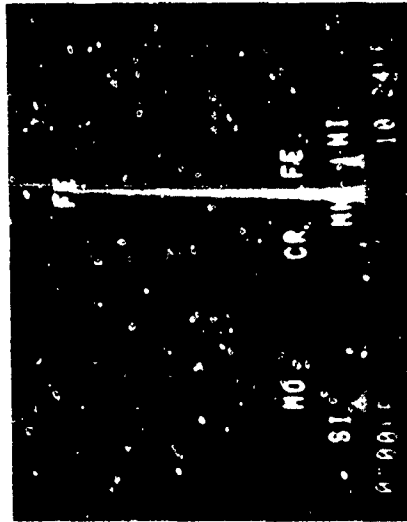


Pitting Attack of Functional
Surface of Roller

Mag 300X



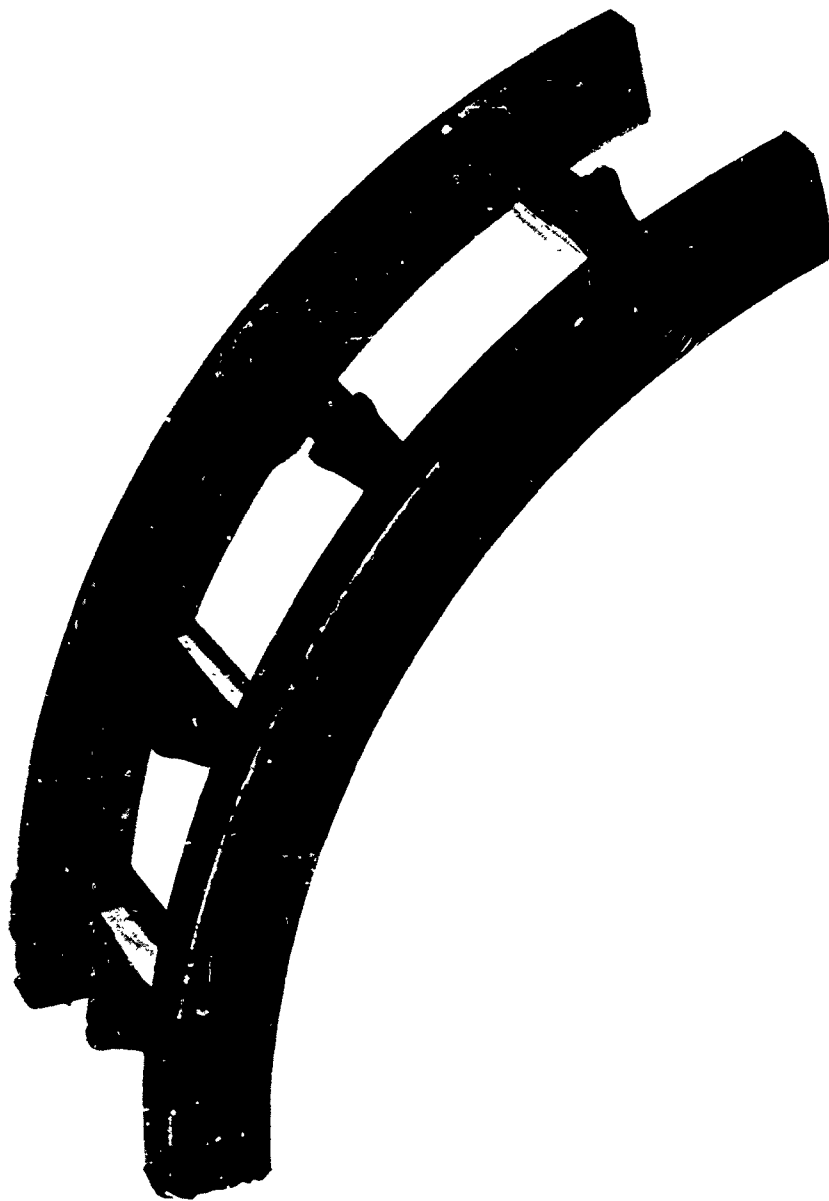
XES Spectra in Pitted Region Showing
Higher Concentration of Alloying
Elements Due to Leaching Effect



XES Spectra of Base
Material for Comparison

FD 2366803

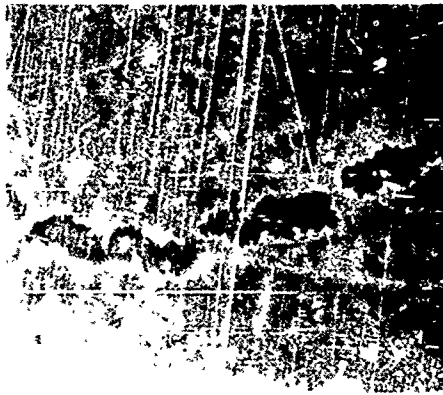
Figure 22. — SEM Photomicrographs and XES Spectra of Area of Pitting Attack (Main Shaft Bearing K)



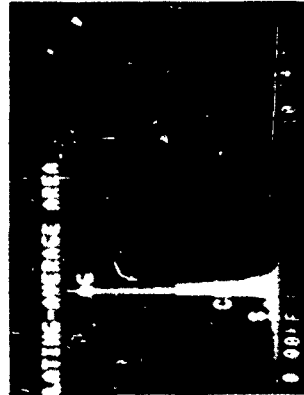
FE 352756

Figure 23 — Section of Cage Examined Via SEM, XES, and MET Analyses for Thin Dark Stains (Accessory Bearing H)

The SEM and XES analyses of M50 steel components revealed characteristics of both storage and service environments. They exhibited the mudcracking and spalling corrosion typical of storage, as well as the indenting, scratches, wear, and embedding of silicon and aluminum (oxide) particles representative of parts exposed to service (Figures 26 and 27).



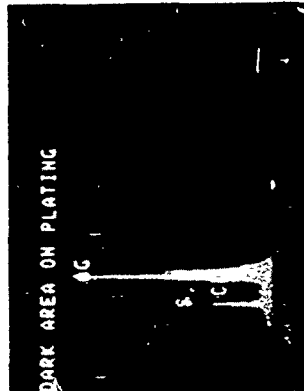
Mag 80X
Thin Dark Stain of Silver Plate



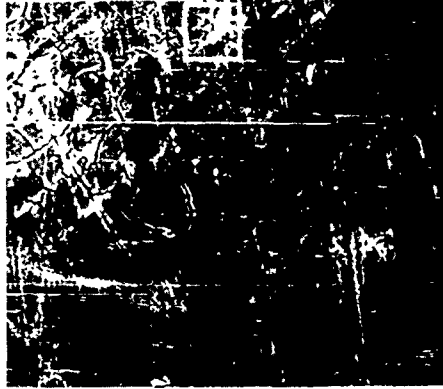
XES Spectra of Unstained Region



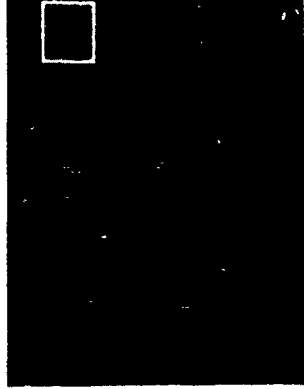
Mag 500X
Thin Dark Stain of Silver Plate Showing
"Mudcracked" Morphology



XES Spectra of Dark Stain Showing
High Sulfur Content



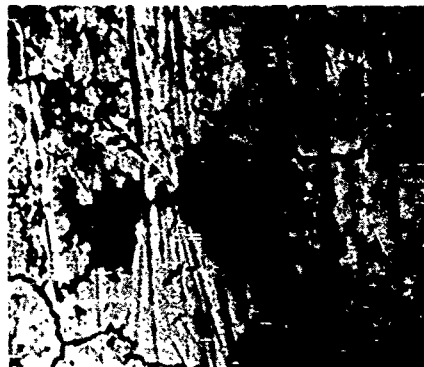
Mag 500X
Spall in "Mudcracked" Region



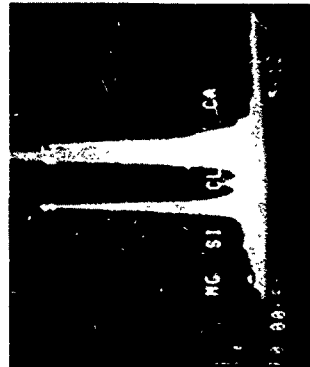
Sulfur X-ray Map of Location Shown Above.
Note Lower Intensity in Region of Spall

FD 235804

Figure 24. — SEM Photomicrographs and XES Spectra of Thin, Dark Stains of Silver-Plated AISI 4340 Steel Showing Mudcracked Morphology and High Sulfur Content in Locations of Corrosive Attack (Accessory Bearing H)



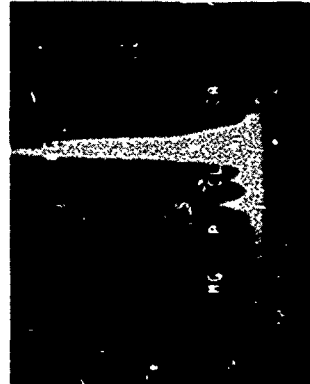
Mag 1000X
 "Mudcracked" Region Showing Location of
 Spalls of Silver/Silver Sulfide



XES Spectra of "Mudcracked" Area
 Adjacent to Pit



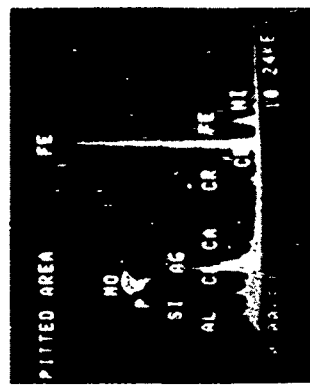
Mag 3000X
 Pit Formed as a Result of Spalling
 of Silver/Silver Sulfide



XES Spectra of Pit Bottom. Note Lower
 Sulfur Intensity (Less Attack) and High Silver
 Intensity (Plate Still Intact)



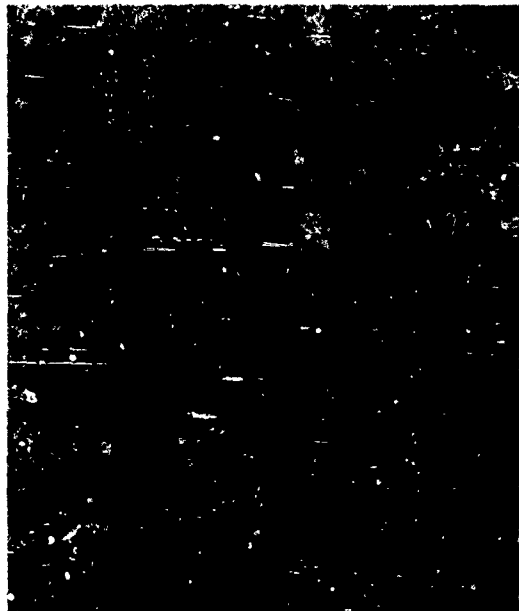
Example of Silver Particle Lodged in
 Extreme Right of Indentation or Incipient
 Spall of Function Surface of Outer Race



XES Spectra of Above Particle
 Note High Silver Intensity

FD 238605

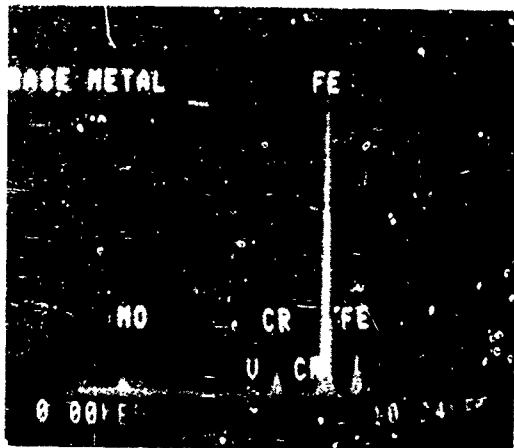
Figure 25. — SF Photomicrographs and XES Spectra of Mudcracked Morphology of Silver-Plated AISI 4340 Steel Cage and Damaged Bower 315 Steel Outer Race (Main Shaft Bearing K)



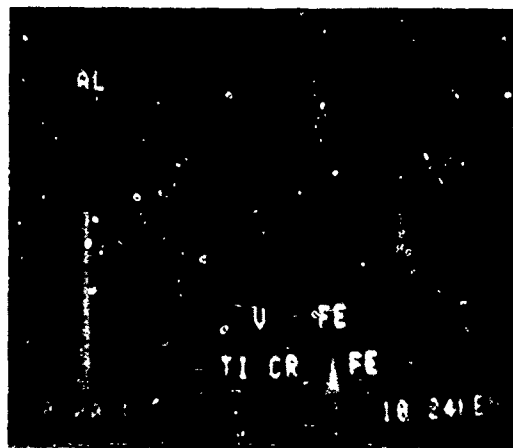
Mag 200X
 Roller Surface Showing Scratches, Indentations, and Mudcracking Corrosion



Mag 2000X
 Embedded Particle in Roller Surface



XES Spectra of M-50 Base Material



XES Spectra in Location of Embedded Particle Above

FD 236806

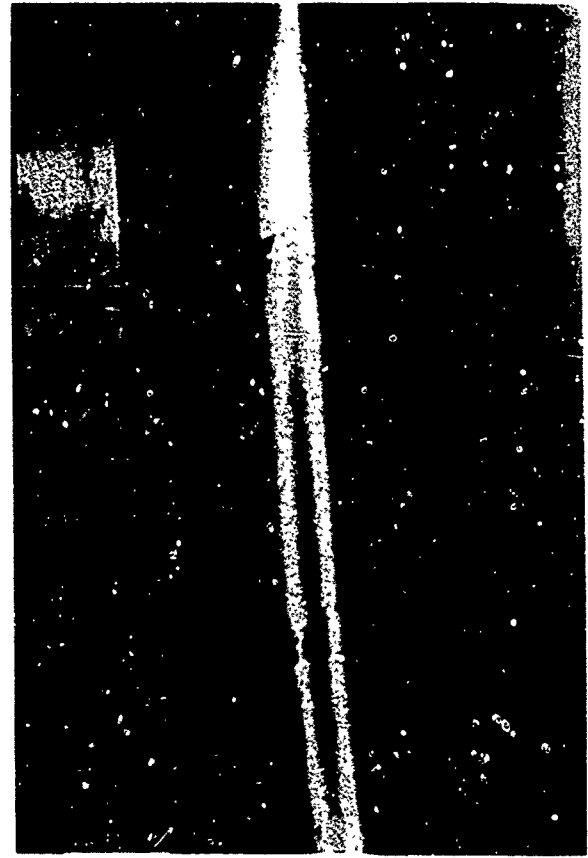
Figure 26 - SEM Photomicrographs and XES Spectra of M50 Steel Roller Exposed to Service and Storage Environments (Accessory Bearing G)

The history of mainshaft bearing D (Figure 28) is somewhat unique. The bearing, presumably protected with the short-term preservative oil MIL-C-15074C, was assembled into its housing and left in a horizontal position for approximately six months before the assembly was completed and the engine run. This was sufficient time for the oil to drain, concentrating a corrosive mixture of absorbed particles of dust, water, salt, etc., on the surface of a puddle in the outer race, leaving the remainder of the bearing exposed to the atmosphere (i.e., equivalent to storage without a preservative). Inspection of the bearing at teardown revealed extensive attack of the bearing including an elliptical zone of heavy pitting in the outer race. The pitting corresponded to the interface of the preservative puddle, air, and M50 steel.



Mag 1 1/2X

Typical Appearance of Corrosion
of Non-Functional Surfaces



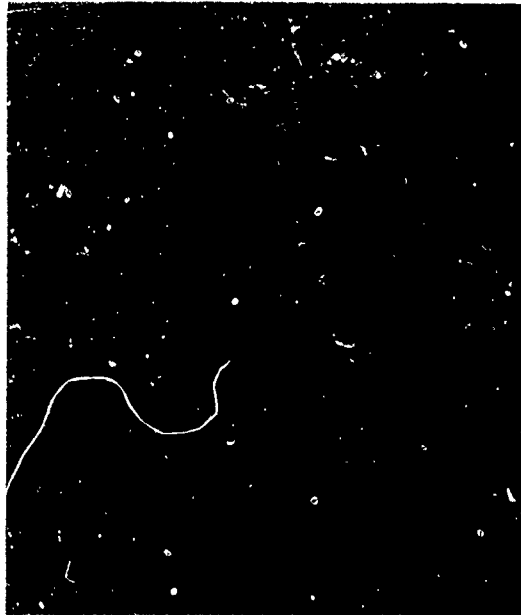
Mag 1 3/4X

Pitting Corrosion at Preservative-Atmosphere
Phase Boundary on Outer Race Surface

FD 230891

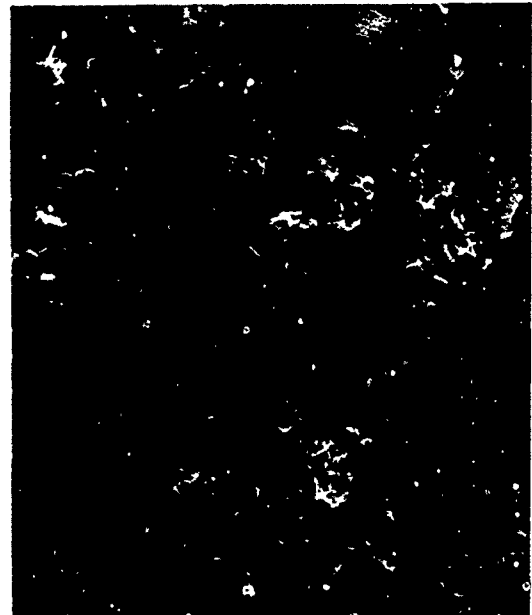
Figure 28. — Corrosion of Main Shaft Bearing D Inadequately Preserved During Delay in Assembly

Mudcracking (characteristic of a storage environment) was the predominant corrosion morphology in nonfunctional areas (Figure 29). Pitting (more typical of the service environment) was found on functional surfaces (Figure 30). These observations tend to verify the hypothesis that the corrosion mechanisms (not rates or modes of initiation) of stored and service bearings are similar (compare Figure 29 with Figure 16, and Figure 30 with Figures 20 and 22).



Mag 60X

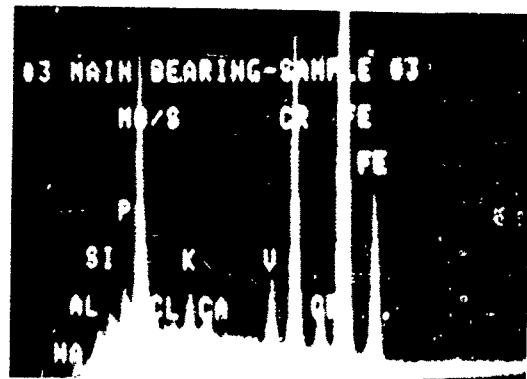
Corrosion of Non-Functional Surface



Mag 200X



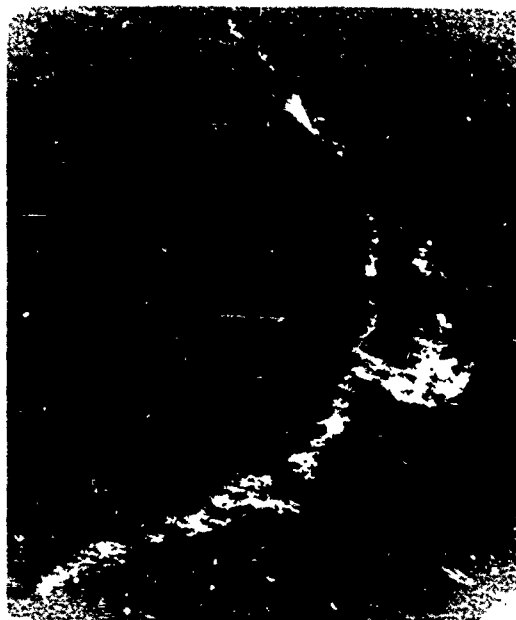
Mag 900X



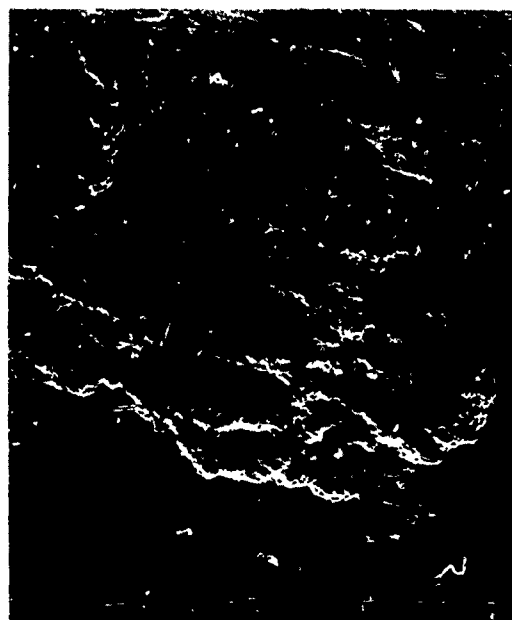
XES Spectra of Scale at Left

FD 236808

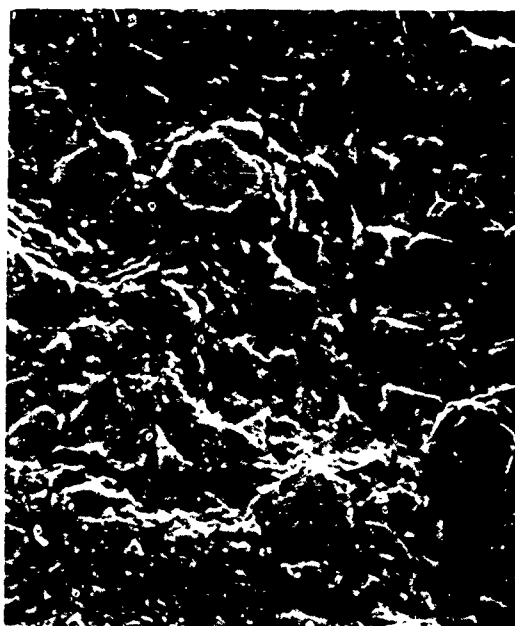
Figure 29 — SEM Photomicrographs and XES Spectra of Mudcracking Corrosion of M50 Steel, Nonfunctional Surfaces (Main Shaft Bearing D)



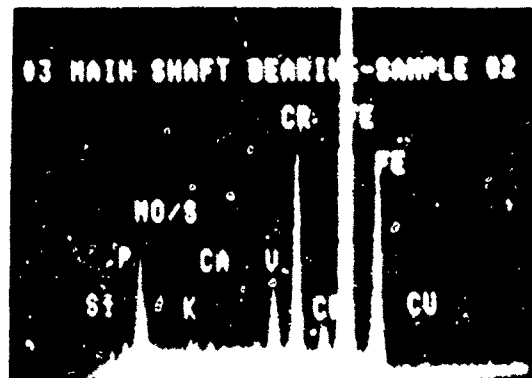
Mag 10X
Crescent Shaped Pitting Attack
Seen in Figure 28



Mag 60X



Mag 400X



XES Spectra in Location at Left

FD 236809

Figure 30 — SEM Photomicrographs and XES Spectra of Pitting Attack of M50 Steel Outer Race Along Phase Boundary (Main Shaft Bearing D)

c. Analyses of Preservatives and Used Engine Oils

To determine the source of reactive species responsible for the corrosion of bearings, short-term preservative MIL-C-15074C, long-term preservatives MIL-C-11796B and MIL-C-16173D, and engine oils MIL-L-7808 and MIL-L-23699 were analyzed.

(1) Storage Preservatives

Samples of storage preservative from three freshly opened mainshaft bearing *skin-packs* (MIL-C-11796B or MIL-C-16173D), as well as samples of a long-term preservative (MIL-C-11796B) and a short-term preservative (MIL-C-15074C) were analyzed for sulfur, chloride, and water content with the following results as listed in Table 1.

TABLE 1.
STORAGE PRESERVATIVES

<i>Preservative</i>	<i>Bearing</i>	<i>Sulfur</i> (%W)	<i>Chloride</i> (%W)	<i>Water</i> (%V)
MIL-C-11796B (or MIL-C-16173D)	M	0.56	≥ 0.0028	Not Run
MIL-C-11796B (or MIL-C-16173D)	N	0.20	≥ 0.0024	0.14
MIL-C-11796B (or MIL-C-16173D)	A	0.13	≥ 0.0023	0.12
MIL-C-11796B	N/A	0.30	≥ 0.0024	0.09
MIL-C-15074C	N/A	0.14	≥ 0.0013	0.06

%W = Percent weight
%V = Percent volume

Despite the lower mobility of ions and water in the viscous preservatives, these levels of contaminants are expected to cause corrosion of bearings based on tests conducted at P&W/GPD and the Navy (Reference 5), where corrosion of M50 steel was observed in oils contaminated with only 0.0003 percent weight (%W) chloride and 0.0600 percent weight water.

(2) Service Oils

Similar efforts were made with the service environment fluids (MIL-L-7808 and MIL-L-23699 oils). Requests to the Air Force and Navy have resulted in samples of used engine oils from a variety of sources (Table 2). Unfortunately, analyses of these oils for the reactive species sulfur, chloride, and water were frustrated because the levels of these contaminants were at or below the threshold of detectability of the available analytical instruments. Because of the lack of resolution, the data remain incomplete, except that the chloride concentration for all of the oils is probably less than 0.0005 percent weight (5 ppm).

TABLE 2.
HISTORY AND ANALYSIS OF USED ENGINE OILS

<i>Base</i>	<i>Total Engine Time (hours)</i>	<i>Oil Type</i>	<i>Time On Oil (hours)</i>	<i>Sulfur (%W)</i>	<i>Chloride (%W)</i>	<i>Water (%V)</i>
366TH TFW	—	7808	501	<0.002	<0.0005	0.01
Mt. Home AFB	—	7808	62	<0.002	<0.0005	0.02
	—	7808	311	<0.002	<0.0005	0.01
	—	7808	248	<0.002	<0.0005	0.01
Oceana NAS	1173	23699	—	<0.002	<0.0005	0.03
VA	1581	23699	190	<0.002	<0.0005	0.02
	902	23699	473	<0.002	<0.0005	0.03
	578	23699	578	<0.002	<0.0005	0.05
27th AGS	1734	7808	268	<0.002	<0.0005	0.025
Cannon AFB	951	7808	18	0.002	<0.0005	0.010
NM	964	7808	13	0.002	<0.0005	0.16
	1210	7808	263	<0.002	<0.0005	0.015
48th TFW	652	7808	652	0.003	Not Run	0.02
Lakenheath	493	7808	493	<0.002	Not Run	0.01
RAFB	489	7808	489	<0.002	Not Run	0.01
England	369	7808	117	<0.002	Not Run	0.01
20th TFW	—	7808	48	<0.002	Not Run	0.01
RAFB, Upper	—	7808	106	<0.002	Not Run	0.01
Heyford	—	7808	297	<0.002	Not Run	0.01
England	—	7808	498	<0.002	Not Run	0.01
48th TFW	2328	7808	562(TSO)	0.002	Not Run	0.12
Lakenheath	1052	7808	468(TSO)	<0.002	Not Run	0.10
RAFB	655	7808	—	<0.002	<0.0005	0.10
England	922	7808	649(TSO)	0.002	Not Run	0.03
P&W-GPD		7808	144	<0.001	Not Run	0.015
		7808	—	Not Run	Not Run	0.015 to 0.040

6710

Higher levels of water contamination were encountered, but no significant trend could be established. Results of oil analyses from water wash tests of a test engine indicate that condensation during cool down and changes of weather are more significant contributors to the water content of the oil than the water washing procedure (Table 3).

d. Galvanic Cell Tests

Galvanic corrosion could multiply the rate of attack above that of crevice or pitting corrosion alone. With the use of dissimilar metals (silver plate vs M50 and AISI 4340 steel) in bearing construction, the confirmed presence of several potentially reactive chemical species that readily dissociate in water solution, and water contamination of preservatives and oils, all of the elements required for galvanic corrosion are present. In a bearing, a local galvanic cell could be formed by interposing between the steel components and the silver plate, condensation water in petroleum solution containing dissolved ions from the surrounding environment.

TABLE 3.
OIL ANALYSIS RESULTS AFTER ENGINE WATER WASHDOWN

Engine Test Conditions	Duration	Material Ingested	Rate of Ingestion	Percent Volume Water in Oil	
				Before	After
Idle	5 hr	Water	10 gal/min	0.015	0.03
Idle	10 min	Water + B&B 3100*	2.5 gal/min	0.04	0.02
Windmill	2 min	Water + B&B 3100	2.5 gal/min	0.02	0.02
Static	Overnight	—	—	0.02	0.04

*B&E 3100 — Concentrated liquid compound for cleaning gas paths in turbine engines (FS N 6850-181-7547).

6-7 M'

To measure the galvanic potential of the silver-M50 and silver-AISI 4340 couples, samples of M50 and AISI 4340 steels were placed one at a time in a 3 percent weight sodium chloride solution coupled across a high impedance, high resolution voltmeter to a silver electrode also immersed in the salt solution. The potential generated for the M50 silver couple rose rapidly to approximately -0.23 vdc then slowed, and finally stabilized around -0.550 ± 0.015 vdc after 45 minutes. A similar performance of the AISI 4340-silver couple was recorded with a final reading of -0.575 ± 0.010 vdc.

Thus, the possibility for galvanic corrosion between the steel components and the silver-plating of bearings was confirmed.

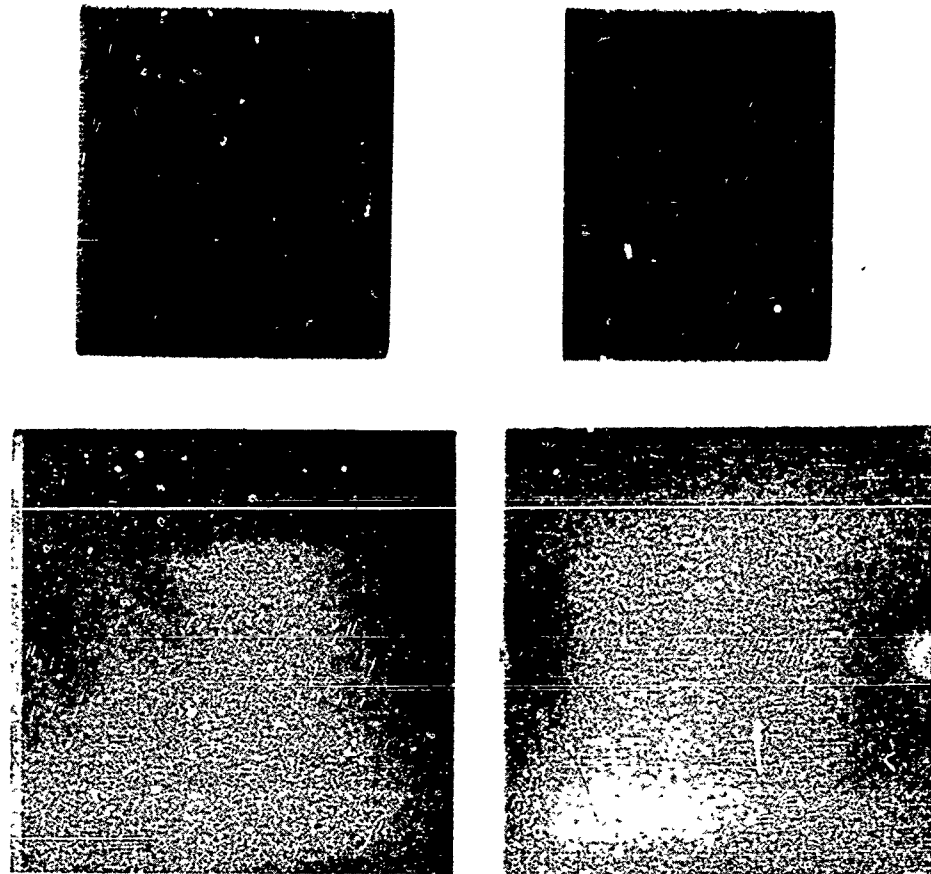
e. Accelerated Corrosion Tests

Tests were conducted to evaluate the effects of various concentrations of sulfur and chloride ions in oil on M50 steel and silver-plated coupons.

Elemental sulfur along with several short chain organic mercaptan compounds dissolved in a neutral medium (water saturated mineral oil) were evaluated in simple qualitative tests for corrosive attack (staining) of silver-plated coupons. Water-saturated mineral oil mixtures evaluated included: sulfur, sulfur dissolved in carbon disulfide, carbon disulfide (control), sulfur dissolved in carbon tetrachloride, carbon tetrachloride (control), thioacetamide, sulfanilic acid, ethanethiol, 2-mercaptoethanol, benzenethiol, and thiophene. Of the mixtures tested, only those containing elemental sulfur and thioacetamide would stain silver plate within a 24-hour period at room temperature. The 2-mercaptoethanol had to be heated to 180°F before it would attack the silver during a similar interval.

Mixtures which produced relatively rapid attack of the silver plate, however, inevitably presented miscibility problems with oils. Therefore, tests were first conducted to evaluate the ability of MIL-C-15074C, MIL-L-7808J, and MIL-L-23699C oils to counteract the corrosive effects of saturation with water, chloride ions, and reactive sulfur. The oils were saturated with these contaminants by first emulsifying water, thioacetamide, and sodium chloride (to an equivalent of 0.1000 percent weight water, 0.0100 percent weight chloride, and 0.0100 percent weight sulfur), allowing time for equilibrium and phase separation, then decanting of the saturated oil over M50 steel/silver plated coupon pairs. Specimens exposed to the contaminated oils, along with controls, were then placed in an oven at 140°F for 24 hours. Results indicated MIL-L-23699C oil was superior followed by MIL-L-7808J then MIL-C-15074C (Figures 31 through 33). The silver-plated coupons exhibited stains ranging from very light (MIL-L-23699)

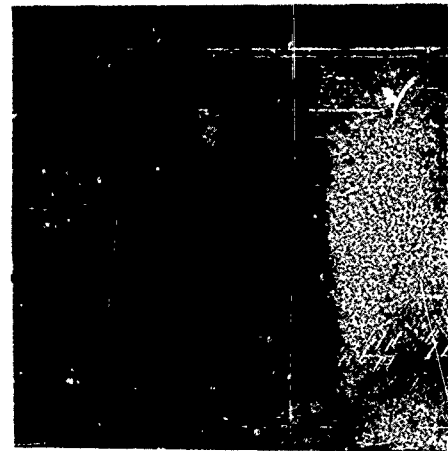
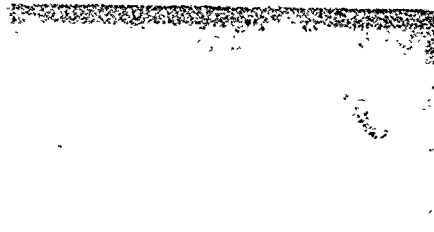
to very heavy (MIL-C-15074C). The M50 steel components were unaffected, indicating the need for longer duration tests.



FE 352627

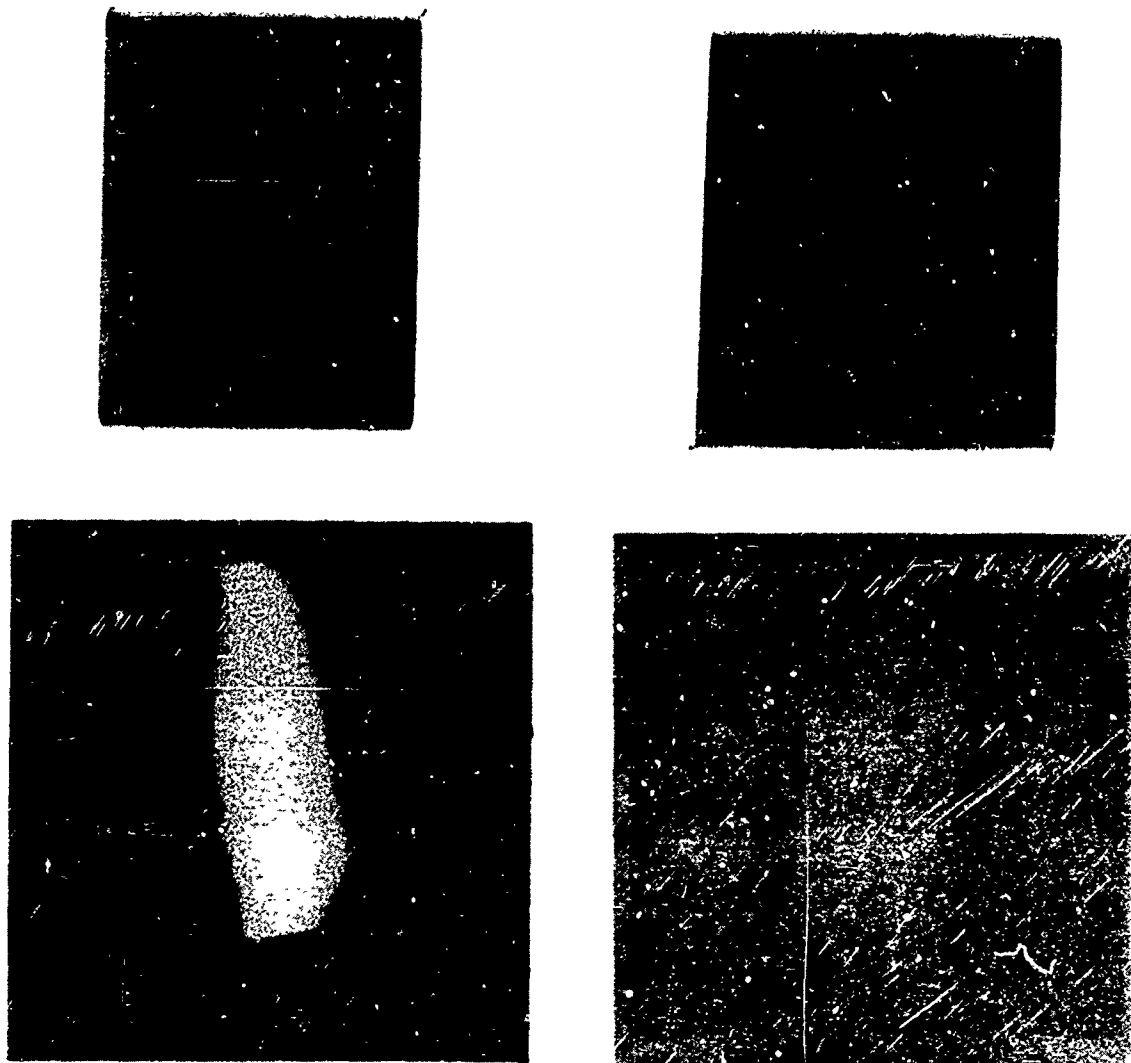
Figure 31. — Specimens (M50 Steel at Top; Silver-Plated Coupon at Bottom) Exposed to MIL-L-23699 Oil (Contaminated at Left, Control at Right) at 140°F for 24 Hours

The M50 steel and silver plated pairs were also tested by immersion in dry mineral oil solutions containing tritylthiol (triphenylmethyl mercaptan) at 0.0100, 0.0020, and 0.005 percent weight sulfur concentrations and solutions containing trityl chloride (chlorotriphenylmethane, triphenylmethyl chloride) at the same levels of chloride concentration. Samples were again placed in an oven at 140°F for 24 hours. Results indicated that the silver plate was the most susceptible material to attack by both chloride ions and reactive sulfur down to the lowest concentrations tested, with sulfur producing the heaviest stains. The M50 steel was unaffected by the reactive sulfur and all but the highest concentrations of chloride ions (Figures 34 through 39).



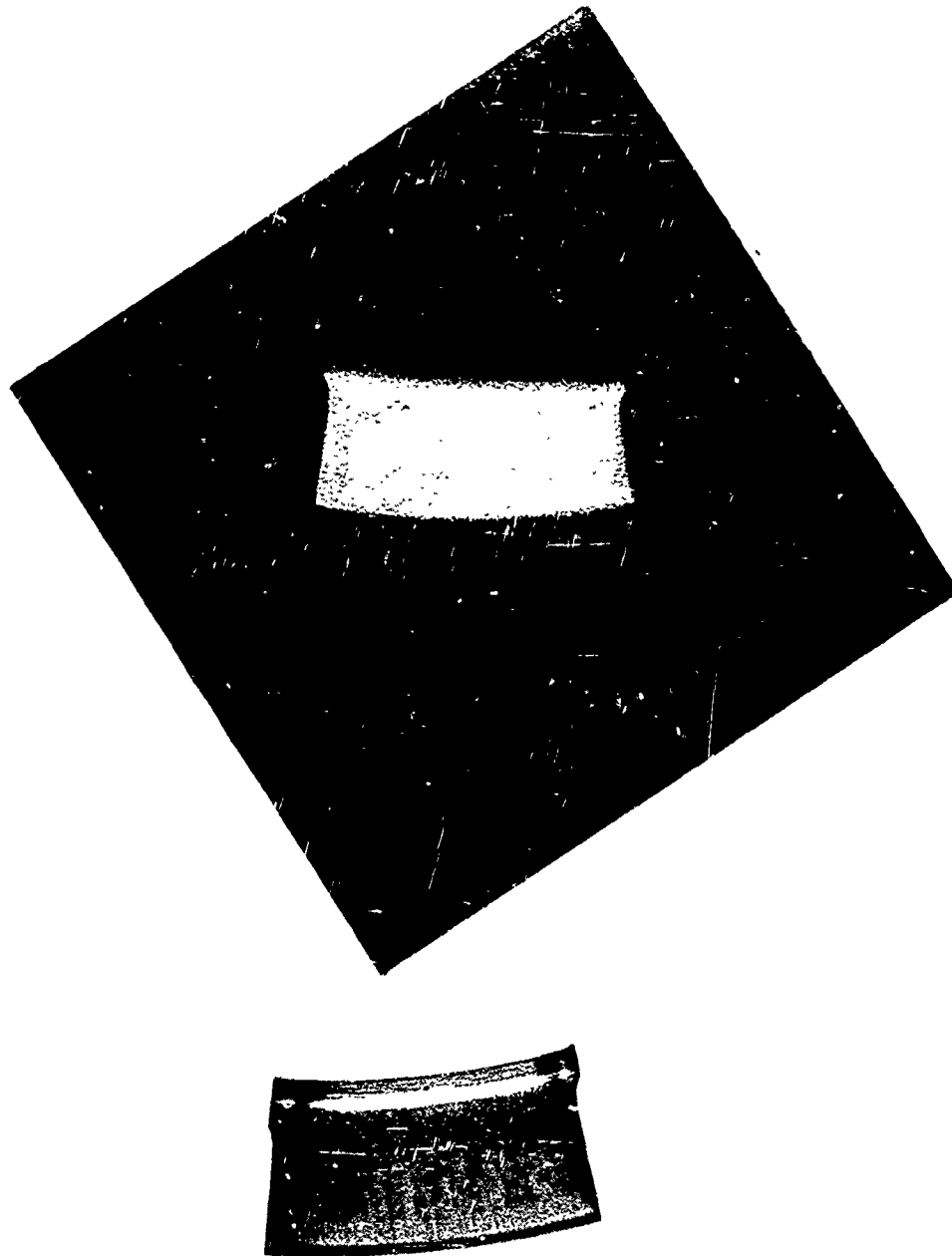
FE 352625

Figure 32. — Specimens (M50 Steel at Top, Silver-Plated Coupon at Bottom) Exposed to MIL-L-7808j Oil (Control at Left; Contaminated at Right) at 140°F for 24 Hours



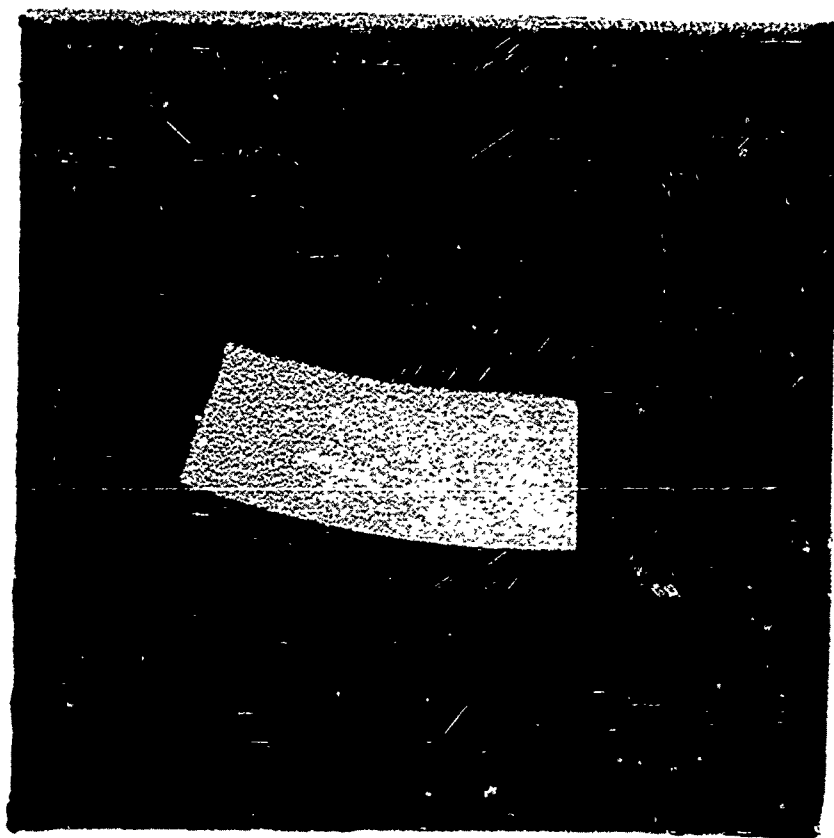
FE 352623

Figure 33 — Specimens (M50 Steel at Top, Silver-Plated Coupons at Bottom) Exposed to M.L-C-15074C Oil (Contaminated at Left; Control at Right) at 140°F for 24 Hours



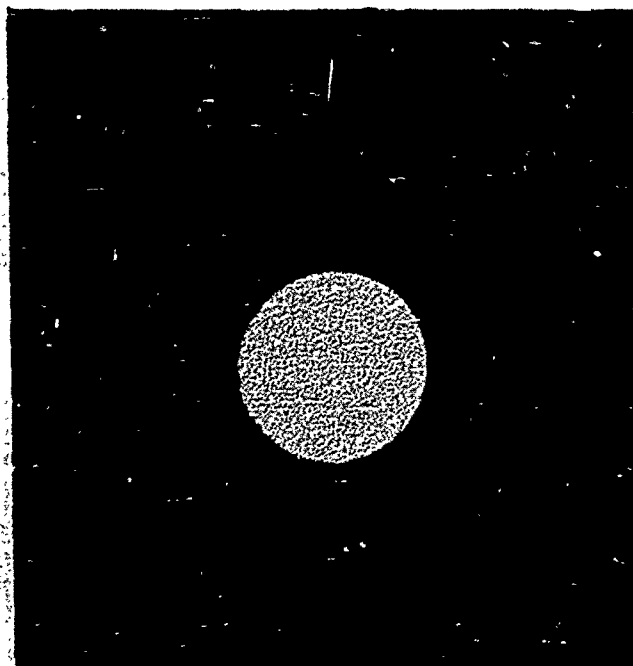
FE 352750

Figure 34 — Specimens (M50 Steel at Bottom, Silver-Plated Coupon at Top) Exposed to 0.0005 Percent Weight Sulfur (as Triethyl Thiob) in Mineral Oil at 140°F for 24 Hours



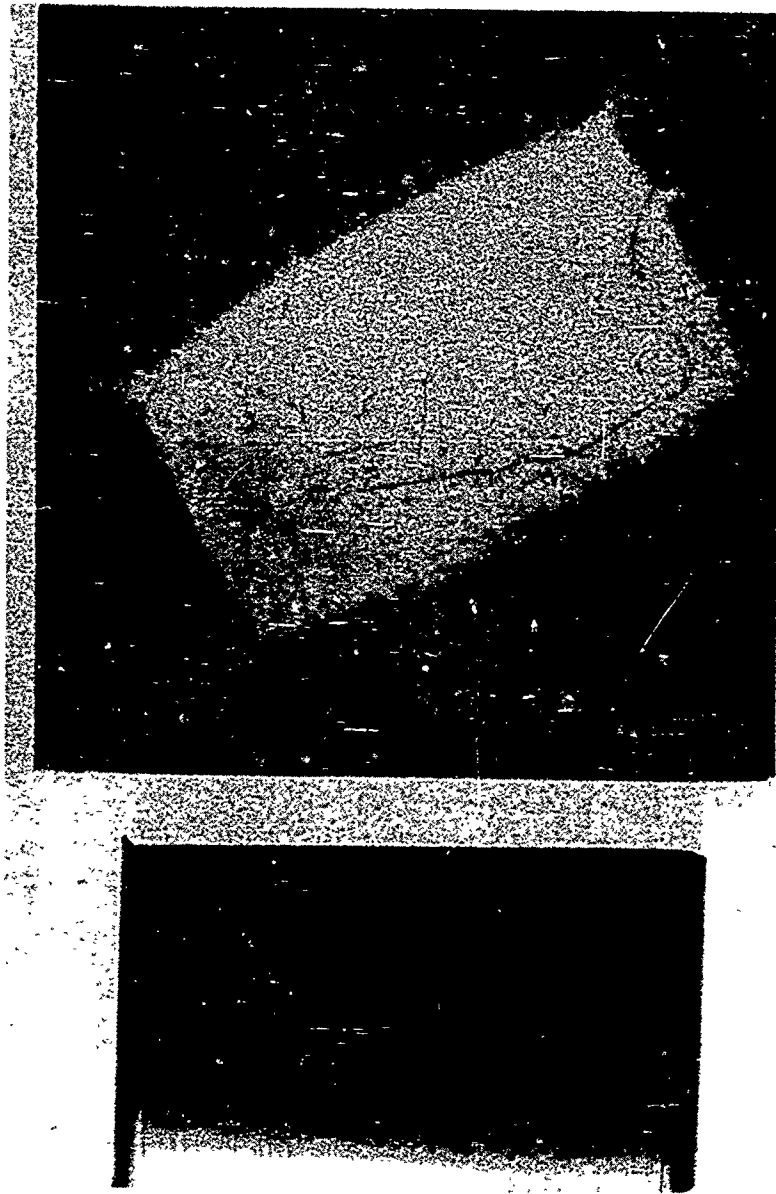
FE 352751

Figure 35. — Specimens (M50 Steel at Bottom, Silver-Plated Coupon at Top) Exposed to 0.0020 Percent Weight Sulfur (as Trityl Thiol) in Mineral Oil at 140°F for 24 Hours



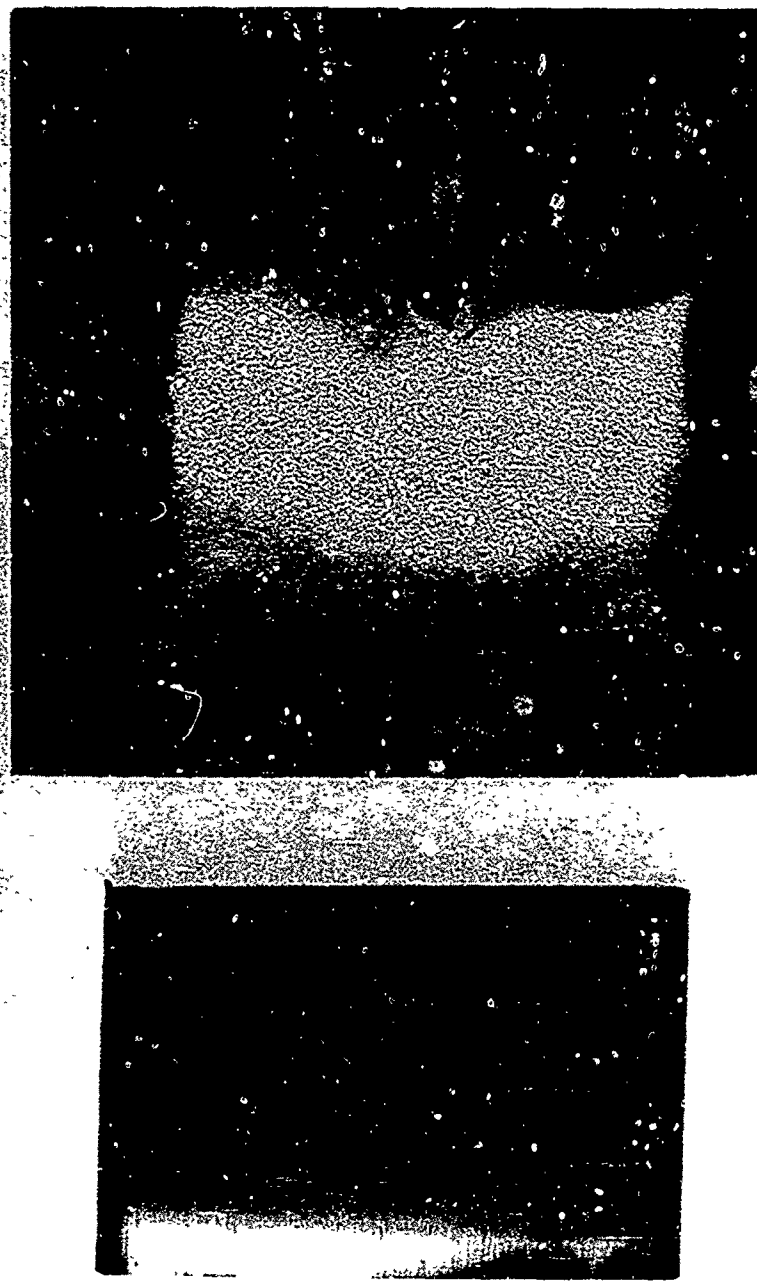
FE 352740

Figure 36. — Specimens (M50 Steel at Bottom, Silver-Plated Coupon at Top) Exposed to 0.0100 Percent Weight Sulfur (as Trityl Thiol) in Mineral Oil at 140°F for 24 Hours



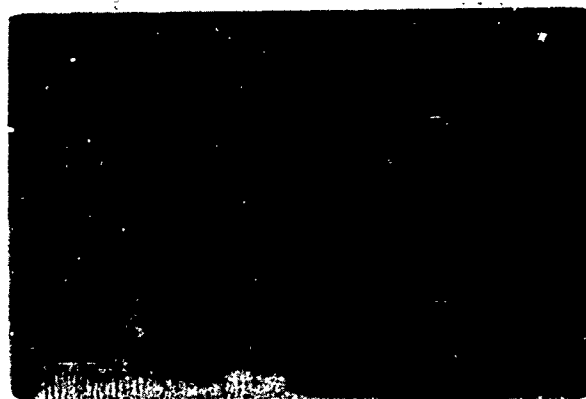
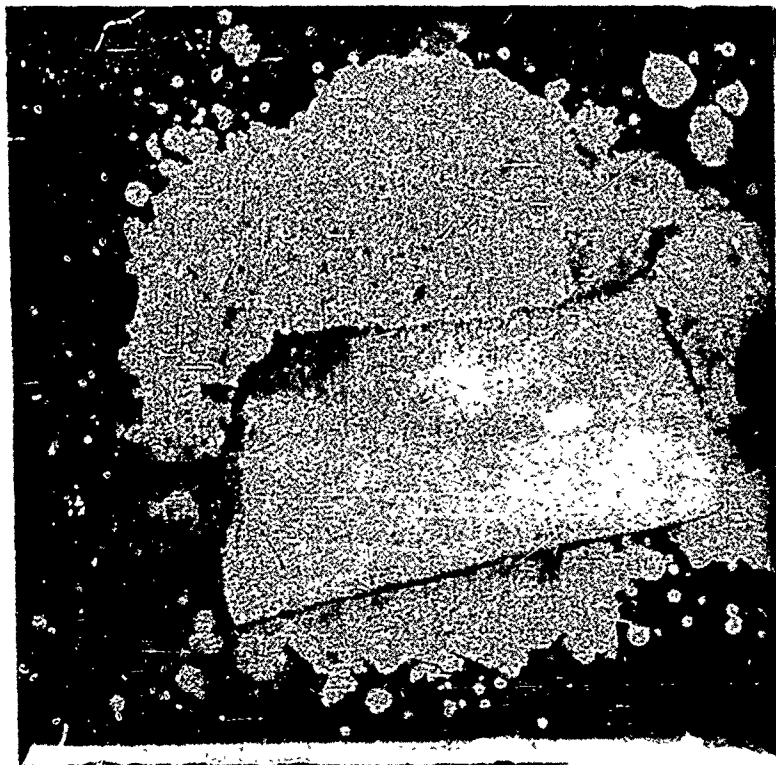
FE 352726

Figure 37. — Specimens (M50 Steel at Bottom; Silver-Plated Coupon at Top) Exposed to 0.0005 Percent Weight Chloride (as Trityl Chloride) in Mineral Oil at 140°F for 24 Hours



FE 352725

Figure 38. — Specimens (M50 Steel at Bottom, Silver-Plated Coupon at Top) Exposed to 0.0020 Percent Weight Chlorid^e (as Trityl Chloride) in Mineral Oil at 140°F for 24 Hours



FE 352724

Figure 39. — Specimens (M50 Steel at Bottom; Silver-Plated Coupon at Top) Exposed to 0.0100 Percent Weight Chloride (as Trityl Chloride) in Mineral Oil at 140°F for 24 Hours

3. CANDIDATE SELECTION

a. Initial Screening

Increased bearing corrosion resistance can be achieved by using corrosion resistant alloys or by providing a protective coating or surface treatment to existing alloys. With either approach,

bearing performance should at least equal the state-of-the-art bearing alloy, VIM-VAR M50. In the initial screening and subsequent testing, candidates had to show superior corrosion resistance, as well as equivalence in rolling contact fatigue, hot hardness, and wear resistance compared to a VIM-VAR M50 baseline.

For the initial screening, the material reference resources and (in the absence of hard data) the metallurgical experience of Pratt & Whitney, TRW Inc., and material supplier contacts were surveyed.

For preliminary consideration, a list of 28 candidates with potential for rolling element bearing application was compiled. The list included some materials which were lacking in certain state-of-the-art turbine engine bearing properties. These materials were included to ensure that consideration was given to materials which potentially might benefit from coatings, surface treatment, or other material processing.

Even as the preliminary list was being generated, the candidates with the greatest and least potential for success were being identified. The first culling reduced the list of 28 candidates to 17 candidates. This ranking was based on obvious and inferred risks and deficiencies with respect to basic bearing material properties.

The list of 17 candidates is presented in Table 4. The list includes 8 alloys and 9 coatings. Seven of the eight alloys (MRC2001, RSR405, BG42, CRB7, WD65, and 14-4 Mo) are high chrome martensitic steels. Studies conducted in the past several years (References 6 and 7) have shown that high-chrome stainless steels, potentially suitable for high-temperature, high-performance bearings, can be developed. These steels achieve corrosion resistance by forming a passive iron-chrome oxide film at the surface. They may be hardened by conventional heat treat techniques. Some of these alloys are currently used in rolling element bearings.

Powder metallurgy is an alternate processing technique with the potential for significant alloy modifications and microstructural improvements. Potential benefits include finer and more uniformly distributed carbides, better homogeneity of alloying elements, and improved material utilization due to near net shape forming.

Four of the alloy candidates considered were powder processed materials: MRC2001, RSR405, WD65, and CRB7 (CRB7 was also considered in wrought form). MRC2001 is an experimental alloy being developed for rolling contact bearing use. It had shown excellent corrosion resistance in preliminary tests at TRW. These tests ranked MRC2001, CRB7, WD65, and M50 in corrosion resistance and included tests identical to the corrosion screening tests performed in Task III of this program, as well as more severe salt spray tests. The properties of MRC2001, including hot hardness, were expected to exceed VIM-VAR M50. The RSR405 is a high chrome, potential bearing alloy which was investigated in a related P&W program, Application of Rapidly Solidified Alloys, Contract F33615-76-C-5136. Rolling contact fatigue test results from this program showed life equal to M50. In an earlier program (Contract F33615-75-C-2009), P&W demonstrated that powder processed CRB7 (AMS5900) had a rolling contact fatigue life (RCF) at least equal to, and in most cases better than, M50 in single ball tests. A concurrent rolling contact fatigue bar test performed by the USAF also showed CRB7 to be at least equal to M50.

TABLE 4.

LIST OF POTENTIAL CANDIDATES

Candidate	Process	Chemical Composition										Hardness		Heat		Impact					
		Cr	C	V	Mo	Co	Ni	Mn	Si	W	F ₂	Other	RT	400	T _{reat}		800				
BG 42	Wrought	15	1.2	1.2	4			0.45	0.3				Bal			62	62	57	2050/950		
14-4 Mo	Wrought	14.5	1.07	0.15	4			1.0	1.0				Bal			60-63	63	54	2000/1000	IZOD 31.0	
CRB7	Wrought	14	1.1	1	2			0.4	0.3				Bal	0.25Cb		61	61	57	2100/400	M/CVN 12	
CRB7	Powder	14	1.1	1	2			0.4	0.3				Bal	0.25Cb		61	61	57	2100/400	Poor	
	Metallurgy																				
WD65	Powder	14	1.1	2.8	4		5.3	0.2		2.4			Bal	0.15S		58-62	54-57	47	2100/1000	Poor	
	Metallurgy																				M/CVN 7-8.5
MRC2001	Powder	15	1.3	1.8	6.5			0.5					Bal	0.05Cb		60-62	54-57	50	2100/1000	Excellent	
	Metallurgy																				M/CVN 8
RSR405	Powder	19	1.3	1	2								Bal								
	Metallurgy																				
CBS 1000M	Wrought	1.07	0.11	0.37	4.5		3.0	0.5	0.5				Bal	0.03Al		61	59	53	2000/1000		
Armloy	Plating																				
Nobilizing	Plating																				
Chrome	Sputter																				
	Coating																				
Nickel	Sputter																				
	Coating																				
Gold	Sputter																				
	Coating																				
Silver	Sputter																				
	Coating																				
Chrome Carbide	Sputter																				
	Coating																				
Titanium Carbide	Sputter																				
	Coating																				
Black Oxide	Salt Bath																				

6174

All the powder processed materials incorporated a degree of risk in that all were unproven experimental bearing alloys, and that the process development and qualification procedures required for production use of powder metallurgy bearings may exceed the 3- to 5-year introduction goal.

Another stainless steel, BG42 (AMS5749), is potentially suitable for high performance bearing applications. Pratt & Whitney has experience with BG42 bearings in the exhaust nozzle air motor for an Air Force F100 engine. In this application, the BG42 bearings operate dry and at a very high temperature, about 700°F. This environment differs radically from that of a mainshaft bearing but it did demonstrate suitability of BG42 for production and for high temperature applications. Rolling contact element life tests comparing VIM-VAR BG42 and VIM-VAR M50, (Reference 6) showed fatigue life at least equal to VIM-VAR M50.

The commercial availability and excellent preliminary rolling contact fatigue results for both CRB7 and BG42 made those two high chrome alloys prime candidates for use in high performance corrosion resistant bearings. Both alloys have demonstrated hot hardness equal to M50 (References 8 and 9). In addition, these alloys are commercially available in wrought form as is the currently used VIM-VAR M50.

A common high carbon stainless steel, AISI 440C is widely used in bearing applications, but is not suitable for gas turbine use because of poor hot hardness characteristics. The 14-4 Mo is a modified form of 440C. It has a molybdenum addition which improves the secondary hardening characteristics and hot hardness. The alloy is commercially available, but has not had extensive development testing for rolling contact bearing applications.

An alternate approach to achieve corrosion resistance is a protective coating or surface treatment applied to existing bearing materials. Coatings and surface treatments have the distinct advantages of being applicable to existing bearings and requiring a minimum amount of strategic elements. A successful coating or surface treatment must adhere to the substrate bearing material and endure millions of rolling contact stress cycles without impairing bearing performance. Conventional electroplates and electroless nickel have failed due to inadequate adhesion, allowing peeling and chipping to occur in the contact area (Reference 10). Three modern coating techniques were considered in this program, i.e., sputter coating, proprietary plating, and black oxide coating processes. Chemical vapor deposition processes were not considered because the high substrate temperatures required would have adversely affected substrate hardness.

Ion implantation is a surface treatment that creates a surface alloy by injecting ions into a substrate. Depending on the ions and the substrate material, the resulting surface alloy can have significantly improved corrosion resistance (Reference 5). The improved corrosion resistance of Cr, Cr+Mo, and Cr+P ion implanted M50 specimens vs baseline M50 has been demonstrated by a joint Naval Air Propulsion Center/Naval Research Laboratory program. The improved corrosion resistance was achieved without expense to the substrate bulk properties. By joint USAF and P&W agreement ion implantation was not considered as a candidate to avoid duplication of effort and to allow as broad a survey as possible of other potential candidates.

Two proprietary plating processes were considered. Armoloy and Nobilizing have both shown potential for use in rolling contact bearing applications (Reference 10). Both of these processes deposit a thin (0.00005 to 0.00025 inch) coating of hard, dense chromium.

TRW Bearings Division has had good experience with Armoloy including ball bearings of both 52100 and M50 steel in a variety of applications including an experimental gas turbine engine. A partial listing of Armoloy-plated bearing applications is shown in Table 5.

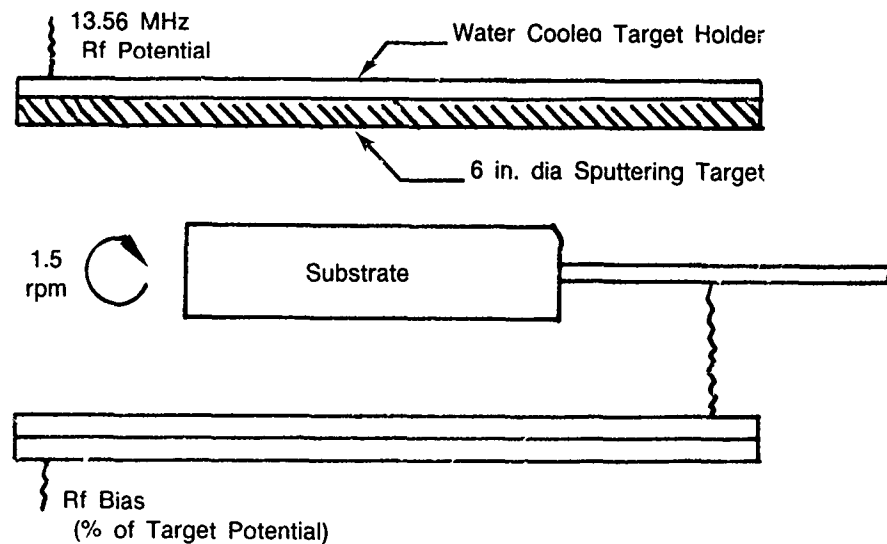
TABLE 5.

ARMOLOY-PLATED BEARING APPLICATIONS

<i>Bearing</i>	<i>Base Material</i>	<i>Application</i>	<i>Environment</i>
7203	52100	Ice Cube Machine	Water
R4	52100	Flow Meter	Sour (NaCl,S) Crude
7224/7228	52100	Stirring Motor	Polyethylene
R1907E101	M50	Exp Gas Turbine Engine	MIL-L-7808
9109UK108	M50	Exp Gas Turbine Engine	MIL-L-7808
2035	52100	Simulated Control Rod Mechanism (Nuclear)	De-Ionized Water

6171C

Sputtering is a physical vapor deposition technique. The coating chamber is evacuated to eliminate atmospheric gases, then back-filled with argon to low pressure, 1 to 30×10^{-3} Torr. Figure 40 is a schematic representation of the radio frequency (RF) diode sputtering process. An application of an RF potential of sufficient voltage to the target creates a plasma and accelerates positive argon ions to the target which is the coating material source. This ionic bombardment ejects (sputters) atoms from the target surface with sufficient energy to traverse the chamber, impact, and bond to the substrate.



Schematic - Not to Scale

FD 270313

Figure 40. — Diagrammatic Representation of the Radio Frequency Diode Sputtering Chamber

Adhesion is achieved by promoting interdiffusion. This may be accomplished by controlling substrate temperatures, which for bearing applications must be below the tempering temperature, and sputter etching of the substrate to remove impurities.

Almost all compounds and elements can be deposited by sputtering. Pratt & Whitney has extensive experience with protective and wear resistant coatings including TiC on 440C and 52100 balls (not rolling element bearing applications, however). Selected initial candidate coating materials are from two classes of materials: (1) hard, wear resistant materials (chrome, chrome

carbide, titanium carbide), and (2) relatively soft, lubricating materials (gold, silver). Corrosion protection is achieved by enveloping the substrate M50 with a protective coating.

An oxide coating was also considered initially. In one study (Reference 11), bearings treated with a commercial black oxide coating and operated in a water environment showed significantly improved corrosion and wear resistance when compared to noncoated bearings.

The natural oxide coating on steels confers a degree of passivity to the base material. This protection has been improved upon by several commercial processes which develop a thicker, stronger oxide film. These films do not provide much protection by themselves, but protective oils are retained by the porous coating.

Future turbine engines will require improved fracture toughness to accommodate anticipated higher rotor speeds. CBS1000M is a high temperature, secondary hardening, carburizing steel with reported improved fracture toughness over M50. However, it has only 1 percent by weight of chrome compared to 4 percent for M50. It was included for consideration as an alloy which would provide an added benefit over M50 with the application of a corrosion resistant coating or surface treatment.

b. Initial Candidate Selection

State-of-the-art turbine engine bearings are made from AISI M50 steel. The material was selected for turbine engine use due to its good rolling contact fatigue (RCF) life and high hot hardness.

In addition to superior corrosion resistance, any candidate selected for material property testing was required to be at least potentially equivalent in rolling contact fatigue, hot hardness, and wear resistance.

All the material property data collected from literature searches and material supplier contacts were compiled for the 17 initial candidates. This initial ranking did not penalize an otherwise worthy candidate because of a lack of data. In order to allow a wider variety of candidates to be considered for basic material property evaluation, the secondary categories of frugal use of strategic elements, cost, other mechanical properties, and potential for 3- to 5-year use were not weighed. It was decided that these criteria would be used to discriminate between otherwise equal candidates once back-to-back property data were available.

Given the lack of rolling contact fatigue data on coated candidates, it was assumed that fatigue life for a coated candidate would be the same as that of the substrate. For each category of RCF, corrosion resistance, wear, and hot hardness a candidate was judged to be either better than (+), equal to (0), or less than (-) M50. A negative in any category was cause for elimination. Table 6 summarizes the results.

The remaining candidates were subdivided into four categories:

- State-of-the-art corrosion resistant alloys
- Advanced powder processed corrosion resistant alloys
- Sputtered coatings (over M50 or CBS1000M)
- Proprietary chrome plating processes (over M50 or CBS1000M).

TABLE 6.
PRELIMINARY TASK 2 CANDIDATE SELECTION

<i>Candidate</i>	<i>Process</i>	<i>RCF</i>	<i>Corrosion Resistance</i>	<i>Wear Res.</i>	<i>Hot Hard</i>
BG 42	Wrought	0	+	0	0
CBS 100M	Wrought	0	+ (with coating)	0	0
CRB7	Powder Metallurgy	0	+	- (Ref 7)	0
CRB7	Wrought	0	+	0	0
MRC001	Powder Metallurgy	0	+	0	0
RSR405	Powder Metallurgy	0	+	0	0
WD 65	Powder Metallurgy	- (Ref 8)	+	0	0
14-4 Mo	Wrought	- (Ref 12)	+	0	0
Armoly	Plating	0	+	0	0
Black Oxide	Salt Bath	0	+	- (Ref 11)	0
Chrome	Sputter Coating	0	+	0	0
Chrome Carbide	Sputter Coating	0	+	0	0
Gold	Sputter Coating	0	+	0	0
Nickel	Sputter Coating	0	+	0	0
Nobilizing	Plating	0	+	0	0
Silver	Sputter Coating	0	+	0	0
Titanium Carbide	Sputter Coating	0	+	0	0

6.17.10

It was decided that risk to the program would be minimized and potential benefit maximized, if at least one candidate from each category were represented in the final list of five candidates.

Consideration was given in each category as to which candidate would provide the maximum information by tying into existing data. There appeared to be little difference between the chemically similar alloys CRB7 and BG42. Wrought CRB7 was chosen over BG42 because

unexplained and disappointing wear data existed on powder processed CRB7 (Reference 7). It was felt that wear data on wrought CRB7 would provide additional data which might help in determining whether the process or the material was the cause of the wear.

Armoloy and Nabilizing were viewed as essentially equal in every respect. Armoloy was chosen because of TRW Bearing Division's previous experience with the process.

The corrosion resistance of all the sputtered coating candidates was judged equal. However, it was felt that the elemental metallic coatings could achieve adequate adhesion at lower substrate temperatures compared to either TiC or CrC. Sputtered elemental chrome was eliminated from consideration because a chrome coating, Armoloy, was already represented. Sputtered nickel was chosen over gold because of the availability and initial costs of target materials. Silver was eliminated because of the potential for galvanic attack at local defects. Nickel, being closer to steel in the galvanic series, should minimize this potential problem.

The M50 was chosen over the CBS1000M as the substrate material because back-to-back comparison with the M50 baseline would provide a means of isolating coating effects on property data.

Both RSR405 and MRC2001 are experimental powder processed high chrome stainless steels. Existing data indicated both had RCF life at least equal to M50; and, with 19 percent and 15 percent chrome, respectively, both were expected to exhibit excellent corrosion resistance. The fourth candidate elected was MRC2001. It was in a more advanced state of development compared to RSR405 and existing preliminary wear and corrosion test results were very promising.

To arrive at a fifth candidate, all categories were reviewed again. Two candidates surfaced as leading contenders: BG42 and RSR405. The BG42 was initially selected over the RSR405 because it was a readily available, lower risk, 15 percent chrome alloy with demonstrated corrosion resistance, whereas RSR405 was an experimental alloy with good potential but which required additional development. However, in subsequent discussions with the Air Force, it was decided that the Improved Corrosion Resistance Turbine Engine Bearings Program would be better served with RSR405, given its higher chrome content (19 percent), its unique rapid solidification rate powder processing, and its encouraging RCF data.

Early in the course of the program RCF testing, the RSR405 candidate experienced several premature spalls. The RCF testing on this candidate was suspended and later examination revealed surface and subsurface aluminum oxide inclusions. There was also some evidence that the interdiffusion layer that existed between extrusion can material and the consolidated powder material after it has been extruded was not completely machined off during RCF specimen preparation.

The source of the aluminum oxide inclusions was traced to a crucible in which the alloy was melted during powder fabrication. In the interim period between the original candidate selection and the mechanical property testing, additional test results had become available from both an on-going P&W Bearing Material Improvement Program and a Defense Advanced Research Project Agency (DARPA) sponsored program. In the DARPA program, Application of Rapidly Solidified Alloys (F33615-76-C-5136), RSR565, an experimental tool steel, had demonstrated superior RCF life compared to both M50 and RSR405. Also, preliminary data from the internal P&W program, indicated that RSR565 had superior hardness retention characteristics compared to RSR405. The RSR565, while not stainless by definition, was also expected to exhibit improved corrosion resistance compared to the M50 because of its higher chrome and alloy content. Also, RSR565 was readily available in form and quantity for Phase I evaluation, therefore, the Air Force program office was requested to, and did, approve the substitution of RSR565 for the RSR405 candidate.

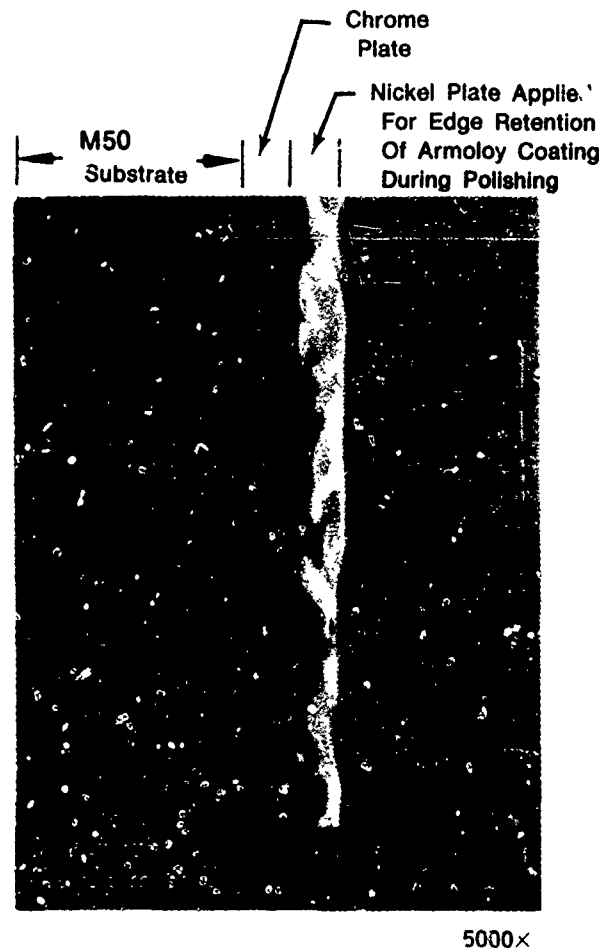
As part of an ongoing P&W material development program, an experimental high chrome RSR material, RSR113, was also evaluated for rolling contact fatigue life and corrosion resistance. The results are included as a part of this report.

c. Test Specimen Fabrication

(1) Armoloy-Coated M50

Armoloy is a proprietary electro-chemical hard chrome plating process. The coating thickness is self-limiting. The coating thickness range is 0.00005 to 0.00025 inch which reportedly is controllable to 0.0001 inch.

The coating thickness of the specimens used in this program ranged from 0.00008 to 0.00009 inch in the as-received condition. An SEM photomicrograph of a cross sectioned Armoloy-coated specimen is presented in Figure 41.



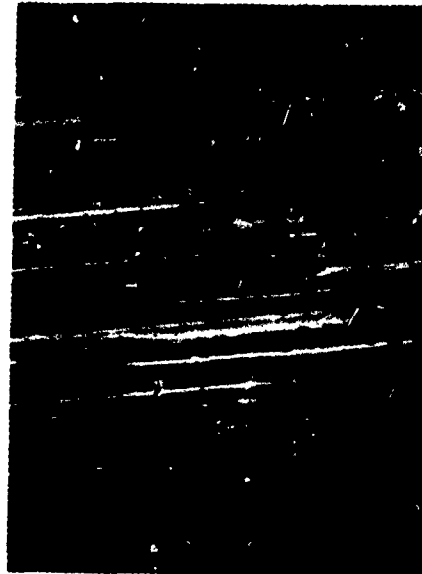
FD 270302

Figure 41. — SEM Photomicrograph of a Cross Sectioned "As-Received" Armoloy-Coated M50 Test Specimen

The Armoloy coating as received had a coarser average surface finish (9.2 microinches) than either the VIM-VAK M50 substrate (4.6 microinches average) or the other candidate test

specimens (4.6 to 5.4 microinches average) used in this program. To determine qualitatively what effect this coarsened surface finish would have on RCF life, the Armoloy test bars were split into two test lots. One lot was left in the as-received condition and the second lot was hand-polished on a coarse natural cellulosic fiber wheel using an iron oxide polishing compound to an average surface finish of 5.4 microinches.

SEM photomicrographs of the surfaces of an M50 test bar prior to coating, an as-received Armoloy coating, and a polished Armoloy coating are presented in Figures 42, 43, and 44, respectively.



Mag 1000x

FD 270307

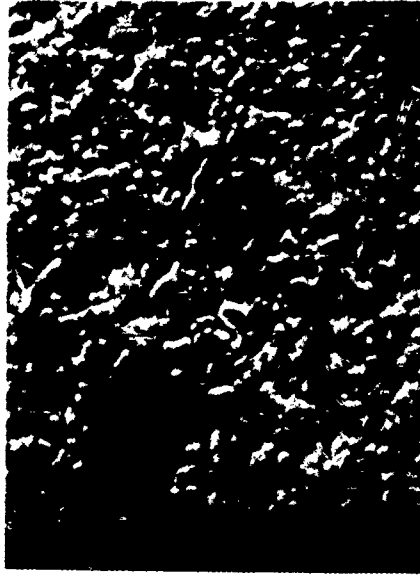
Figure 42. — SEM Photomicrograph of the Surface of a Typical VIM-VAR M50 Baseline Test Specimen and Coating Substrate Specimen

The Armoloy coating was applied by the Armoloy Co. of Dekalb, Illinois. Within a half-hour after processing, all Armoloy test bars were subjected to a stress relief cycle of 425°F for 4 hours. A post-processing bake is not a standard requirement in the proprietary Armoloy process. It has been TRW's experience, however, that AISI 52100 bearings suffered a reduction in RCF life after Armoloy processing unless they were post-process baked.

(2) Nickel Sputter-Coated M50

The nickel sputter coating was applied by the Pratt & Whitney/Government Products Division, Materials Development Laboratory.

A cryopumped RF diode sputtering system which employs a 1 kW RF power supply was used to sputter coat nickel over a VIM-VAR M50 substrate. Substrate temperatures typically did not exceed 400°F. The substrates were coated while rotating at 1 rpm, 1 inch below a water cooled, sputtering target. The target, a flat disk 15.24 cm in diameter and 0.95 cm thick (6.00 inches in diameter by 0.375 inch thick) was machined from commercial quality Ni-200 plate stock. Standard XES analysis run on a sample of this material revealed no trace elements present in excess of 0.1 percent weight concentration.



Mag 1000x

FD 270306

Figure 43. — SEM Photomicrograph of the Surface of a Typical "As-Received" Armoloy-Coated M50 Test Specimen

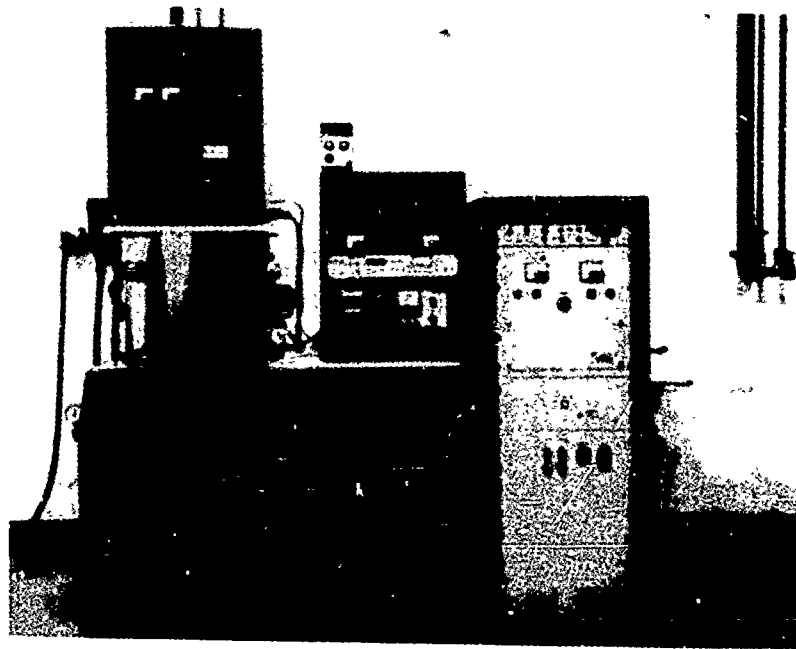


Mag 1000x

FD 270305

Figure 44. — SEM Photomicrograph of the Surface of a Typical Polished Armoloy-Coated M50 Test Specimen

The RF sputtering system is shown in Figure 45; the coating chamber was previously illustrated in Figure 40.



FD 270314

Figure 45. — Planar Target Radio Frequency Diode Sputtering System

The substrates were cleaned just prior to fixturing in the coater, or stored in a clean stainless steel container under an argon gas atmosphere until used, to prevent contamination of the freshly cleaned surface. The cleaning procedure which produced the most satisfactory results was as follows:

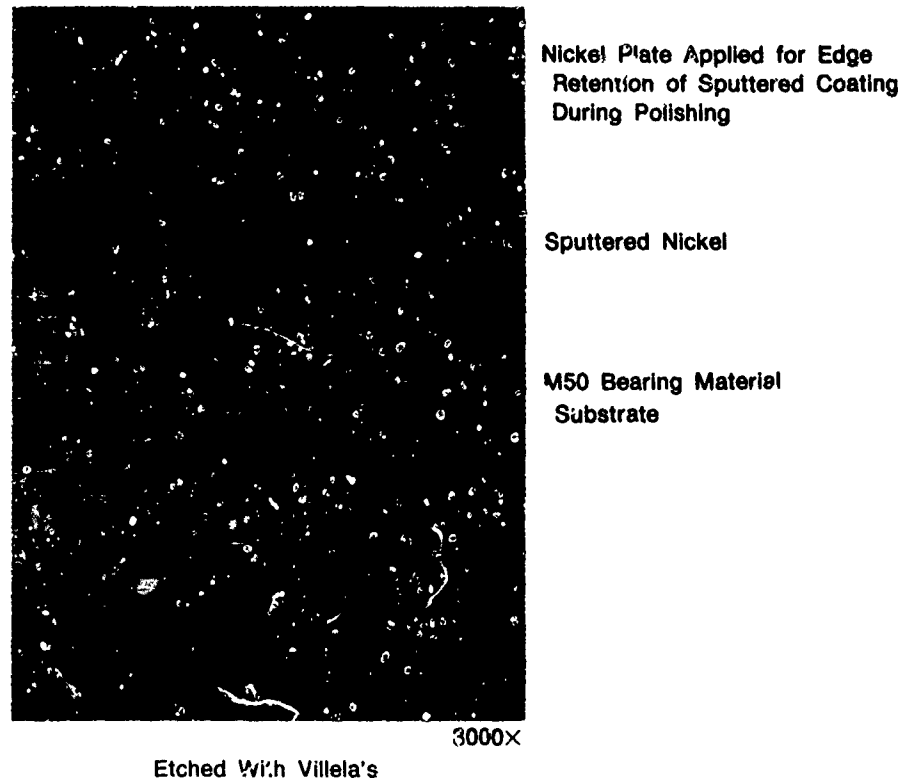
- Three 5-minute ultrasonic baths in clean freon
- A 5-minute ultrasonic bath in soap/water solution
- Clean tap water rinse
- A 2-minute ultrasonic bath in clean ethyl alcohol
- Rinse in reagent grade ethyl alcohol
- Forced warm air dry.

Four experimental coating cycles were run in the RF diode coater to obtain process parameters which would yield coatings with the desired characteristics. Once these parameters were finalized, coating of the actual bearing material began. All thirty of the bearing stock test specimens were coated using the following procedures:

- The loaded chamber was pumped down to the low 10^{-6} Torr range.
- The chamber was back-filled with argon gas to approximately 6×10^{-3} Torr.
- A plasma was established by applying 3 kv RF to the target.

- A bias voltage of 100v RF was applied to the substrate for the first 10 minutes of deposition to assure a good coating bond.
- After 10 minutes the bias voltage was removed from the substrate. The deposition process was continued to complete a full 2-hour coating period.

The thickness of the sputtered deposit was determined from a SEM photomicrograph of polished cross sections of coated trial specimens. Measurements taken from these photos showed that a 2-hour deposition cycle would yield a coating approximately 0.000045 inch (11,300 angstroms) thick as illustrated in Figure 46.



FD 270311

Figure 46. — SEM Photomicrograph of a Cross Section of Sputtered Nickel on M50 Bearing Stock

The nickel coating appeared shiny and virtually defect-free to the unaided eye. Scratches, nicks, and other defects which were present on the original bearing surfaces were mirrored by the thin nickel coating. Figure 47 illustrates the typical *as-coated* surface finish of test specimens used in this study.

Coating adhesion was determined using a Sebastian 1 adherence tester on a witness tab which was coated along with the first M50 test specimen. The coating on this tab did not debond within the 10,000 psi limit of this tester, but the epoxy used to bond the witness tab to the tester loading mechanism failed at 9820 psi halting the test sequence.



Mag 1000×

FD 270299

Figure 47. — SEM Photomicrograph of the Surface of a Typical Nickel Sputter-Coated M50 Test Specimen

The hardness of the bulk M50 bearing material was measured before and after coating experiments using a Zwick microhardness tester with a diamond pyramid indenter under a 5 kg load. The as-received bulk hardness was found to be 739 HV (Rockwell "C" (Rc) 61.8) and the hardness after nickel coating was 800 HV (Rc 64). This indicates that the hardness of the bulk material was virtually unaffected by the RF diode sputtering process.

(3) VIM-VAR M50 Baseline

VIM-VAR M50 (Fe-4.25Cr-4.25Mo-1.0V-0.8C-0.25Mn) is a lean molybdenum type, through hardened high speed steel. It possesses high strength and high hot hardness and is considered state-of-the-art high performance turbine engine bearing material. However, the material has low corrosion resistance. All the VIM-VAR material used in this program was the same heat lot (Altech Metals heat lot 46734). The baseline M50 test bars and coating candidate substrate bars were processed identically. The M50 heat treatment schedule is presented in Table 7.

(4) MRC2001 Candidate

MRC2001 (Fe-15.2Cr-6.74Mo-1.81V-1.51C-0.32Mn-0.1Si) is a martensitic, high carbon, corrosion resistant and oxidation resistant alloy steel. The powder for this program was fabricated from vacuum melted prealloyed material which was atomized in a nitrogen gas atmosphere. The powder for the test specimens was encapsulated and hot outgassed at approximately 10^{-4} Torr. It was then extruded at 1950°F and a 14 to 1 reduction ratio. The MRC2001 heat treatment schedule is presented in Table 8.

TABLE 7.
HEAT TREATMENT OF M50

	<i>Temperature (°F)</i>
Preheat	1550
Austenitize	2025
Quench	1100
Martemper	350
Air Cool	
Wash	
Temper	1000
Temper	1000
Temper	1000

6.17 (C)

TABLE 8.
HEAT TREATMENT OF MRC2001

	<i>Temperature (°F)</i>
Preheat	1500
Austenitize	2150
Martemper	350
Wash	
Air Cool	
Deep Freeze	-110
Liquid Nitrogen	-320
Temper	1000
Deep Freeze	-110
Liquid Nitrogen	-320
Temper	1000
Temper	1000

6.17 (C)

(5) **Wrought CRB7 Candidate**

CRB7 (Fe-14.0Cr-2.07Mo-1.06V-1.11C-0.43Mn-0.29Si) is a patented, corrosion resistant secondary hardening tool steel with reported high temper resistance, hot hardness, and wear resistance (Reference 8). The alloy was developed by the Carpenter Steel Division of the Carpenter Technology Corporation for improved hot workability compared to 14-4 Mo and WD65.

Wrought 0.520-inch diameter round stock was purchased from Carpenter Steel Co. (heat Lot 83434).

The CRB7 heat treatment schedule is presented in Table 9.

TABLE 9.
HEAT TREATMENT OF CRB7

	<i>Temperature (°F)</i>
Preheat	1550
Austenitize	2100
Martemper	350
Air Cool	
Wash	
Deep Freeze	-110
Liquid Nitrogen	-320
Temper	1000
Deep Freeze	-110
Liquid Nitrogen	-320
Temper	1000
Temper	1000

617 H'

(6) *RSR565 Candidate*

RSR565 (Fe-9Cr-2Mo-1V-4Co-1C-0.2Mn-0.2Si) is a powder metallurgy, corrosion resistant secondary hardening tool steel developed on AF Contract F33615-76-C-5136. The alloy was designed to give adequate corrosion resistance to a lubricated bearing via the 9 percent Cr addition while minimizing the number of grain boundary chromium rich carbides so prevalent in 14 percent Cr bearing steels. The 4 percent Co addition was designed to raise the martensitic start (MS) temperature so complete transformation of austenite to martensite would occur without cold treatment. The alloy had superior rolling contact fatigue properties when compared to M50 tool steel in preliminary APL conducted tests. The test material for this program was made at P&W by direct extrusion of prealloyed RSR140 mesh powder at 1700°F and a 20:1 reduction ratio. The RSR565 heat treatment schedule is presented in Table 10.

TABLE 10.
HEAT TREATMENT OF RSR565

	<i>Temperature (°F)</i>
Austenitize	2100
Air Cool	
Liquid Nitrogen	-320
Temper	1000
Air Cool	
Liquid Nitrogen	-320
Temper	1000
Air Cool	
Liquid Nitrogen	-320

617 H'

(7) *RSR405*

RSR405 (Fe-19Cr-2Mo-1V-1.25C-0.2Mn-0.2Si) is a powder metallurgy, ultra-high chromium tool steel developed on AF Contract F33615-76-C-5136. The alloy was designed so that it would have more corrosion resistance than any other commercially available tool steel due to its very high chromium content. It was hoped that rapid solidification, powder metallurgy

processing would help minimize an expected massive chromium rich carbide network at the prior austenite grain boundaries. The alloy had similar rolling contact fatigue properties when compared to M50 tool steel in APL conducted tests. The test material for this program was made at P&W by direct extrusion of prealloyed RSR140 mesh powder at 1700°F and a 20:1 reduction ratio. The RSR405 heat treatment schedule is presented in Table 11.

TABLE 11.
HEAT TREATMENT OF RSR405

	<i>Temperature (°F)</i>
Austenitize	2100
Air Cool	
Liquid Nitrogen	-320
Temper	400
Air Cool	
Liquid Nitrogen	-320
Temper	400
Air Cool	

6.17 (1)

(8) RSR113

RSR113 (Fe-14Cr-4Mo-1V-2Co-1C-1Cb-0.2Mn-0.2Si) is a powder metallurgy modified version of the CRB7 tool steel developed by Carpenter Technology. The alloy was designed so it would contain more beneficial wear resistant MC and M₂C type carbides than are present in the CRB7 tool steel. This was achieved by increasing the molybdenum and columbium content of the alloy while adding cobalt to partially offset the reduction in MS temperature. This alloy has superior corrosion resistance due to its high chromium content. The alloy was not tested in rolling contact fatigue and wear prior to incorporation in this program. The test material for this program was made at P&W by direct extrusion of prealloyed RSR -140 + 325 mesh powder at 1750°F and a 12:1 reduction ratio. The RSR113 heat treatment schedule is presented in Table 12.

TABLE 12.
HEAT TREATMENT OF RSR113

	<i>Temperature (°F)</i>
Austenitize	2130
Air Cool	
Liquid Nitrogen	-320
Temper	925
Air Cool	
Liquid Nitrogen	-320
Temper	925
Air Cool	
Temper	925
Air Cool	

6.17 (1)

All the alloy candidate test bars and the baseline M50 test bars were centerless ground at TRW to final size (0.5 inch diameter) and finish (4 to 6 microinches) using a 20-inch, 100 grit, A100M5 wheel rotating at 1300 rpm.

The metallurgical parameters of CRB7, MRC2001, RSR565, RSR113, and the VIM-VAR M50 baseline material are summarized in Table 13.

TABLE 13.
METALLURGICAL PARAMETERS OF ALLOY CANDIDATES, RSR113 AND VIM-VAR M50 BASELINE

Candidate Material	Chemistries (%W)										Rockwell Hardness (Rc)	Percent Retained Austenite	ASTM Grain Size
	C	Cr	V	Mo	Mn	Co	Si	Nb	O ₂	Cb			
CRB7	1.11	14.0	1.06	2.07	0.43	—	0.29	—	—	0.31	62.5 62.9	3	9.1
MRC2001	1.51	15.2	1.81	6.74	0.32	—	0.1	—	28ppm	—	62.6 63.1	3	12+
RSR565	1	9	1	2	—	4	—	—	—	—	62.6 63.0	4	5-8
RSR113	1	13.8	1.09	3.95	0.31	1.95	0.3	1.02	—	—	62.5 63.2	27* 9**	13-14
VIM-VAR M50 Base Mat'l	0.80	4.25	1.0	4.25	0.25	—	—	—	—	—	62.1 62.3	3	8.9

*Transverse
**Axial

637 X

Figure 48 shows SEM photomicrographs of the M50 baseline, alloy candidates, and RSR113 microstructure.

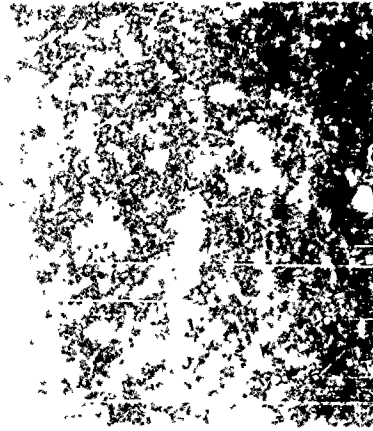
d. Phase I Test Results

(1) Rolling Contact Fatigue Testing

The rolling contact fatigue characteristics of the above materials were investigated through performance testing on RCF-1 rolling contact fatigue testing machines (Figure 49), produced by Polymet Corporation, Cincinnati, Ohio. This type of RCF test is widely used throughout industry to reliably rank candidate materials.

The RCF-1 tester, uses test specimens (0.50-inch diameter rods, 3 inches long) mounted in a precision chuck, rotating at 7000 rpm. The rotating test rod is diametrically loaded in rolling contact by two large contacting rollers (or loading disks) pendulum supported, and mechanically loaded against the test rod. The test load is continuously monitored by a strain analyzer. A fatigue spall is detected by an adjustable velocity vibration pickup with an automatic shutdown feature which senses the vibration increase associated with spalling. Lubrication was provided with a gravity flow, once through lubricant system using MIL-L-23699 fluid. Total test specimen revolutions are automatically counted.

VIM-VAR M50



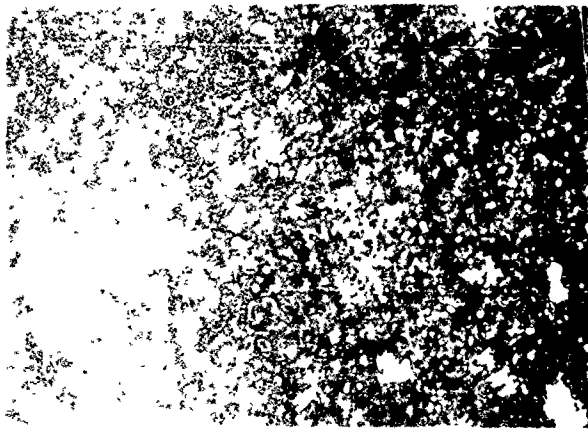
Alloy Carbide Size and Distribution in a Tempered Martensitic Matrix Is Typical of Wrought Ingot Metallurgy Magnification 400X

MFC2001



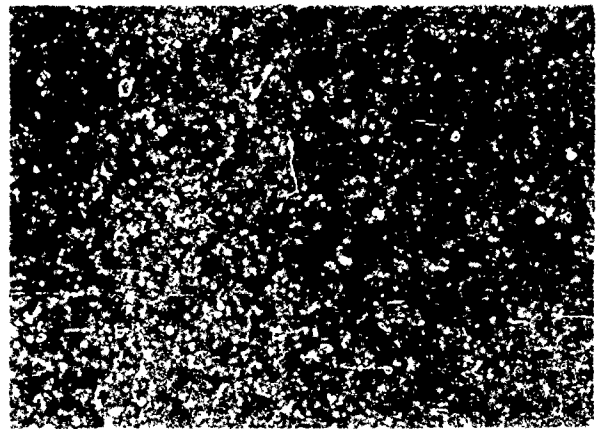
Evenly Dispersed Alloy Carbides of the MC and M_6C_{23} Type in a Matrix of Tempered Martensite Magnification 1000X

CRB 7



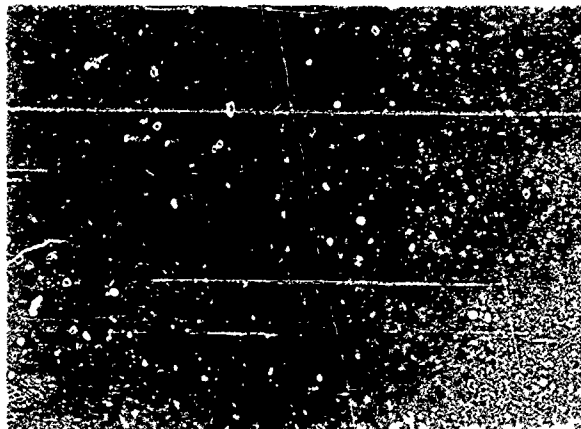
Carbides of Varying Size, Typical of High Purity Martensitic Stainless Steel Produced by Ingot Metallurgy Magnification 400X

RSR565

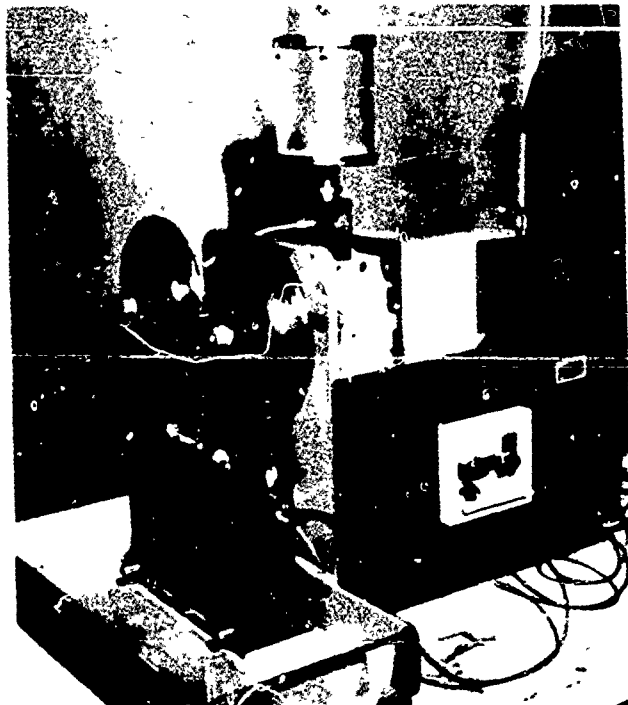


Evenly Dispersed Alloy Carbides in a Tempered Martensitic Matrix Magnification 400X

RSR113



Evenly Dispersed Alloy Carbides in a Tempered Martensitic Matrix Magnification 400X



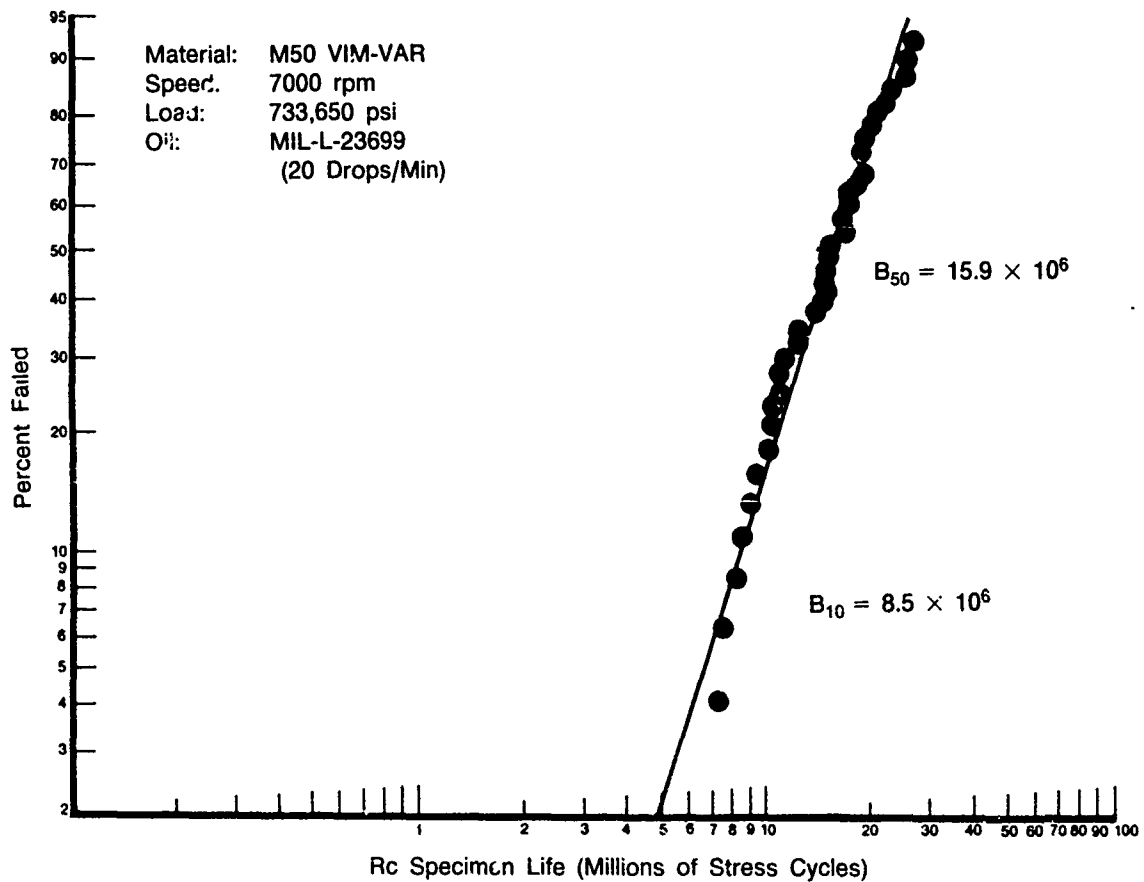
FD 216723

Figure 49. — Overall View of the Rolling Contact Fatigue Rig (Top), Closeup View of Specimen and Test Rolls (Bottom)

The loading disks (composed of CVM M50 steel, R: 61 to 64, 7.5 inches in diameter by 0.5 inch thick, and with a 0.25-inch contact radius) exert a maximum Hz stress test load on the test rod of 733,650 psi.

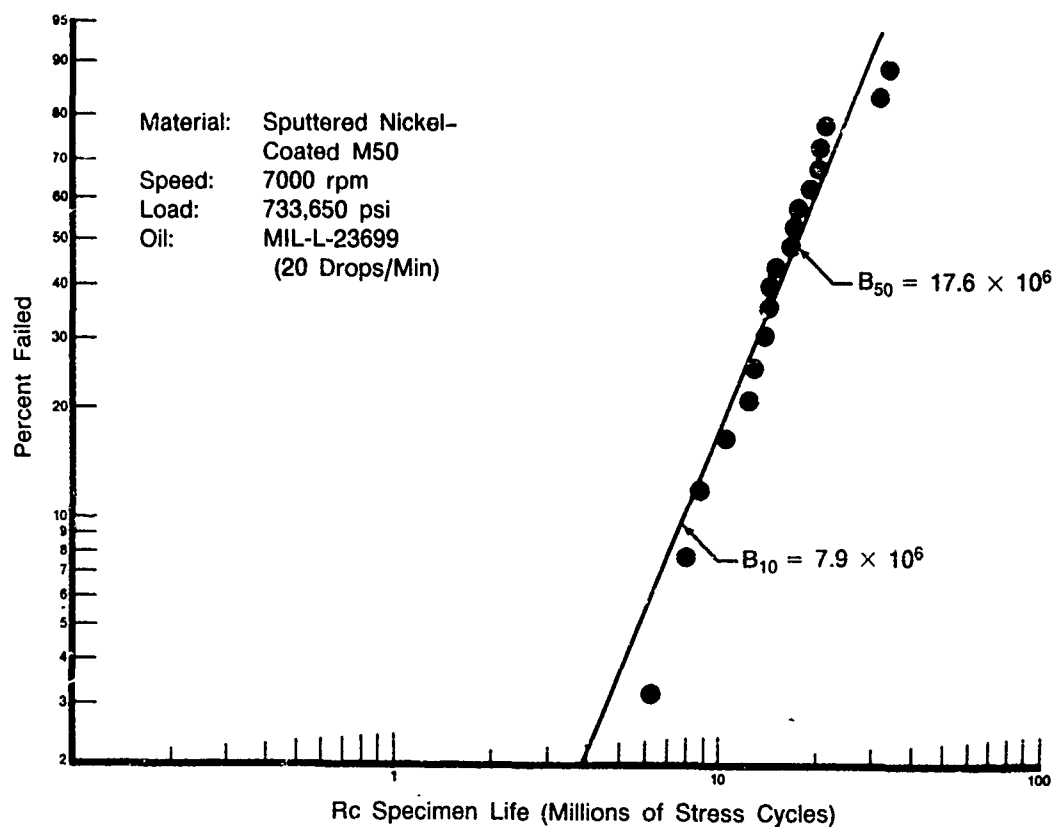
A minimum of 20 rolling contact fatigue tests were produced for each candidate and reference M50 material.

Figures 50 through 57 are individual Weibull plots of the RCF test results. A data summary sheet and composite Weibull are presented in Table 14 and Figure 58, respectively. Of particular note is the outstanding performance of the VIM-VAR M50 reference material. Compared to other RCF studies conducted on 0.5-inch diameter rod specimens, the M50 demonstrated both a steep Weibull slope and a high L_{10} life. Confidence numbers were generated for the L_{10} and L_{50} lives using L. G. Johnson's technique (Reference 12). A 95 percent or greater confidence number (a 2σ confidence level) is indicative of a high degree of confidence.



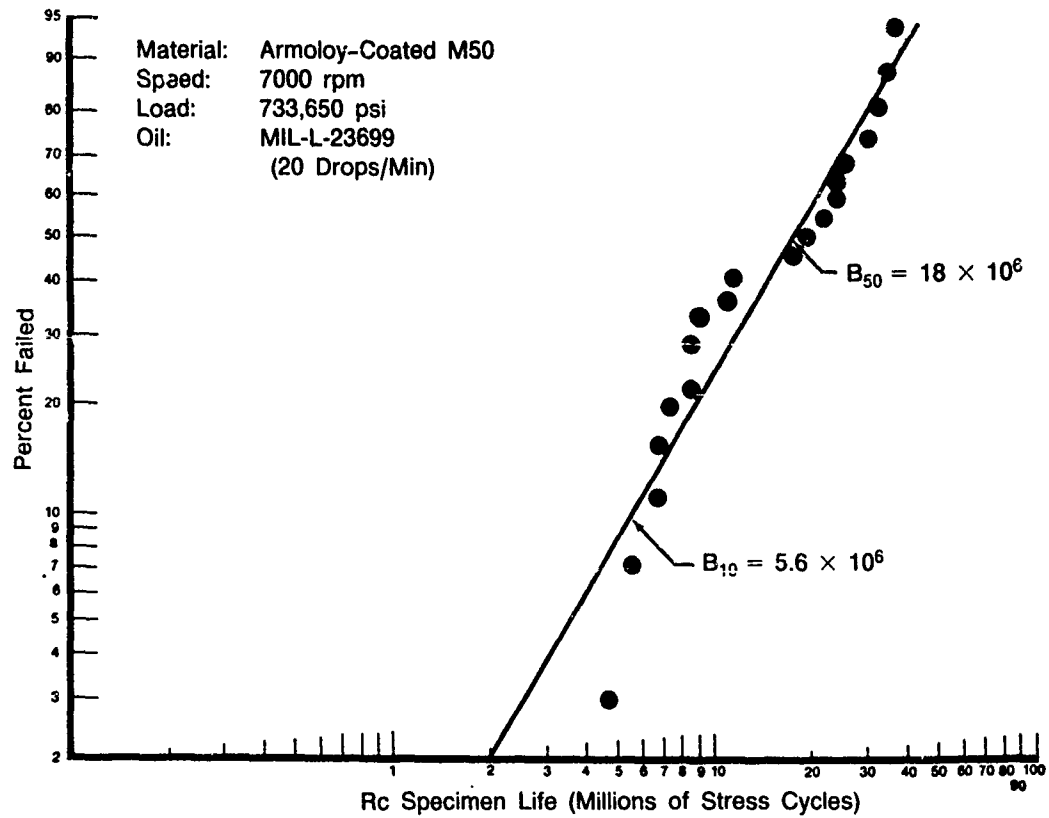
FD 270297

Figure 50. — Weibull Plot of Baseline M50 Rolling Contact Fatigue Test Results



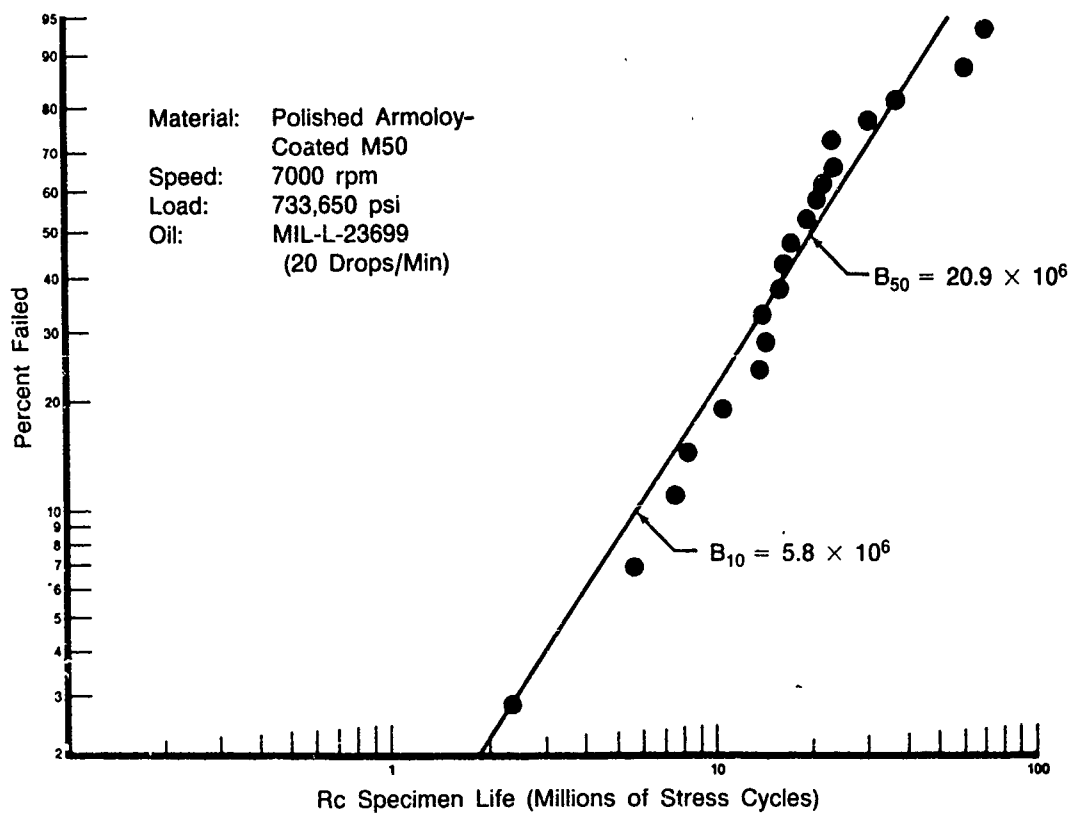
FD 270292

Figure 51. — Weibull Plot of Nickel Sputter-Coated M50 Rolling Contact Fatigue Test Results



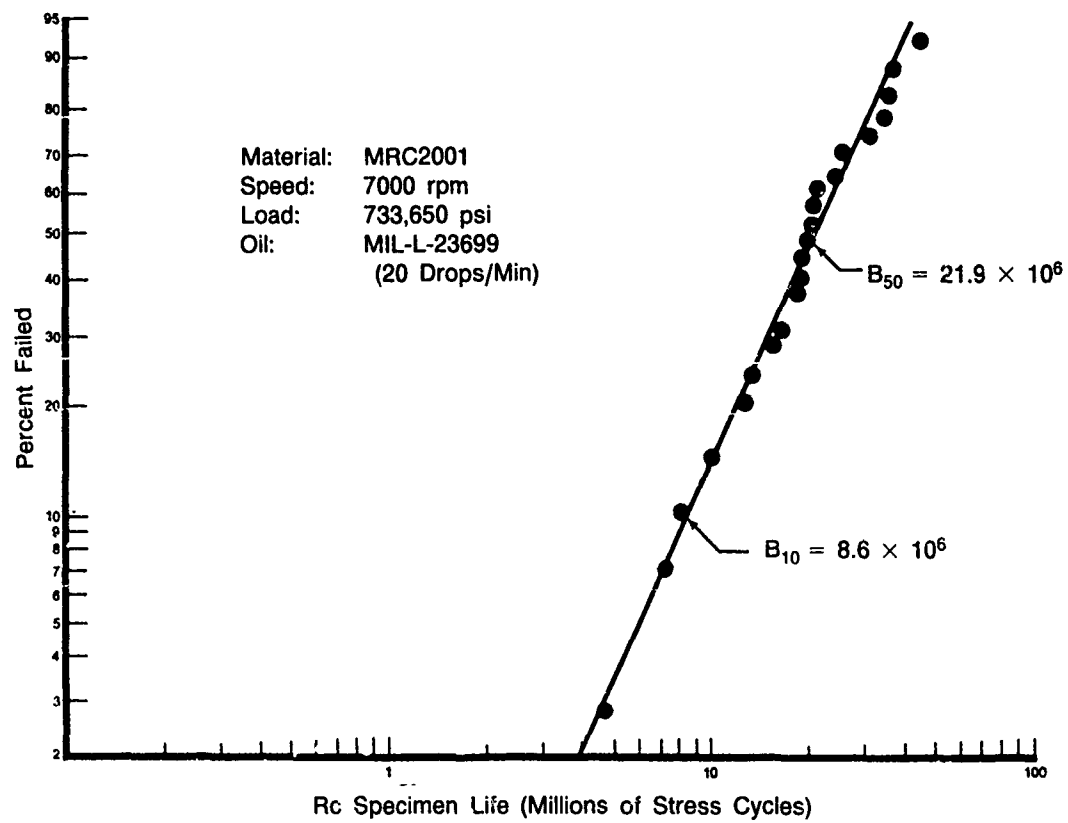
FD 270291

Figure 52. — Weibull Plot of As-Received Armoloy-Coated M50 Rolling Contact Fatigue Test Results



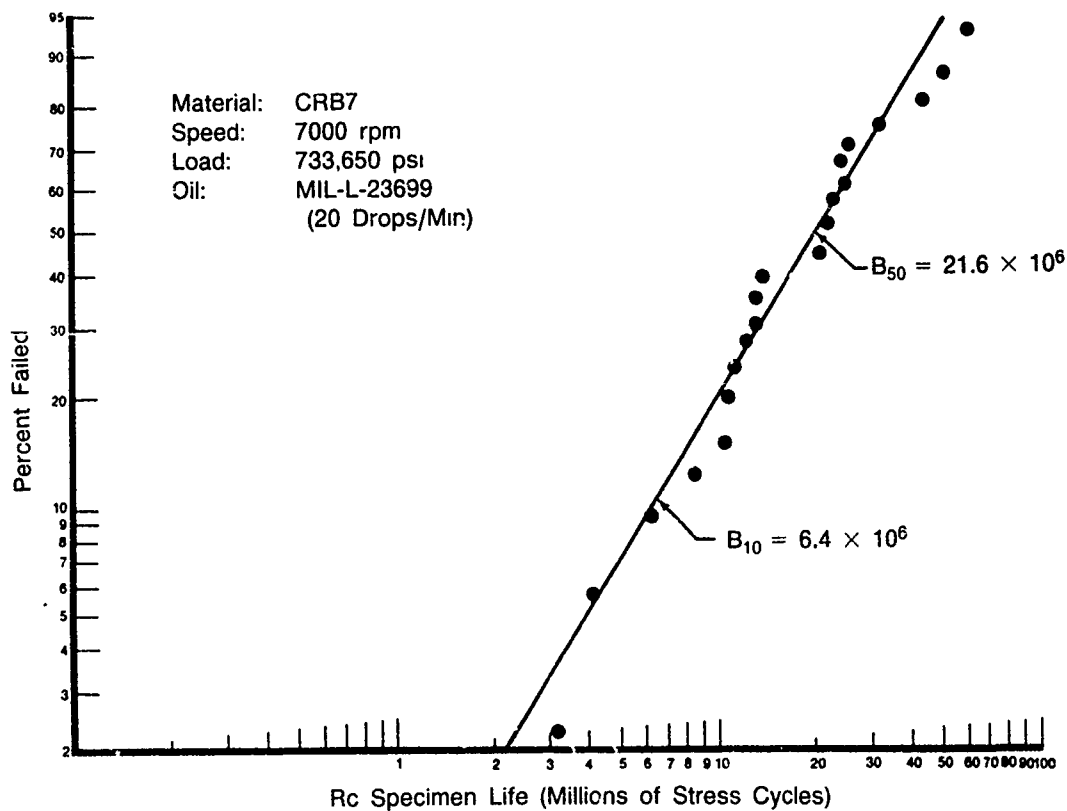
FD 270290

Figure 53. — Weibull Plot of Polished Armoloy-Coated M50 Rolling Contact Fatigue Test Results



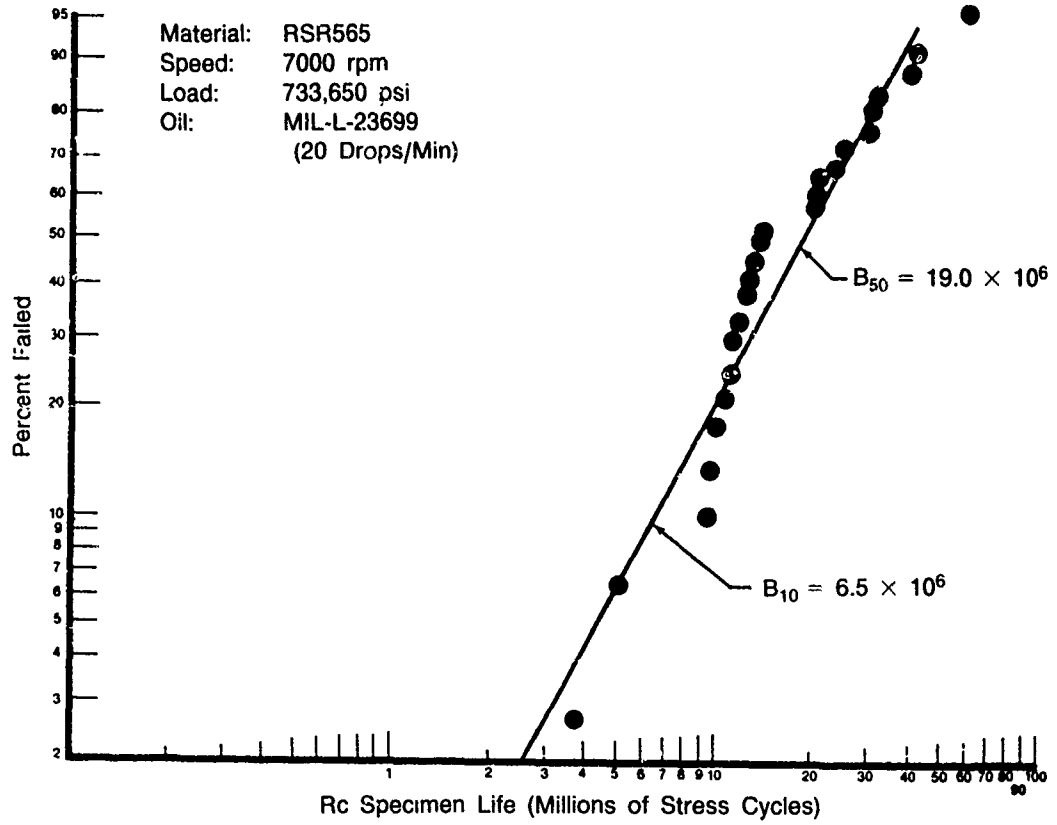
FD 270293

Figure 54. — Weibull Plot of MRC2001 Rolling Contact Fatigue Test Results



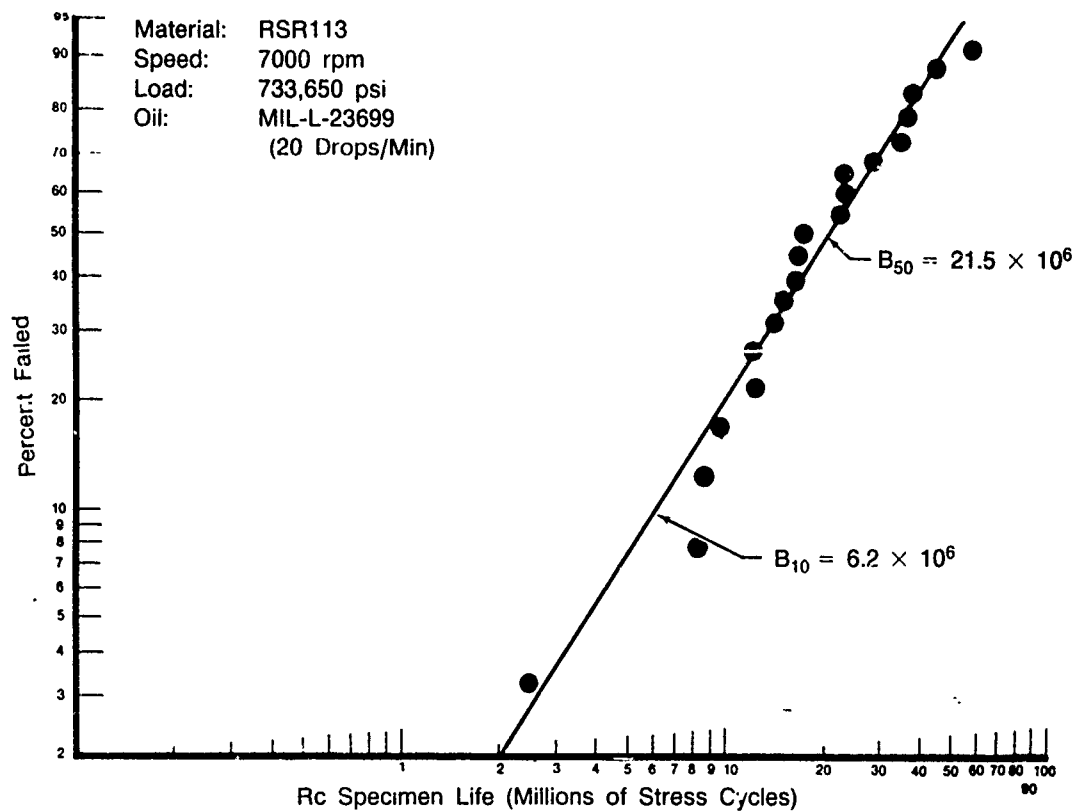
FD 270296

Figure 55. — Weibull Plot of CRB7 Rolling Contact Fatigue Test Results



FD 270295

Figure 56. — Weibull Plot of RSR565 Rolling Contact Fatigue Test Results



FD 270294

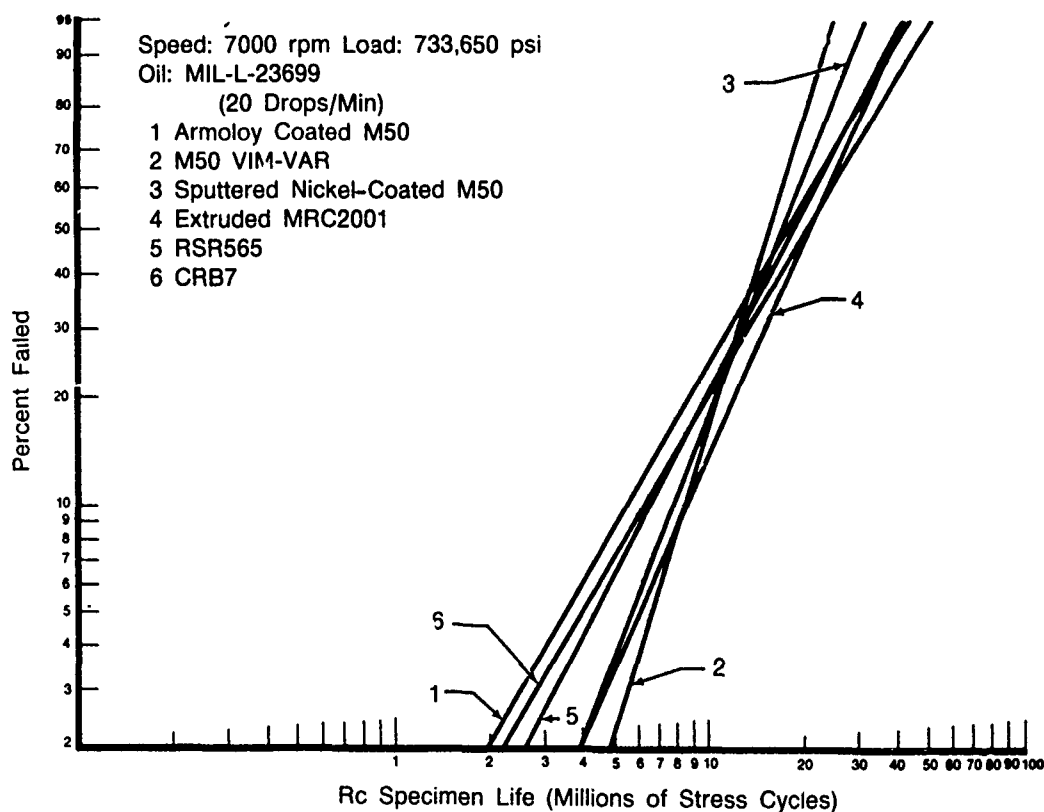
Figure 57. — Weibull Plot of RSR113 Rolling Contact Fatigue Test Results

TABLE 14.

ROLLING CONTACT FATIGUE TEST RESULTS

Candidate Material	Life Stress Cycles — 10^6		Weibull Slope	Life Ratio to M50		Confidence Relative to M50	
	L_{10}	L_{50}		L_{10}	L_{50}	L_{10}	L_{50}
Armloy-Coated M50 — Polished	5.8	20.9	1.47	0.68	1.31	90% Inferior	96% Superior
Armloy-Coated M50 — Unpolished	5.6	18.0	1.60	0.66	1.13	90% Inferior	85% Superior
Nickel Sputter- Coated M50	8.0	17.6	2.37	0.94	1.11	No Significant Difference	85% Superior
MRC2001 Extruded	8.6	21.9	2.01	1.01	1.38	No Significant Difference	98% Superior
RSR113	6.2	21.5	1.52	0.73	1.35	90% Inferior	98% Superior
RSR565	6.5	19.0	1.82	0.78	1.24	80% Inferior	94% Superior
CRB7	6.4	21.6	1.56	0.75	1.36	80% Inferior	98% Superior
Reference M50	8.5	15.9	2.98	1	1		

6.178C



FD 270298

Figure 58. — Composite Weibull Plot of Candidate and VIM-VAR M50 Rolling Contact Fatigue Test Results

None of the candidates were shown, to a high degree of confidence, to be inferior to the M50 L_{10} RCF life although all but MRC2001 had lower measured L_{10} lives. All candidates had higher measured L_{50} lives and three candidates (MRC2001, Armoloy-coated M50, and CRB7) had, to a high degree of confidence, superior L_{50} lives compared to M50. However, the maximum spread in either the L_{10} or L_{50} life relative to M50 was 38 percent. The M50 used in this program was from one heat lot. Given the variability of RCF life between different heat lots and between different hardness values in one heat lot, a 38 percent difference in RCF life is not considered significant.

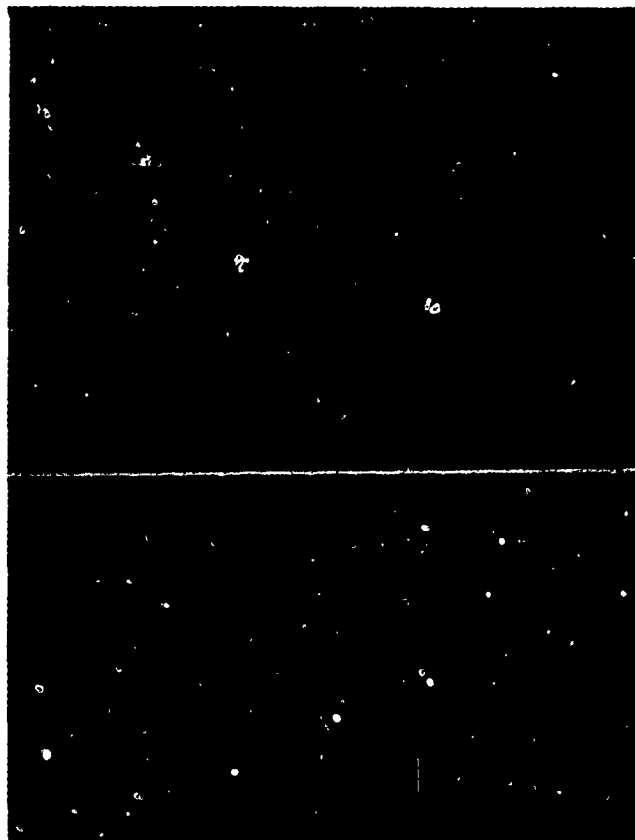
Three nickel sputter-coated bars and 5 Armoloy-coated M50 bars were subjected to SEM and Energy Dispersive X-ray (EDXR) analyses following the fatigue endurance testing of those bars. The purpose of these evaluations was three-fold:

- Determine physical characteristics of roller tracks
- Evaluate integrity of surface treatment in tracks
- Determine uniformity of surface treatments.

The results of the SEM and EDXR analyses are as follows:

- Sputtered nickel does not stand up under the contact pressures of this test. See Figures 59 through 62.

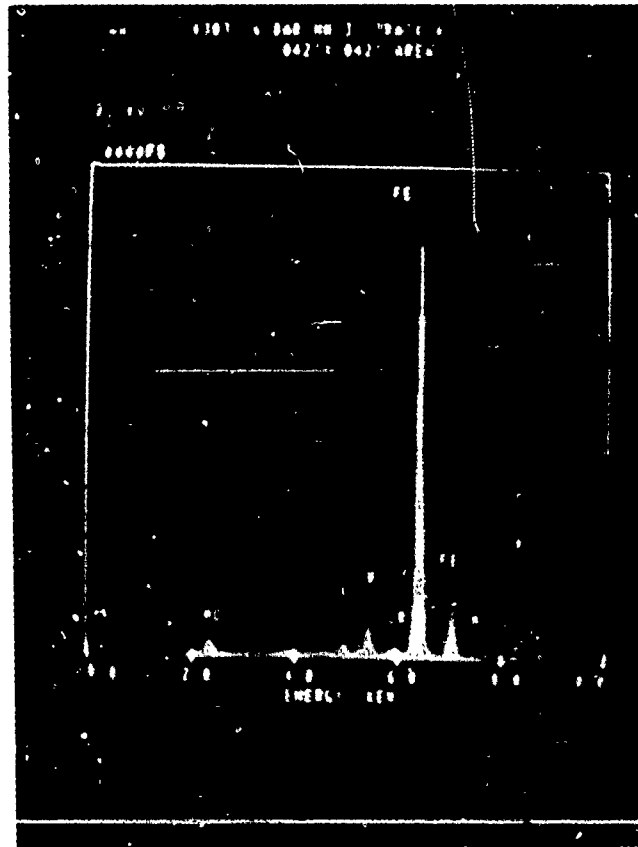
- The chrome plating applied by Armoloy Corporation tends to have a pebbly surface. See Figures 63, 64, and 43.
- The pebbly surface described above, can be removed by polishing. Compare Figures 62, 64, and 43 with Figures 65, 66, and 44. However, EDXR examinations of polished chrome surfaces show some iron. See Figures 67 through 70.
- The chrome plating, polished or unpolished, did not flake or crack under rolling contact.



FC 90354

*Figure 59. — EDXR Analysis of Nickel Sputter-Coated Bar Outside of Roller Track
(Note Nickel Lines)*

Figures 71 through 76 are SEM photographs of typical fatigue spalls from Rc test bars of M50 and five candidate materials. (Nickel sputter-coated M50 is omitted here because the nickel coating has disintegrated from the contact zone before fatigue failure.) The photos demonstrate that the same type of failure mechanism was at work in all materials. Failure initiated at a point, then progressed in a somewhat fan-shaped pattern in the direction of rolling. In Figures 71 and 76, flaking started near the bottom of the photos and progressed toward the top. In Figure 72, failure initiated at the top of the photo. In Figures 73, 74, and 75, spalling progressed from left to right. All show further cracks developing from the spalls. In each case the time lapse from the start of flaking until rig rotation stopped was a matter of seconds.



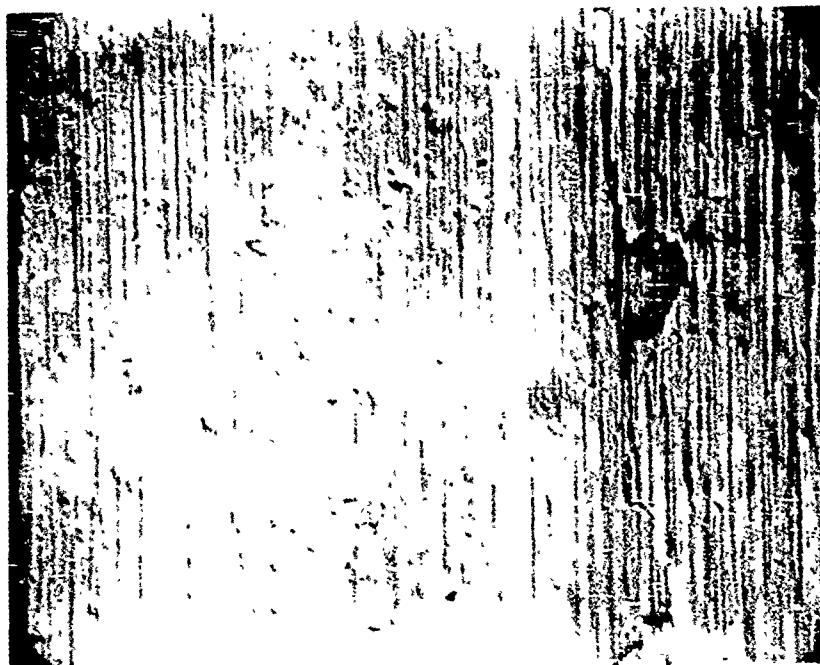
FC 90355

Figure 60. — EDXR Analysis of Nickel Sputter-Coated Bar Roller Track (Nickel Has Been Lost)



FC 90356

Figure 61. — SEM Photomicrograph of Roller Track on Nickel Sputter-Coated Bar HN-2 (Note Flaking; Magnification: 50×)



FC 90357

Figure 62. — SEM Photomicrograph of Roller Track on Nickel Sputter-Coated Bar HN-2 (Magnification: 200×)



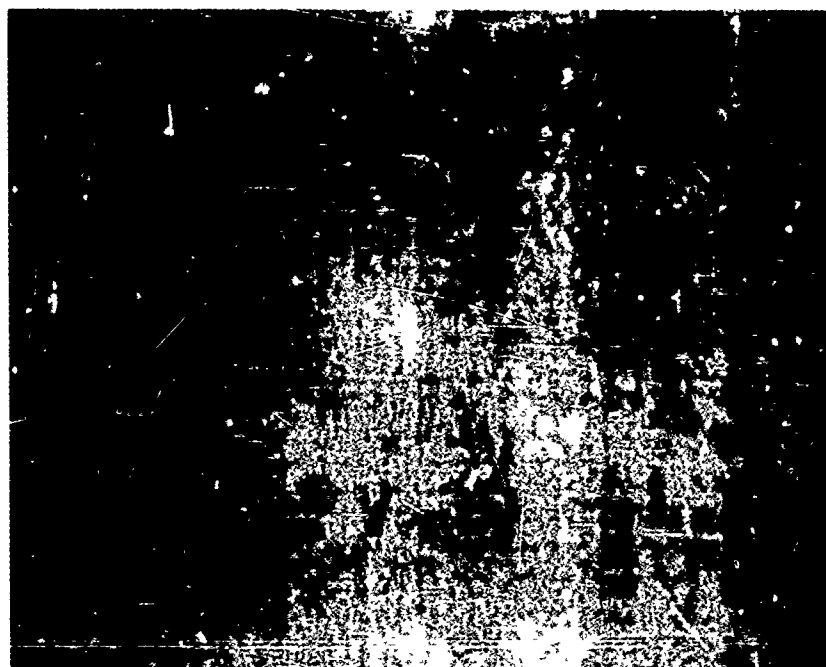
FC 90358

Figure 63. — SEM Photomicrograph of Roller Track No. 3 on Chrome-Plated Bar HA-5
(Note Pebbled Surface Outside of Roller Path; Magnification: 50×)



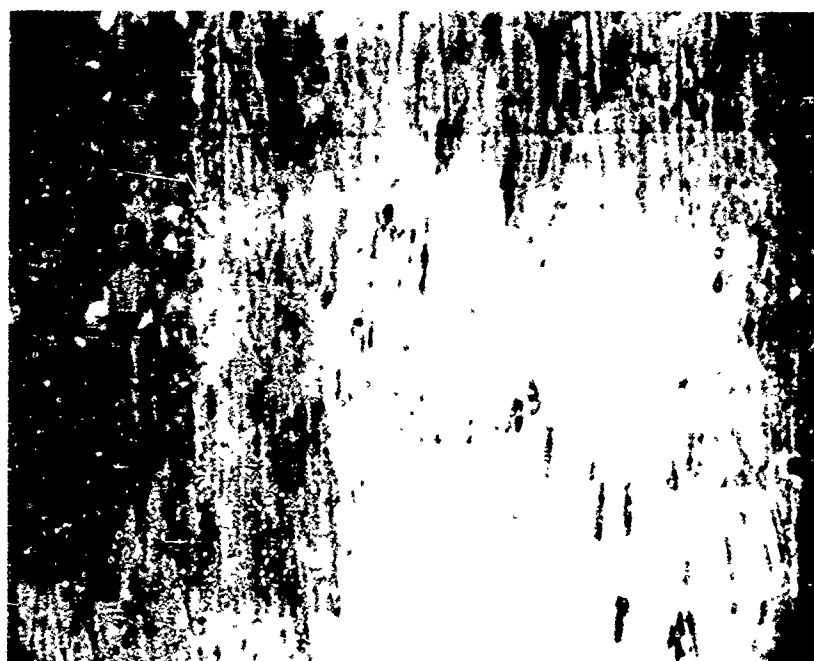
FC 90359

Figure 64. — SEM Photomicrograph of Roller Track No. 3 on Chrome-Plated Bar HA-5
(Note Smeared Surface; Magnification: 200×)



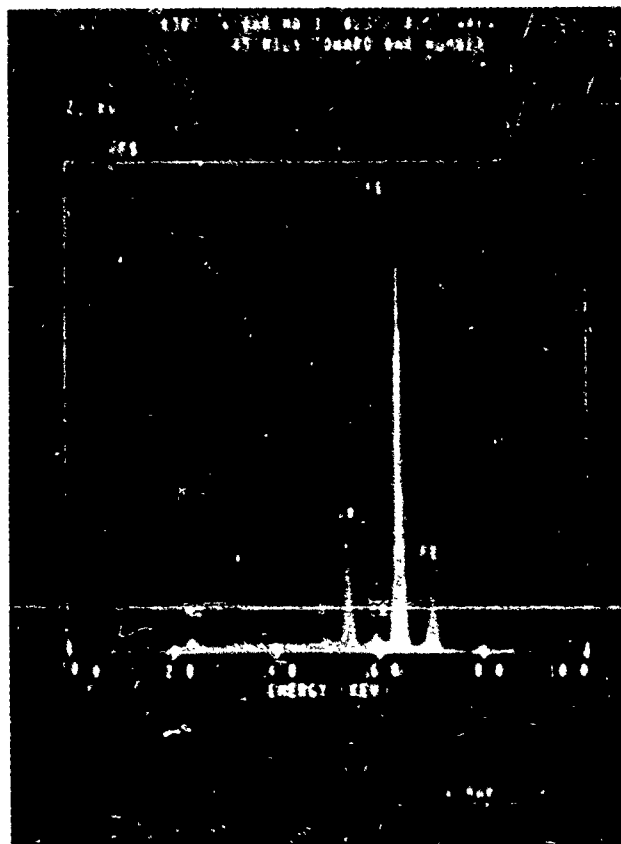
FC 90360

Figure 65. — SEM Photomicrograph of Roller Track No. 6 on Chrome-Plated, Subsequently Polished, Bar HA-3; (Magnification: 50×)



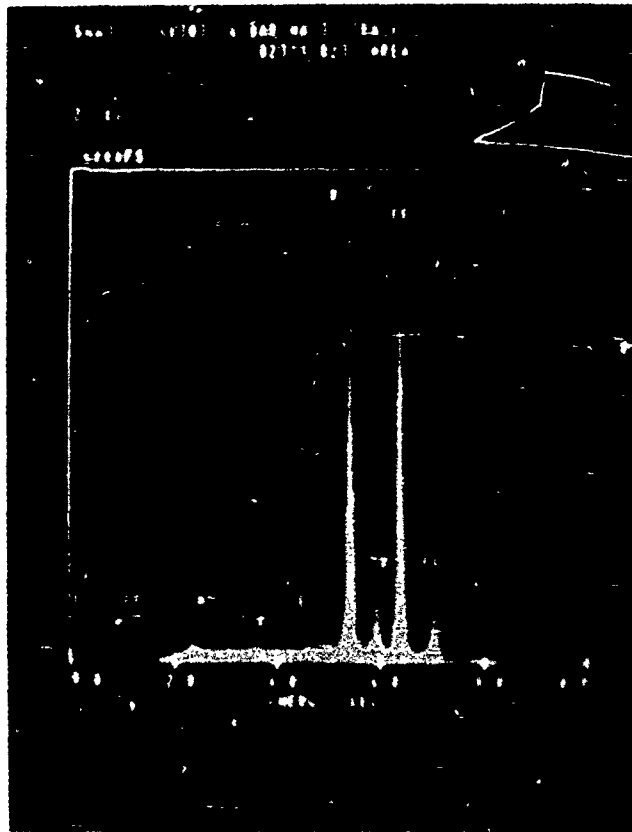
FC 90361

Figure 66 — SEM Photomicrograph of Roller Track No. 6 on Chrome-Plated, Subsequently Polished, Bar HA-3 (Magnification: 200×)



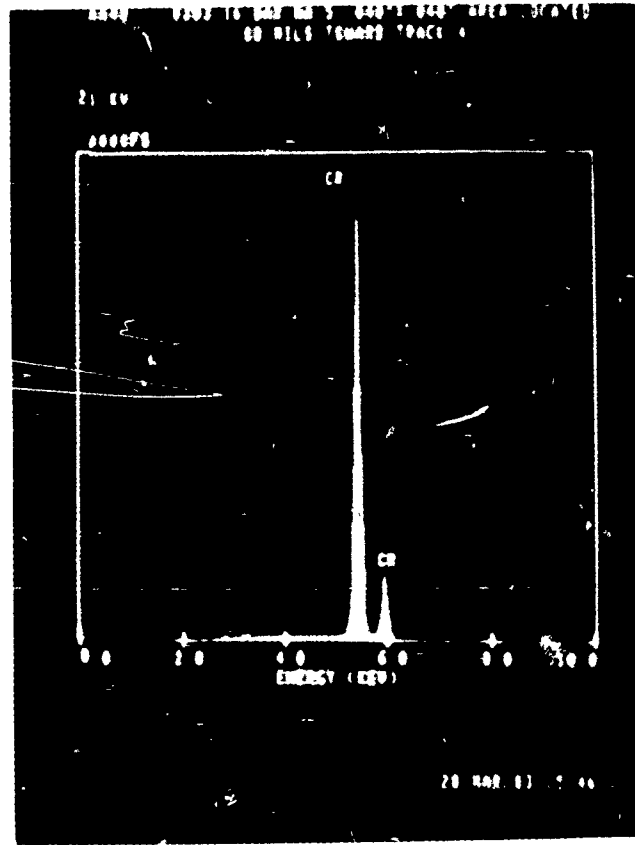
FC 90362

*Figure 67. — EDXR Analysis of Chrome-Plated, Subsequently Polished, Bar HA-3
Outside of Track (Note Iron Lines)*



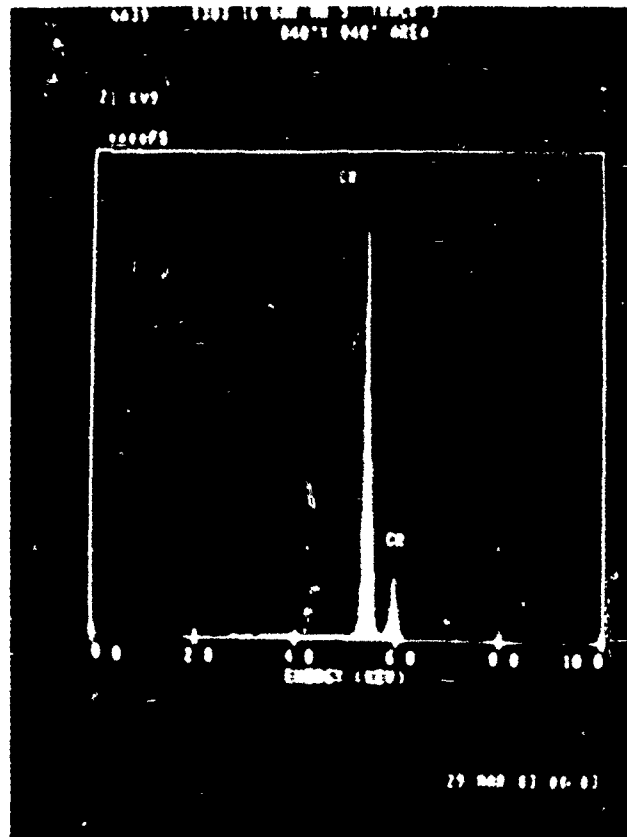
FC 90363

Figure 68. — EDXR Analysis of Chrome-Plated, Subsequently Polished, Bar HA-3 in Track 1 (Note That Iron Is Present but Chrome Is Thicker Than in Figure 67)



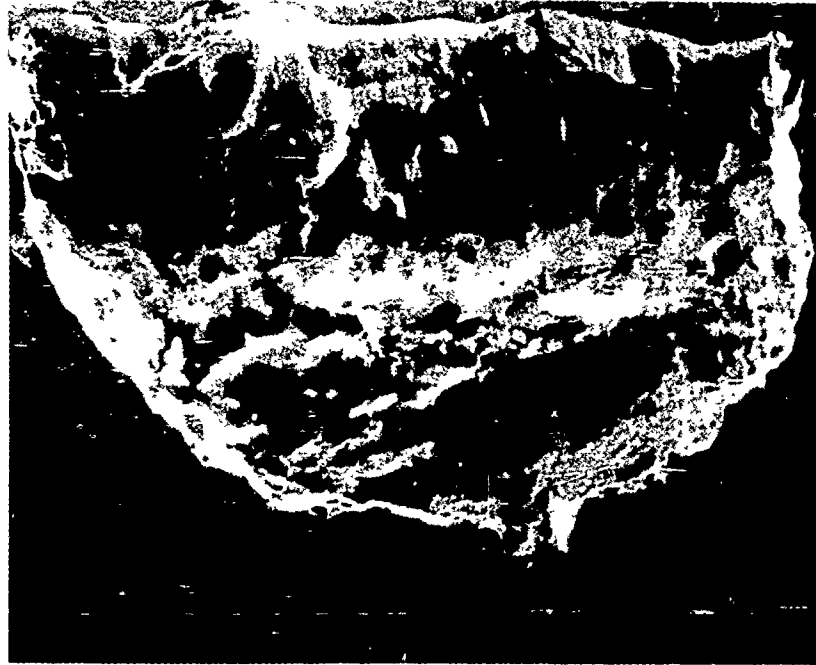
FC 90364

Figure 69. — EDXR Analysis of Chrome-Plated Bar HA-5 Outside of Track



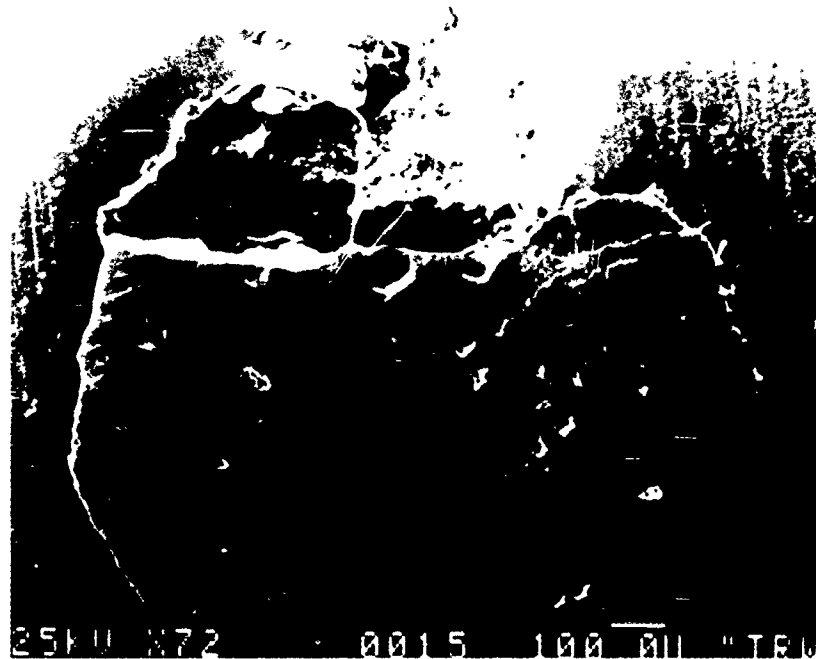
FC 90365

Figure 70. — EDXR Analysis of Chrome-Plated Bar HA-5 in Track 3



FC 90366

Figure 71 — SEM View of Typical Spall in M50 Reference Test Bar H-4
(Magnification: 110X)



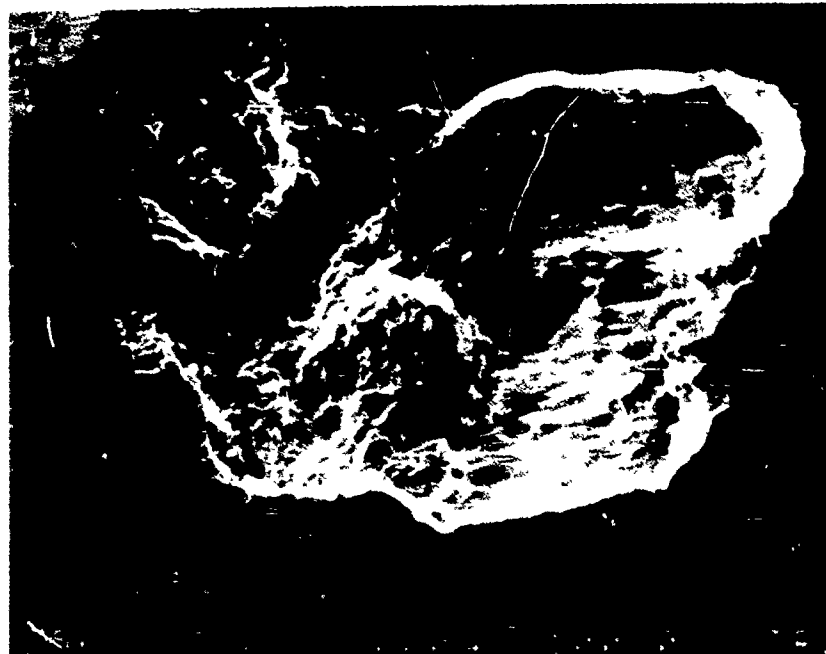
FC 90367

Figure 72 — SEM View of Spall in Chrome-Plated Test Bar HA-1
(Magnification: 72X)



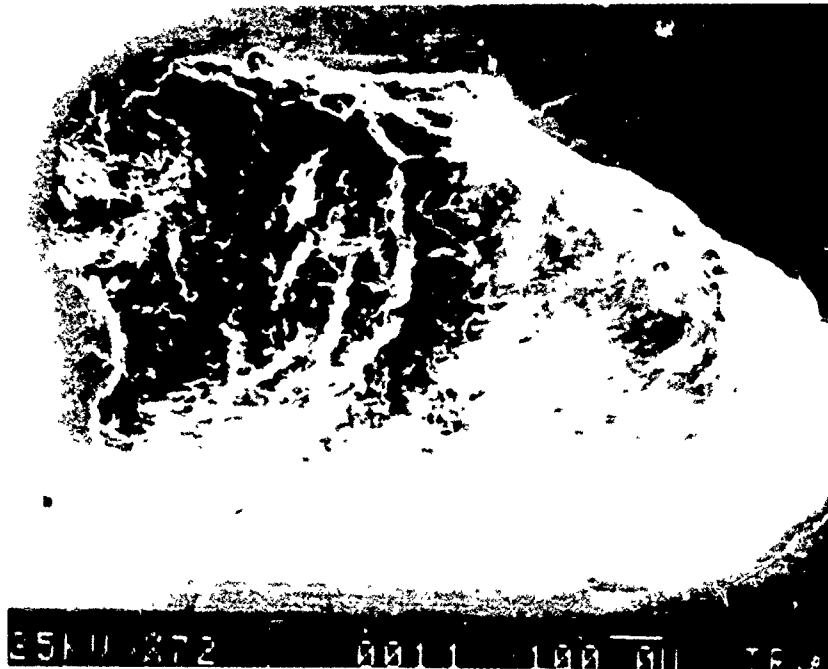
FC 90368

Figure 73. — SEM View of Spall in CRB7 Test Bar HC-2 (Magnification: 72 \times)



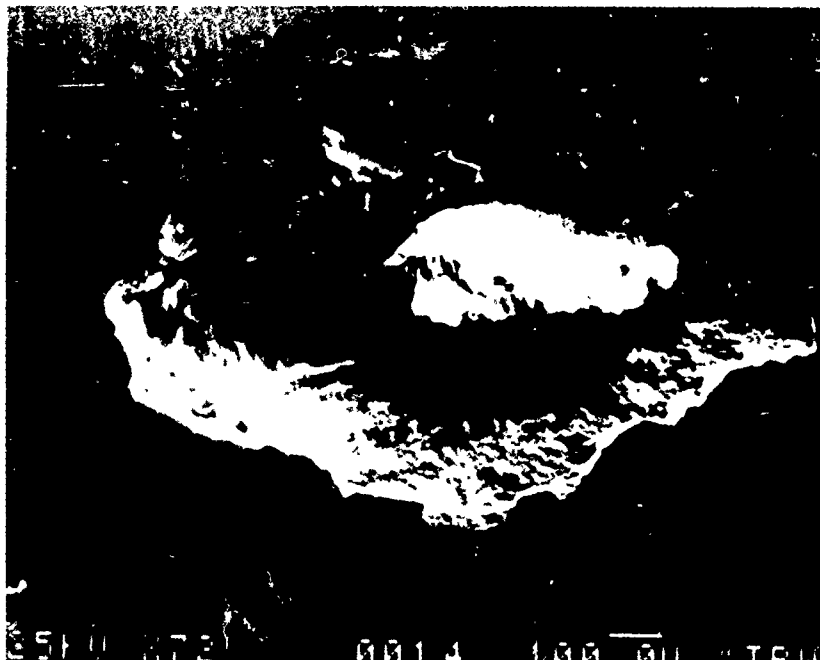
FC 90369

Figure 74. — SEM View of Spall in RSR565 Test Bar HR-1 (Magnification: 72 \times)



FC 90370

Figure 75 — SEM View of Spall in FSR113 Test Bar HB-2 (Magnification: 72X)



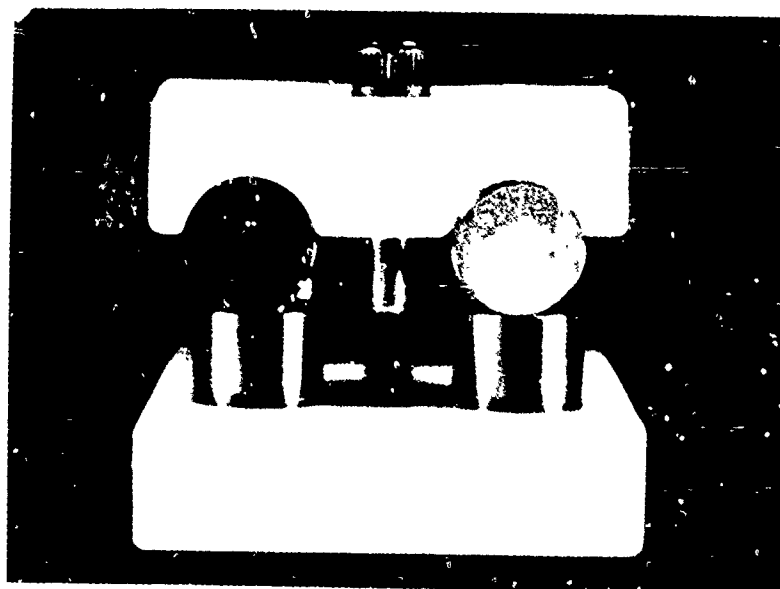
FC 90371

Figure 76 — SEM View of Spall in MRC2001 Test Bar HE-2 (Magnification: 72X)

(2) Corrosion Resistance Testing

Material specimens approximately 0.500 inch in diameter by 0.500-inch long were cleaned in two successive washings in separate baths of toluene, ethanol, hexane, and acetone, in that order. The specimens were allowed to drain between solvent baths. After the final bath the specimens were air dried at 65°C for 10 minutes.

Specimens were installed in fixtures, Figure 77, so that they could be tested in pairs. The cylindrical surface of one specimen was pressed against the flat surface of another. Each pair consisted of like materials. Four pairs were installed in each of six fixtures so that 24 pairs of specimens were tested at a time. Typically, there were three pairs of samples of one material tested simultaneously; these three pairs were spread among the six fixtures so that there was no more than one pair of a particular material in a single fixture.

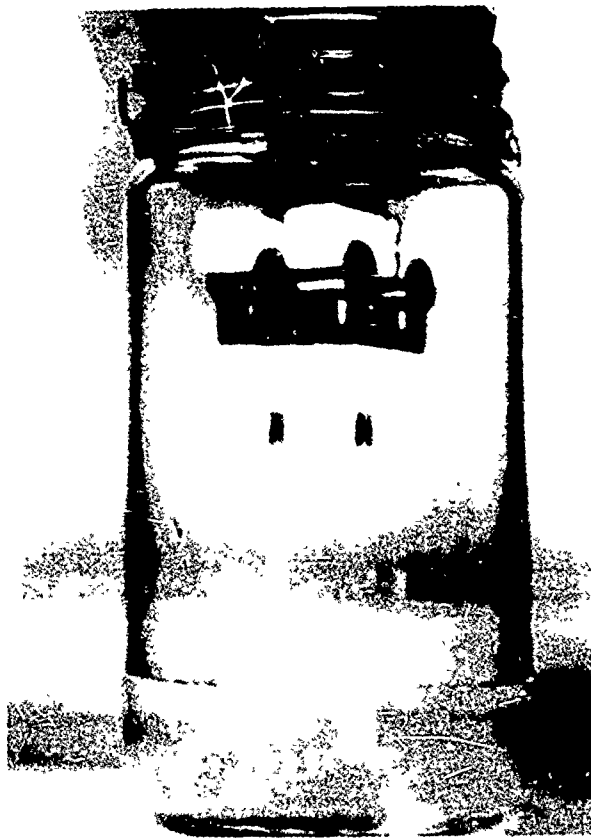


FC 90372

Figure 77 — Corrosion Test Fixture With Four Pairs of Specimens

Using ASTM D665, synthetic seawater with three parts per million (ppm) by weight of chlorides was added to MIL-L-7808H oil. The water content of the lubricant was then adjusted to 600 ppm by weight total by the addition of distilled water. The fixtured test specimens were immersed in the doped lubricant at room temperature and were allowed to soak for one hour, during which time the doped lubricant was agitated periodically. The specimens were then removed from the lubricant and allowed to drain for 30 minutes at ambient temperature.

Corrosion test cells were prepared which consisted of a 1-liter glass bottle fitted with a rubber stopper. A 100 ± 1 ml portion of distilled water was added to each cell. The fixtured test specimens were then hung in the test cells shown in Figure 78 using a corrosion resistant suspension. The cells were loosely closed with a rubber stopper and placed in an oven set at $65^{\circ}\text{C} \pm 1^{\circ}\text{C}$ for 8 hours. The cell was then placed in a refrigerator set at $3^{\circ}\text{C} \pm 2^{\circ}\text{C}$ for 16 hours. This procedure was repeated an additional 13 times. After 14 days of thermal cycling, the specimens were prepared for inspection by cleaning with hexane and acetone and a second set of 24 specimen pairs were subjected to the same test.



FC 90373

Figure 78. — Corrosion Test Setup

Results may be summarized as follows:

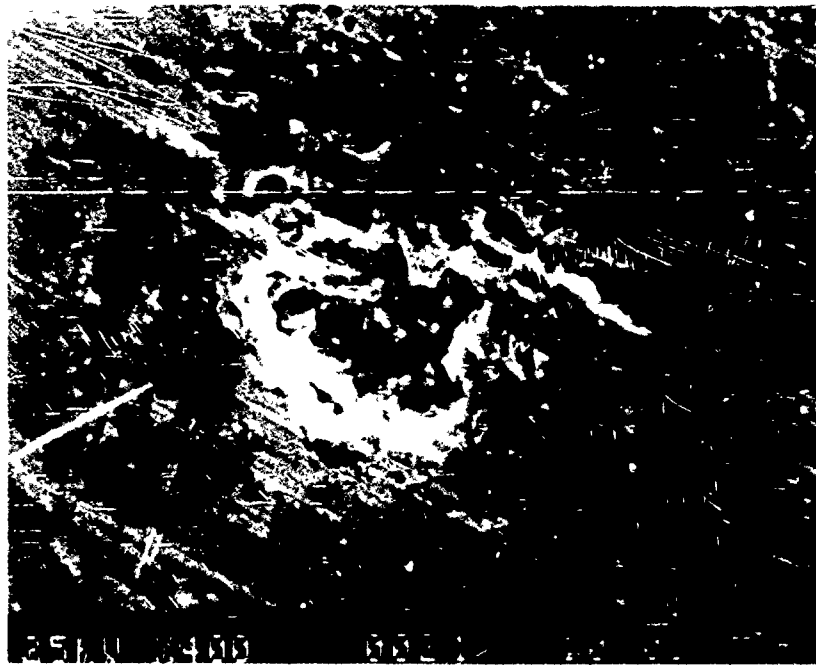
- M50 steel reference specimens experienced the most severe corrosion.
- All other materials and coatings were significantly better than the reference M50 in resisting corrosion at the contact between specimens.
- All coatings appeared to have occasional flaws; corrosion at these flaws was quite marked.
- Changes in specimen weight during the course of corrosion testing were small.
- Many specimens experienced significant corrosion at the contact between the plastic holder and the specimen. This was particularly the case with vertical members of a pair.
- Several vertical specimens experienced corrosion on the upper flat surface, but at a distance from the contact with the horizontal specimen; specimens which were so affected were two M50 reference, one nickel-coated, one chrome-plated, two RSR565, two hipped 2001, and two extruded 2001. In each case, the corrosion was miniscule compared to the corrosion in the contact area.

Figures 79 through 81 show corrosion in the contact meniscus area on specimens 5 and 6. These were reference M50 steel specimens.



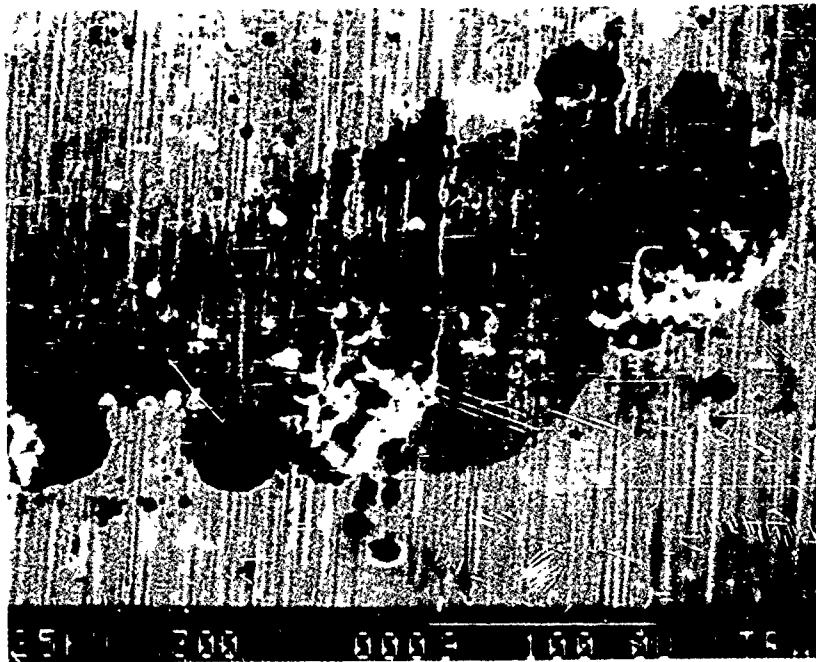
FC 90374

Figure 79. — M50 Reference Specimens 5 and 6



FC 90375

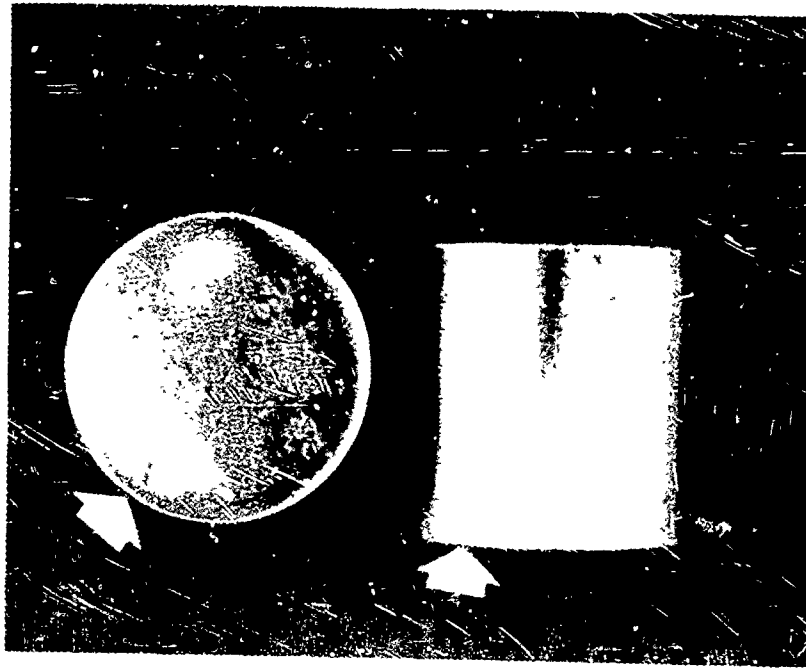
Figure 80. — Stained and Pitted End Surface M50 (Magnification: 400×)



FC 90376

Figure 81 — Stained and Pitted OD Surface M50 (Magnification. 300×)

Figure 82 shows corrosion in the contact meniscus area on specimens 19 and 20. These specimens were chrome plated by Armoloy Corporation. Arrows point to the corrosion indications. The horizontal specimen has a large mark which is not corrosion, but relates to the plating process. Corrosion data are presented in Tables 15 through 21.



FC 90377

Figure 82. — Chrome-Plated Specimens 19 and 20 After Corrosion Test (Arrows Point to Corroded Areas)

TABLE 15.

VIM-VAR M50 CORROSION TEST DATA

Serial Number	Material	Orientation	Corrosion in Miniscus Area (Square Inch)	Weight Change	Corrosion in Other Areas
1	M50	Vertical	0.0100	+0.00016	Severe
2	M50	Horizontal	0.0090	+0.00008	Severe
3	M50	Vertical	0.0135	-0.00003	Severe
4	M50	Horizontal	0.0115	+0.00011	Severe
5	M50	Vertical	0.0225	-0.00003	Severe
6	M50	Horizontal	0.0200	+0.00005	Incidental
51	M50	Vertical	0.000009	-0.00008	Severe
52	M50	Horizontal	0.000007	-0.00003	Severe
53	M50	Vertical	0.000009	+0.00003	Severe
54	M50	Horizontal	0.000007	+0.00010	Severe
55	M50	Vertical	0.000009	-0.00010	Severe
56	M50	Horizontal	None	+0.00022	Incidental
AVERAGE			0.0072	+0.00004	

6533

TABLE 16.

NICKEL SPUTTER-COATED M50 CORROSION TEST DATA

<i>Serial Number</i>	<i>Material</i>	<i>Orientation</i>	<i>Corrosion in Miniscus Area (Square Inch)</i>	<i>Weight Change</i>	<i>Corrosion in Other Areas</i>
7	Nickel-Sputtered	Vertical	None	-0.00002	None
8	Nickel-Sputtered	Horizontal	None	0.00000	None
9	Nickel-Sputtered	Vertical	None	+0.00011	Incidental
10	Nickel-Sputtered	Horizontal	None	+0.00004	None
11	Nickel-Sputtered	Vertical	None	+0.00003	None
12	Nickel-Sputtered	Horizontal	None	0.00000	Incidental
57	Nickel-Sputtered	Vertical	None	+0.00012	Slight
58	Nickel-Sputtered	Horizontal	None	+0.00014	None
59	Nickel-Sputtered	Vertical	None	+0.00022	Slight
60	Nickel-Sputtered	Horizontal	None	+0.00026	Slight
61	Nickel-Sputtered	Vertical	None	+0.00028	None
62	Nickel-Sputtered	Horizontal	None	-0.00002	Severe
AVERAGE			None	+0.00010	

6.17.11

TABLE 17.

ARMOLOY-COATED M50 CORROSION TEST DATA

<i>Serial Number</i>	<i>Material</i>	<i>Orientation</i>	<i>Corrosion in Miniscus Area (Square Inch)</i>	<i>Weight Change</i>	<i>Corrosion in Other Areas</i>
19	Chr. Pl	Vertical	0.0005	+0.00004	Slight
20	Chr. Pl	Horizontal	0.0015	+0.00010	None
21	Chr. Pl.	Vertical	None	+0.00016	Incidental
22	Chr. Pl.	Horizontal	None	+0.00008	Slight
23	Chr. Pl. Polished	Vertical	None	+0.00002	Slight
24	Chr. Pl. Polished	Horizontal	None	+0.00008	Slight
71	Chr. Pl.	Vertical	None	+0.00036	None
72	Chr. Pl.	Horizontal	None	+0.00035	None
73	Chr. Pl.	Vertical	None	+0.00042	None
74	Chr. Pl.	Horizontal	None	+0.00035	Slight
75	Chr. Pl. Polished	Horizontal	None	+0.00032	None
76	Chr. Pl. Polished	Vertical	None	+0.00039	None
AVERAGE			0.00017	+0.00022	

6.17.11

(3) Selection of the Three Candidates for Hot Hardness and Wear Testing

(a) Selection Criteria

At the conclusion of the RCF and corrosion testing, all candidates were ranked according to the following criteria.

- Corrosion resistance
- Rolling contact fatigue

- Hot hardness
- Wear resistance
- Mechanical properties, i.e., strength, HCF, etc.
- Adhesion (coatings only)
- Ability for application without affecting substrate properties (coatings and surface treatments only)
- Suitability for production incorporation in 3 to 5 years
- Cost
- Frugal use of strategic elements
- Environmental impact.

TABLE 18.

CRB7 CORROSION TEST DATA

<i>Serial Number</i>	<i>Material</i>	<i>Orientation</i>	<i>Corrosion in Miniscus Area (Square Inch)</i>	<i>Weight Change</i>	<i>Corrosion in Other Areas</i>
25	CRB7	Vertical	None	-0.00008	Incidental
26	CRB7	Horizontal	None	+0.00004	None
27	CRB7	Vertical	None	-0.00006	Slight
28	CRB7	Horizontal	None	+0.00002	Slight
29	CRB7	Vertical	None	+0.00004	Slight
30	CRB7	Horizontal	None	-0.00008	None
77	CRB7	Vertical	None	+0.00012	None
78	CRB7	Horizontal	None	+0.00010	Slight
79	CRB7	Vertical	None	+0.00026	None
80	CRB7	Horizontal	None	+0.00026	Slight
81	CRB7	Vertical	None	+0.00036	Slight
82	CRB7	Horizontal	None	+0.00026	None
AVERAGE			None	+0.00010	

61710

(b) Candidate Ranking

A point value was assigned to each criteria based on the criteria's relative importance with respect to a state-of-the-art turbine engine bearing application. The candidate ranked best received the maximum point value. The second, third, fourth, and fifth ranked candidates received 80 percent, 60 percent, 40 percent, and 20 percent respectively. Where rank between candidates could not be established the candidates were awarded the same point value. Failure to demonstrate superiority in corrosion resistance and at least equivalence in rolling contact fatigue life, hot hardness, and wear resistance to the M50 baseline was cause to eliminate a candidate from further consideration. Additionally, a coated candidate was eliminated from further consideration if either the coating or coating process was found to be deleterious to the M50 substrate mechanical properties or if a coating failed to adhere during property testing.

TABLE 19.

RSR565 CORROSION TEST DATA

Serial Number	Material	Orientation	Corrosion in Miniscus Area (Square Inch)	Weight Change	Corrosion in Other Areas
31	RSR565	Vertical	None	-0.00021	Incidental
32	RSR565	Horizontal	None	-0.00006	Severe
33	RSR565	Vertical	None	0.00000	Slight
34	RSR565	Horizontal	None	-0.00006	Incidental
35	RSR565	Vertical	None	0.00000	Slight
36	RSR565	Horizontal	None	0.00000	Incidental
83	RSR565	Vertical	None	+0.00013	Incidental
84	RSR565	Horizontal	None	+0.00005	None
85	RSR565	Vertical	None	+0.00010	None
86	RSR565	Horizontal	None	+0.00010	Slight
AVERAGE			None	+0.00000	

647M'

TABLE 20.

MRC2001 CORROSION TEST DATA

Serial Number	Material	Orientation	Corrosion in Miniscus Area (Square Inch)	Weight Change	Corrosion in Other Areas
37	2001-Hipped	Vertical	None	-0.00004	Incidental
38	2001-Hipped	Horizontal	None	-0.00002	None
39	2001-Hipped	Vertical	None	-0.00013	Incidental
40	2001-Hipped	Horizontal	None	-0.00008	Slight
41	2001-Hipped	Vertical	None	-0.00014	Incidental
42	2001-Hipped	Horizontal	None	-0.00022	None
87	2001-Hipped	Vertical	None	+0.00035	Slight
88	2001-Hipped	Horizontal	None	+0.00030	None
89	2001-Hipped	Vertical	None	+0.00034	Incidental
90	2001-Hipped	Horizontal	None	+0.00025	Slight
AVERAGE			None	+0.00005	
43	2001-Extruded	Vertical	None	-0.00034	Incidental
44	2001-Extruded	Horizontal	None	0.00000	None
45	2001-Extruded	Vertical	None	-0.00027	Severe
46	2001-Extruded	Horizontal	None	-0.00007	Incidental
91	2001-Extruded	Vertical	None	+0.00042	Incidental
92	2001-Extruded	Horizontal	None	+0.00046	Incidental
AVERAGE			None	+0.00002	

647M'

- *Rolling Contact Fatigue — 15 Points Maximum*

No significant differences between candidates or between candidates and the M50 baseline. Points were not awarded for this criteria.

TABLE 21.

RSR113 COPROSION TEST DATA

<i>Serial Number</i>	<i>Material</i>	<i>Orientation</i>	<i>Corrosion in Miniscus Area (Square Inch)</i>	<i>Weight Change</i>	<i>Corrosion in Other Areas</i>
47	RSR113	Vertical	None	-0.00042	Slight
48	RSR113	Horizontal	None	-0.00034	None
93	RSR113	Vertical	None	+0.00026	Slight
94	RSR113	Horizontal	None	+0.00026	Slight
95	RSR113	Vertical	None	+0.00024	None
96	RSR113	Horizontal	None	+0.00018	Slight
97	RSR113	Vertical	None	+0.00026	Slight
98	RSR113	Horizontal	None	+0.00036	None
AVERAGE			None	+0.00007	

6.17 K

● *Corrosion Resistance — 15 Points Maximum*

All candidates were judged superior to M50. MRC2001, RSR565, CRB7, and the nickel sputter coating had virtually no corrosion and were judged equal. Armoloy-coated M50, while superior to M50, was slightly less corrosion resistant than the other four candidates as follows:

- MRC2001 — 15 points
- RSR565 — 15 points
- CRB7 — 15 points
- Nickel sputter-coated M50 — 15 points
- Armoloy-coated M50 — 12 points.

● *Hot Hardness — 15 Points Maximum*

● *Wear Resistance — 15 Points Maximum*

Points were not awarded pending hot hardness and wear resistance test results.

● *Coating Adhesion — 15 Points Maximum*

All alloy candidates were awarded maximum points. The Armoloy-coated candidate did not exhibit any sign of cracking or peeling under rolling contact. The nickel sputter-coated candidate was eliminated from further consideration because it failed to adhere under rolling contact. Points were awarded as follows:

- RSR565 — 15 points
- MRC2001 — 15 points
- CRB7 — 15 points
- Armoloy-coated M50 — 15 points
- Nickel sputter-coated M50 — 0 points.

● *Coating Application Without Affecting Substrate Properties — 15 Points Maximum*

All alloy candidates were awarded the maximum points. Both coating processes expose the substrate to conditions which, while not demonstrated in this program, could be deleterious to the substrate material properties, i.e., Armoloy-hydrogen embrittlement; nickel sputtering — elevated substrate temperatures. Points were awarded as follows:

- CRB7 — 15 points
- MRC2001 — 15 points
- RSR565 — 15 points
- Armoloy-coated M50 — 2 points
- Nickel sputter-coated M50 — 12 points.

● *Other Mechanical Properties (High Cycle Fatigue, Strength, Fracture Toughness, etc.) — 10 Points Maximum*

Lacking data to the contrary all candidates were judged equivalent to M50 and points were not awarded for this criteria.

● *Three- to Five-Year Production Incorporation — 10 Points Maximum Candidates Were Ranked in the Following Order:*

CRB7 — 10 Points

Wrought CRB7 is an existing commercially available bearing alloy.

Armoloy-Coated M50 — 8 Points

Armoloy is an existing commercially available plating process. However, before being qualified for production turbine engine bearing applications, the process would require some development to ensure process uniformity.

MRC2001 — 6 Points

MRC2001 is fabricated using a commercially available powder processing technique, however, the powder consolidation processes will require development.

RSR565 — 4 Points

Both the powder fabrication and consolidation processes will require development. The powder fabrication capacity would limit early usage.

Nickel Sputter-Coated M50 — 2 Points

The sputter coating process would require considerable development. The processing capacity is very limited and the impact of the process on substrate properties is not defined.

● *Cost — 10 Points Maximum*

Candidates were ranked in the following order:

Armoloy-Coated M50 — 10 Points

The Armoloy-coated candidate was considered the least costly of the candidates. The plating process and associated process controls would result in a modest increase in cost compared to uncoated M50 material.

CRB7 — 8 Points

CRB7 has a higher chrome content and a lower machinability compared to M50.

MRC2001 — 6 Points

The powder fabrication and consolidation processes as well as higher chrome and alloy content would increase costs over the above candidates.

RSR565 — 4 Points

RSR565 contains 4 percent cobalt and has a higher chrome content than M50. The RSR powder fabrication process is also somewhat more costly than other powder fabrication techniques.

Nickel Sputter-Coated M50 — 2 Points

The coating process and associated quality control would require added costly manual operations.

● *Frugal Use of Strategic Elements — 5 Points Maximum*

Nickel Sputter-Coated M50 — 5 Points

(4.25 Cr, 0.8 C, 1.0 V, 4.25 Mo, 0.24 Mn, Fe)

Armoloy-Coated M50 — 4 Points

(4.25 Cr, 0.8 C, 1.0 V, 4.25 Mo, 0.24 Mn, Fe)

CRB7 — 3 Points

(14.0 Cr, 1.11 C, 1.06 V, 2.07 Mo, 0.43 Mn, 0.29 Si, Fe)

MRC2001 — 2 Points

(15.2 Cr, 1.51 C, 1.81 V, 6.74 Mo, 0.32 Mn, 0.1 Si, Fe)

RSR565 — 1 Point

(9 Cr, 1 C, 1 V, 2 Mo, 4 Co)

● *Environmental Impact — 5 Points Maximum*

The Armoloy-coated M50 candidate was rated fifth because of the attendant treatment and disposal of the chrome plating baths. The first four candidates are rated in order of their anticipated energy consumption as follows:

Nickel Sputter-Coated M50 — 5 Points
CRB7 — 4 points
MRC2001 — 3 points
RSR565 — 2 points
Armoloy-Coated M50 — 1 point.

Based on the above evaluations MRC2001, Armoloy-coated M50, and CRB7 were selected as the three most promising candidates for wear resistance and hot hardness testing. A summary of the ranking criteria results is presented in Table 22.

(A) ***Wear Resistance Testing***

Rolling contact bearings are subject to some sliding contacts which promote wear. A ball rolling on a raceway under angular contact, a roller contacting the flanges of the guiding race, balls or rollers pushing against cage pockets, and raceway shoulders contacting cage bores or ODs are all examples of sliding action. Thus, a bearing material must accept sliding with minimum wear.

To evaluate wear resistance of candidate materials, a cross cylinder wear apparatus was used. Figure 83 shows the rig schematically, while Figure 84 is a photograph of the rig. Essentially, a half-inch diameter cylinder was rotated against a fixed half-inch diameter rod, with axes inclined 90 degrees to each other. In representing the sliding effect of a ball on a race, or a roller against raceway flanges, cylinders of the same material were run against each other. In representing the action of bearing steel against cage material, a silver plated AMS6415 bar was rotated against a bar of the candidate material. Because aircraft bearing contacts are lubricated, wear tests were conducted in the presence of MIL-L-7808 oil.

Test conditions may be summarized as follows:

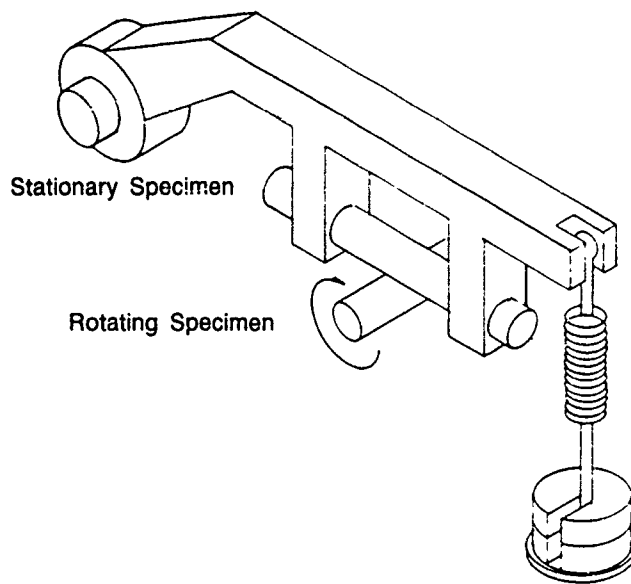
- Specimen size — 0.500 + 0.0015 inch diameter × 3 inches long
- Surface finish — 4 to 6 microinches, except Armoloy-coated M50 (reference Section II.3.C(1) paragraph 3)
- Rotating speed — 1200 rpm
- Applied load — 25 pounds on load arm
- Lubrication — MIL-L-7808 oil, applied by contacting wick
- Duration — 5 minutes per test.

The effective load on the contact was 53 pounds, due to mechanical advantage of the rig and weight of the load arm. This resulted in a maximum Hz stress at the start of a test of 340,000 psi. Stress reduced rapidly, but at an indeterminate rate as wear increased the contact area.

TABLE 22. TASK III RANKING SUMMARY

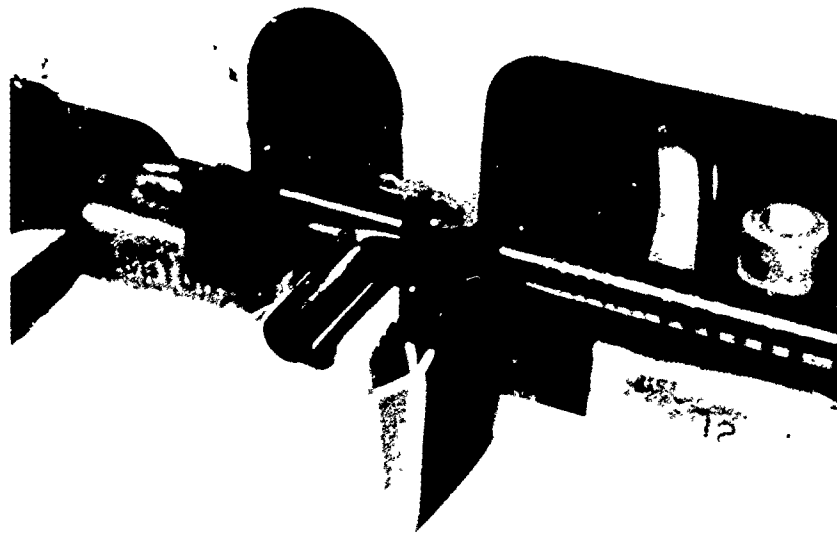
Maximum Points	Task 3			Task 4			Tasks 3 & 4							Total				
	15	15	15	15	15	15	10	10	10	15	15	15	10		10	5	5	5
	RCF	Corrosion	Hot Hardness	Wear	Mechanical Properties	Adhesion	Appl. W/O Affecting Properties	3-5 Years Production Incorporation	Cost	Strategic Elements	Environmental Impact							
CRE7	*	15		*	15	15	10	15	15	15	15	10	10	6	3	4		Task 3 Total - 70
MRC2001	*	15		*	15	15	10	15	15	15	15	10	10	6	2	3		Task 3 Total - 62
RSR 565	*	15		*	15	15	10	15	15	15	15	10	10	4	1	2		Eliminated in Task 3 Candidate Selection Based on Point Rank (Task 3 Total - 56)
Armoloy	*	12		*	15	15	10	15	15	15	15	10	10	4	1	1		Task 3 Total - 62
Sputtered Ni	*	15		*	15	15	10	15	15	15	15	10	10	2	5	5		Eliminated; Coating Failed During Task 3 RCF Tests

* No Significant Difference



FD 216726

Figure 83. — Schematic of Wear Test Apparatus

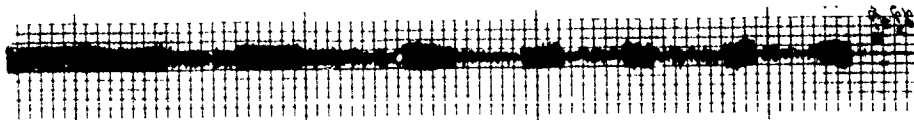


FC 90378

Figure 84. — Wear Test Rig Showing Wick Lubrication

The rotating bar produced an elliptical wear scar on the stationary bar. When like materials were run together, this scar became practically round. When silver plated bars were run against test bars, the scars on the test bars were very small and elliptical in shape. Before and after each test, both rotating and stationary bars were weighed to the nearest 0.0001 gram to determine change in mass.

An accelerometer was mounted on the load arm directly above the contact between the two bars. The output of the accelerometer, as charted by a Brush recorder, produced a measure of the stick-slip behavior of the materials (Figures 85 and 86).



M50 vs M50 Run 5



Armoloy Coated M50 vs Armoloy Coated M50 Run 3



MRC2001 vs MRC2001 Run 4



CRB7 vs CRB7 Run 3



RSR565 vs RSR565 Run 2

FD 270308

Figure 85 — Sample Traces of Vibration Data From Wear Tests

Wear test changes in mass are presented in Table 23 and summarized in Table 24. The most significant changes were those of the stationary specimens when like materials were run against each other; the changes in stationary specimen mass are shown graphically in Figure 87.



M50 vs Ag-Plated AMS 6415 Run 2



Armoloy Coated M50 vs Ag-Plated AMS 6415 Run 5



MRC 2001 vs Ag-Plated AMS 6415 Run 2



CRB7 vs Ag-Plated AMS 6415 Run 2



RSR 565 vs Ag-Plated AMS 6415 Run 3

FD 270309

Figure 86. --- Sample Traces of Vibration Data From Wear Tests

TABLE 23.

WEAR TEST DATA

Test No	Wt Loss Stationary (gm)	Wt Loss Rotating (gm)	Wt Loss Stationary (gm)	Wt Loss Rotating (gm)
<i>M50 vs M50</i>				
1	0.0040	0.0020 (gain)	0.0007 (gain)	0.0029
2	0.0049	0.0008 (gain)	0.0010	0.0026
3	0.0055	0.0003	0.0002	0.0031
4	0.0112	0.0020	0.0001	0.0012
5	0.0087	0.0007	0.0002	0.0045
6	0.0112	0.0006 (gain)	0.0002	0.0024
<i>M50 vs Silver-Plated AMS 6415</i>				
1	0.0121	0.0008	0.0003	0.0027
2	0.0193	0.0050	0.0001	0.0037
3	0.0142	0.0002	0.0001	0.0028
4	0.0174	0.0022	0.0009	0.0040
5	0.0135	0.0062	0.0005	0.0034
6	0.0161	0.0046	0.0009 (gain)	0.0026
<i>Armoloyed M50 vs Armoloyed M50</i>				
<i>Armoloyed M50 vs Silver-Plated AMS 6415</i>				
1	0.0415	0.0034	0.0002	0.0012
2	0.0317	0.0017 (gain)	0.0001 (gain)	0.0006
3	0.0407	0.0031	0.0005	0.0015
4	0.0314	0.0004 (gain)	0.0003	0.0033
5	0.0400	0.0046	0.0003 (gain)	0.0002
6	0.0508	0.0019 (gain)	0.0011	0.0027
<i>CRB7 vs CRB7</i>				
<i>CRB7 vs Silver-Plated AMS 6415</i>				
<i>MRC2001 vs MRC2001</i>				
<i>MRC2001 vs Silver-Plated AMS 6415</i>				
1	0.0062	0.0028	0.0006	0.0026
2	0.0011 (gain)	0.0008 (gain)	0.0001 (gain)	0.0030
3	0.0038	0.0011 (gain)	0.0002	0.0020
4	0.0040	0.0038 (gain)	0.0011 (gain)	0.0007
5	0.0043	0.0023	0.0023	0.0027
6	0.0001 (gain)	0.0009 (gain)	0.0012	0.0049
7	0.0047	0.0023		
8	0.0034	0.0017		
<i>RSR565 vs RSR565</i>				
<i>RSR565 vs Silver-Plated AMS 6415</i>				
1	0.0438	0.0004	0.0003	0.0003 (gain)
2	0.0346	0.0008 (gain)	0.0009	0.0037
3	0.0684	0.0046 (gain)	0.0005 (gain)	0.0034
4	0.0535	0.0010 (gain)	0.0015	0.0002
5	0.0532	0.0023 (gain)	0.0002	0.0020
6	0.0527	0.0001 (gain)	0.0013 (gain)	0.0034

6378

TABLE 24.
WEAR TEST RESULTS SUMMARY

Candidate	Weight Loss	
	Stationary Element	Rotating Element
<i>Candidate vs Candidate</i>		
MRC2001	0.0032 Gram Average	(-) 0.0003 Gram Average
M50	0.0076 Gram Average	(+) 0.0001 Gram Average
Armoloy-Coated M50	0.0154 Gram Average	(-) 0.0032 Gram Average
CRB7	0.0394 Gram Average	(-) 0.0012 Gram Average
RSR565	0.0510 Gram Average	(+) 0.0014 Gram Average
<i>Candidate vs Silver-Plated 4340</i>		
MRC2001	0.0005 Gram Average	(-) 0.0026 Gram Average
M50	0.0002 Gram Average	(-) 0.0028 Gram Average
Armoloy-Coated M50	0.0002 Gram Average	(-) 0.0032 Gram Average
CRB7	0.0003 Gram Average	(-) 0.0016 Gram Average
RSR565	0.0002 Gram Average	(-) 0.0021 Gram Average

6.17.87

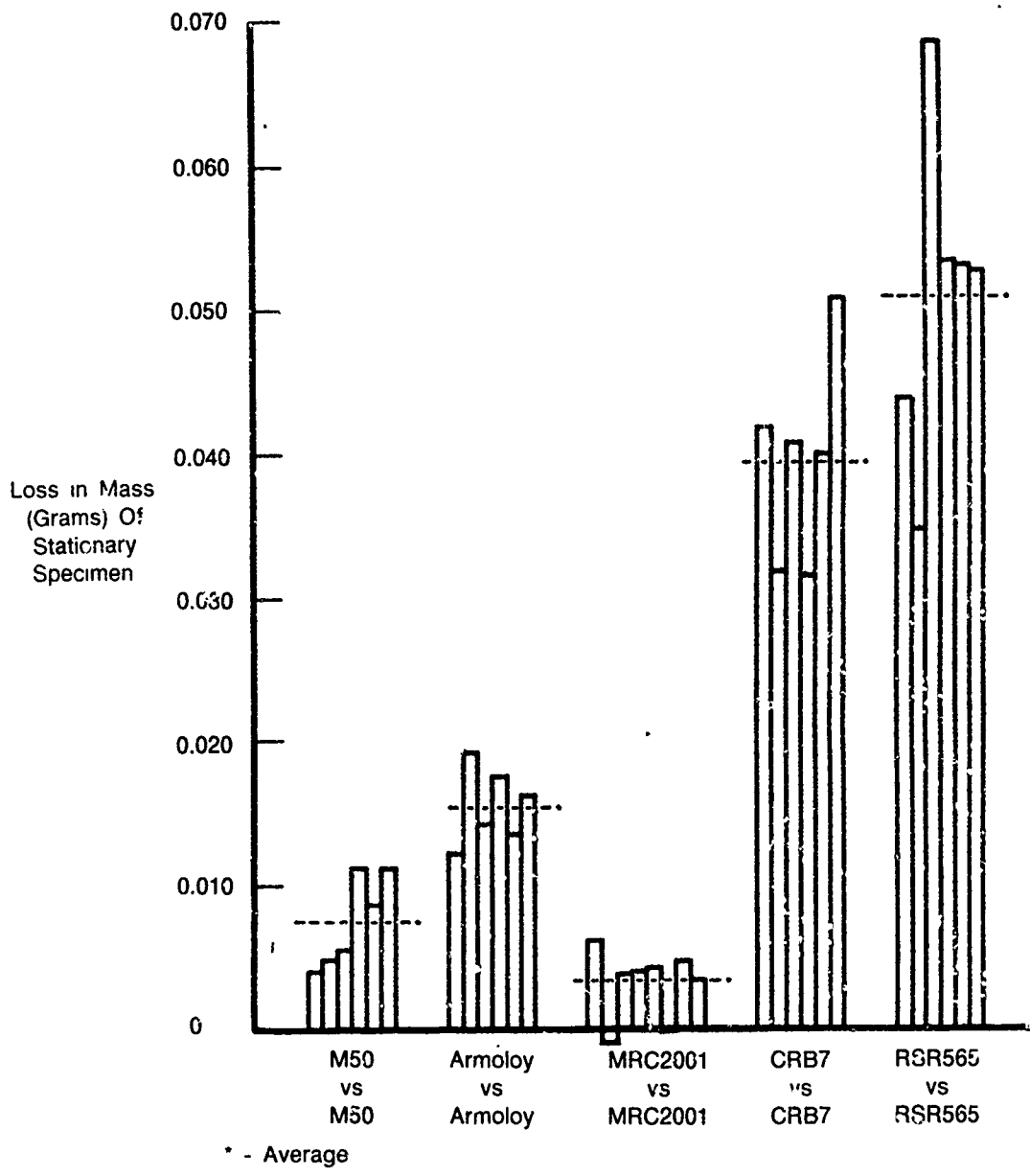
Based on this weight loss data, materials may be ranked in the following order:

- MRC2001 (best, with least material loss)
- M50 Baseline
- Armoloy-coated M50
- CRB7
- RSR565.

The difference in performance between the M50 reference material and the Armoloy-coated M50 is believed to be the slightly rougher, pebbly surface of the Armoloy coating; the chrome surface of the rotating bar cut through the chrome surface of the stationary bar and then tended to abrade the M50 base material.

Changes in mass of rotating bars were all small, with little difference between materials. When silver-plated AMS6415 bars were run against test materials, mass changes in test bars and silver-plated bars were very small, but with generally greater changes occurring in the rotating, silver-plated bars than in the stationary bars. Silver plate had been applied to the AMS6415 steel 0.0005 to 0.0015 inch thick per AMS2412, corresponding to the normal processing of steel cages. While these data provide little means of contrasting wear resistance in the test materials, they demonstrate that silver plate is an effective boundary lubricant.

Figures 88 and 89 are photographs of wear test bars, or sections of wear bars, showing representative wear scars on the stationary specimens. It was necessary to use some of the bars for hot hardness tests following completion of wear tests. The Armoloy-coated specimen and the RSR565 specimen in Figure 89 were sectioned from the original bars and heated; thus, the wear scars are somewhat darkened. The M50 reference bar, as shown in Figure 89, was sectioned to permit insertion into our Scanning Electron Microscope. These photos demonstrate the difference in size of wear scars on the several materials.



FD 270301

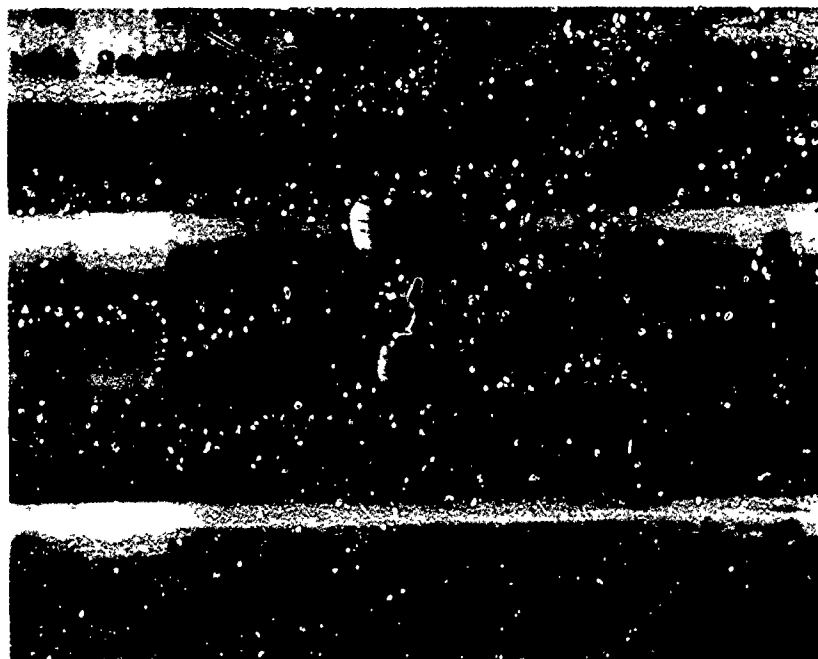
Figure 87 — Bar Chart Showing Mass Change of Stationary Specimens Used in Candidate vs Candidate Wear Tests

Figures 90 and 91 are photographs of rotating wear test bars, showing difference in width of the tracks. These widths correspond to diameters of the wear scars on the stationary bars with which they were associated.



FC 90344

Figure 88 — Sections of Wear Test Bars Showing Representative Scars on M50, Armoloy-Coated M50, and RSR565 Material (Latter Two Bars Were Also Subjected to Hot Hardness Tests)



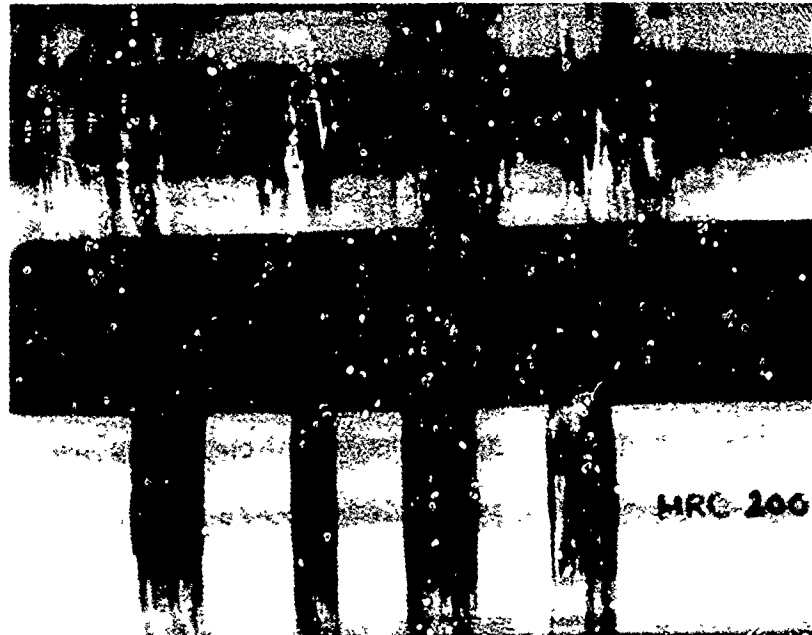
FC 90343

Figure 89 — Wear Test Bars Showing Representative Scars on MRC2001, CRB7, and M50 Material (Scale Magnification Approximately 2.5×)



FC 9034C

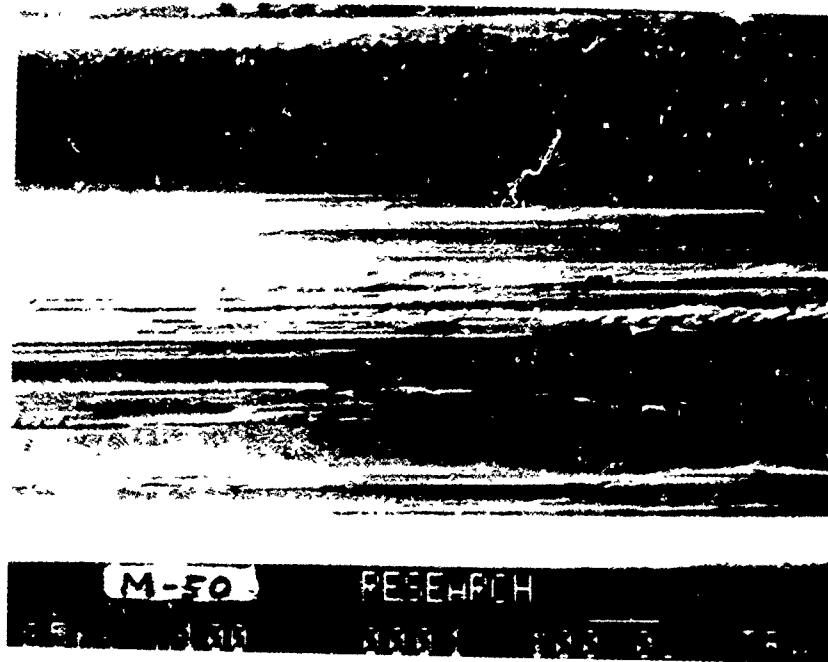
Figure 90. — Rotating Wear Test Bars Showing Representative Tracks on M50 and MRC2001 Specimens (Scale Magnification Approximately 3×)



FC 90346

Figure 91. — Rotating Wear Test Bars Showing Representative Tracks on MRC2001 and CRB7 Specimens (Scale Magnification Approximately 3×)

Figures 92, 93, and 94 are SEM photographs of representative wear scars on the stationary bars of M50, MRC2001, and CRB7, respectively.



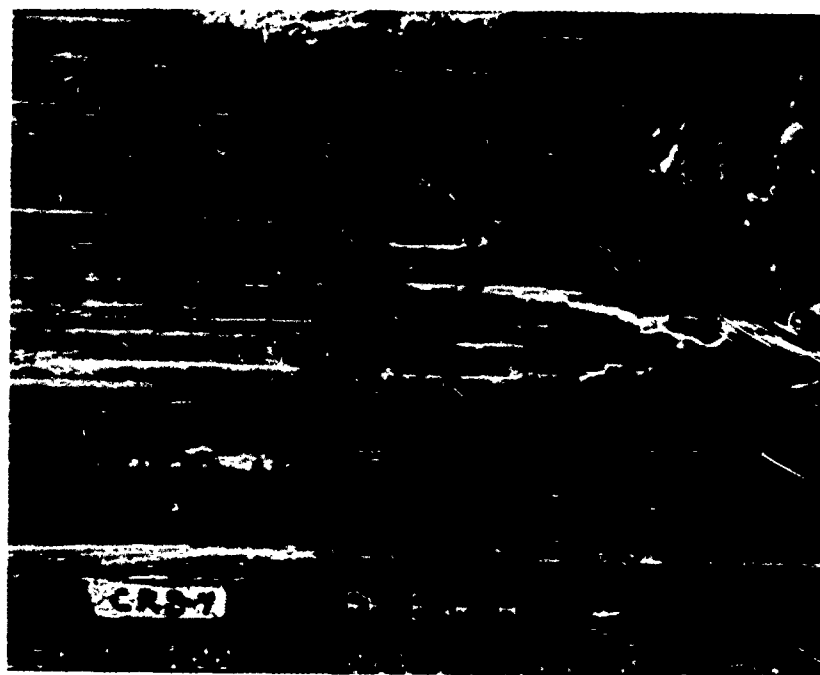
FC 90347

Figure 92. — SEM Photograph of the Bottom of a Typical Wear Scar on an M50 Stationary Bar (Magnification: 100X)



FC 90348

Figure 93. — SEM Photograph of the Bottom of a Typical Wear Scar on an MRC2001 Stationary Bar (Magnification: 100X)



FC 90349

Figure 94. — SEM Photograph of the Bottom of a Typical Wear Scar on a CRB7 Stationary Bar (Magnification: 100×)

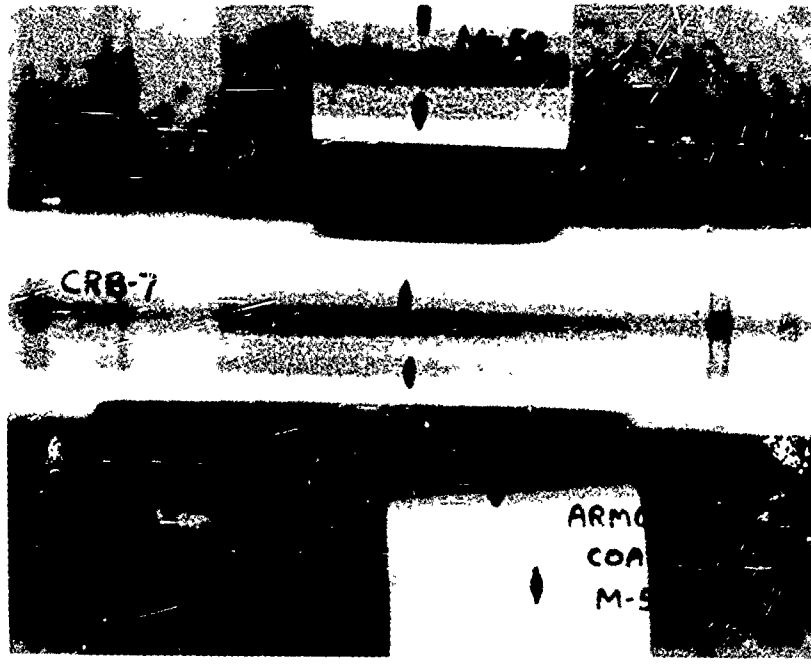
Figure 95 is a photograph of representative wear scars on M50, Armoloy-coated M50, CRB7, and RSR565, run against rotating silver-plated AMS6415 bars. All scars are very small, as would be indicated by weight loss data on Table 23. Wear scars on MRC2001 from this test were apparently destroyed when the bar was sectioned to make hot hardness test specimens. Discoloration of the RSR565 bar was caused by a hot hardness test.

Figure 96 is a photograph of two representative silver-plated bars used in the wear test. One of these bars was sectioned and the wear track was examined metallographically. Figure 97 shows a section across the wear track; there are still traces of silver in the bottom of the track.

Recordings of vibration data from the early part of one run from each of the ten sets of runs were shown previously in Figures 85 and 86. These recordings, which include some variations in chart speed and recorder attenuation, do not demonstrate the wide divergence which is found in the weight loss data. The fact that contacts were lubricated probably minimizes the effect of stick-slip.

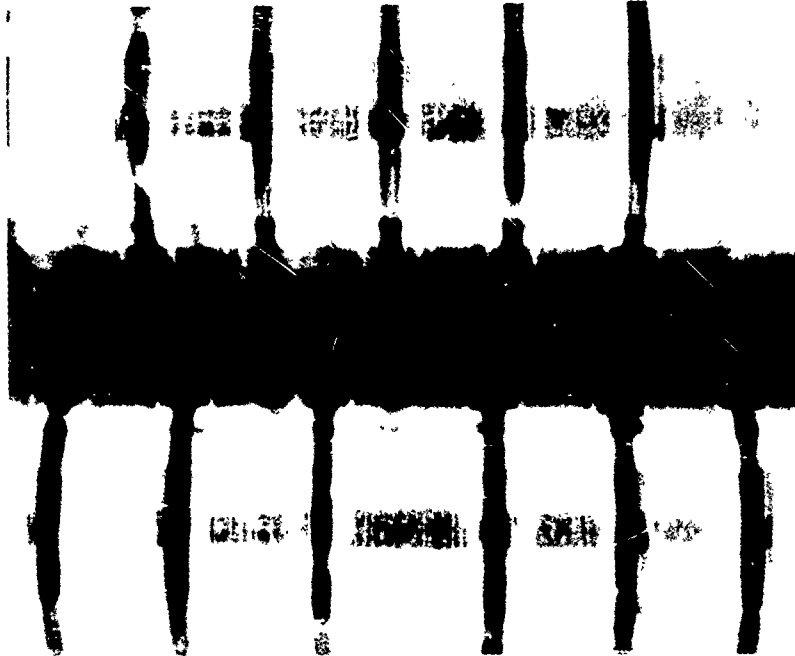
(5) Hot Hardness Testing

Hardnesses of the five test materials, VIM-VAR M50, Armoloy-coated VIM-VAR M50, MRC2001, CRB7, and RSR565, were determined at room temperature, 400°F, 500°F, 600°F, and 800°F, in a standard Detroit Testing Brinell machine set up for hot hardness testing. Details of the equipment are shown schematically in Figure 98. The furnace is insulated to minimize heat transfer away from the test zone. The controller holds specimen temperature to within 5°F.



FC 90350

Figure 95. — Wear Scars on M50, Armoloy-Coated M50, CRB7, and RSR565 Run Against Silver-Plated Steel (RSR565 Specimen Was Discolored Subsequent to the Wear Test)



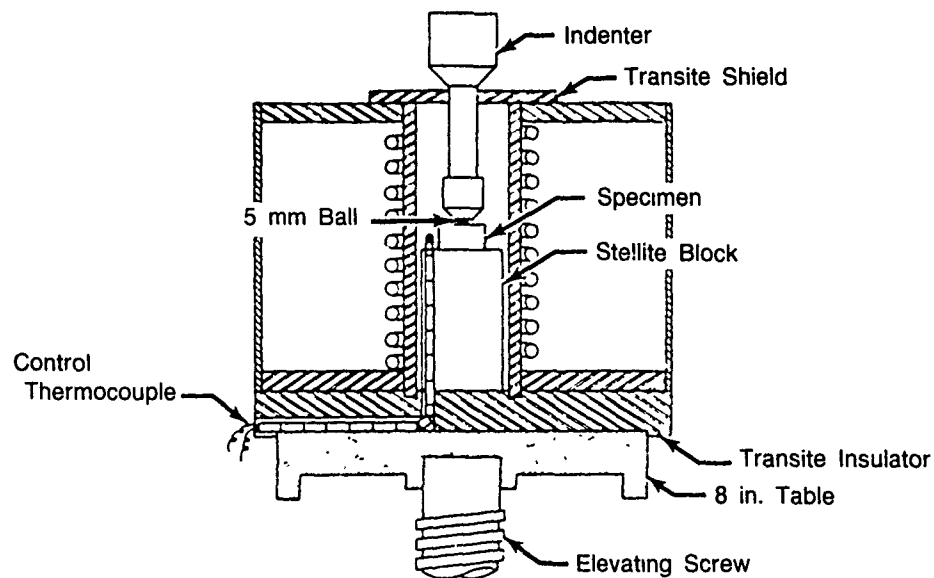
FC 90351

Figure 96. — Rotating Wear Test Bars, Silver-Plated AMS 6515 Steel, Showing Representative Wear Tracks (Scale Magnification Approximately 3X)



FC 90352

Figure 97. — *Metallographic Examination of Cross Section of Wear Track on a Silver-Plated Steel Bar (Magnification: 400×)*



FD 216729

Figure 98. — *Schematic of Hot Hardness Test Apparatus*

Hardness test specimens were 0.5-inch diameter cylinders, 0.5-inch long with ends ground flat and parallel. These specimens were prepared from wear test bars. Care was taken in preparing specimens to prevent overheating or cold working of the surfaces.

In performing a hot hardness test, a specimen and the 5-mm diameter chromium carbide indenter were installed in the preheated furnace and held at test temperature for 20 minutes.

During this stabilization of conditions, the indenter was positioned adjacent to, but not contacting, the upper end of the specimen. Then a 750 Kg load was applied for precisely 20 seconds, forcing the 5-mm diameter indenter into the end of the test specimen. After removal of load, the specimen was removed from the oven and allowed to air cool.

The impression of the indenter was then measured to the nearest 0.025 mm with a standard Brinell Microscope. Two measurements were made at 90 degrees to each other and the average taken. Brinell hardness was then calculated by the formula:

$$\text{BHN} = \frac{P}{\frac{\pi D}{2} (D - \sqrt{D^2 - d^2})}$$

where: P = Load in kilograms
D = Diameter of ball in millimeters
d = Diameter of impression in millimeters.

Four hot hardness tests were made with each material at each temperature. Results are presented in Table 25 and summarized in Table 26. A normalized plot of average hardness values converted to approximate Rc equivalents, is presented in Figure 99. Figure 100 is a photograph of two representative test specimens, showing indentations.

Bearing hardnesses are usually presented as readings on the Rc scale. A Rockwell Hardness Tester is not able to function at high temperature, so it is necessary to convert Brinell hardness readings to Rc values by approximate methods. In presenting Rc values in Table 25 and Figure 99 we have used the table, "Approximate Equivalent Hardness Numbers for Brinell Hardness Numbers for Steel", from ASM's Metals Handbook, Volume 1. The room temperature hardness values obtained in this test are slightly, but consistently, lower than hardnesses reported earlier using a Rockwell Hardness Tester.

Performances of all materials in the hot hardness test were quite comparable, with much of the small scatter probably due to resolution of the indentation measurement. We should expect M50 and Armoloy-coated M50 to produce identical readings, for instance, but we see variations of up to 1.0 on the Rc scale. Both MRC2001 and RSR565 have as high or higher hardness values than M50 over the entire temperature range. CRB7 exhibited lower hardness values than M50 at some temperatures, but these differences are small, particularly after the data are normalized to account for initial room temperature hardness.

(6) Selection of Single Best Candidate for Phase II Evaluation.

In order to be considered for Phase II evaluation a candidate, as a minimum, had to demonstrate equivalence to M50 in hot hardness and wear resistance.

- *Hot Hardness — 15 points maximum.*

CRB7 demonstrated superior hot hardness compared to M50. All other candidates were judged equal to M50.

TABLE 25.

HOT HARDNESS TEST DATA

(Hardness values in BHN, with averages converted to approximate Rockwell "C" equivalents. Indentation diameters in millimeters.)

	Room Temperature		400°F		500°F		600°F		800°F	
	Dia.	BHN	Dia.	BHN	Dia.	BHN	Dia.	BHN	Dia.	BHN
M50	1.20	653	1.20	653	1.25	601	1.25	601	1.30	555
(Reference)	1.20	653	1.20	653	1.225	626	1.225	626	1.30	555
	1.15	712	1.20	653	1.20	653	1.20	653	1.275	578
	1.20	653	1.20	653	1.225	626	1.25	601	1.30	555
		668		653		627		620		561
		(60.9 Rc)		(60.0 Rc)		(58.7 Rc)		(58.3 Rc)		(55.1 Rc)
Armolov-Coated	1.20	653	1.20	653	1.20	653	1.25	601	1.275	578
	1.20	653	1.20	653	1.225	626	1.25	601	1.30	555
M50	1.20	653	1.20	653	1.20	653	1.20	653	1.30	555
	1.20	653	1.20	653	1.20	653	1.25	601	1.30	555
		653		653		646		614		561
		(60.0 Rc)		(60.0 Rc)		(59.7 Rc)		(58.0 Rc)		(55.1 Rc)
MRC2001	1.175	682	1.20	653	1.20	653	1.225	626	1.275	578
	1.15	712	1.20	653	1.20	653	1.225	626	1.275	578
	1.20	653	1.20	653	1.20	653	1.20	653	1.275	578
	1.15	712	1.20	653	1.20	653	1.225	626	1.275	578
		690		653		653		633		578
		(62.1 Rc)		(60.0 Rc)		(60.0 Rc)		(59.0 Rc)		(56.0 Rc)
CRB7	1.20	653	1.225	626	1.225	626	1.25	601	1.25	601
	1.20	653	1.225	626	1.225	626	1.275	578	1.25	601
	1.20	653	1.20	653	1.20	653	1.25	601	1.25	601
	1.20	653	1.20	653	1.25	601	1.25	601	1.275	578
		653		640		627		595		595
		(60.0 Rc)		(59.3 Rc)		(58.7 Rc)		(57.0 Rc)		(57.0 Rc)
RSR565	1.20	653	1.20	653	1.20	653	1.225	626	1.275	578
	1.15	712	1.20	653	1.225	626	1.225	626	1.300	555
	1.175	682	1.20	653	1.20	653	1.225	626	1.275	578
	1.20	653	1.20	653	1.20	653	1.225	626	1.275	578
Average		675		653		646		626		572
		(61.3 Rc)		(60.0 Rc)		(59.7 Rc)		(58.6 Rc)		(55.7 Rc)

617 W

- *Wear Resistance — 15 points maximum.*

The only candidate to demonstrate wear resistance equal to or better than the M50 baseline was MRC2001.

TABLE 26.
SUMMARY OF HOT HARDNESS TEST RESULTS

Brinell Hardness (Brinell 650 \approx Rc 60)					
<i>Candidate</i>	<i>Room Temp</i>	<i>400°F</i>	<i>500°F</i>	<i>600°F</i>	<i>800°F</i>
		M50 (Ref)	668	653	627
Armoloy-Coated M50	653	653	646	614	561
MRC2001	690	653	653	633	578
CRB7	653	640	627	595	595
RSR565	675	653	646	626	572

6.17 K

Table 27 summarizes candidate ranking at the conclusion of Phase I property testing.

Based on the above results, the USAF program office was advised and subsequently approved MRC2001 as the single best candidate to be carried into Phase II full-scale bearing development and testing.

4. PHASE II BEARING FABRICATION AND TEST

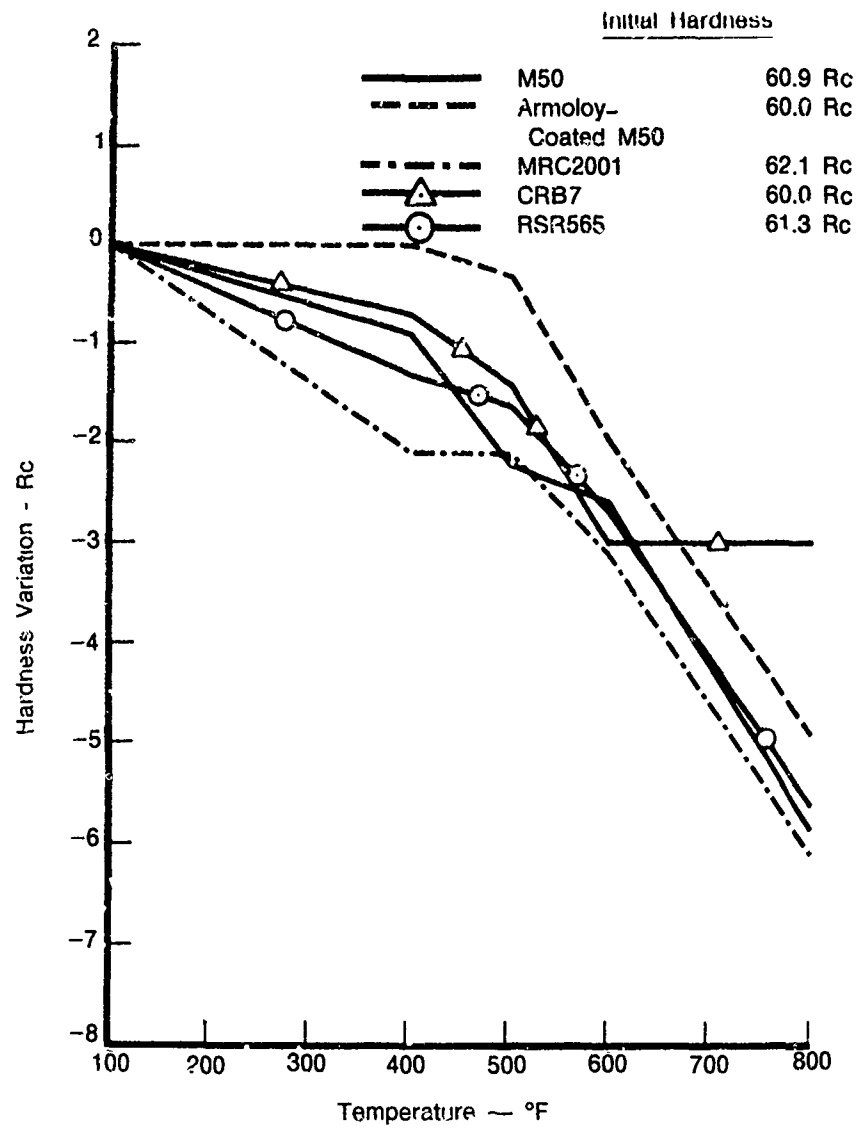
In Phase II, full-scale bearing life tests were performed to substantiate the MRC2001 candidate selection.

a. Task VI — Bearing Fabrication

Twenty each MRC2001 and M50 baseline MRC207S ball bearings were fabricated. The MRC207S bearing design has a 35-mm bore and a 72-mm outside diameter (Figure 101). The bearings conformed to ABEC Grade 5 standards and were assembled with a molded Nylon snap-in cage. One performance bearing was fabricated from MRC2001. The bearing selected for the performance demonstration test was the front half of the TF30 No. 4 ball bearing (PW 5362 10); it is also used to support the high rotor of an advanced demonstrator engine. This bearing is a 110-mm bore by 175-mm outside diameter split inner ring angular contact duplex ball bearing.

The MRC2001 powder used for the test bearings was fabricated from vacuum melted prealloyed material which was atomized in a nitrogen gas atmosphere. The powder was then encapsulated and hot outgassed at approximately 10^{-4} Torr. Table 28 outlines the thermomechanical material consolidation processes for the different MRC2001 rings fabricated for this program. The MRC2001 ball stock for both the 35-mm and 110-mm bearings was extruded at 1950°F and at a 14 to 1 reduction ratio to hot heading size. The extruded ball stock was annealed, hot-headed, rough ground, heat treated, finish ground, and lapped to finished size balls at TRW's Colebrook ball plant.

After annealing and rough turning, one 110-mm performance bearing inner race and one outer race were selected at random and cut into several segments. One segment from each ring was subjected to the standard MRC2001 heat treatment (reference Table 8). The inner ring sample responded normally but the outer ring segment grew significantly and developed numerous radial cracks. A study was undertaken to determine the cause of this abnormal heat treat response and to determine a means of sorting good and bad rings.



FD 270300

Figure 99 — Plot of Normalized Hardness vs Temperature for Candidates and VIM-VAR M50 Baseline Material



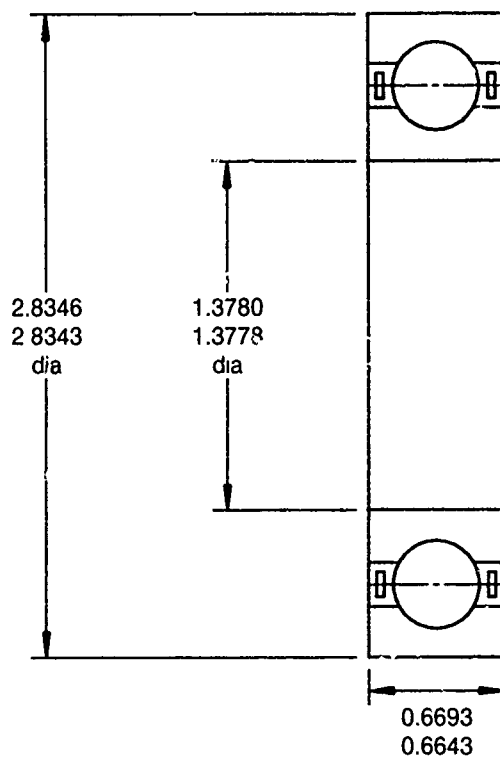
FC 90353

Figure 100. — Typical Indentations on Hot Hardness Test Specimens

TABLE 27. TASK IV RANKING SUMMARY

Maximum Points	Task 3			Task 4			Tasks 3 & 4					Total
	15	15	15	15	15	15	15	10	10	10	5	
	RCF	Corrosion	Hot Hardness	Wear	Mechanical Properties	Adhesion	Appl. W/O Affecting Properties	3-5 Years Production Incorporation	Cost	Strategic Elements	Environmental Impact	
CRB7	*	15	0	*	15	15	15	10	8	3	4	Eliminated: Failed Task 4 Wear Resistance Criteria. Task 3 Total - 70
MRC2001	*	15	15	*	15	15	15	6	6	2	3	77 (Task 3 Total - 62)
RSR 565	*	15	(*)	*	**	15	15	4	4	1	2	Eliminated in Task 3 Candidate Selection Based on Point Rank (Task 3 Total - 56)
Armoloy	*	12	0	*	15	12	8	10	4	4	1	Eliminated/ Failed Task 4 Wear Resistance Criteria (Task 3 Total - 62)
Sputtered Ni	*	15		*	0	12	2	2	5	5	5	Eliminated; Coating Failed During Task 3 RCF Tests

*No Significant Difference
 **Tested (But Not Officially Ranked) for Task 4 Wear and Hot Hardness as Part of P&W's
 Planned and Ongoing Bearing Material Improvement Programs



FDA 300505

Figure 101. — MRC207S 35-mm Endurance Test Bearing

TABLE 28.

THERMOMECHANICAL PROCESSING OF MRC2001 RACE BLANKS

<i>Process</i>	<i>Condition</i>
• Powder Consolidation — Hot Isostatic Press (HIP)	30 ksi at 2125°F
• Strip HIP Can and Cut into Forging Mults	
• Upset Forge	2 to 1 Reduction Ratio
• Pierce Bore — 110-mm Race Blanks Drill Bore — 35-mm Race Blanks	
• Ring Hammer Forge (Except 35-mm Inner Rings)	2050 to 2100°F
• Rough Turn	
• Heat Treat	Reference Table 8

The 110-mm bearing race blanks as well as the remaining pieces of the samples used for the heat treat trial were inspected for whole part density to determine if a significant difference existed.

Densities were determined via the Archimedes technique, i.e., weighing to the fourth decimal place, in air, then in water. Results are listed in Table 29. Results for the unused heat treat trial samples were clearly different and agree with the metallographic examination discussed later.

TABLE 29.

DENSITY VALUES FOR 110-MM RINGS

<i>Inner Ring</i>	<i>Density g/cc</i>	<i>Outer Ring</i>	<i>Density g/cc</i>
1	7.771	1	7.797
2	7.768	2	7.797
3	7.769	3	7.799
4	7.791	4	7.798
5	7.770	5	7.798
6	7.740	6	7.797
7	7.767	7	7.798
8	7.770	8	7.797
9	7.731		
10	7.794		
11	7.796		
12	7.793		
13	7.773		
14	7.710		

<i>Heat Treat Trial Segment -- Inner Ring</i>	
a	7.7534
b	7.7560
c	7.7309

<i>Heat Treat Trial Segment -- Outer Ring</i>	
d	7.6719
e	7.6730
f	7.6828

6176

The scatter for the eight 110-mm outer rings was minimal; the values all fell in the range of 7.797 to 7.799 g/cc. However, there was considerable scatter among the 14 110-mm inner rings; these ranged from a low of 7.710 to a high of 7.796 g/cc.

An attempt at differentiating between the "good" and "bad" ring sections via eddy current was totally unsuccessful. The parameter being assessed, electrical conductivity, varied from location to location on a given ring, and it was impossible to differentiate the two rings.

An effort was also made to measure the sonic velocity of the two ring segments. It was determined that the speed of sound through "good" inner ring sections, "bad" outer ring sections, and "good" (higher density) outer rings were all consistently within experimental error of the average value which was 6100 meters/second. Sonic velocity was, therefore, incapable of detecting defective rings.

A metallographic examination was performed to determine if the microstructural differences in the heat treat samples could explain the abnormal heat treat response.

The "good" inner is shown in Figure 102 in the annealed condition. The unetched view shows that the material is nearly 100 percent dense; two or three very tiny voids are evident.

The etched view shows that the carbides are beginning to coalesce. This is an indication of exposure to high temperature. However, this structure is believed to be fully acceptable.

By contrast, note in Figure 103 that there are definitely voids in the outer ring section in the annealed condition. The etched view shows evidence of carbide coalescence.

Figure 104 shows both rings after hardening. The inner is not appreciably changed from the annealed condition. However, in the outer, there is some evidence of burning. The carbides have developed "tails" and are penetrating into grain boundaries. Figure 105 more clearly shows the appearance of outer ring voids/cracks.

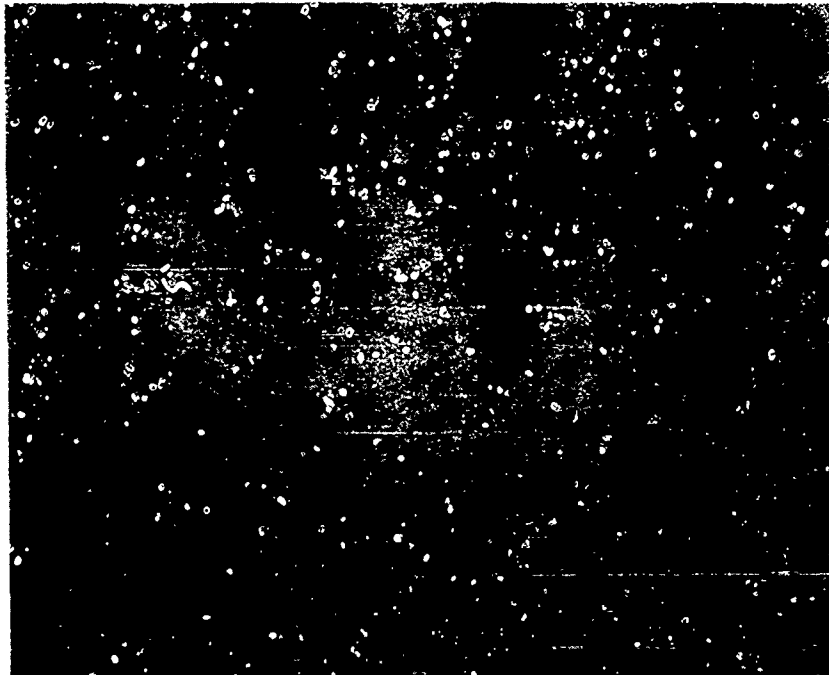
The possibility of healing the damage by reHIPping (HIP — hot isostatic press) the material was explored. A sample of the "bad" outer ring was re-HIPped at 30,000 psi and 2125°F for two hours. After HIPping, the density was determined to be 7.741 g/cc; this represents an increase from the 7.67 to 7.68 values determined prior to HIPping. The sample was then heat treated and while it did not swell as did the rest of the same ring, it did develop internal cracks.

The initial evidence acquired in the abnormal heat treat response study tended to indicate that the material was damaged by burning prior to heat treatment. However, it was later determined that the voids were the result of thermally induced porosity (TIP) caused by a leak in one of the HIP cannisters. The spherical pores which are normally associated with TIP and which are the result of the thermal expansion of small hubbles of entrapped inert gas have been masked in Figures 103, 104, and 105 by the thermomechanical working to which the rings were subsequently subjected.

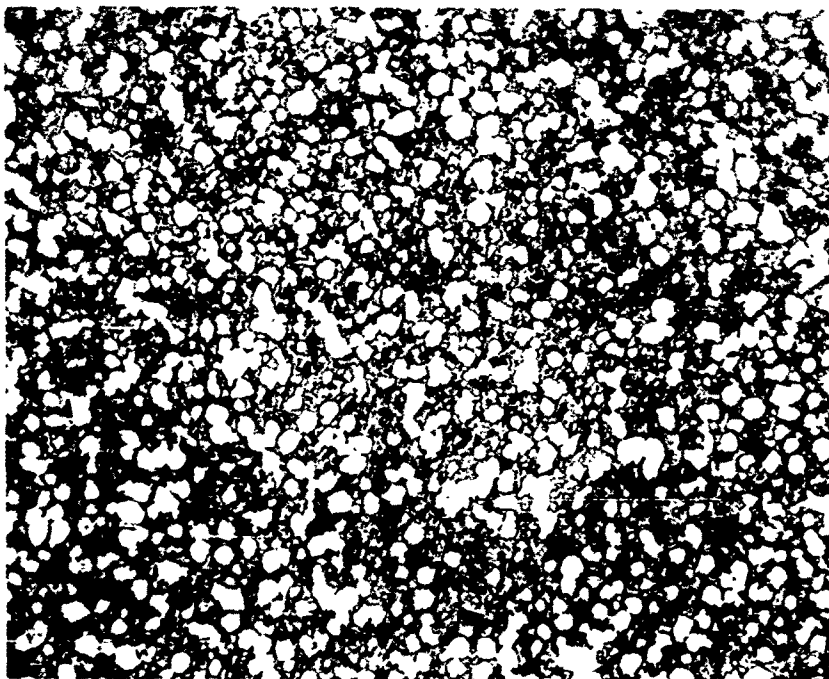
At the conclusion of the above study it was decided to proceed with the heat treatment of all the remaining 35-mm and 110-mm race blanks and employ nondestructive test methods to screen defective races. All raceway blanks were subjected to the standard MRC2001 heat treatment. Post heat treatment inspections for hardness, density, and microstructure anomalies were completed for the 35-mm and 110-mm bearing components.

The 110-mm inner race blanks demonstrated considerable variability in hardness and density after heat treatment and two of the inner race blanks developed gross microcracks in a radial direction. The MRC2001 35-mm endurance bearing race blanks did not show any evidence of microcracks after heat treatment and had uniform hardness and density. Post-heat treat density and hardness results are listed in Tables 30 through 33 for each of the 35-mm and 110-mm inners and outers.

In response to the density and hardness variability and microstructure defects observed in the heat treated 110-mm race blanks, a second study was undertaken. The purpose of the study was to establish correlations between whole part density, hardness, ultrasonic, and eddy current test indications, and microstructural anomalies as a means to evaluate post-heat treat part integrity of the 35-mm and 110-mm race blanks.



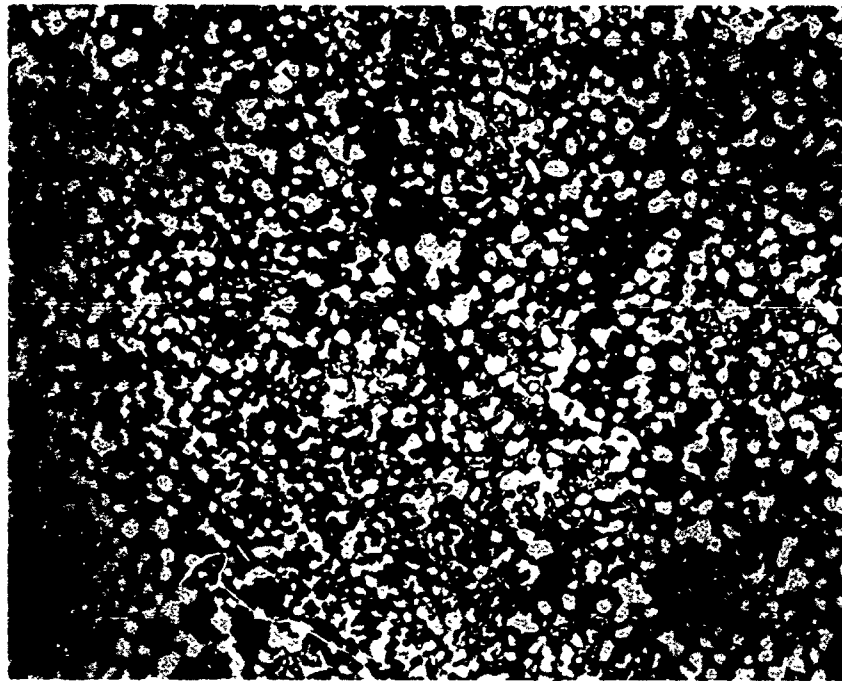
Unetched (100X)



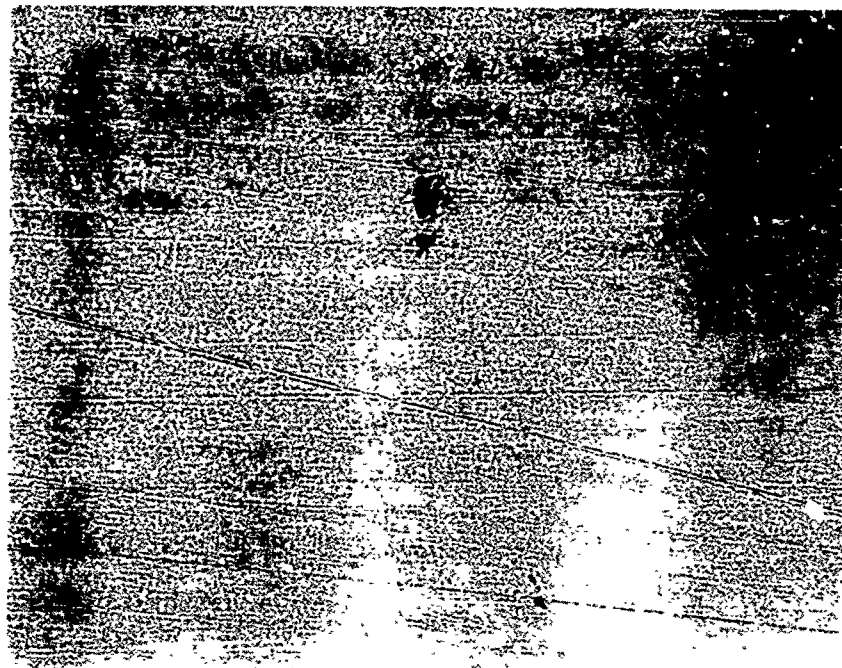
Marbles Etched (1000X)

FD 300524

Figure 102. — SEM Photomicrograph of Annealed Inner Ring Segment Which Exhibited Normal Heat Treat Response



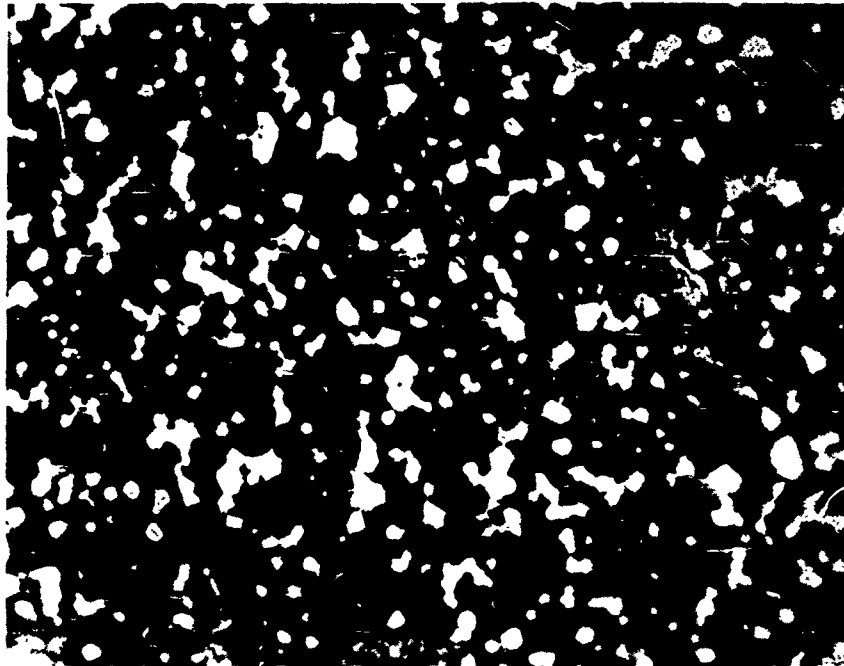
Marbles Etched (1000×)



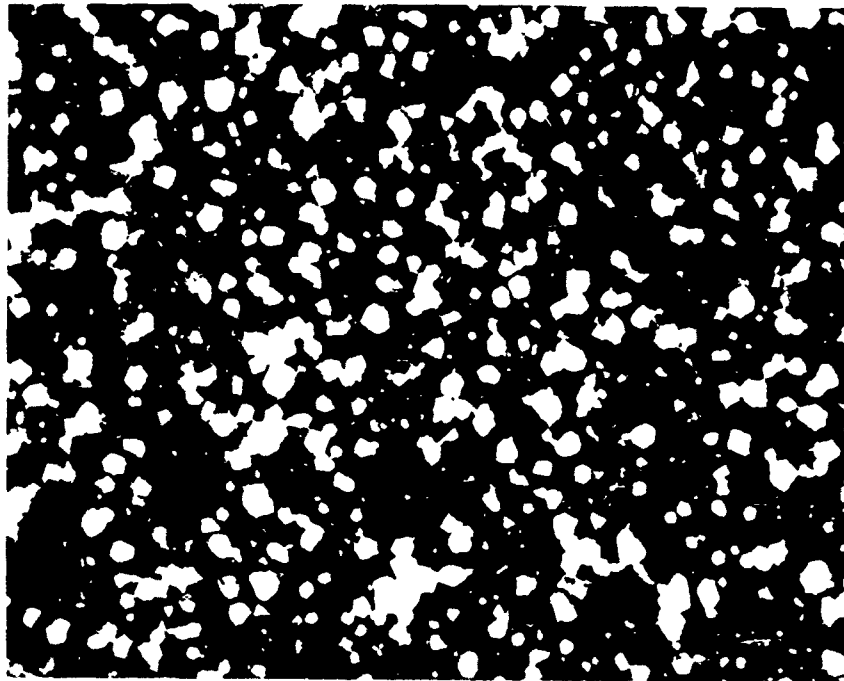
Unetched (400×)

FD 300510

Figure 103. — SEM Photomicrograph of Annealed Outer Ring Segment Which Exhibited Abnormal Heat Treat Response



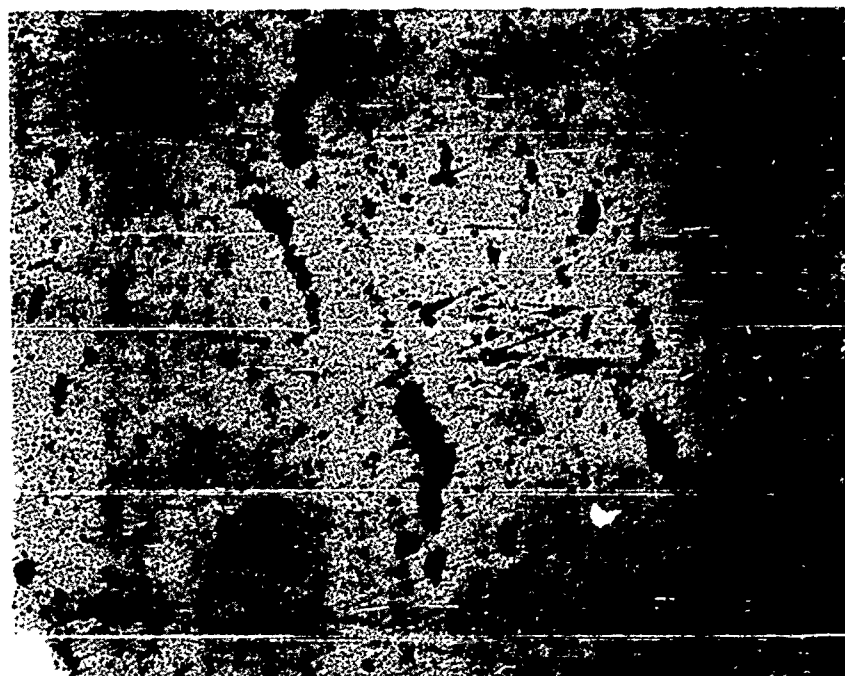
Outer Race Marbles Etched (1000X)



Inner Race Marbles Etched (1000X)

FD 300508

Figure 104 — SEM Photomicrograph of Hardened and Tempered Inner and Outer Ring Segments Presented in Figures 102 and 103 Respectively



FD 300509

Figure 105. — SEM Photomicrograph of Outer Race Segment Voids/Cracks After Heat Treatment (Unetched; 100X)

TABLE 30.

POST-HEAT TREAT HARDNESS VS DENSITY FOR 110-MM OUTER RING BLANKS

<i>Process Number</i>	<i>Hardness (Rc)</i>	<i>Density (g/cc)</i>
1	59.1 — 59.4	7.74
2	61.1 — 61.7	7.78
3	61.1 — 61.6	7.75
4	61.2 — 62.0	7.77
5	60.3 — 60.6	7.74
6	61.2 — 61.7	7.77
7	60.1 — 60.6	7.77

6.179C

In Figure 106, the degree of scatter between the 110-mm inners is plotted against the hardness range within the respective parts. Over the entire range, the correlation coefficient, as determined by linear regression analysis, is 0.60 and 0.79 for the 110-mm outer and inner rings, respectively. Note that 1.0 is perfect correlation and 0 is complete absence of any correlation; thus, these coefficients indicate that a statistical relationship does exist between density and attainable hardness.

TABLE 31.

POST-HEAT TREAT HARDNESS VS DENSITY FOR 110-MM INNER RING BLANKS

<i>Process Number</i>	<i>Hardness (Rc)</i>	<i>Density (g/cc)</i>
1	58.0 — 60.0	7.25
2	57.2 — 59.2	7.49
3	60.9 — 61.3	7.78
4	61.4 — 61.6	7.76
5	58.8 — 59.7	7.56
6	58.3 — 60.2	7.50
7	59.5 — 60.5	7.52
8	57.3 — 60.3	7.55
9	61.1 — 61.7	7.60
10	57.0 — 60.8	7.53
11	57.9 — 58.6	7.52
12	62.4 — 63.0	7.76

6.176C

The 35-mm inners and outers exhibited very little scatter as was expected with respect to initial hardness measurements. Most of the post-heat treat densities fell between 7.77 and 7.78 g/cc.

Ultrasonic C-scans were used to determine the presence of anomalies within both the inner and outer rings. Evaluation was based only on axial measurements. The decision to use axial instead of radial scans stemmed from observing the heat treated outer ring which exhibited gross microcracking; cracking seemed to propagate along the transverse axis, possibly due to forging practice.

Wrought M50 35-mm inner and outer rings were used for ultrasonic inspection setup and "standardization". The C-scans performed on these rings were used to determine the sonic velocity and sensitivity which was then used on the MRC2001 bearings.

In general, all of the 35-mm inners and outers appeared to be sound, whereas, very few of the 110-mm rings gave no indication of flaws. The C-scans of the 110-mm inners showed catastrophic cracking throughout with the exception of parts 3, 4, 9, and 12. The ultrasonic C-scans on the 110-mm outer rings revealed discrete voids and/or more localized cracking. Two of these outer rings (No. 2 and No. 4) appeared completely sound. A third, No. 6, was considered sound enough for rig testing inasmuch as the possible defects are some distance away from the race.

The 35-mm ball bearings and 110-mm ball bearings made from MRC2001 steel were subjected to eddy current and magnaflux inspection for surface defects. The baseline 35-mm ball bearings of M50 steel were also subjected to magnaflux inspection.

TABLE 32.

POST-HEAT TREAT HARDNESS VS DENSITY FOR MRC2001 35-MM INNER RACE
BLANKS

<i>Process No.</i>	<i>Hardness Range (HRc)</i>	<i>Hardness Average (HRc)</i>	<i>Density (g/cc)</i>
1	61.3 - 61.5 - 61.5	61.4	7.77
2	61.0 - 62.0 - 62.3	62.1	7.75
3	61.0 - 61.7 - 61.8	61.8	7.76
4	61.7 - 61.8 - 61.9	61.8	7.77
5	61.4 - 61.7 - 61.7	61.6	7.77
6	61.7 - 62.0 - 62.3	62.0	7.78
7	62.1 - 62.4 - 62.4	62.3	7.78
8	61.5 - 61.7 - 62.0	61.7	7.74
9	61.4 - 61.7 - 61.8	61.6	7.78
10	61.4 - 61.6 - 62.0	61.7	7.77
11	61.1 - 61.2 - 61.7	61.3	7.77
12	61.7 - 61.9 - 62.0	61.9	7.77
13	61.2 - 61.4 - 61.6	61.4	7.77
14	62.2 - 62.2 - 62.2	62.2	7.77
15	61.6 - 61.8 - 62.0	61.8	7.78
16	61.2 - 61.5 - 61.7	61.5	7.77
17	61.7 - 61.7 - 62.2	61.8	7.77
18	61.6 - 61.8 - 62.0	61.8	7.77
19	61.6 - 61.6 - 61.7	61.7	7.77
20	61.3 - 61.6 - 61.9	61.6	7.69
21	61.5 - 61.6 - 61.9	61.7	7.77
22	61.4 - 61.5 - 61.8	61.6	7.78
23	61.5 - 61.5 - 61.6	61.5	7.78
24	61.3 - 61.3 - 61.6	61.5	7.76
25	61.7 - 61.8 - 61.8	61.8	7.77
26	61.0 - 61.4 - 61.5	61.3	7.77
27	61.2 - 61.3 - 61.6	61.4	7.77
28	61.8 - 62.1 - 62.3	62.1	7.78
29	61.4 - 61.4 - 61.4	61.4	7.79
30	61.7 - 61.8 - 61.9	61.8	7.77
31	61.5 - 61.7 - 61.8	61.7	7.78
32	61.5 - 61.7 - 61.8	61.7	7.78
33	61.6 - 61.8 - 61.9	61.8	7.78
34	61.5 - 61.6 - 61.7	61.6	7.78

64700

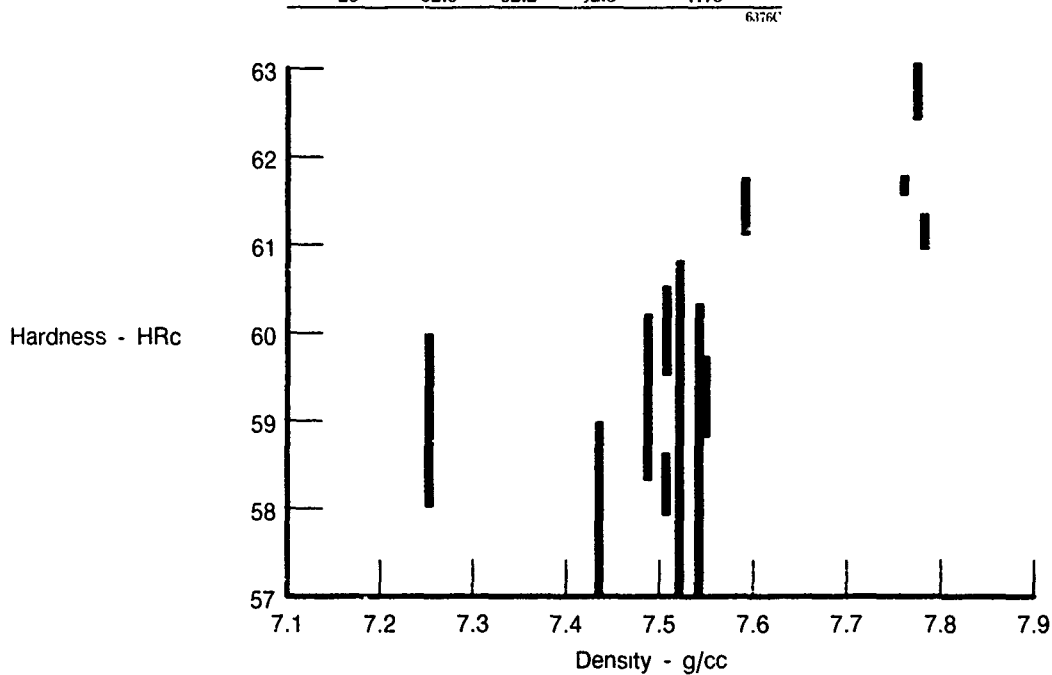
Tables 34, 35, and 36 summarize the detailed dimensional and quality inspection data on the 35-mm MRC2001 ball bearings, baseline 35-mm M50 ball bearings, and 110-mm ball bearings (made from MRC2001 steel but otherwise conforming to the forward bearing of the PW 536343 duplex pair), respectively.

All the 35-mm bearings met dimensional specifications. Noise level data, as measured by the Anderometer, showed no difference between the two lots of 35-mm ball bearings, and that all bearings were very quiet. Anderometer readings are a measure of vibration and include the effects of surface finish, raceway waviness, eccentricity, and ball quality.

TABLE 33.

POST-HEAT TREAT HARDNESS VS DENSITY FOR MRC2001 35-MM OUTER RACE BLANKS

Process No	Hardness Range (HRc)	Density (g/cc)
1	62.4 — 62.5 — 62.5	7.77
3	61.8 — 62.2 — 62.4	7.76
4	62.0 — 62.2 — 62.6	7.76
5	62.0 — 62.3 — 62.4	7.77
6	61.4 — 61.7 — 61.9	7.75
7	62.0 — 62.0 — 62.3	7.78
8	62.0 — 62.2 — 62.5	7.77
9	62.1 — 62.2 — 62.4	7.77
11	61.5 — 61.8 — 62.2	7.77
12	62.3 — 62.6 — 62.6	7.77
13	62.1 — 62.3 — 62.4	7.78
14	62.0 — 62.2 — 62.2	7.78
15	62.2 — 62.2 — 62.3	7.78
16	62.3 — 62.4 — 62.4	7.78
17	61.5 — 61.8 — 62.2	7.73
18	61.8 — 62.1 — 62.5	7.77
19	61.9 — 62.2 — 62.5	7.77
20	61.7 — 62.0 — 62.4	7.77
21	62.6 — 62.7 — 62.8	7.75
22	62.2 — 62.5 — 62.7	7.78
23	62.1 — 62.3 — 62.5	7.78
24	62.6 — 62.6 — 62.8	7.78
25	62.0 — 62.2 — 62.3	7.75



FDA 300504

Figure 106. — Plot of Hardness Range vs Density for 110-mm Inner Ring Blanks

TABLE 34.

DIMENSIONAL AND QUALITY INSPECTION DATA FOR MRC2001 35-MM
ENDURANCE BEARINGS

Bearing S/N	Inner Process No.	Outer Process No.	Inner Bore	Outer OD	Radial Clearance	Ball Weight ± 0.0002 gm	Anderometer					
							Lo	Med	Hi	Lo	Med	Hi
E1	22	1	1.37788	2.83450	0.0007	6.8572	5	20	40	5	25	40
E2	4	3	1.37794	2.83445	0.0007	6.8568	5	20	40	5	15	25
E3	25	4	1.37796	2.83456	0.00075	6.8564	5	20	25	5	15	25
E4	23	5	1.37790	2.83457	0.0008	6.8564	5	15	30	5	15	30
E5	24	6	1.37789	2.83452	0.00065	6.8562	5	15	35	5	10	30
E6	9	7	1.37787	2.83443	0.0009	6.8562	5	15	30	5	10	30
E7	14	8	1.37788	2.83457	0.0007	6.8562	5	20	20	5	15	25
E8	10	9	1.37788	2.83450	0.0007	6.8559	10	20	30	5	15	30
E9	33	11	1.37793	2.83445	0.0006	6.8559	5	10	25	5	10	20
E10	6	12	1.37787	2.83450	0.00065	6.8559	5	15	30	5	15	30
E11	16	13	1.37792	2.83450	0.00075	6.8556	5	10	25	5	15	30
E12	17	14	1.37793	2.83440	0.0006	6.8556	5	15	35	5	25	35
E13	12	15	1.37791	2.83456	0.00085	6.8556	5	15	25	5	20	35
E14	13	16	1.37790	2.83442	0.0007	6.8556	5	20	30	10	15	25
E15	11	18	1.37789	2.83450	0.0007	6.8552	5	15	30	5	15	30
E16	18	20	1.37790	2.83455	0.00075	6.8552	5	15	35	5	10	30
E17	29	21	1.37795	2.83454	0.0006	6.8548	5	15	30	5	15	30
E18	31	22	1.37788	2.83448	0.0008	6.8548	5	15	30	5	10	30
E19	27	23	1.37792	2.83450	0.0007	6.8548	5	15	30	5	15	30
E20	26	25	1.37788	2.83447	0.0007	6.8545	5	20	35	5	15	35
E21	19	19	1.37792	2.83455	0.0008	6.8545	5	15	40	5	15	30
E22	15	24	1.37792	2.83435	0.0006	6.8542	5	15	25	5	15	25

Surface Finish Races 2 μ -in. to 4 μ -in.

Ball Diameter 0.46899 inch, Hardness Rc 61.9 - 62.4

61764

The outer and inner races of the 35-mm MRC2001 ball bearings were subjected to eddy current inspections after finishing. Outer rings were finished and examined before inner races were match ground. Inner races were examined after match grinding. None of the eddy current traces indicated surface defects. All of the rings also passed magnaflux inspection.

The 110-mm outer and inner races were also subjected to eddy current inspection. The five outer races showed no surface defects. Other inspections: ultrasonic scans, density, and hardness indicated that specimen No. 2 and No. 4 were superior to the others. Specimen No. 6, which appeared relatively good during preliminary inspections, was scrapped during grinding. Outer ring specimen No. 5 was selected to form part of a third bearing. The eddy current traces of five of the six inner ring halves showed no surface defects. Four of those five were also good on the basis of ultrasonic, density, and hardness inspections. The sixth race (No. 5 \times , originally No. 11) showed a definite surface defect. The surface defect was visible on the race. The four inner ring halves which were good on the basis of ultrasonic scan, density, hardness, and eddy current were installed in bearing specimen No. E001 and No. E002.

TABLE 35.

DIMENSIONAL AND QUALITY INSPECTION DATA FOR M50 35-MM BASELINE
ENDURANCE BEARINGS (VIM-VAR M50 INNERS, OUTERS, BALLS)

Bearing S/N	Inner Bore	Outer OD	Radial Clearance	Anderometer					
				Lo	Med	Hi	Lo	Med	Hi
1	1.37794	2.83447	0.0007	10	20	20	10	20	25
2	1.37790	2.83453	0.0010	10	20	20	10	20	20
3	1.37793	2.83446	0.0009	10	15	30	10	20	30
4	1.37797	2.83454	0.0009	10	30	25	10	20	25
5	1.37792	2.83448	0.0009	15	15	30	5	15	25
6	1.37790	2.83457	0.0009	5	15	20	5	15	25
8	1.37791	2.83458	0.0010	5	20	25	5	25	25
9	1.37793	2.83457	0.0010	10	25	25	10	25	25
10	1.37791	2.83450	0.0007	10	25	40	10	30	10
11	1.37790	2.83455	0.0008	10	25	20	10	20	20
12	1.37788	2.83445	0.0009	5	15	20	10	15	20
13	1.37785	2.83441	0.0011	5	15	20	10	15	25
14	1.37793	2.83450	0.0011	5	15	20	5	10	20
15	1.37792	2.83451	0.0011	10	15	30	5	15	25
16	1.37791	2.83447	0.0009	10	20	45	10	20	40
17	1.37794	2.83449	0.0010	10	25	20	10	15	20
18	1.37796	2.83450	0.0012	15	25	25	5	20	25
19	1.37797	2.83451	0.0008	10	15	25	10	25	30
20	1.37786	2.83457	0.0008	10	20	25	5	30	40
22	1.37792	2.83450	0.0010	10	30	20	10	25	25
23	1.37788	2.83454	0.0009	10	30	15	5	15	20
24	1.37797	2.83449	0.0011	10	15	20	5	15	20
25	1.37791	2.83460	0.0009	10	15	25	5	15	20
26	1.37799	2.83452	0.0008	5	20	25	5	25	20

Hardness -- HRc

Inner Rings 61.8-62.2

Outer Rings 61.4-61.7

Ball Diameter 0.46909, Hardness 61 minimum

The nondestructive test (NDT) inspection results of the MRC2001 rings are summarized below:

- 35-mm Inner Rings (20 Required)

All 34 rings were considered usable; however, based on density results, numbers 2, 3, 8, and 20 were viewed as suspect.

- 35-mm Outer Rings (20 Required)

Of the 23 rings tested, only four (No. 6, 17, 21, and 25) had densities of 7.75 g/cc or less. These were regarded as suspect.

- 110-mm Inner Rings (1 Required)

Four rings (No. 3, 4, 9, and 12) appeared to be acceptable, based upon all evaluation criteria. All others were deemed unacceptable.

- 110-mm Outer Rings (1 Required)

Two rings, No. 2 and 4, appeared to be acceptable based upon all evaluation criteria. Also, No. 6 had acceptable hardness and density but showed indications away from the race in the C-scan; this ring was regarded as suspect. All others were deemed unacceptable.

At the conclusion of the hardness and density inspections the acceptable rings were ground to size using a two step grinding process. In the latter "finish grind" step, the races were individually ground to match with specific outer race and ball sets. Stock removal during the finish grind operation amounts to the last few thousandths of material. Following the finish grind operation, the inner races were honed to improve the surface parameters.

The grinding and honing processes used for the MRC2001 bearing races were essentially the same as those used for the reference M50 tool steel bearings.

b. Endurance Test Facility

Testing of bearings was performed in a battery of 8 identical machines, referred to as "Model A Test Machines". Figure 107 is a photograph of part of the battery of the machines and Figure 108 is a schematic of an individual machine.

Each machine has its own drive and controls but shares a common lubrication and hydraulic system.

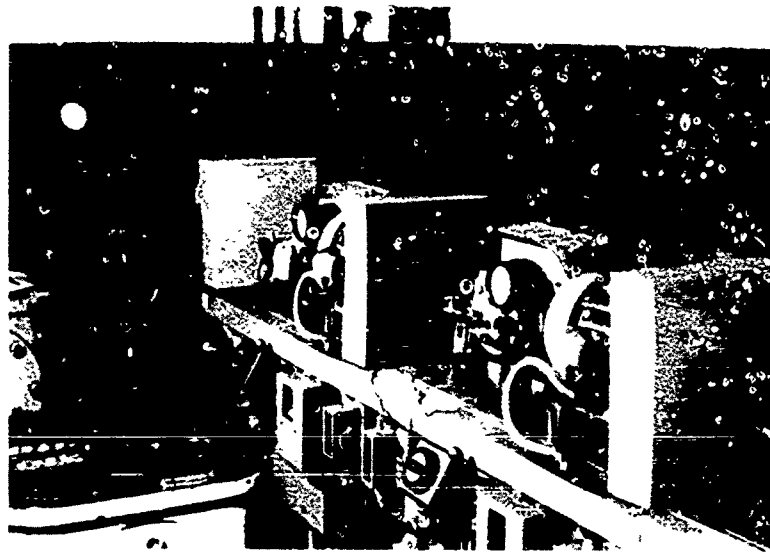
Machines are driven at constant speed by ac electric motors through a V-belt and sheave arrangement. A slave spindle in each machine accepts belt tension loads and transmits torque to the test bearing shaft through a splined coupling.

TABLE 36.

DIMENSIONAL INSPECTION DATA FOR MRC2001 110-MM PERFORMANCE BEARINGS
(SAME CONFIGURATION AS FORWARD BEARING OF PWA 536343 DUPLEXED PAIR)

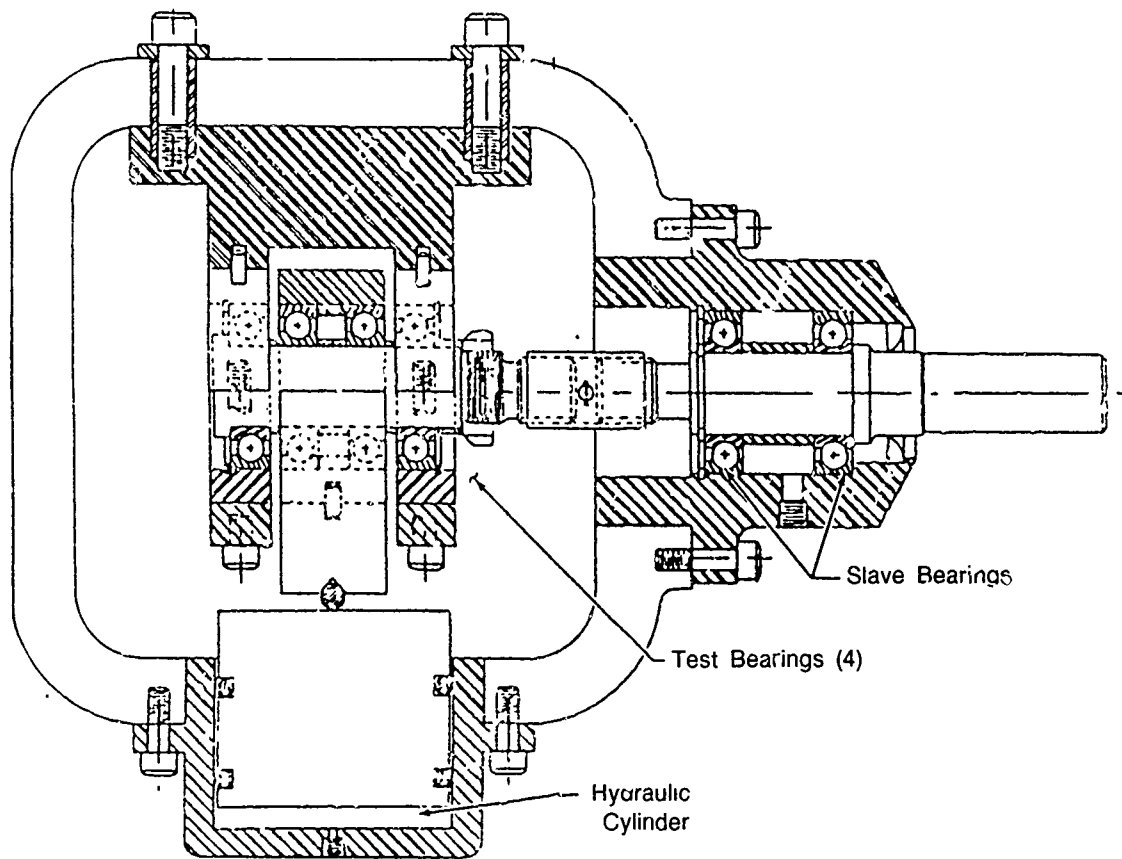
Bearing S/N	Component	Current Component		Weight	Bore	OD	Radial Clearance	End Play	Contact Angle	Circumferential		Surface Finish
		S/N	Original Component S/N							Waivness In	30 Deg Arc, Max	
E001	Outer	2	2	28.040 to 28.042 gm	6.0525	6.88942	0.0046	0.019	25°	62 μ-in. 38 μ-in.	2.5 μ-in. 2 μ-in. 3 μ-in.	
	Plain Inner	2	4		4.33054	5.31135						
	Puller Inner	2X	12		4.33052	5.31135						
	Balls											
E002	Outer	4	4	28.042 to 28.047 gm	6.0525	6.88965	0.0047	0.019	25°	46 μ-in. 24 μ-in.	4 μ-in. 2.5 μ-in. 3 μ-in.	
	Plain Inner	4	4		4.33052	5.3114						
	Puller Inner	4X	9		4.33055	5.31135						
	Balls											
E003	Outer	5	5	28.036 to 28.040 gm	6.0527	6.88964	0.0047	0.0195	26°40'	44 μ-in. 29 μ-in.	3 μ-in. 2 μ-in. 3 μ-in.	
	Plain Inner	5	5		4.33052	5.31145						
	Puller Inner	5X	11		4.33054	5.31115						
	Balls											

Ball diameter 0.75004, Hardness Rc 60.7-61.2, Surface Finish < 0.5 μ-in.



FC 850210

Figure 107 — Part of Battery of Model A Test Machines



FD 216731

Figure 108. — Schematic of TRW's Model A Test Rig

Four bearings are tested at a time under radial load in each machine. Load is applied to the center two bearings which are surrounded by a single housing, and resisted by the two bearings at the ends of the shaft. Axial location of housings and shaft positions is tightly held so that the two end bearings resist load equally. Internal diametral clearance of the two center bearings in each setup is matched as closely as possible, normally within 0.0001 inch, to facilitate load sharing.

A motor-driven pump delivers oil at approximately 200 psi to each machine. Pressure is individually regulated at each machine to provide 157 psi pressure to the radial load cylinder, and oil flow at substantially reduced pressure to the test and slave spindle bearings. Scavenged oil flows by gravity back to the central sump where it is recirculated. Lubricant is jetted into each test bearing at 600 to 700 cc per minute and drains from both sides of each bearing. Within the sump, on the suction line to the pump is a screen-type filter.

Each test machine incorporates redundant shut-off devices which are actuated by a bearing failure. The first, and most sensitive, is a piezo-electric accelerometer which is mounted on the base of the spindle and transmits signals to a meter and switch. The second device, which is fail-safe, is an electrical grid placed under the bearings; a metallic chip, 0.005 to 0.010 inch in width, will produce an electrical short in the grid and open the motor control circuit. In addition, a pressure switch in the hydraulic lubrication system of each machine will shut the machine down if pressure drops. A circuit breaker element in each motor control will also shut a machine down in case of increased torque.

A thermocouple contacts each outer ring for temperature measurement. The temperature of the outer rings, oil-in and scavenge oil are measured and recorded on a multipoint recorder.

c. Test Facility Calibration

(1) Loading

Radial load is applied by a hydraulic cylinder whose piston has been accurately machined and measured. The pressure gage on each cylinder is periodically checked on a dead weight tester. As a check on the system, a 20,000 pound capacity strain gage type load cell is installed in the machine casting with test spindle removed. Load cell output is compared with output generated when the cell is loaded in a Timas-Olsen Tester. Calibrations indicated loading accuracy within ± 1.5 percent.

(2) Lubrication

The oil flowrate in each machine was calibrated at normal operating temperature by flowing the oil into a graduated cylinder.

(3) Speed

Rotational speed of each machine was checked by a strobe-type tachometer, which is calibrated against 60 Hz ac electric current.

d. Endurance Test Conditions

The following were the established bearing endurance test conditions:

- Speed — 5500 rpm
- Load — 1975 lb Radial
- Lubrication — MIL-L-7808
- Temperature — No heat added.

It was considered desirable to mix the bearings within the machines to prevent idiosyncracies of individual machines from influencing overall results. Since the center two bearings operate in a slightly different thermal regime than the outboard bearings, the test bearings were also mixed in the various test positions. The two center bearings for each machine were matched to within 0.0001 inch in internal diametral clearance. This practice provided a constraint within which bearings could be installed in particular locations. When the 8 machines were initially set up, each bearing lot was divided almost equally between center positions and end positions. As bearing were replaced they were matched as closely as possible by bearing with the same internal clearance.

e. Task VII — Endurance Test Results

Endurance testing of the 35-mm bearings fabricated in Task VI was terminated when 8 of the MRC2001 bearings developed classic subsurface fatigue spalls 0.008 to 0.010 inch deep within 439 hours while only one M50 bearing developed a spall. The M50 spall was in the inner race which is the characteristic location for this bearing in the Model A endurance test rig. However, the MRC2001 spalls occurred on three inners, two outers, and three balls. Figures 109 through 112 present photographs of typical bearing component spalls. The predictions from these tests using Weibull analyses established the MRC2001 bearing B_{10} life (all component failures) at 75.1 hours versus 977 hours for M50 (Figure 113). The test results are presented in Table 37.

An investigation to determine the cause of the unexpected low endurance life of the MRC2001 35-mm bearings was undertaken. The following summarizes the results of the investigation.

(1) Metallurgical Studies

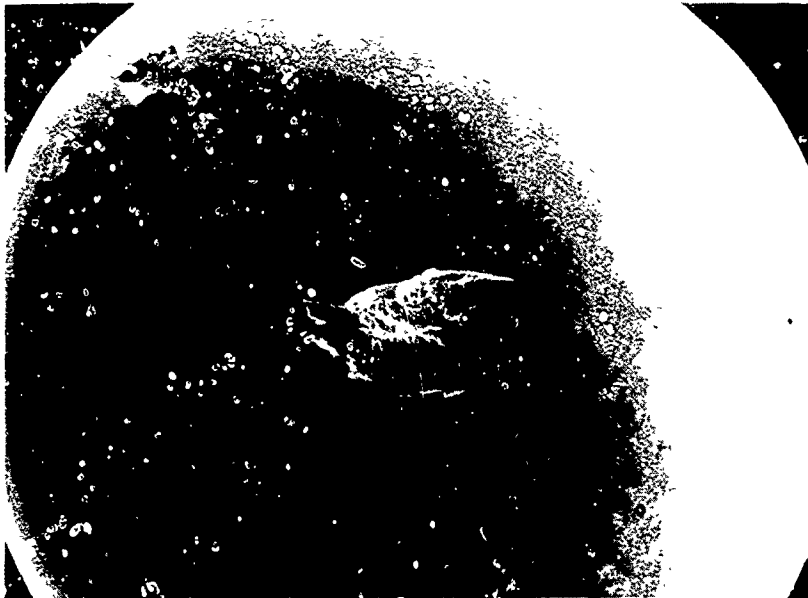
The purpose of the study was to find microstructural reasons why the Phase I MRC2001 RCF test specimens performed better compared to M50 than the MRC2001 35-mm endurance bearings. The overall conclusion of the metallurgical investigation is that no obvious microstructural problem was responsible for the disappointing performance of the MRC2001 35-mm bearings. Differences in thermomechanical processing techniques used to fabricate the RCF bar samples and the various bearing components had only modest effects on final alloy microstructure. Findings of the specific studies are as follows.

(a) Grain Size

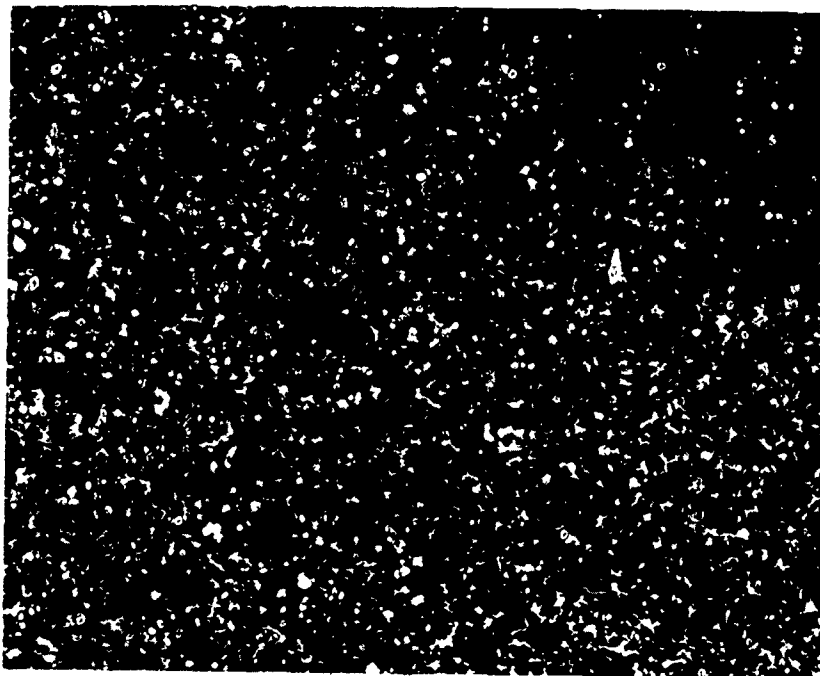
MRC2001	Inner Race	--	ASTM 13-14
	Outer Race	—	ASTM 13-14
	Ball	—	ASTM 12-13
	RCF Test Specimen	-	ASTM 13-14

(b) Crack Propagation Analysis

Secondary cracks adjacent to the primary bearing fatigue spall followed prior austenite grain boundaries (Figure 114). The cracks only followed a martensite-carbide boundary when a grain boundary was also present. This type of fracture path has been observed in the past for other powder metallurgy high chromium bearing alloys. It was not possible to precisely determine the fracture path of the primary spall on either the RCF bar or the bearing, however, the fracture path for both spalls appeared to also follow the prior austenite grain boundaries. The RCF bars did not exhibit secondary cracking around the primary spall possibly because there was less secondary damage after the spall.



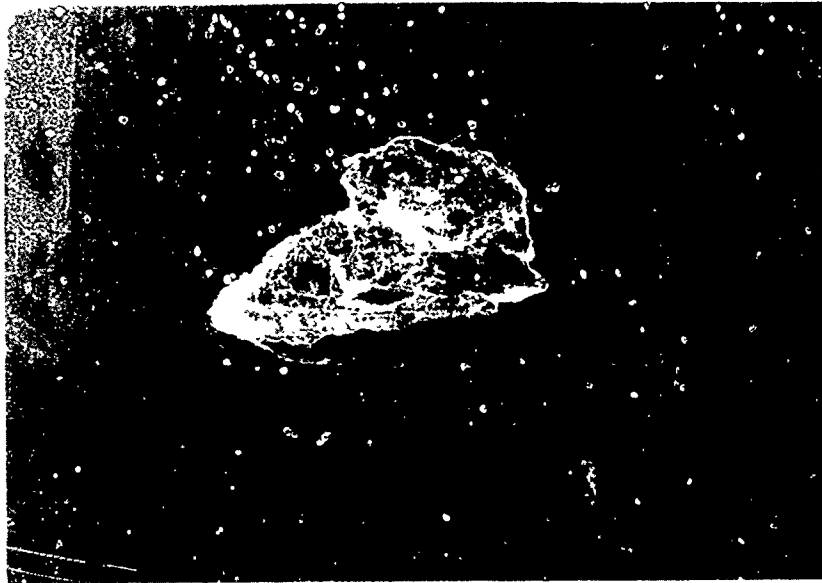
Ball Spall (20X)



E2 Ball Spall Cross Section (400X)

FD 300520

Figure 109. — MRC200j 35-mm Endurance Bearing S/N E2 Spalled Ball



Inner Race Spall (20×)



E20 Inner Race Spall Cross Section (100×)

FD 300521

Figure 110. — MRC2001 35-mm Endurance Bearing S/N E20 Spalled Inner Race



FC 85729

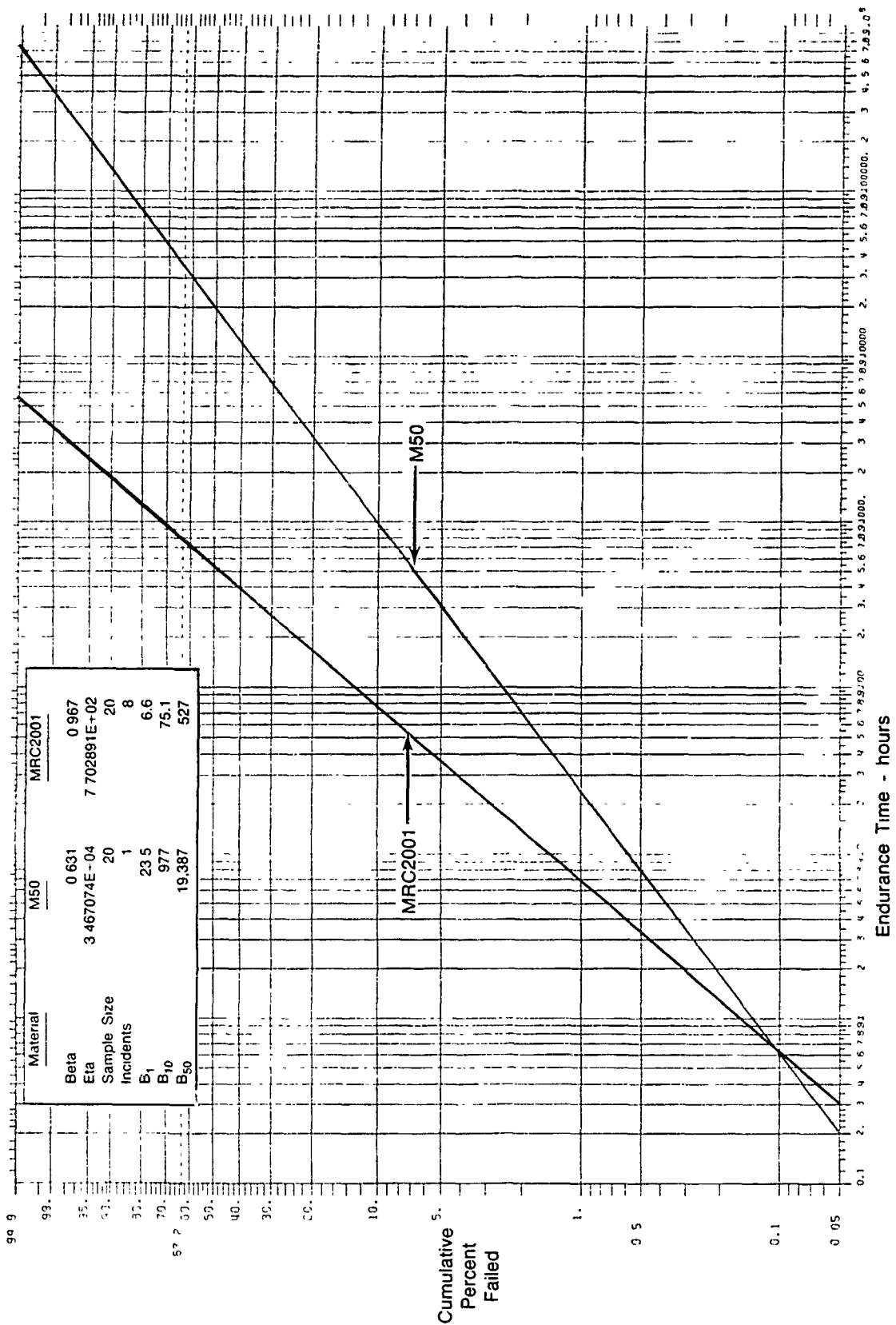
Figure 111. — MRC2001 35-mm Endurance Bearing S/N E12 Outer Race Spall (20 \times)



FD 300519

Figure 112. — M50 35-mm Endurance Bearing S/N 17 Inner Race Spall (20 \times)

Thin foil transmission electron microscopy revealed that a continuous film of carbide did not exist along all prior austenite grain boundaries for MRC2001 alloy. A spalled RCF bar and a spalled bearing ball were studied (Figures 115 and 116). A great deal of carbide agglomeration was observed in both samples which was also observable at lower magnifications.



FD 300529

Figure 113. — Composite Maximum Likelihood Weibull Distribution Plot of M50 and MRC2001 Task VII Endurance Bearing Failure

TABLE 37.

TASK VII 35-MM BEARING ENDURANCE TEST LOG

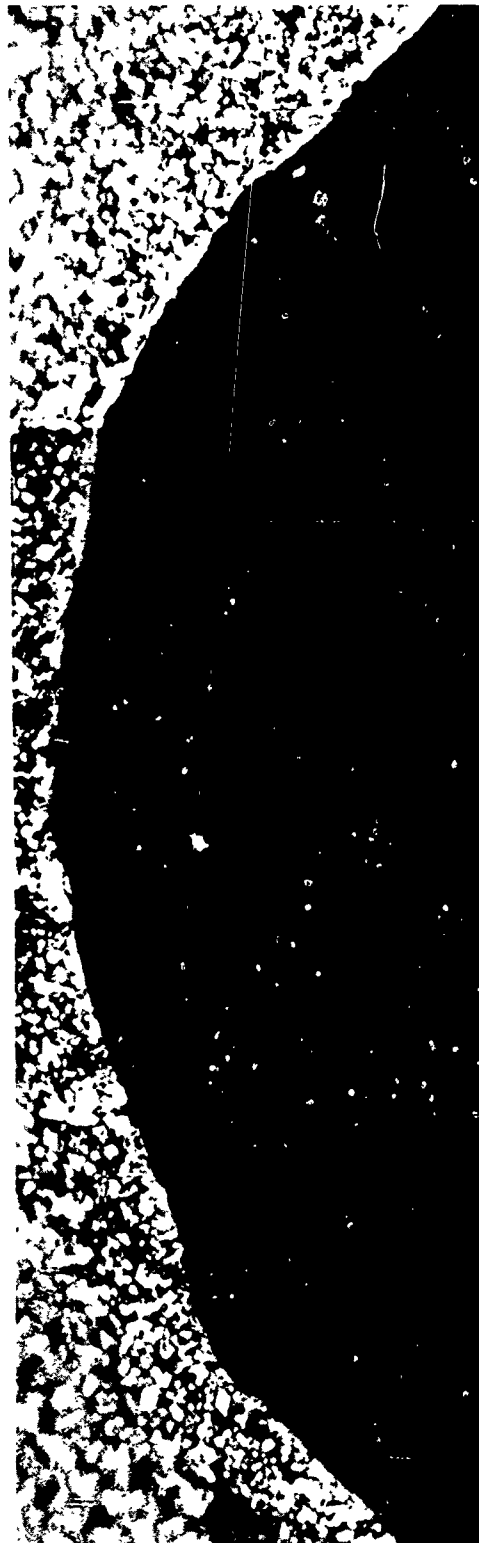
<i>MRC2001 Bearings</i>			<i>M50 Baseline Bearings</i>		
<i>Bearing S/N</i>	<i>Logged Endurance Time (hr)</i>	<i>Status</i>	<i>Bearing S/N</i>	<i>Logged Endurance Time (hr)</i>	<i>Status</i>
E1	439.9	Ball Spall	1	360	Suspended
E2	112.7	Ball Spall	2	37	Suspended
E3	145.2	Inner Race Spall	3	415	Suspended
E4	428	Suspended	4	415	Suspended
E5	Not Run		5	360	Suspended
E6	424	Suspended	6	138	Suspended
E7	439	Suspended	8	15	Suspended
E8	346	Suspended	9	428	Suspended
E9	125.9	Inner Race Spall	10	Not Run	
E10	26.9	Ball Spall	11	203	Suspended
E11	428	Suspended	12	439	Suspended
E12	84.8	Outer Race Spall	13	383	Suspended
E13	367	Suspended	14	424	Suspended
E14	415	Suspended	15	424	Suspended
E15	383	Suspended	16	273	Suspended
E16	273	Suspended	17	69.5	Inner Race Spall
E17	360	Suspended	18	Not Run	
E18	424	Suspended	19	367	Suspended
E19	69.2	Outer Race Spall	20	383	Suspended
E20	341	Inner Race Spall	22	Not Run	
E21	367	Suspended	23	439	Suspended
E22	Not Run		24	428	Suspended
			25	Not Run	
			26	367	Suspended

64784



(1000X)

Secondary Cracking Around Fatigue
Spall of 35 mm Bearing Inner Race
Nital-Picral Etch



(1000X)

MRC2001 Rolling Contact Fatigue
Specimen Spall Nital-Picral Etch

FD 300518

Figure 114. — Photomicrograph of Primary Fatigue Spall of MRC2001 RCF Specimen
and MRC2001 Inner Race



Figure 115. — Thin Film Transmission Electron Micrograph of MRC2001 RCF Specimen

FD 300517



36,000x



60,000x



100,000x

This area appears to be slightly overtempered. The small area appears to be ferrite with many temper carbides; however Vicker's DPH = 826 (= 65 Rc), so overtempering is doubtful.

FD 300516

Figure 116 — Thin Film Transmission Electron Micrograph of MRC2001 35-mm Endurance Bearing Ball

(c) Retained Austenite

The retained austenite content of a failed MRC2001 outer bearing race sample was determined to be less than five percent volume. The large volume fraction of Cr_{23}C_6 carbides in this alloy prevented a more precise determination to be made. The retained austenite content of the MRC2001 RCF specimens used in the Phase I specimen screening tests was determined at the conclusion of the screening tests to be less than 3 percent volume. The difference in the measured volume percent threshold is measuring technique related and is not considered significant.

(d) Carbide Quantitative Metalography

Quantitative metallographic analysis precisely determined the volume percent carbide in an RCF bar, a spalled inner race, and a spalled ball.

RCF bar = 23.0 percent volume carbide
Inner race = 21.0 percent volume carbide
Ball = 22.2 percent volume carbide.

The size distribution of carbide in all samples was close to the same. Precise size numbers could not be determined since many carbides were agglomerated together.

(e) Microstructure

Only slight microstructural differences were observed between the spalled MRC2001 bearings and the spalled RCF bars. None of the slight differences observed, i.e., grain size, number of ultrafine temper carbides, carbide agglomeration, or carbide percent volume could explain the disappointing performance of the MRC2001 bearings. However, the martensite in the RCF bars did etch much darker than the martensite in the ball and inner and outer bearing race samples when a grain boundary attacking etch was applied (Figure 117). While inconclusive, this can be an indication of a difference in residual stress magnitude or pattern between the RCF bar and the bearing component parts. The heat treatment history of all MRC2001 test rods and bearing component parts was reviewed and determined to be essentially identical.

(f) Thermomechanical Processing

The microstructure, fracture toughness, density, and hardness were traced through the different thermomechanical processing steps to which the MRC2001 rings were subjected (Figures 118 through 121). It was concluded from this study that the forging process had no apparent effect on fracture toughness, and that the upset and ring hammer forge tended to eliminate mottled structure and refine microstructure. It was also noted that the heat treatment caused agglomeration of carbides into large triangular/multisided carbide formations.

(2) Visual, Dimensional, Residual Stress, and Quali., Inspections

- Generally, both M50 and MRC2001 races exhibited dented raceways under magnified inspection. MRC2001 typically exhibited banded balls compared to M50. The banded balls were determined to be the result of an unintended axial load component caused by a seizing compound. The seizing compound was applied to the outer races to prevent the race from spinning in its housing.

- Surface measurements of inner and outer rings of run bearings exhibited no significant difference between M50 and MRC2001. For both materials, inner ring finish was much better than outer ring. Surface finish (random inspection) of MRC2001 balls of run bearings tended to be rougher than M50 balls.
- Residual stress/depth gradient for M50 inner/outer rings and MRC2001 outer rings exhibit typical profiles consistent with acceptable grinding practices. MRC2001 inner rings exhibit a tensile residual stress profile suspected to be associated with burnished/polished surface texture (Figure 122).
- SEM replications corroborate the differences in finishes observed and measured between inner and outer rings (Figure 123). Grinding furrows are more evident and distinct in the MRC2001 outer rings than in M50 rings, even after hours of running.
- Bearing inspection data were reviewed and the 35-mm bearings for both materials met all production requirements.

(3) Oil Analysis

Oil samples taken from both before and after the endurance rig's lubrication system filters were examined to obtain information on oil quality, debris type, particle size, and chip morphology. The lubrication system had three filters in series, the first being a coarse screen followed by two 10 μ nominal paper cartridges. Separate analyses were conducted at AFWAL/POSL and P&W laboratories. Both analyses found the level of debris to be more than was expected for a test rig and that the type of debris generally associated with rolling contact fatigue was not prominent.

The P&W study examined the chip size and found many particles in excess of 15 μ in the oil sample taken downstream of the final 10 μ nominal filter. The oil analysis conducted by AFWAL/POSL found the MIL-L-7808J lubricant to be in good condition with total acid numbers (TAN) and viscosities well within limits.

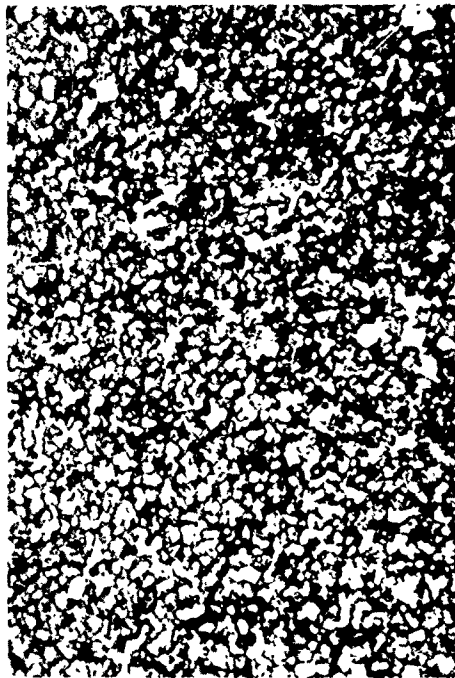
For the endurance test rig used in this program the inner race is the highest stressed test bearing component. Of the 8 MRC2001 bearings that failed, 3 were ball failures, 3 were inner race failures, and 2 were outer race failures; this indicates that the failures were not related to material durability.

Given the results of the above investigations it was reasoned that the low endurance life experienced by the MRC2001 35-mm bearings (compared to the M50 baseline 35-mm bearings) was induced by surface distress resulting from oil system debris contamination and less than optimum grinding practice.

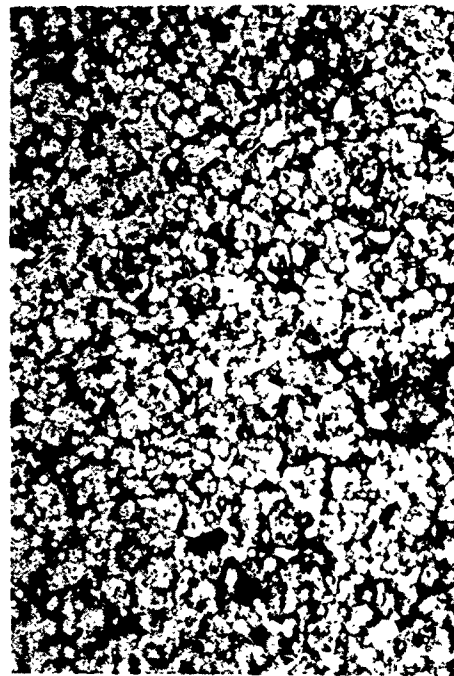
f. Redirected Bearing Fabrication and Endurance Program

(1) Task 421 — Bearing Fabrication

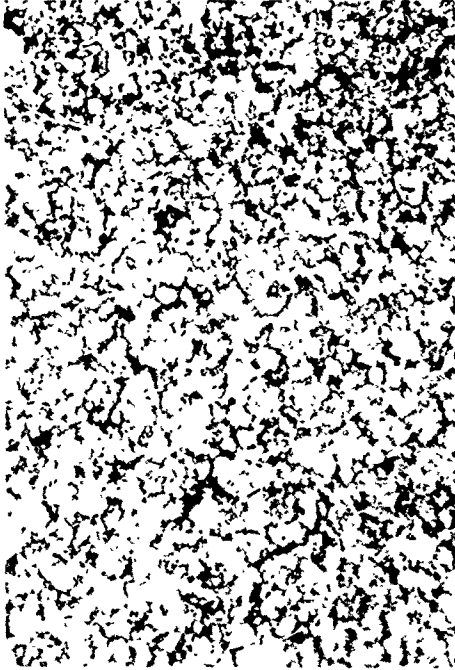
As a result of the low endurance life investigation, the Phase II bearing fabrication and test program was redirected. Task VII — Bearing Life Testing and Analysis; Task VIII — Bearing Performance Testing; and Task IX — Bearing Corrosion Testing were terminated. Tasks 421 and 422 were constituted



MRC2001 Rolling Contact Fatigue Bar (1000X)
Nital-Picral Etch
Grain Size = ASTM 13-14



MRC2001 Outer Bearing Race (1000X)
Nital-Picral Etch
Grain Size = ASTM 13-14



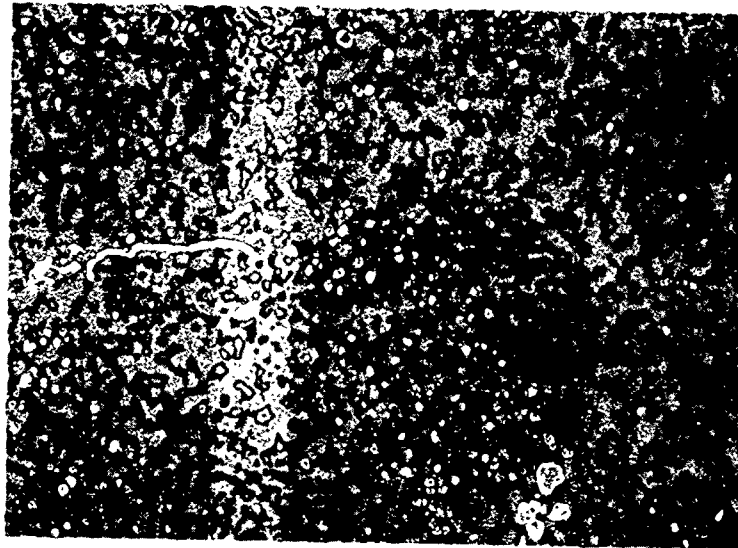
MRC2001 Ball (1000X)
Nital - Picral Etch Grain Size = ASTM 12-13



MRC2001 Inner Race Failure (1000X)
Nital - Picral Etch
Grain Size = ASTM 13-14

FD 300515

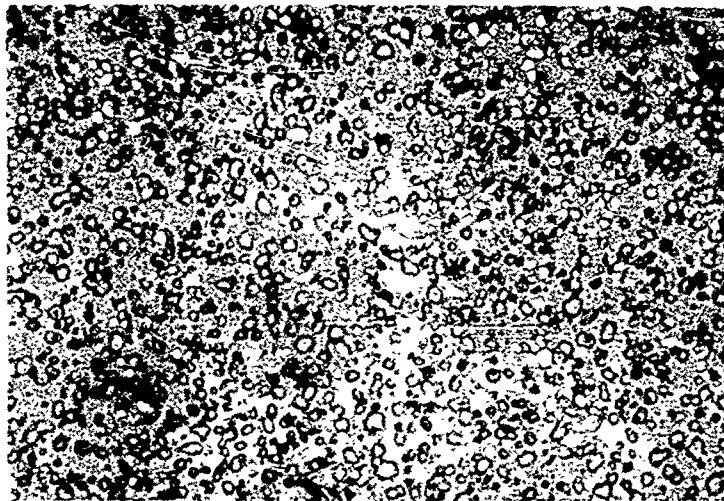
Figure 117. — MRC2001 Microstructure, Grain Size, and Etch Response Comparison



Fracture Toughness - 15.13 psi√in. (After Sample Was Hardened)

FD 300514

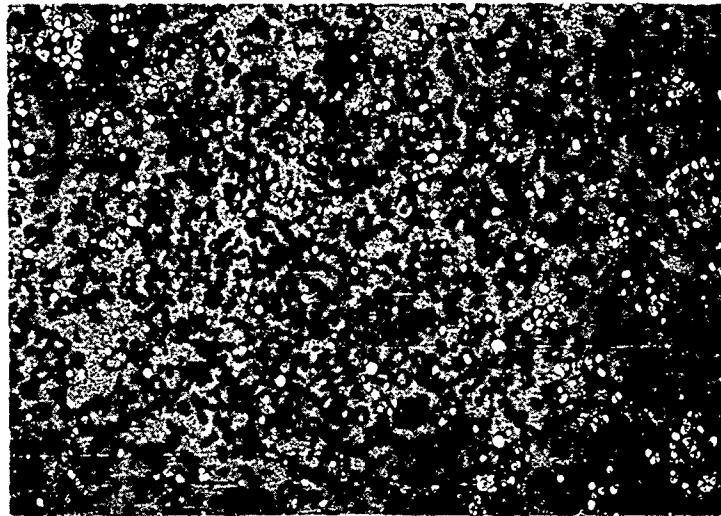
Figure 118. — MRC2001 35-mm Bearing Ring Microstructure as HIPped (1000X)



Hardness - Rc 35-36
 Density - 7.766-7.763 (After Hardening)
 Fracture Toughness - 15.11 ksi √in. (After Sample Was Hardened)

FD 300513

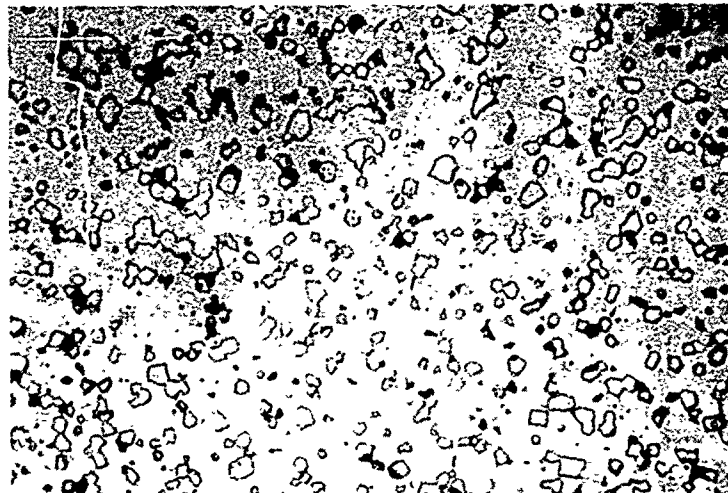
Figure 119 — MRC2001 35-mm Bearing Ring Microstructure After HIPping, Upsetting, and Drilling (1000X)



Hardness - Rc 36.5
 Density - 7.661 - Cracks at Circumference Make Measurement Doubtful
 Fracture Toughness - Ring too Small to Obtain Specimen

FD 300511

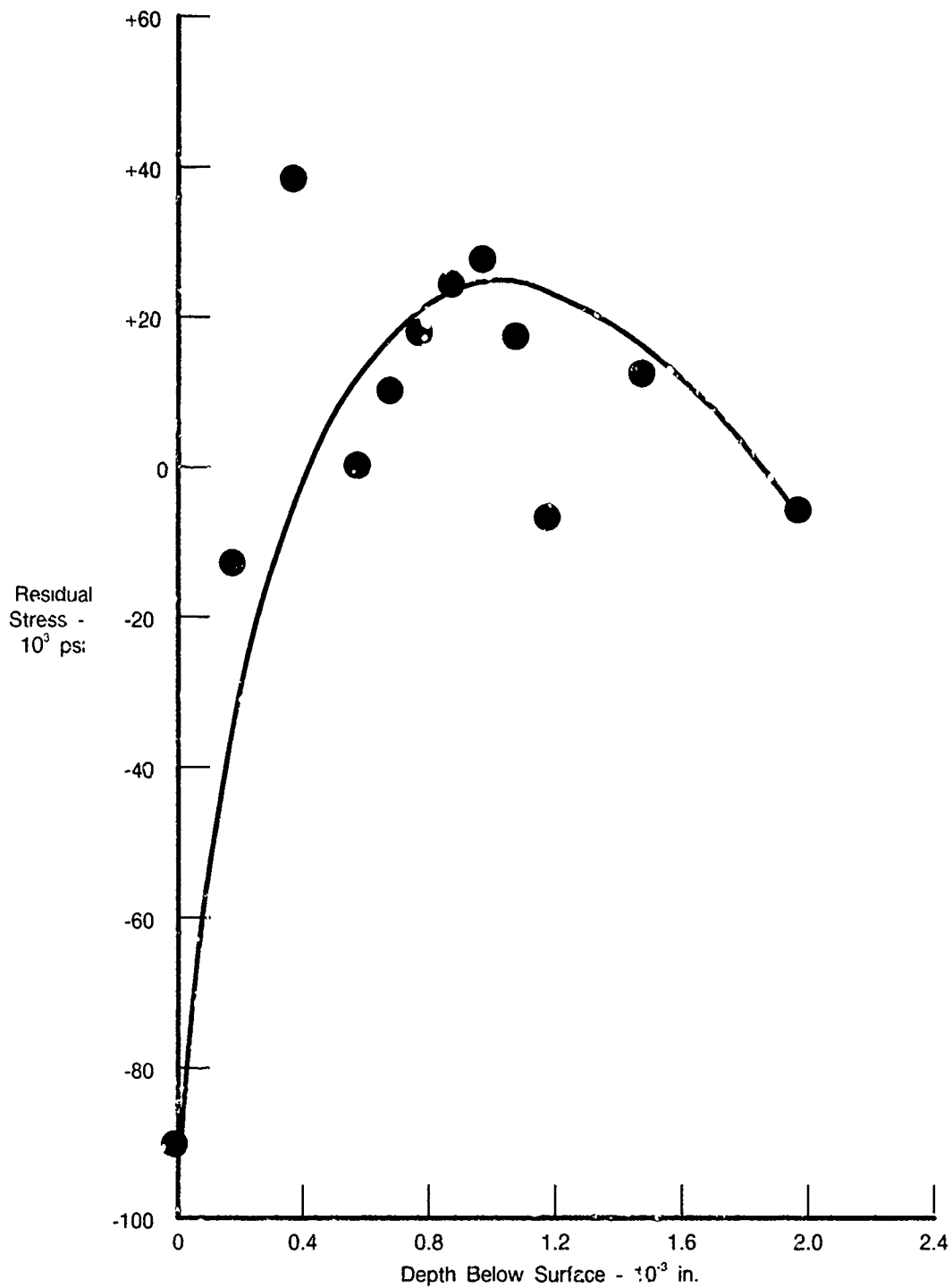
Figure 120. — MRC2001 35-mm Outer Ring Microstructure After HIPping, Upsetting, and Hammer Forging (1000X)



Hardness - Rc 61-66
 Density - 7.661
 Fracture Toughness - Ring too Small to Obtain Specimen

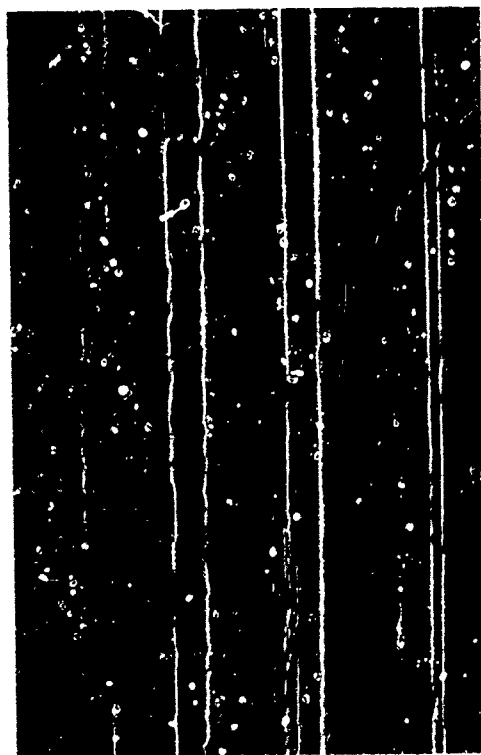
FD 300512

Figure 121. -- MRC2001 35-mm Outer Ring Microstructure After HIPping, Hammer Forging, and Hardening (1000X)



FDA 300506

Figure 122. — Tensile Residual Stress Profile of MRC2001 Inner Race S/N E22



Replica S/15 Outer
M50 Outer Race S/N 15



Replica S/N 13 Inner
M50 Inner Race S/N 13



Replica E17 Outer
MRC2001 Outer Race S/N E17



Replica 110 Inner
MRC2001 Inner Race S/N E15

Figure 123. --- Comparison of Typical MRC2001 and M50 Race Surface (1000X)

In Task 421, the fifteen remaining unspalled MRC2001 inner races were reground using a grinding practice optimized for the MRC2001 material. These inner races were then matched with new M50 balls and outer races. Since the inner ring is the highest stressed component in the Model A endurance rig, this approach permitted a demonstration of MRC2001 rolling contact fatigue potential in full-scale bearings without the influence of the different outer race and ball manufacturing processes. Twenty new M50 baseline bearings were also manufactured. These two lots of bearings were endurance tested in Task 422.

The low endurance life investigation, in particular the results of the etch response study and residual stress analysis, suggested that the grinding process used in the manufacture of the MRC2001 endurance bearing races resulted in an unfavorable (tensile) surface condition.

A grinding study was undertaken by TRW to optimize the grinding parameters used in the manufacture of MRC2001 bearing inner races. Because of the limited availability of MRC2001 stock, BG42, another high chrome steel (Fe-15Cr-4Mo-1.2V-1.2C-0.45Mn-0.3Si), was used in a series of "one factor at a time" tests to establish acceptable grinding and honing parameters. The selected parameters were then applied to the MRC2001 material to substantiate the surface condition improvement. Residual stress analyses results are presented in Figure 124.

At the completion of the grinding study the raceway and bore surfaces of the remaining original 35-mm, MRC2001 inner races were refurbished using the optimized proprietary grinding practice. The inner races were then assembled with new M50 ball and outer race components and new nylon snap-in separators.

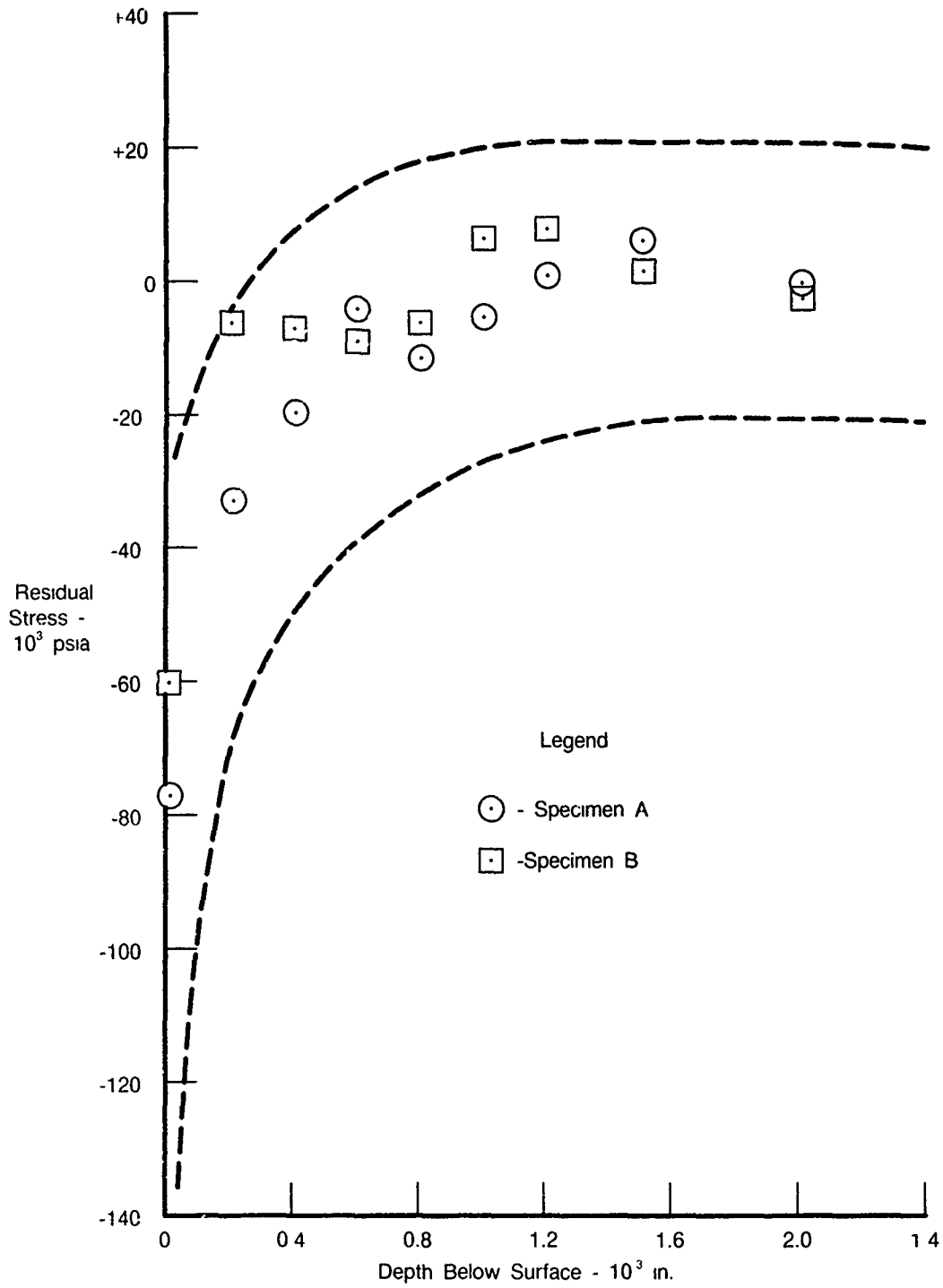
Twenty new M50 baseline 35-mm endurance bearings were also fabricated. As part of a parallel but separately funded program, twenty RSP565 MRC207S 35-mm endurance bearings were also fabricated. RSP565 is the conventional argon atomized powder version of RSR565 material evaluated in the Phase I specimen tests (reference Section II 3.c.(6)).

The RSP565 powder used for the test bearings was fabricated from a vacuum induction melted prealloyed ingot which was atomized in an argon atmosphere. Table 38 outlines the thermomechanical material consolidation processes for the RSP565 endurance bearing races.

All RSP565 raceway components were fabricated using the same grinding procedure developed for MRC2001. The RSP565 ball stock was extruded at 2000°F and at a 43 to 1 reduction ratio. The stock was then centerless ground to hot heading size and annealed. The annealed ball stock was hot headed at 1950°F, ground, and lapped to finished ball size at the Industrial Tectonics, Inc., Ann Arbor, Michigan ball plant. The RSP565 ball and race heat treatment schedule is presented in Table 39.

The RSP565 bearings were incorporated into the MRC2001/M50 endurance test program to provide back to back test result comparisons for each program.

Inspection data are presented in Tables 40 through 43. Figures 125 through 128 illustrate the range of surface texture and residual stress profiles achieved for each bearing lot.



FDA 300503

Figure 124 — Residual Stress Profile of MRC2001 Test Rings

TABLE 38.

THERMOMECHANICAL PROCESSING OF THE RSP565 RACE BLANKS

<i>Process</i>	<i>Condition</i>
HIP (Hot Isostatic Press) Encapsulated Powder	1925°F at 15 ksi
Strip HIP Can	
Press Forge	3 to 1 Diameter Reduction at 2050°F
Furnace Cool Mill Anneal	1600°F
Isothermal Forge (GATORIZED™)	9 to 1 Height Reduction
Ring Blanks Wire Electrical Discharge Machined from GATORIZED™ Pancake	

6.56C

TABLE 39.

RSP565 HEAT TREAT SCHEDULE

<i>Process</i>	<i>Temperature (°F)</i>
Preheat	1550
Austenitize	2000
Marquench	500
Air Cool	
Wash	75
Air Cool	
Deep Freeze	-320
Temper	950
Air Cool	
Aqua Quench	100
Deep Freeze	-320
Temper	950
Air Cool	
Aqua Quench	100
Temper	950
Air Cool	
Aqua Quench	100
Temper	950
Air Cool	
Aqua Quench	100
Temper	950
Air Cool	80

6.56D

TABLE 40.

INSPECTION DATA FOR 35-MM BEARINGS WITH MRC2001 INNERS, M50 BALLS AND OUTER RACES

S/N	Bore	OD	Radial Clearance	Inner Race Surface Finish		Outer Race Surface Finish		Hardness Rc		Anderometer			Stock Removal Inner Race from Previous Grind	
				μ in. AA	Curvature	μ in. AA	Curvature	Inner	Outer	Lo	Med	Hi	Inner	Previous Grind
1	1.3830	2.8345	0.0025	2	0.5185	4	0.5185	61.4	62.8	10	15	35	0.0197*	
2	1.38299	2.8345	0.0012	1	0.5190	1.5	0.5185	62.3	63.0	5	20	30	0.0189*	
9	1.3830	2.8344	0.0010	1.5	0.5195	3	0.5185	61.6	63.3	5	15	20	0.0047	
10	1.3829	2.8345	0.0010	1.5	0.5195	1.5	0.5190	61.7	63.1	10	20	35	0.0035	
11	1.3829	2.8345	0.0023	2	0.5185	1	0.5190	61.3	62.9	5	10	20	0.0042	
12	1.38295	2.8345	0.0020	1.5	0.5185	1.5	0.5185	61.9	63.1	15	20	35	0.0033	
14	1.38295	2.8344	0.0009	2.5	0.5195	1.2	0.5190	62.0	62.8	10	15	25	0.0033	
16	1.3828	2.8344	0.0016	1.5	0.5190	2	0.5190	61.5	62.8	5	20	20	0.0129	
19	1.3829	2.8345	0.0012	1.3	0.5185	1.2	0.5190	61.7	63.1	10	15	25	0.0102	
21	1.3829	2.8345	0.0025	2.5	0.5185	1	0.5190	61.7	63.2	5	15	35	0.0234*	
22	1.38285	2.8345	0.0013	1.5	0.5185	1.8	0.5185	61.6	62.9	5	10	20	0.0051	
23	1.3829	2.8345	0.0011	1.5	0.5190	2.5	0.5190	61.5	62.8	15	20	35	0.0041	
30	1.3829	2.8344	0.0011	1.2	0.5190	2	0.5185	61.8	62.9	5	15	30	0.0260*	
31	1.38285	2.8345	0.0014	1.5	0.5185	1.8	0.5190	61.7	62.9	10	15	30	0.0092	
34	1.3829	2.8344	0.0019	1.5	0.5190	2	0.5190	61.7	63.1	5	15	30	0.0263*	

*These inner rings had not been match ground earlier.

In addition, race finishes of each bearing were examined by SEM, and each inner race was inspected by eddy current.

TABLE 41.
INSPECTION DATA FOR 35-MM M50 BEARINGS

S/N	Bore	OD	Radial Clearance	Inner Race		Outer Race		Hardness Rc		Anderometer		
				Surface Finish μ in. AA	Curvature	Surface Finish μ in. AA	Curvature	Inner	Outer	Lo	Med	Hi
1	1.38292	2.8344	0.0009	1	0.5197	2.5	0.5195	62.4	63.0	5	15	30
2	1.3829	2.8345	0.0010	1.5	0.5197	2	0.5190	62.7	63.0	10	30	35
3	1.38288	2.8345	0.0009	1.2	0.5197	1.2	0.5195	62.5	62.8	10	20	35
4	1.3829	2.8345	0.0011	1	0.5197	1.2	0.5197	62.5	62.9	10	15	30
5	1.38289	2.8344	0.0012	1	0.5197	2.5	0.5192	63.0	63.1	15	25	30
6	1.38288	2.8346	0.0008	1	0.5197	2	0.5190	62.8	63.0	10	20	25
7	1.38232	2.8345	0.0010	1	0.5200	2	0.5192	62.3	62.8	5	20	35
8	1.3829	2.8345	0.0010	1	0.5197	2.5	0.5197	62.4	62.8	15	20	30
9	1.38285	2.8344	0.0009	1.4	0.5197	1	0.5190	62.7	62.9	15	20	35
10	1.38291	2.8345	0.0011	1	0.5197	1.5	0.5197	62.5	63.0	5	15	30
12	1.38295	2.8344	0.0010	1	0.5197	3	0.5192	62.6	62.7	10	20	35
13	1.3828	2.8346	0.0010	1	0.5197	1.8	0.5192	62.7	63.1	5	15	15
14	1.38285	2.8345	0.0010	1	0.5200	2.5	0.5195	62.5	63.0	10	20	35
15	1.38285	2.8345	0.0011	1.5	0.5195	2	0.5195	62.3	62.7	5	20	20
16	1.3829	2.8345	0.0010	1	0.5200	4	0.5197	62.7	62.9	10	15	30
17	1.3829	2.8344	0.0012	1.5	0.5197	2	0.5197	63.0	63.2	15	25	35
18	1.3829	2.8345	0.0010	1	0.5195	4	0.5192	62.6	62.8	10	20	25
19	1.3829	2.8346	0.0009	1	0.5195	1.8	0.5195	62.8	63.0	15	15	30
20	1.38285	2.8345	0.0011	1.3	0.5197	2	0.5192	62.3	62.8	10	25	30
21	1.38285	2.8345	0.0009	1	0.5197	3	0.5195	62.3	62.9	15	20	40

In addition, race finishes of each bearing were examined by SEM, and each inner race was inspected by eddy current.

6377K

TABLE 42.

INSPECTION DATA FOR 35-MM RSP565 BEARINGS

S/N	Bore	OD	Radial Clearance	Inner Race Surface Finish		Outer Race Surface Finish		Hardness Rc		Anderometer		
				μ in. AA	Curvature	μ in. AA	Curvature	Inner	Outer	Lo	Med	Hi
1	1.38292	2.8344	0.0025	1.8	0.5195	3	0.5190	61.8	60.8	10	15	25
2	1.3829	2.8344	0.0020	2	0.5195	2	0.5192	61.3	61.5	10	20	20
3	1.38287	2.8345	0.0019	1.8	0.5195	4	0.5190	61.4	61.6	5	20	30
4	1.38292	2.8344	0.0018	1.8	0.5195	2	0.5195	62.3	61.0	15	20	35
5	1.38295	2.8345	0.0019	2.5	0.5192	3	0.5190	61.6	61.5	10	15	30
8	1.38289	2.8345	0.0014	1.7	0.5195	4	0.5188	61.0	61.4	5	15	25
10	1.38285	2.8346	0.0016	2	0.5190	4	0.5185	61.1	61.5	10	20	25
11	1.38286	2.8344	0.0018	1.5	0.5190	3	0.5190	61.6	61.1	5	20	15
12	1.3828	2.8344	0.0014	1	0.5190	2	0.5190	61.4	61.7	15	15	30
13	1.3829	2.8345	0.0011	2.5	0.5195	2	0.5192	61.3	60.9	10	15	30
14	1.3829	2.8345	0.0012	2	0.5190	3	0.5190	61.4	61.6	10	20	25
16	1.3828	2.8345	0.0013	2.5	0.5185	3	0.5190	61.5	61.8	10	15	30
17	1.3829	2.8345	0.0018	2	0.5185	3	0.5190	61.7	61.2	5	10	30
18	1.3829	2.8346	0.0018	2.5	0.5185	1.8	0.5190	61.1	61.4	15	15	35
19	1.3828	2.8345	0.0021	2	0.5185	3	0.5190	61.1	61.2	15	20	20
20	1.3829	2.8346	0.0019	2	0.5185	3	0.5190	61.4	61.0	5	20	15
21	1.3829	2.8344	0.0019	2	0.5185	1.8	0.5192	62.0	61.3	15	20	15
22	1.38285	2.8344	0.0020	2	0.5185	2	0.5192	61.2	61.5	10	15	25
23	1.3829	2.8345	0.0014	4	0.5195	2.5	0.5190	61.9	61.4	10	20	30
24	1.3828	2.8345	0.0018	2.5	0.5185	3	0.5190	62.1	61.1	10	20	15

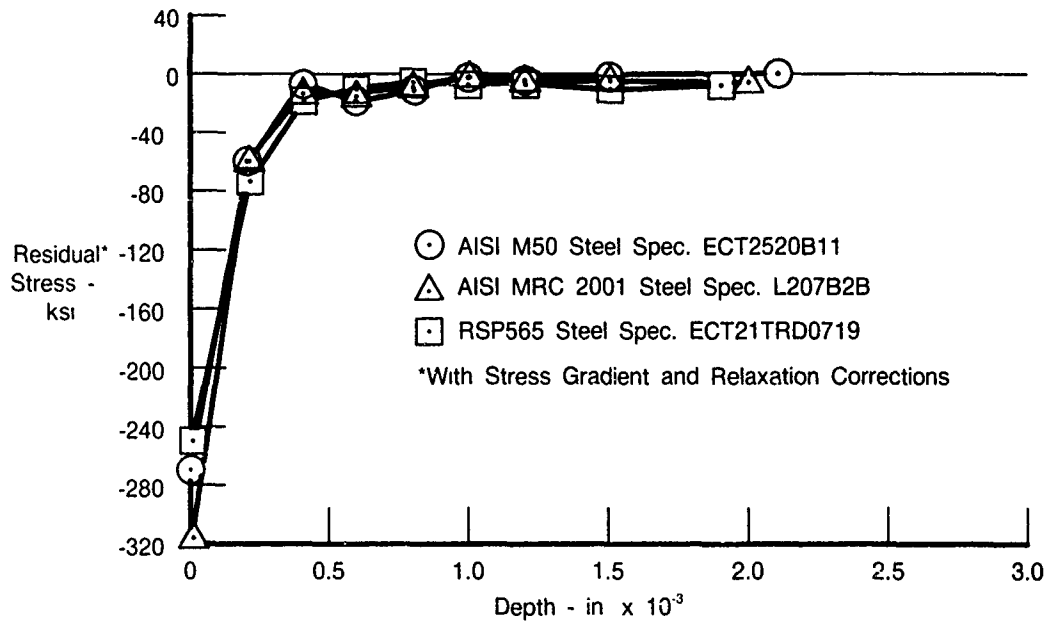
In addition, race finishes of each bearing were examined by SEM, and each inner race was inspected by eddy current.

NIKE

TABLE 43.
INNER RACE FITS AND BEARING INTERNAL CLEARANCES

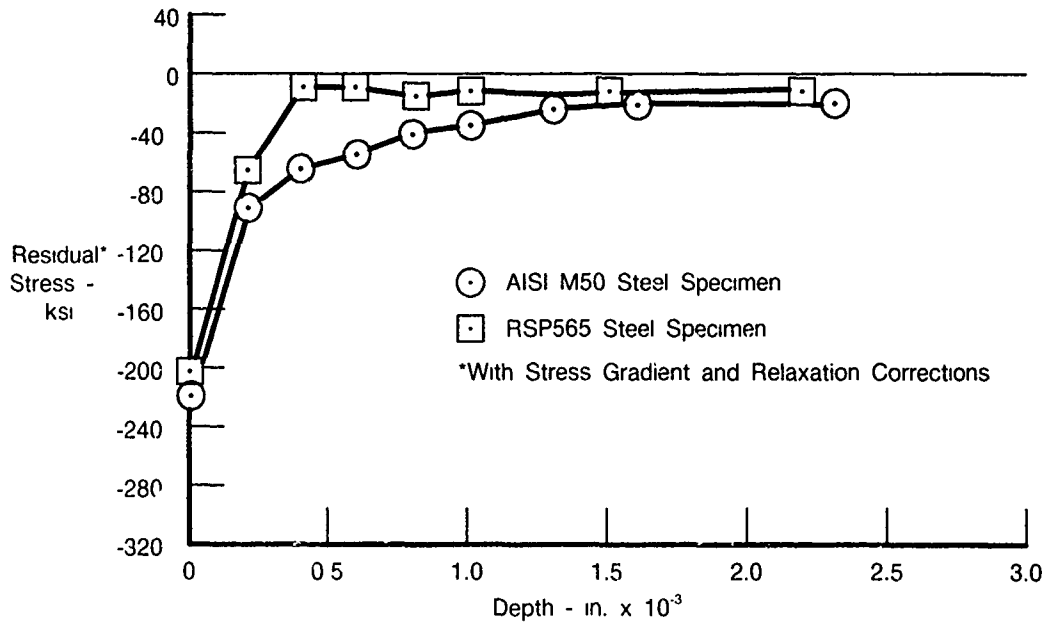
M50 Bearings			RSP565 Bearings			Bearing with MRC2001 Inners		
S/N	Interference Fit, Inner	Internal Clearance	S/N	Interference Fit, Inner	Internal Clearance	S/N	Interference Fit, Inner	Internal Clearance
520-1	0.00063	0.0009	519-1	0.00063	0.0025	521-1	0.00065	0.0025
520-2	0.00065	0.0010	519-2	0.00095	0.0020	521-2	0.00056	0.0012
520-3	0.00095	0.0009	519-3	0.00068	0.0019	521-9	0.00055	0.0010
520-4	0.00052	0.0011	519-4	0.00063	0.0018	521-10	0.00050	0.0010
520-5	0.00066	0.0012	519-5	0.00060	0.0019	521-11	0.00095	0.0023
520-6	0.00067	0.0008	519-8	0.00045	0.0014	521-12	0.00060	0.0020
520-7	0.00073	0.0010	519-10	0.00075	0.0016	521-14	0.00045	0.0009
520-8	0.00095	0.0010	519-11	0.00100	0.0018	521-16	0.00075	0.0016
520-9	0.00100	0.0009	519-12	0.00075	0.0014	521-19	0.00070	0.0012
520-10	0.00049	0.0011	519-13	0.00070	0.0011	521-21	0.00065	0.0025
520-12	0.00060	0.0010	519-14	0.00070	0.0012	521-22	0.00075	0.0013
520-13	0.00075	0.0010	519-16	0.00080	0.0013	521-23	0.00070	0.0011
520-14	0.00070	0.0010	519-17	0.00065	0.0018	521-30	0.00065	0.0011
520-15	0.00070	0.0011	519-18	0.00065	0.0018	521-31	0.00075	0.0014
520-16	0.00065	0.0010	519-19	0.00065	0.0021	521-34	0.00065	0.0019
520-17	0.00070	0.0012	519-20	0.00050	0.0019			
520-18	0.00065	0.0010	519-21	0.00065	0.0019			
520-19	0.00050	0.0009	519-22	0.00055	0.0020			
520-20	0.00075	0.0011	519-23	0.00065	0.0014			
520-21	0.00070	0.0009	519-24	0.00105	0.0018			

6172K



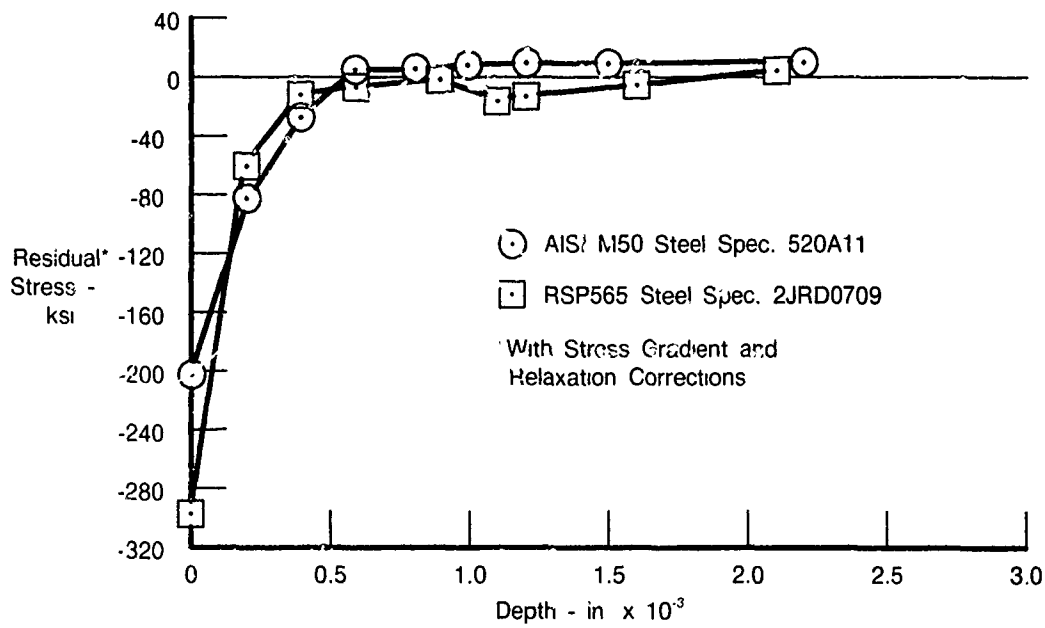
FDA 300498

Figure 125. — Circumferential Residual Stress vs Depth for Inner Raceways at Center Ball Track Location



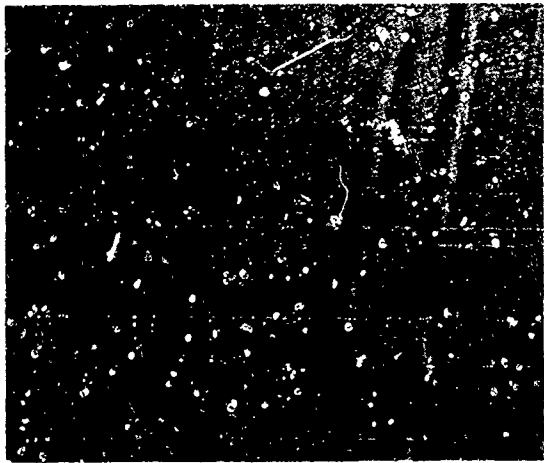
FDA 300499

Figure 126. — Residual Stress vs Depth at Arbitrary Location on Ball

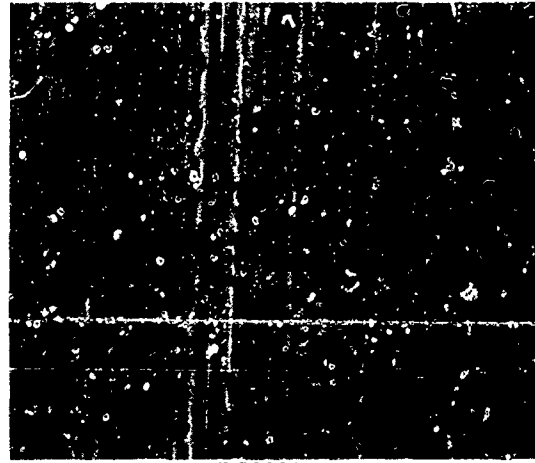


FDA 300500

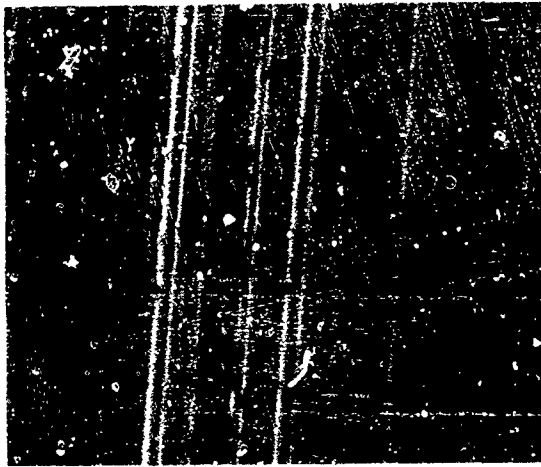
Figure 127. — Circumferential Residual Stress vs Depth for Outer Raceways at Center Ball Track Location



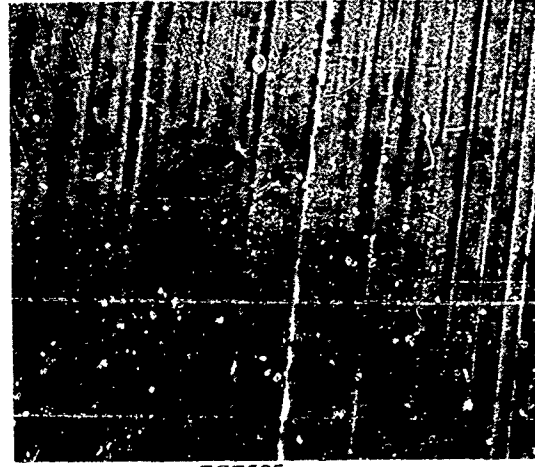
MRC2001 1000x
S/N 1



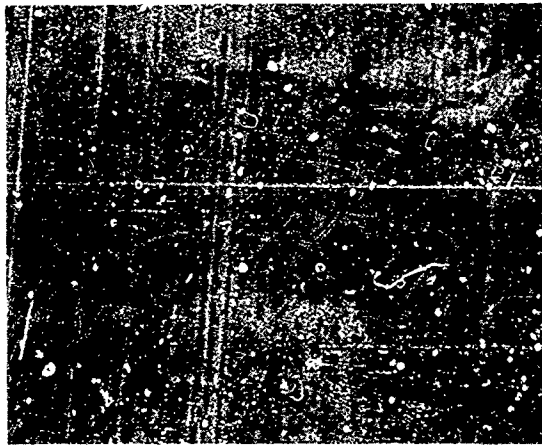
MRC2001 1000x
S/N 10



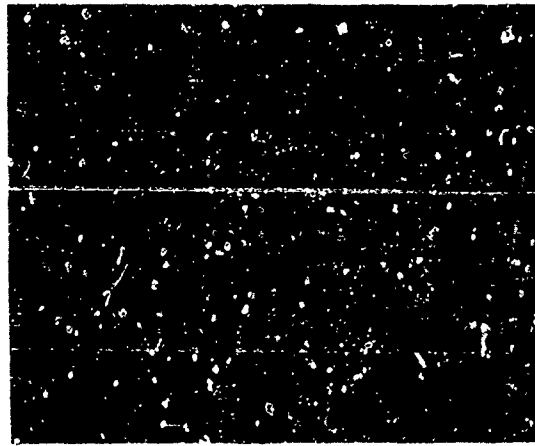
RSP565 1000x
S/N 2



RSP565 1000x
S/N 18



M50 1000x
S/N 20



M50 1000x
S/N 1

FD 300522

Figure 128 Range of Inner Race Surface Finish for MRC2001, RSP565, and M50

(2) Task 422 — Endurance Testing

The test facility/rig previously described in Section II.4.b "Endurance Test Facility" was modified per the following prior to the start of Task 422 endurance testing:

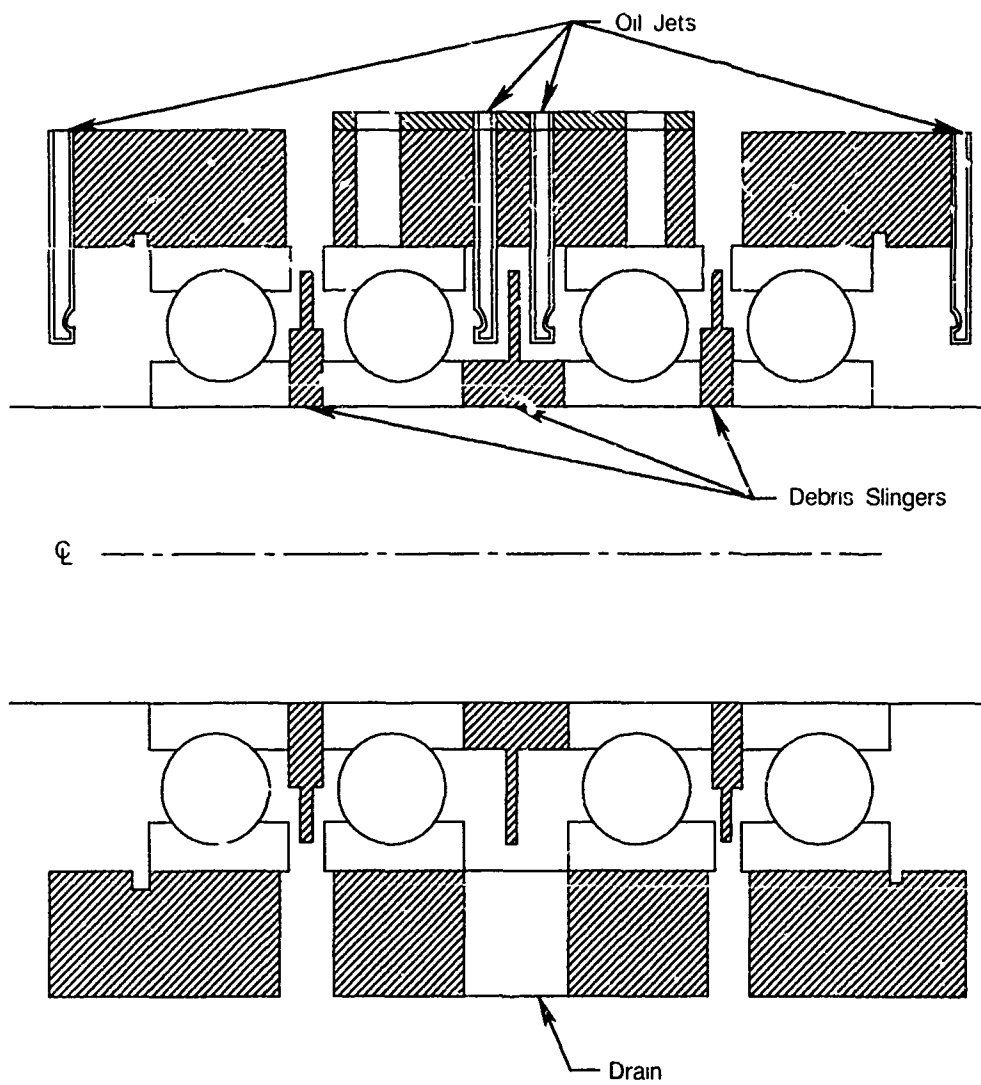
- Results of the oil analyses conducted as part of the Phase II low endurance life investigation indicated that the 10 micron nominal oil filtration system then in use was inadequate for the endurance test program. On the output line from the lubrication system oil supply pump, a 10 micron nominal filter (Lenz DH750-800 housing and 8-03 filter) followed by a 3.3 micron 99.9 retention efficiency filter (Balston 20/80-800 housing and 200-80-BX filter) were installed in place of the then existing system. Both filters were removed and replaced once a week during the endurance test program.
- Slings were incorporated between test bearing inner races (Figure 129) to prevent spall debris generated during a failure from migrating into an adjacent bearing.
- All the endurance rig test bearing inner race journals were reworked to accommodate the refurbished MRC2001 endurance bearing bore diameters and provide a 0.0005 to 0.0010 inch interference fit.
- To avoid any possibility of incorporating thermally induced stress on axial load components, all the endurance rig test bearing outer race housing journals were either reworked or replaced to provide a 0.0001 to 0.0004 inch loose outer race operating fit.

The applied endurance test conditions remained unchanged from the previous endurance program, conducted in Task VII.

Speed	— 5500 rpm
Load	— 1975 lb radial
Lubrication	— MIL-L-7808 at 600 to 700 cc/min per bearing
Temperature	— No heat added (steady-state contact zone temperature \approx 145 to 155°F)

The 1975 lb radial load at operating bearing clearances provided approximately 483,000 psi maximum Hz stress at the inner race contact. Table 44 summarizes the range of calculated bearing life versus the various extremes in bearing and test conditions. The bearing life predictions are calculated without an applied material/process factor.

When the eight machines were initially set up, the 32 bearings in test were divided among 10 RSP565, 11 M50 baseline, and 11 MRC2001. Each lot was divided almost equally between center positions and end positions. As bearings were replaced they were matched as closely as possible by bearings with the same internal clearance.



FDA 300502

Figure 129. — Slinger to Prevent Adjacent Bearing Contamination

All endurance bearings were either tested to failure or for a minimum of approximately 2000 hours. The test results are presented in Table 45. A composite maximum likelihood Weibull distribution plot of M50, MRC2001, and RSP565 inner race failure data is presented in Figure 130.

A statistical evaluation of the MRC2001 and RSP565 Weibulls of inner race failures determined that the rolling contact fatigue life was equivalent to VIM-VAR M50 at the 95 percent confidence level with a minimum P value of 0.3 (where $(1 - P) \times 100$ percent is the lowest level of confidence for which Weibulls will be considered the same).

TABLE 44.
CALCULATED BEARING LIFE FOR THE RANGE OF BEARING GEOMETRIES AND ENDURANCE TEST
CONDITIONS

Contact Zone Temperature (°F)	Running Diametral Clearance (in.)	Max Ball Load (lb)	Hz Mean Stress (psi)		B ₁₀ Life Inner Race (hr)	Race	Surface Finish (rms)		Film Thickness (μ in)	Lambda (Δ)	F Factor**	L ₁₀ Life* (hr)
			Outer Race	Inner Race			Race	Ball				
145	-0.0001	1066	256,910	315,550	38.6	Outer	2.0	0.5	3.80	1.84	2.1	88.1
						Inner	1.0	0.5	3.19	2.85	2.5	88.1
145	0.0020	1207	267,760	328,880	32.3	Outer	1.0	0.5	3.77	1.83	2.1	73.7
						Inner	1.0	0.5	3.16	2.83	2.5	73.7
155	-0.0001	1066	256,910	315,550	38.6	Outer	4.0	0.5	3.35	0.811	0.27	12.2
						Inner	3.0	0.5	2.81	0.924	0.38	12.2
155	0.0020	1207	267,760	328,880	32.3	Outer	4.0	0.5	3.32	0.823	0.27	10.1
						Inner	3.0	0.5	2.78	0.915	0.37	10.1

*Material/Process Factor Excluded
**Life Factor Due to Lubrication Effects

6379C

TABLE 45.

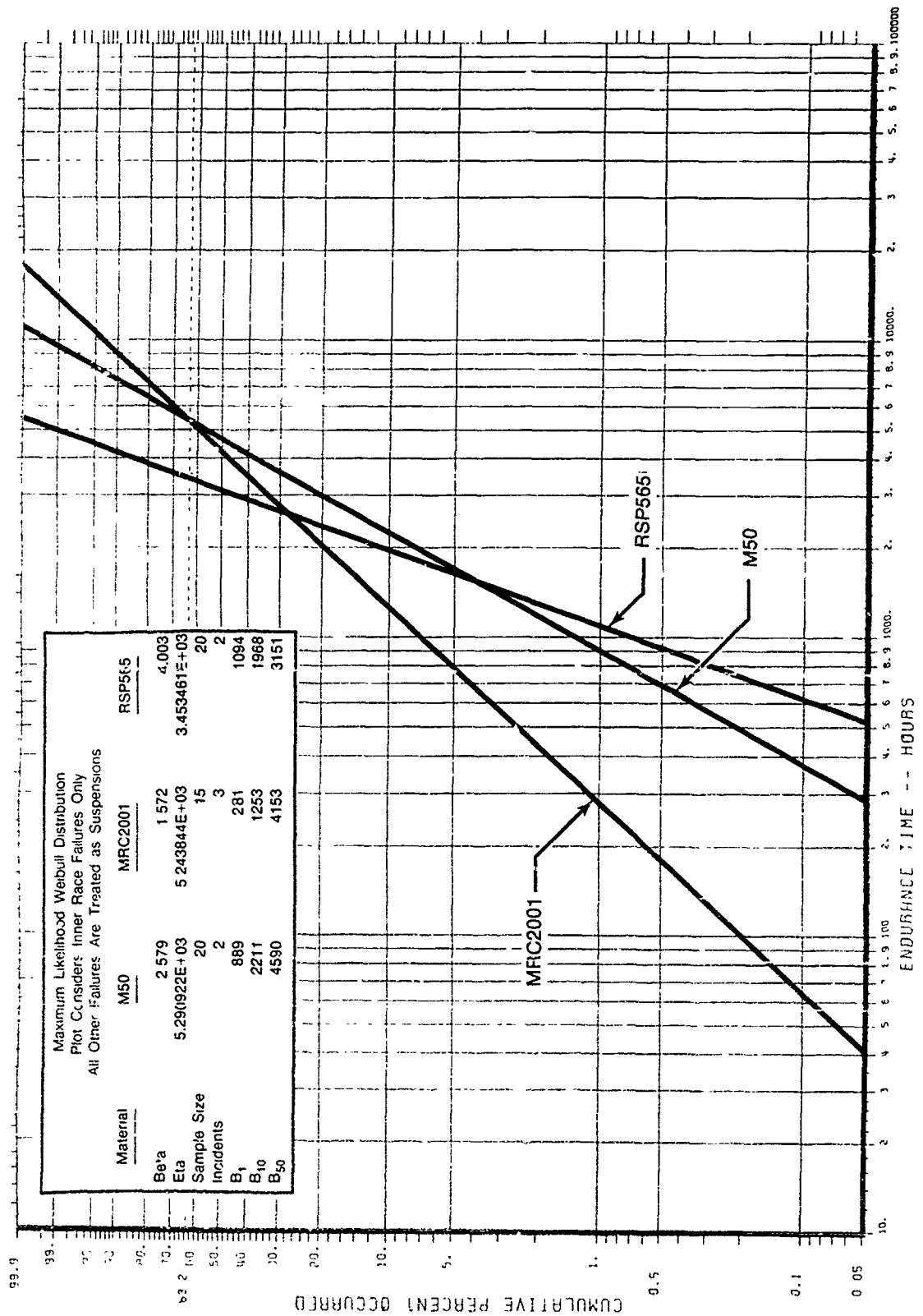
35-MM ENDURANCE BEARING TEST RESULTS

Machine Number	Material Evaluated/Endurance Time		
	S/N - hr (Status)		
	RSR565	M50	MRC2001
20	1- 863.2 (BALL)	1-2001.4 (SUSP)	1-2001.4 (SUSP)
	19-3030.8 (O/R)	6-1148.0 (I/R)	21-2003.8 (SUSP)
		16-2003.8 (SUSP)	
		21-2821.2 (SUSP)	
21	3-1716.7 (I/R)	2-2010.9 (SUSP)	9-2030.5 (SUSP)
	21-2324.7 (SUSP)	12-2030.5 (SUSP)	12-2030.5 (SUSP)
		18-2010.9 (SUSP)	34- 599.5 (I/R)
22	4- 404.6 (BALL)	5-2047.3 (SUSP)	2-1081.1 (I/R)
	5- 404.6 (SUSP)	7-2055.1 (SUSP)	
	13-1843.2 (I/R)	13-3021.3 (SUSP)	
	17-2000.1 (SUSP)	14-2909.0 (SUSP)	
	18-2000.1 (SUSP)		
23	8-2048.8 (SUSP)	4-2048.8 (SUSP)	10-2048.8 (SUSP)
	20-2042.5 (SUSP)	10-2048.8 (SUSP)	14-2042.5 (SUSP)
	22-2042.5 (SUSP)	19-2042.5 (SUSP)	
24	2-2034.6 (SUSP)	3-2034.6 (SUSP)	11-2034.6 (SUSP)
	11-2061.2 (SUSP)	8-2061.2 (SUSP)	
	24-2061.2 (SUSP)	9-2034.6 (I/R)	
25	12- 667.4 (BALL)	15-2078.8 (SUSP)	16-2004.8 (SUSP)
	23- 73.9 (SUSP)		30-1705.3 (I/R)
26	10-2027.1 (SUSP)	20-2066.1 (SUSP)	23-2066.1 (SUSP)
	16- 39.0 (BALL)		31-2066.1 (SUSP)
27	14- 456.0 (BALL)	17-2057.0 (SUSP)	19-2057.0 (SUSP)
			22-2057.0 (SUSP)
Total Endurance Time	30142.2	42531.8	27829.0
Total Bearing Hours on Project --	100,503.0		
Legend.	I/R = Inner Ring Failure O/R = Outer Ring Failure BALL = Spalled Ball SUSP = Suspension		

6176C

The procedure used to test whether two samples come from the same Weibull distribution is based on maximum likelihood estimation and the likelihood ratio. Maximum likelihood is a method for using data to estimate the parameters of a distribution. The technique finds the values of the parameters that maximize the likelihood of observing that particular sample of data.

The likelihood ratio procedure calculates a statistic based on the maximum likelihood estimates. In this particular test the slopes (or betas) of the Weibulls derived from the samples are compared first by calculating a likelihood ratio based statistic from these samples and comparing this statistic to a chi square value. This chi-square value is determined by the confidence level of the test. If the test statistic does not exceed this chi-square value, then the characteristic lives of the Weibulls are compared in a similar manner. If both of these test statistics are found to be less than the critical chi-square value, then the Weibulls are not significantly different (Reference 14).



FD 300527

Figure 130. — Composite Maximum Likelihood Weibull Distribution Plot of M50, MRC2001, and RSP565 Inner Race Failure Data

The bearing failures appear to be classic subsurface initiated spalls. Typical component spalls are illustrated in Figures 131 and 132. Detailed post-endurance test visual inspection results are presented in Appendices A, B, and C. In general all bearings regardless of material type, which did not experience a component spall, exhibited microscopic denting on the raceway surfaces and had fretting to a varying degree on the inner race bore and outer race outer diameter. The balls were typically excellent.

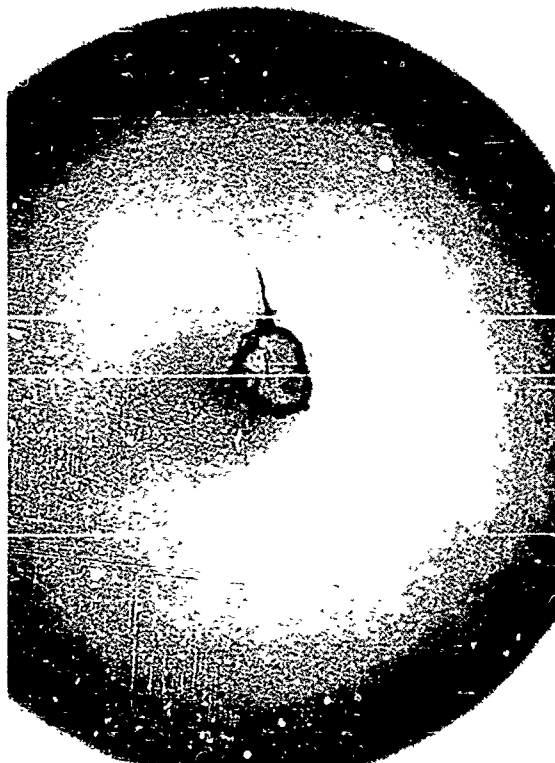
A composite Weibull of Task 422 RSP 565 and Task VII MRC2001 bearing life considering only ball failures is presented in Figure 133. The Weibull in phantom in Figure 133 treats all the RSP565 bearings exceeding 439 hours endurance time as suspensions to eliminate the influence of the difference in Task VII and Task 422 test duration. The statistical technique described in a preceding paragraph determined that at the 95 percent confidence level, no significant difference existed between the RSP565 and MRC2001 Weibulls. The P value for the Weibull comparison was less than 0.5. The Weibull slope associated with the RSP565 (0.6240, 0.8315) and MRC2001 (0.892) ball failures suggests an infant mortality mode of failure.



M50 Inner Race Spall
S/N 9
Endurance Time 2034.6 Hours
20X



MRC2001 Inner Race
Spall S/N 34
Endurance Time 599.5 Hours
20X

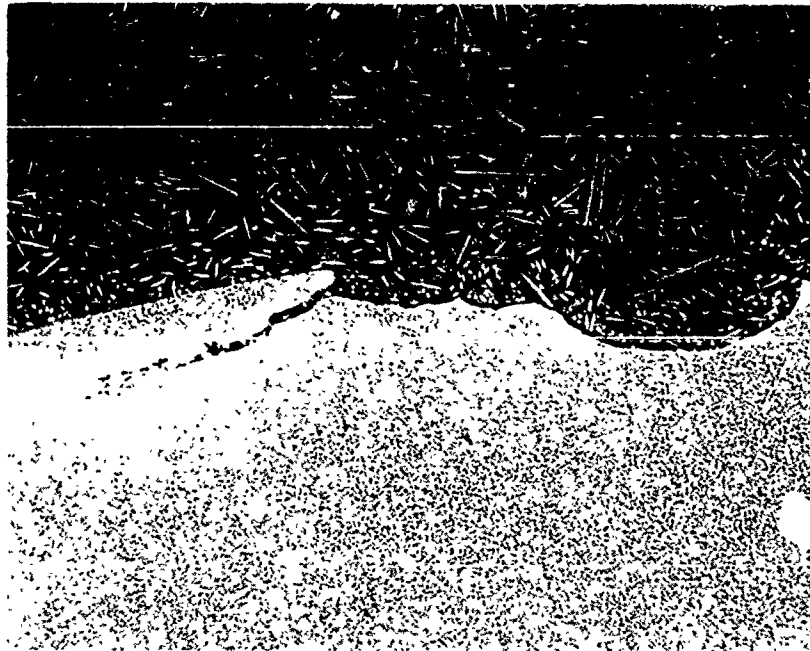


RSP565 Inner Race
Spall S/N 3
Endurance Time 1716.7 Hours
10X



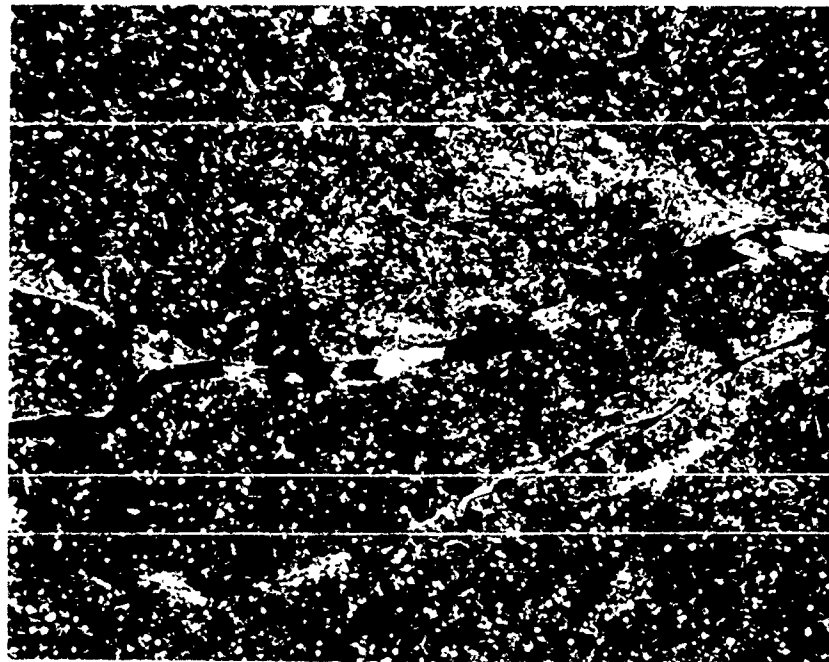
RSP565 Ball Spall
S/N 4
Endurance Time 404 Hours
10X

Figure 131. — Typical 35-mm Bearing Component Spalls



Overview

50x

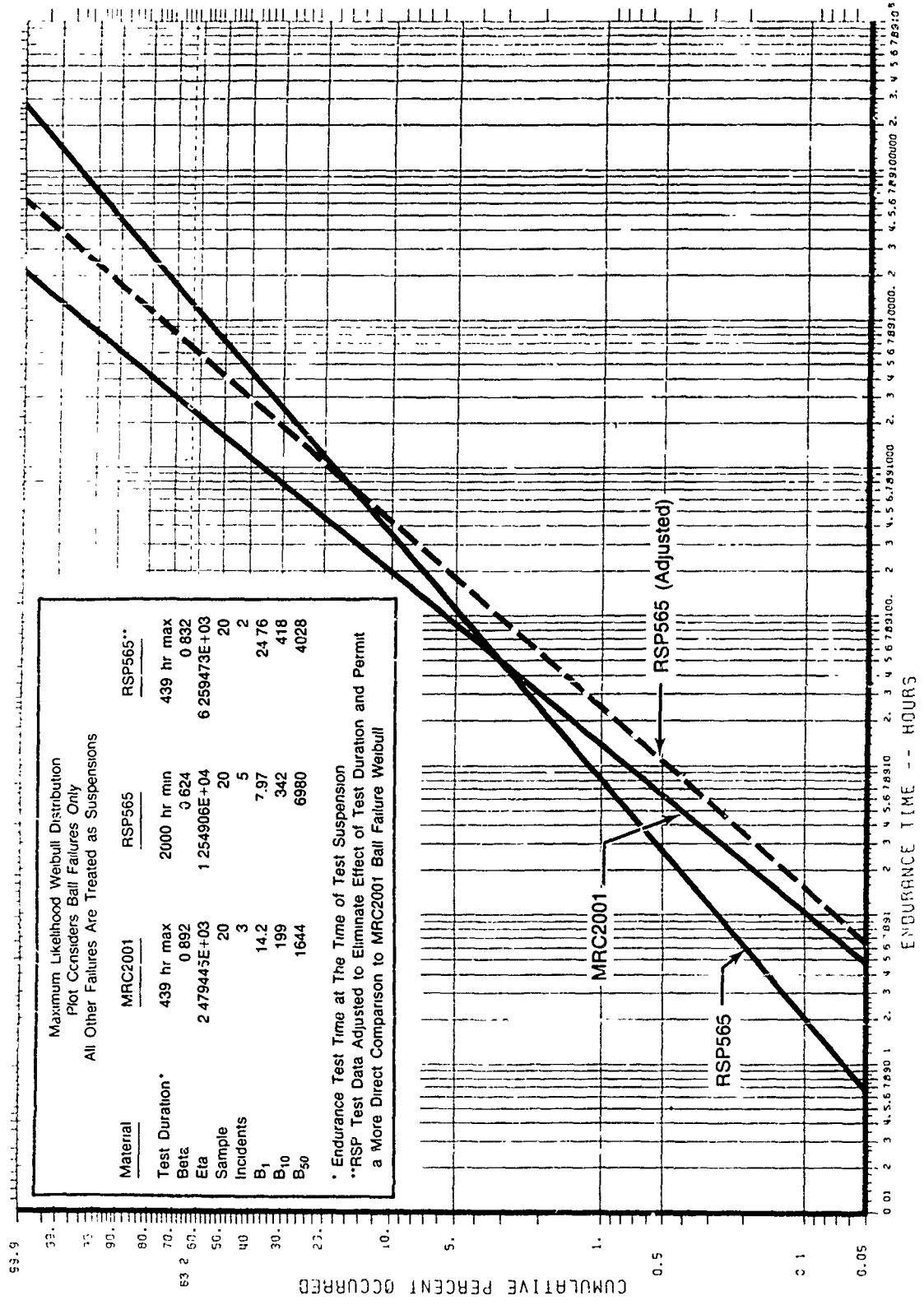


Far Left

500x

FD 300525

*Figure 132. — RSP565 35-mm Endurance Bearing S/N 4 Spalled Ball Cross Section
(Endurance Time of 101 Hours)*



Maximum Likelihood Weibull Distribution
Plot Considers Ball Failures Only
All Other Failures Are Treated as Suspensions

Material	MRC2001	RSP565	RSP565**
Test Duration*	439 hr max	2000 hr min	439 hr max
Beta	0.892	0.624	0.832
Eta	2.479445E+03	1.254906E+04	6.259473E+03
Sample Incidents	20	20	20
B ₁	3	5	2
B ₁₀	14.2	7.97	24.76
B ₅₀	199	342	418
	1644	6980	4028

* Endurance Test Time at the Time of Test Suspension
**RSP Test Data Adjusted to Eliminate Effect of Test Duration and Permit a More Direct Comparison to MRC2001 Ball Failure Weibull

FD 300528

Figure 133. — Composite Maximum Likelihood Weibull Distribution Plot of MRC2001 and RSP565 Ball Failure Data

SECTION III

CONCLUSIONS

1. SUMMARY

The objective of the Improved Corrosion Resistant Turbine Engine Bearing contract was the demonstration of an alternate bearing material which would reduce the occurrence of corrosion by at least 90 percent. The material was also required to be equivalent to VIM-VAR M50 in rolling contact fatigue life, wear resistance, and hot hardness.

The material selected in this program was MRC2001, a 15 percent chrome, powder metallurgy steel which demonstrated the corrosion resistance characteristic of stainless materials. It also demonstrated equivalent rolling contact fatigue life and hot hardness and superior wear resistance during element screening tests. In full-scale bearing endurance tests MRC2001 inner races demonstrated equivalent rolling contact fatigue life compared with baseline VIM-VAR M50 inner races.

2. PRINCIPAL RESULTS

a. Corrosion Mechanism Investigation

Analyses of bearing materials subjected to corrosive attack both by service and storage environments indicate that once corrosion of the steel is initiated, it proceeds by a common mechanism, i.e., autocatalytic pitting corrosion, in both environments. Bearing operation can mechanically remove the corrosion products, thus changing the visual appearance. Superficially, therefore, there appears to be different mechanisms for storage and service bearing corrosion. Corrosive attack of new steel bearing surfaces during storage probably initiates at or is more rapid along grain boundaries due to stress concentrations at these interfaces. The corrosive attack then progresses to autocatalytic pitting corrosion, characterized by mudcracking morphology and typically exhibiting higher X-ray emission spectroscopy (XES) intensities for the alloying elements. By contrast, corrosive attack of steel surfaces of bearings exposed to a service environment is probably initiated directly by autocatalytic pitting corrosion at sites of physical damage. These areas usually appear rough and pitted especially in locations of bearing functioning, and are characterized by more normal XES spectra.

Silver-plated bearing components seem more susceptible to initial attack by reactive species present in storage and service environments, particularly sulfur. The possibility of accelerated attack due to galvanic potential between silver-plated materials and bearing steels has also been shown.

The presence of reactive species in sufficient concentration to cause corrosion of bearing components has been confirmed in preservatives and is suspected in engine oils.

b. Initial Candidate Screening

Using literature searches, material supplier contracts, and available experience, 17 candidates were identified which had potential application to aircraft bearings. These candidates were ranked using all available data and perceived material properties. The five most promising candidates were:

- Armoloy-coated VIM-VAR M50
- CRB7 in wrought form

- MRC2001 conventional powder process material
- RSR565 rapid solidification powder process material
- Nickel sputter-coated VIM-VAR M50.

c. Initial Testing

The five selected candidates were evaluated in rolling contact fatigue and corrosion resistance. Rolling contact fatigue results indicated no significant difference existed between the selected candidates and VIM-VAR (vacuum induction melt, vacuum arc remelt) M50. Post RCF inspection indicates that the nickel sputter-coated VIM-VAR M50 candidate coating failed to adhere during RCF testing.

Compared to the VIM-VAR M50 baseline, all candidates showed superior corrosion resistance with CRB7, MRC2001, RSR565, and sputter nickel-coated VIM-VAR M50 having virtually no corrosion. Based on criteria established in Task II and RCF and corrosion test results, three candidates were selected for further evaluation. These were:

- Armoloy-coated VIM-VAR M50
- CRB7
- MRC2001.

d. Mechanical Property Evaluation

The three selected candidates were tested for wear resistance and hot hardness. All were considered equivalent to VIM-VAR M50 in hot hardness. Only MRC2001 was considered equal to or better than VIM-VAR M50 in wear resistance.

e. Selection of One Candidate

Using established criteria, MRC2001 was evaluated as the single most promising candidate to be carried into Phase II full-scale bearing development and testing.

f. Full-Scale Development and Test

Full-scale 35-mm MRC2001 endurance bearings and 110-mm performance bearings were fabricated. The original grinding practice employed in the MRC2001 race manufacture produced poor surface finish and an unfavorable residual stress profile. This condition in conjunction with lubrication system debris resulted in premature MRC2001 bearing failure and low endurance life compared to M50. Endurance testing was terminated after 439 hours. As a result, a grinding optimization study was conducted.

Results of this race grinding study were used to reprocess the MRC2001 inner rings. The refurbished races were mated to M50 outer races and balls. In a separate, but parallel, program RSP565, a 9 percent chrome material, was used to fabricate 35-mm endurance bearings. The improved grinding practice used to grind the MRC2001 inner races was also employed to grind the RSP565 inner and outer races. Back to back endurance tests were conducted on the 35-mm RSP565, M50 baseline, and refurbished MRC2001 endurance bearings. Considering inner race failures only, Weibull analysis determined that the rolling contact fatigue life of MRC2001 and RSP565 was equivalent to VIM-VAR M50.

3. CONCLUSIONS

a. Corrosion Investigation

The corrosion investigation indicated that water, chloride ions, reactive sulfur, and oxygen are the principal contaminants responsible for corrosion of bearings. The principal sources of contaminants include:

- Water* — Condensation in the lubrication system and preservation processing operations.
Improper handling procedures.
- Chloride Ions* — Improper handling procedures.
Occurs as a standard petroleum contaminant.
- Reactive Sulfur* -- Occurs as a standard petroleum contaminant.
Possible result of a reduction of sulfur compound in bearing corrosion inhibitors.
- Oxygen* — Air in lube system.
Also occurs dissolved in water and oil.

Random instances where improper handling procedures are employed are also contributing factors in that they impact the above conditions. Temperature and temperature cycles also contribute to the corrosion problem as they effect reaction rates and the saturation level of contaminants in oils and preservatives.

It has also been concluded that the corrosion mechanism responsible for the attack of bearings in storage and service are similar in nature and include pitting and intergranular corrosion.

b. Bearing Material Evaluation

MRC2001, as well as RSP565 raceways have demonstrated rolling contact fatigue life equivalent to VIM-VAR M50. Post-test visual and dimensional inspections of the endurance test bearings could not show any wear difference attributable to material type. This result suggests that the specimen wear test conducted in Phase I was too severe for ranking lubricated rolling contact bearing materials in wear resistance.

The improvement in M50 rolling contact fatigue life between the tests in Task VII and Task 422 can only be attributed to the improvements in raceway surface finish and lubrication cleanliness. This performance improvement was also noted for the MRC2001 and RSP565 endurance tests when compared with theoretical expectations. This suggests that all bearings would benefit from these improved conditions, a conclusion which is fully supported by other published research (References 15 and 16).

These results also indicate that the fundamental life prediction system, as defined by Lundberg and Palmgren, seriously underestimates life of current bearings. This conclusion is also supported by reports from recent research (References 17 and 18).

4. RECOMMENDATIONS

a. Ball Manufacturing

The powder metallurgy MRC2001 and RSP565 balls demonstrated poor endurance life and post-test evaluations could not define a cause. Wrought M50 balls performed excellently with no

ball failures during the M50 endurance program. At the same time, balls from these two experimental stainless materials suffered many premature failures. These stainless balls were made by different ball manufacturers which is suggestive of a generic problem with high chrome alloy powder metallurgy ball manufacture. An extended study to understand the cause of these premature ball failures is required. This should then be used to assist in the development of an optimum ball manufacturing process. Ball manufacturing progress can be easily monitored with 35-mm endurance tests using M50 rings.

b. Performance Demonstration Bearings

The 110-mm performance test bearing fabricated during Task IV should be tested at main shaft operating conditions. This would provide a full-scale demonstration of a powder metallurgy corrosion resistant bearing and would begin the process of engine verification of these type bearings.

c. Rolling Contact Fatigue Endurance

The exceptionally long life demonstrated in this program, when well finished bearings are tested in a clean environment, supports the potential for an endurance limit for rolling contact fatigue (References 17 and 18). This possibility needs further study and verification if possible. Current design practice for rolling element bearings tends to sacrifice reliable performance in order to achieve a theoretical life goal e.g., in a given bearing design, spin to roll ratio and ball excursion (performance characteristics) may be compromised for increased contact angle and raceway conformance (increased theoretical life).

A program to define rolling contact fatigue at reasonable stress levels is needed. Current knowledge is sufficient to show that surface effects, from poor grinding for example, can substantially shorten bearing life. With this knowledge, a program that takes special care to preserve surface quality can be structured.

A natural second step would be to investigate methods to improve performance under conditions that promote surface damage. Low EHD film thickness applications such as slow speed gearbox bearings will never operate with full separation, thus, any process that will mitigate surface damage has the potential for substantial life improvement.

d. Corrosion Resistance Verification

The corrosion resistance verification tests using failed endurance test bearings should be conducted as originally planned in Task IX. The purpose of these tests would be to provide confirmation that the improved corrosion resistance demonstrated in specimen tests is retained even after extensive bearing operation.

REFERENCES

1. Cunningham, Jr., J. S. and M. A. Morgan, "Review of Aircraft Bearing Rejection Criteria and Causes," *Lubrication Engineering*, Vol. 35, 8, pp 435-441, Aug. 1979
2. P&WA Internal Correspondence, Memo, H. L. Hess to L. M. Mazer, "Bearing Design System" 21 April 1980
3. Warner, P. A., G. C. Brown, R. J. Meehan, and W. J. Purvis, "Corrosion Inhibiting Engine Oils," AFWAL TR-81-4028
4. Brown, C. and F. Feinberg, "Development of Corrosion Inhibited Lubricants for Gas Turbine Engines and Helicopter Transmissions," ASLE 80-AM-6C-3
5. Valori, R., G. K. Hubler, and D. Popgoshev, "Ion Implanting Bearing Surfaces for Corrosion Resistance," ASME Paper 82-LUB-23
6. Parker, R. J. and R. S. Hodder, "Rolling Element Fatigue Life of AMS 5749 Corrosion Resistant High Temperature Bearing Steel," ASME paper 77-Lub-3
7. Brown, P. F. and J. R. Potts, "Evaluation of Powder Processed Turbine Engine Ball Bearings," AFAPL-TR 77-26
8. Philip, T. V. "A New Bearing Steel; A New Hot Work Die Steel," *Metal Progress*, Feb. 1980
9. Johnson, B. L., "A Stainless High Speed Steel for Aerospace Applications," *Metal Progress*, Sept 1964
10. Nimos, N. J., D. E. Hahn, and R. E. Maurer, "Research Report on Functional Testing of Armoloy, Nobilizing and Electroless Nickel Coating in Rolling Contact," SKF Industries, Inc., Report AL76M001
11. Wensel, R. G., "Testing of Unlubricated Water Immersed Carbon-Steel Ball Bearings," Atomic Energy of Canada Limited, AECL-5824
12. Parker, T. D. "14%Cr-4%Mo the Stainless Bearing and Tool Steel," Climax Molybdenum Co., 1962
13. Johnson, L. G. "The Statistical Treatment of Fatigue Experiments," Elsevier Publishing Co., 1964
14. Lawless, J. F., "Statistical Models and Methods for Lifetime Data," John Wiley and Sons, 1982
15. "Life Adjustment Factors for Ball and Roller Bearings," ASME Engineering Design Guide
16. Sayles, R. S. and P. B. Macpherson "Influence of Wear Debris on Rolling Contact Fatigue," Rolling Contact Fatigue Testing of Bearing Steels ASTM STP 771, J J. C. Hoo Ed., American Society for Testing Materials, 1982

17. Zwirlein, O., H. Schlicht "Rolling Contact Fatigue Mechanisms — Accelerated Testing Versus Field Performance," Rolling Contact Fatigue Testing of Bearing Steels, ASTM 771, J. J. C. Hoo, Ed., American Society for Testing and Materials, 1982
18. Ioannides, E., T. A. Harris "A New Fatigue Life Model for Rolling Bearings," ASME paper 84-Trib-28

APPENDIX A

VISUAL INSPECTION DOCUMENTATION OF THE 35-MM ENDURANCE BALL BEARINGS WITH MRC2001 INNER RINGS, M50 BALLS, AND OUTER RINGS

S/N 1 (Run 2001.4 Hours)

Inner — Very few microscopic dents (20× scope). Heavy fretting on bore.

Outer — Very few microscopic dents.

Balls — Excellent.

S/N 2 (Run 1081.1 Hours, spalled inner)

Inner — Spall 0.040 × 0.065 inch, centered in race. Denting downstream from spall. Mild fretting in bore.

Outer — Denting in loaded zone; fretting on OD; has turned in housing.

Balls — Light denting.

S/N 9 (Run 2030.5 Hours)

Inner — Few microscopic dents (20× scope). Mild fretting face and bore.

Outer — Few microscopic dents; heavy fretting on OD.

Balls — Excellent.

S/N 10 (Run 2048.8 Hours)

Inner — Few microscopic dents (20× scope). Heavy fretting on bore.

Outer — Few microscopic dents; light fretting on OD.

Balls — Excellent.

S/N 11 (Run 2034.6 Hours)

Inner — Two dents 0.010 to 0.015 inch long plus a few microscopic dents. Mild fretting on face and bore.

Outer — A few microscopic dents; OD is fretted and turned in housing.

Balls — Excellent.

S/N 12 (Ran 2030.5 Hours)

Inner — A few microscopic dents (20× scope). Light fretting on face and bore.

Outer — A few microscopic dents; fretting on OD; turned in housing.

Balls — Excellent.

S/N 14 (Ran 2042.5 Hours)

Inner — A few microscopic dents (20×). Slight indication of rolling, sliding zones. Mild fretting on bore, faces.

Outer — Very few microscopic dents. Moderate fretting on OD.

Balls — Good.

S/N 16 (Ran 2004.8 Hours)

Inner — Very few microscopic dents (20× scope). Light fretting face and bore.

Outer — Very few microscopic dents.

Balls — Excellent.

S/N 19 (Ran 2057.0 Hours)

Inner — Few microscopic dents (20× scope). Mild fretting face and bore.

Outer — Few microscopic dents; heavy fretting on OD; turned in housing.

Balls — Excellent.

S/N 21 (Ran 2003.8 Hours)

Inner — A few microscopic dents (20×). Slightly cloudy ball path. Severe fretting on bore, mild fretting on one face.

Outer — A few microscopic dents. Moderate fretting on OD.

Balls — Good.

S/N 22 (Ran 2057.0 Hours)

Inner — Few microscopic dents (20× scope). Mild fretting face and bore.

Outer — Few microscopic dents; fretting on OD; turned in housing.

Balls — Excellent.

S/N 23 (Ran 2066.1 Hours)

Inner — Few microscopic dents (20× scope); mild fretting face and bore.

Outer — Few microscopic dents; fretting on OD.

Balls — One shows slight band, otherwise excellent.

S/N 30 (Ran 1705.3 Hours, spalled inner)

Inner — Spall approximately 0.040 × 0.065 inch, centered in race. Dents downstream from spall. Mild fretting on face and bore.

Outer — Dents in loaded zone; fretted on OD.

Balls — Light banding.

S/N 31 (also marked 37) (Ran 2066.1 Hours)

Inner — Very few microscopic dents (20× scope); light fretting bore and face.

Outer — Very few microscopic dents; light fretting on OD.

Balls — Excellent.

S/N 34 (Ran 599.5 Hours, spalled inner)

Inner — Spalled area approximately 0.080 × 0.085 inch. Deepest part of spall is in center of race with flaked area as a whole off-centered about 0.015 inch. Dents down-stream from spall; slight fretting on bore.

Outer — Numerous small dents in loaded zone; mild fretting on OD.

Balls — Incidental dents.

APPENDIX B

VISUAL INSPECTION DOCUMENTATION OF THE
M50 BASELINE 35-MM ENDURANCE BALL BEARINGS

S/N 1 (Ran 2001.4 Hours)

Inner — Faint indications of rolling, sliding zones. A number of microscopic dents (20× scope); slight fretting on bore.

Outer — Microscopic denting; OD fretted.

Balls — Excellent.

S/N 2 (Ran 2010.9 Hours)

Inner — A few microscopic dents (20×) on race. Mild fretting on bore and one face. Slight indication of rolling, sliding zones.

Outer — A few microscopic dents on race. Moderate fretting on OD; turned in housing.

Balls — Good.

S/N 3 (Ran 2034.6 Hours)

Inner — Few microscopic dents (20× scope); mild fretting bore and face.

Outer — Few microscopic dents; mild fretting on OD.

Balls — Excellent.

S/N 4 (Ran 2048.8 Hours)

Inner — Few microscopic dents (20× scope); fretting on bore.

Outer — Few microscopic dents in outer; fretting on OD.

Balls — Excellent.

S/N 5 (Ran 2047.3 Hours)

Inner — Several microscopic dents (20× scope); mild fretting on bore and face.

Outer — Microscopic dents in outer; mild fretting on OD; turned in housing.

Balls — Excellent.

S/N 6 (Ran 1148.0 Hours, spalled inner)

Inner — Spalled area approximately 0.220×0.080 inch, denting. Considerable fretting on bore.

Outer — Numerous small dents; fretting on OD.

Balls — Dented.

S/N 7 (Ran 2055.1 Hours)

Inner -- One dent about 0.003 inch in diameter, a few microscopic ones (20×). Mild fretting on bore, one face. Distinct rolling, sliding zones

Outer — One dent about 0.007 inch in diameter and a few microscopic dents. Very mild fretting on OD.

Balls — Good.

S/N 8 (Ran 2061.2 Hours)

Inner — One narrow dent 0.030 inch long. Numerous microscopic dents (20×). Distinct rolling, sliding zones. Light fretting on bore but heavy fretting on one face (possible source of material which dented race). A few scuff marks made at disassembly.

Outer — Numerous microscopic dents. Light fretting on OD.

Balls — Good.

S/N 9 (Ran 2034.6 Hours, spalled inner)

Inner — Spalled area approximately 0.120×0.080 inch, denting. Light fretting on bore.

Outer — Dented; fretting on OD.

Balls — Dented.

S/N 10 (Ran 2048.8 Hours)

Inner — One dent approximately 0.015 inch long, few microscopic dents (20× scope); some fretting in bore.

Outer — A few microscopic dents; fretting on OD.

Balls — Excellent.

S/N 12 (Ran 2030.5 Hours)

Inner — Looks good to naked eye. However, a multitude of microscopic crescent shaped dents caused by a damaged ball. A few conventional type microscopic dents (20× scope); mild fretting on face and bore.

Outer — Same as inner race; mild fretting on OD.

Balls — Two balls have creases, as if forced against a sharp edge. Raised metal around one or both of these creases must have generated the crescent-shaped dents on the races.

S/N 13 (Ran 3021.3 Hours)

Inner — One dent about 0.007 inch in diameter, a few microscopic ones (20×). Distinct rolling, sliding zones. Heavy fretting bore, light fretting on face.

Outer — A few microscopic dents, OD is good.

Balls — Good.

S/N 14 (Ran 2909.0 Hours)

inner — One dent about 0.005 inch in diameter, a few microscopic ones (20×). Distinct rolling, sliding zones. Moderate fretting bore, heavy on one face.

Outer — A few microscopic dents. Mild fretting on OD.

Balls — Good.

S/N 15 (Ran 2078.8 Hours)

Inner — One dent approximately 0.020 inch long, a few microscopic dents (20× scope); fretting on both faces and bore.

Outer — A few microscopic dents; fretting on OD; turned in housing.

Balls — Excellent.

S/N 16 (Ran 2003.8 Hours)

Inner — A few microscopic dents (20×). Distinct rolling, sliding zones. Heavy fretting on bore, one face.

Outer — A few microscopic dents. Moderate fretting on OD.

Balls — Good.

S/N 17 (Ran 2057.0 Hours)

Inner — A few microscopic dents (20× scope); heavy fretting on face, fretting on bore.

Outer — A few microscopic dents; fretting on OD; turned in housing.

Balls — Excellent.

S/N 18 (Ran 2010.9 Hours)

Inner — A shallow dent about 0.020 inch long in bottom of race. Slight indication of rolling, sliding zones. A few microscopic dents (20×). Mild fretting on bore and one face.

Outer — A few microscopic dents on race. Heavy fretting on OD.

Balls — Good.

S/N 19 (Ran 2042.5 Hours)

Inner — A few microscopic dents (20×). Slight indication of rolling, sliding zones. Moderate fretting on bore.

Outer — Very few microscopic dents. Very little fretting on OD.

Balls — Good.

S/N 20 (Ran 2066.1 Hours)

Inner — A row of 0.005 inch dents about 0.040 inch long on edge of ball path. Several microscopic dents (20× scope); light fretting on face and bore.

Outer — Several microscopic dents; light fretting on OD.

Balls — Excellent.

S/N 21 (Ran 2821.2 Hours)

Inner — Numerous microscopic dents (20×). Cloudy ball path. Very heavy fretting on bore, mild fretting on face.

Outer — A few microscopic dents, OD good.

Balls — Good.

APPENDIX C

VISUAL INSPECTION DOCUMENTATION OF THE RSP565 35-MM ENDURANCE BALL BEARINGS

S/N 1 (Ran 863.2 Hours)

Inner — A large number of crescent shaped dents from contact with the edges of a spall on a ball. A few 0.005-inch diameter dents in addition. Mild discoloration in bore.

Outer — Slightly roughened surface in loaded zone from contact with spalled ball. Three narrow dents approximately 0.030 inch long. Moderate fretting on OD.

Balls — One ball spalled. Other balls show microscopic dents and scratches.

S/N 2 (Ran 2034.6 Hours)

Inner — One dent approximately 0.010-inch diameter, several microscopic dents (20× scope); mild fretting on bore.

Outer — Microscopic denting; fretting on OD; turned in housing.

Balls — Excellent.

S/N 3 (Ran 1716.7 Hours, spalled inner)

Inner -- Spalled area 0.210 inch long × 0.060 inch to 0.120 inch wide, with incidental denting. A scuff mark apparently generated after completion of test. Severe fretting on bore.

Outer — Considerable denting; moderate fretting on OD; turned in housing.

Balls — Dented.

S/N 4 (Ran 404.6 Hours)

Inner — A number of long, scratch-like marks across the race, probably from contact with a spall on a ball.

Outer — A large number of dents or surface blemishes, from less than 0.001 inch to 0.002 inch in loaded zone. Almost no fretting on OD.

Balls — One ball spalled. Others show a few fairly deep dents under magnification.

S/N 5 (Ran 404.6 Hours)

Inner — Several dents up to 0.005-inch diameter on raceway. The bore is in good condition.

Outer — Several dents 0.002-inch to 0.007-inch diameter on raceway. Cloudy areas under 10× magnification, consisting of marks less than 0.001 inch. Three spots on side of loaded zone, visible to naked eye, which appear to be variations in finish. Moderate fretting on OD.

Balls — Three balls have streaks of shallow parallel grooves, visible at 30× and higher magnification. One ball is especially marked. Also there are apparent cuts. It is believed these balls did not clean up during finishing. The other five balls show a very few small dents.

NOTE: Machine 22, which incorporated this bearing, experienced several automatic shutoffs during early running. Upon restarts, no normal failure pattern was indicated. It is believed that a particular orientation of the worst ball was necessary to actuate the automatic monitor. After S/N 4 failed and was replaced, the machine continued to shut down; a technician thought he detected audible indications of failure so the setup was again dismantled. Small spots in the finish of the outer race of S/N 5 were observed. The bearing was replaced, after which the problem ceased.

S/N 8 (Ran 2048.8 Hours)

Inner — An indentation about 0.030 inch long, 0.001 inch wide, possibly a scratch. Very few microscopic dents (20× scope); heavy fretting on bore.

Outer — Very few microscopic dents; moderate fretting on OD; turned in housing.

Balls — Excellent.

S/N 10 (Ran 2027.1 Hours)

Inner — A very few microscopic dents (20× scope). Fretting on face and bore.

Outer — Few microscopic dents; fretting on OD.

Balls — Excellent.

S/N 11 (Ran 2061.2 Hours)

Inner — Several microscopic dents in race (20×). Several scuff marks in race which were generated after test during rig disassembly. Rolling, sliding zones evident. Light fretting on bore and face.

Outer — A few microscopic dents, some scuff marks. Light fretting on OD.

Balls — Good.

S/N 12 (Ran 667.4 Hours, spalled ball)

Inner — Light denting; slight fretting on bore.

Outer — Substantial shallow denting; slight fretting on OD.

Balls — One is spalled, approximately 0.104×0.090 inch.

S/N 13 (Ran 1843.2 Hours, spalled inner)

Inner — Spalled area 0.340 inch long \times 0.080 inch, incidental denting; fretting on face.

Outer — Substantial denting; OD fretted.

Balls — Slight banding, perhaps from running over spall on inner.

S/N 14 (Ran 456.0 Hours)

Inner — A large number of small crescent marks, from contact with spall on a ball, plus a few separate 0.005 -inch to 0.010 -inch dents. The bore is in good condition.

Outer — A large number of marks, from less than 0.001 -inch to 0.002 -inch diameter in loaded zone. Very light fretting on OD.

Balls — One ball spalled. Another ball has long circular scratches, probably from spall material which became trapped in a cage pocket. Some dents which can be seen at $30\times$.

S/N 16 (Ran 39.0 Hours)

Inner — Two dents, approximately 0.060×0.015 inch and several 0.020×0.030 inch and some smaller ones in raceway. There are also marks which appear to result from contact with sharp edges of a spalled ball. No fretting on bore.

Outer — One dent 0.040×0.020 inch, and a few smaller ones. There are marks from contact with edges of a spalled ball. There is mild fretting on the OD.

Balls — One ball spalled. Other balls are dented; one has a dent approximately 0.050×0.010 inch and another 0.060×0.015 inch.

S/N 17 (Ran 2000.1 Hours)

Inner — One dent approximately 0.007 inch long; a few microscopic dents ($20\times$ scope); fretting on face and slightly on bore.

Outer — A few microscopic dents; fretting on OD; turned in housing.

Balls — Excellent.

S/N 18 (Ran 2000.1 Hours)

Inner — Very few microscopic dents ($20\times$ scope); light fretting on face.

Outer — Very few microscopic dents; OD fretted.

Balls — Excellent.

S/N 19 (Ran 3030.8 Hours, spalled outer)

Inner — Many dents caused by spall debris. Raceway is cloudy. Severe fretting on bore, light fretting on face.

Outer — A spall approximately 0.120×0.170 centered in race. Outer turned in housing with substantial fretting.

Balls — Dented

S/N 20 (Ran 2042.5 Hours)

Inner — A few microscopic dents (20 \times) on race. Slight indication of rolling-sliding zones. Mild fretting on bore and one face.

Outer — Very few microscopic dents. Light fretting on OD.

Balls — Good.

S/N 21 (Ran 2324.7 Hours)

Inner — A few microscopic dents (20 \times) on race. Substantial fretting on bore and one face. Distinct ball path.

Outer — Very few microscopic dents in race. Considerable fretting on OD. Turned in housing.

Balls — Good.

S/N 22 (Ran 2042.5 Hours)

Inner — A narrow indent about 0.025 inch long near edge of loaded zone, also a scuff mark. Otherwise a few microscopic dents (20 \times) on race. Somewhat cloudy ball path with slight differentiation due to rolling, sliding zones. Mild fretting on bore.

Outer — A few microscopic dents in race. Fretting on OD.

Balls — Good.

S/N 23 (Ran 73.9 Hours)

Inner — A few dents in raceway approximately 0.001-inch diameter. Bore is in good condition.

Outer — There is a 0.007-inch diameter spot in the loaded zone but out of the central area. This is not a dent and its origin is unknown. It has some depth and was originally believed to be cause of rig shutdown. There are a few crescent shaped marks 0.003 to 0.005 inch in loaded zone. The limited number and sharpness of these suggest they occurred immediately before shutdown. Light fretting on OD.

Balls — One ball appears to be defective. There are two small cavities, one about 0.005-inch diameter, which do not appear to be conventional dents or

spalls. There are also a few grinding marks which did not clean up during finishing. Some other balls show dents up to 0.005-inch diameter.

NOTE: It is now believed that failure indication was initiated by the apparently defective ball.

S/N 24 (Ran 2061.2 Hours)

Inner — One shallow dent 0.010 inch in diameter. A few microscopic dents (20×). Numerous light scratches and scuff marks transverse of race made after completion of test, apparently at disassembly. Rolling, sliding zones evident. Mild fretting on OD and one face.

Outer — One dent 0.005 × 0.10 inch and a few microscopic dents. Scuff marks which were generated after the test. Light fretting on OD.

Balls — Good.